# COMPLEX P-T-T-D HISTORY OF SUPRACRUSTAL ROCKS OF THE METAMORPHIC INTERNAL ZONE OF THE SOUTHERN WOPMAY OROGEN, NT

by

LEANNE MARIE SMAR

B.Sc. Hons, Carleton University, 2008

A THESIS SUBMITTED IN PARTIAL FULFILLMENT OF

THE REQUIREMENTS FOR THE DEGREE OF

MASTER OF SCIENCE

in

THE FACULTY OF GRADUATE AND POSTDOCTORAL STUDIES

(Geological Sciences)

THE UNIVERSITY OF BRITISH COLUMBIA

(Vancouver)

April 2015

ABSTRACT

An abundance of Paleoproterozoic orogenic belts are distributed globally, as peripheral terranes accreted against the margins of Archean cratons. The abundance of these terranes indicates a period of tectonic activity between 2.1 and 1.8 Ga. The study of such belts has offered insight into the nature and rate of tectonic activity in the Paleoproterozoic. Analysis of thermo-tectonic events, paired with the collection of geochronological data has led to the discovery of a supercontinent that existed before the formation of Rodinia, called Columbia. The 1.9 Ga Wopmay Orogen in northern Canada is a Paleoproterozoic belt, comprising a complex amalgamation of tectonic elements, which is thought to have formed during the assembly of Columbia.

The advent of new geochronological data has demanded that the current P-T-t-d (Pressure-Temperature-time-deformation) model of the Wopmay Orogen be reconsidered. To reconstruct the evolution of an orogenic belt, structural analysis of overprinting kinetic fabrics, thermodynamic analysis of metamorphic mineral assemblages, and the determination of absolute timing of thermo-tectonic events are required.

Two map areas were chosen to conduct an analysis of the kinetic and metamorphic evolution of the southern Wopmay Orogen, a region of the belt that has historically been under-studied. The Brown Water and the Little Crapeau Lake areas are situated south of 65˚N in the Metamorphic Internal zone of the orogen, and are bounded to the east and west by the Archean Slave craton and the ca. 1850 Ma Great Bear Magmatic zone, respectively. The areas comprise a sequence of pelitic to semi-pelitic schists and gneisses that overlie parautochthonous Archean basement. Rocks in both areas show evidence for five generations of overprinting fabrics, $S_{1C}$-$S_{5C}$ at Little Crapeau Lake, and $S_{1B}$-$S_{5B}$ at Brown Water Lake. Conditions of peak metamorphism were attained synchronous with the intrusion of the ca. 1877 Ma Little Crapeau Sill, and the regionally expansive ca. 1850 Ma Rodrigues granite. At Brown Water Lake peak metamorphic conditions were reached syn-$S_{5B}$ at 3.1-4.2 kbars and 570-670˚C, and syn-$S_{2C}$ at 3.1-3.9 kbars and 570-630˚C at Little Crapeau Lake. Chemical and isotopic geochronological dating of monazite provided metamorphic age constraints that concurred with ages of local intrusions.

# PREFACE

This dissertation is original, unpublished, independent work by the author, L. Smar.

TABLE OF CONTENTS

LIST OF TABLES

LIST OF FIGURES

ACKNOWLEDGEMENTS

First and foremost, I would like to give special thanks to my main supervisors, Valerie Jackson at the Northwest Territories Geoscience Office (NTGO), and Ken Hickey at the University of British Columbia (UBC), for their time, guidance, and patience throughout this project. Their invaluable experience in and out of the field, thoughtful discussions, and overall thoroughness and dedication to scientific research came together to help create a final product that I am proud of. Luke Ootes of the NTGO also made significant contributions in and out of the field, particularly when it came to big picture ideas and the tectonic history of the Wopmay Orogen.

Also much gratitude is given to the field assistants who were part of a great team during the 2009-10 field seasons. Special thanks to Duncan Mackay for his expert assistance in the field over two summers, for ten o'clock snacks, and for Pirate Days on our Lonely Island 2010 fly camp.

External help was also provided by Dave Hirsch at the University of Western Washington, by Mike Williams, Mike Jercinovic and Julien Allaz at the University of Massachusetts at Amherst, and by Bill Davis, Nicole Rainer and Tom Pestaj at the GSC SHRIMP lab in Ottawa. Much appreciation to them.

And last but not least, sincere and enormous thanks goes to my family and friends, officemates and others, for their loving support over the years.

# 1 INTRODUCTION

Paleoproterozoic orogenic belts are distributed globally as peripheral terranes accreted against Archean cratonic shields (Zhao et al., 2002). Peripheral orogenies are belts of orogenic rocks that occur at the exterior margin of a supercontinent, of Archean age in this case (Murphy and Nance, 1991). They are often preserved in the middle of continents, frozen in time and space during crustal assembly. They can be complex in nature, comprising many tectonic elements, and having been affected by a long tectonic history which can include extension, collision, and thickening, with thrust and fold components (Hoffman et al., 1988; Thompson et al., 1987). The detailed reconstruction of such complex histories into a relative sequence of deformational and metamorphic events is critical in the understanding of Proterozoic tectonic activity and its relationship to Archean cratons.

An abundance of 2.1-1.8 Ga orogenic belts worldwide indicates a period of abundant tectonic activity whereby Archean and Paleoproterozoic cratonic blocks were welded together during collisional orogeny (Zhao et al., 2002; Zhao et al., 2004). This provides evidence for the formation of a Paleo-mesoproterozoic supercontinent that preceded Rodinia, named Columbia or Nuna (Zhao et al., 2002). Study of these early Proterozoic belts helps to further our understanding of earth's early tectonic history.

The Wopmay orogen, which borders the Archean Slave craton in the Northwest Territories, Canada, is a Paleoproterozoic orogen that has had a long history of study. Its southern extent is located approximately 140 km northwest of Yellowknife, NT (Fig. 1.1 a). The orogen is exposed over >450 km north to south, and is variable in width from ~250 km tapering to a point at its southern extent (Fig. 1.1 b). Over several decades, numerous mapping and geochronological studies across the orogen have defined its main tectonic components and have attempted to unravel its tectonic and thermal history (Bowring, 1985; Davis et al., 2011; Hildebrand and

Bowring, 1984; Hildebrand et al., 1987; Hildebrand et al., 1991; Hoffman, 1980, 1984; Hoffman and Bowring, 1984; Hoffman and Hall, 1993; Janots et al., 2009; King, 1986). These regional studies have however focused largely on the northern half of the orogen, above 65°N, where stratigraphic sequences are well exposed, and where workers have been able to reconstruct a fold and thrust belt (Grotzinger and Hoffman, 1983; Tirrul, 1983). Crustal-scale imaging studies, such as the SNORCLE profile produced by Canada's National Lithoprobe Geoscience Project, as well as regional magnetic surveys have shed light on the geometry of the deep Archean and Proterozoic crust; however these provide little insight into the processes and deformation phases that lead to their current geometry. This can be resolved through highly detailed microstructural and metamorphic studies.

A regional geological mapping project by the Northwest Territories Geoscience Office (NTGO) has gathered widespread geochronological data to reconstruct the timing and relationships of many crustal scale intrusive suites (Jackson et al., 2013) (Fig. 1.1 c). This study has yielded geochronological data that has provided evidence for the presence of more intrusive suites than were previously recognized, therefore requiring reassessment of the tectonic evolution of the Wopmay Orogen. Whereas heating in the orogen was once attributed to two distinct intrusive phases, the Hepburn and Bishop intrusive suites, it is now evident that there was a longer period of magmatic activity spanning nearly 40 million years. The new mapping initiatives across the southern Wopmay orogen cover both the Metamorphic Internal zone (MIz) and the Great Bear Magmatic zone (GBMz) (Fig. 1.2). With the advent of this new data, redefining of previous orogenic models has been necessary, requiring the need for detailed structural and metamorphic analysis to rebuild a more accurate model to fit current knowledge.

The research presented herein represents part of such a metamorphic-structural study of the Wopmay Orogen. The overall goal was to decipher the P-T-t-d history of the Metamorphic

Internal zone of the southern Wopmay Orogen and assess the implications this may have for its tectonic evolution. Points addressed are: 1) The geometric and kinematic evolution of ductile deformation structures, especially foliations, 2) The timing of metamorphic mineral growth relative to foliations, 3) The pressure and temperature conditions that accompanied metamorphic mineral growth, and 4) Absolute age of these metamorphism and deformation.

The study has regional-scale implications for the new orogenic model, and speculates on the nature and importance of Paleoproterozoic belts worldwide. For this study, two areas were chosen to highlight differences and similarities in deformation and metamorphic history in the Metamorphic Internal zone of the southern Wopmay Orogen (Fig. 1.3). The field areas are approximately 250 km to the north-northwest of Yellowknife, and are approximately 40 km apart from one another (Fig. 1.3). The Brown Water Lake area abuts the Archean Slave craton to the southeast (Fig. 1.4). The Little Crapeau Lake area is bordered by the Wopmay Fault zone to the northwest (Fig. 1.5). The Brown Water Lake area was the main focus for study, while Little Crapeau Lake served as a source for structural, metamorphic and chronological comparison.

## 1.1 Wopmay Orogen

The Wopmay Orogen is a Paleoproterozoic orogenic belt that straddles the western margin of the Archean Slave craton in the Northwest Territories, Canada (Fig. 1.2). It is exposed over >500 km in north-south strike length, and is up to 200 km in width. It is overlain by Paleozoic cover to the west. From east to west, the orogen is comprised of several main tectonic elements: the Coronation Margin (~1.92-.188 Ga), the Coronation Supergroup (~1.92 Ga), the Great Bear Magmatic zone (<1.85 Ga), and the Hottah Terrane (>2.0 Ga). The tectonic history and evolution of the orogen is under debate and is currently being remodeled, however the current understanding is that rifting on the western margin of the Slave craton was initiated around

2014.32 ± 0.89 Ma (Hoffman et al., 2011). Following this, a sequence, several hundred kilometres thick, of rift, passive margin and collisional foredeep sediments and rift-related volcanic was deposited on the margin between ca. 2015-1882 Ma (Hildebrand et al., 2010; Hoffman et al., 2011). These sediments comprise the Coronation margin (Fig. 1.2). They are interpreted to represent the sedimentary infill of a rift basin, and it has been proposed that the sediments are derived from an allochthonous source based on detrital zircon ages (Bowring and Grotzinger, 1992). The origin of the sedimentary and plutonic rocks however remains unresolved (Bennett and Rivers, 2006; Bowring and Grotzinger, 1992; Jackson et al., 2013; Lalonde, 1989; St-Onge et al., 1987). A maximum deposition age for these sediments has been given at 1.92 Ga (Bennett and Rivers, 2006).

During the ca. 1885 Calderian orogeny, these rocks were shortened, deformed and translated eastward over the Slave craton (Tirrul, 1982, 1983). Thin-skinned thrusting and folding of the Coronation margin resulted in the formation of the Asiak Thrust and Fold Belt (Fig. 1.1 b, 1.2). The Metamorphic Internal zone is thought to have formed as a result of the closing of the rift basin (King, 1986; Lalonde, 1989). It is uncertain whether and if so, how far the rocks of the Coronation Supergroup were transported during basin closure.

The crustal-scale 1890-1875 Ma Hepburn Intrusive suite (Fig. 1.2 b) intrudes rocks of the MIz and is thought to have been emplaced synchronous with ductile deformation and eastward translation of the Coronation margin (Bowring and Grotzinger, 1992). Related plutons are not found to intrude Archean basement (St-Onge et al., 1984). The post-orogenic Bishop Intrusive suite (Fig. 1.2 b) also intrudes rocks of the MIz, and is synchronous with initiation of magmatism in the Great Bear magmatic zone (Lalonde, 1989).

To the west of the Coronation Supergroup are rocks of the Great Bear Magmatic zone and the Hottah Terrane. The Great Bear magmatic zone is separated from the Metamorphic Internal

zone by the ~500 km long Wopmay Fault zone (Fig. 1.2, 1.3). It is comprised of arc-like volcanic rocks and extensive plutonic rocks that range in age from 1875 to 1850 Ma (Gandhi et al., 2001; Hildebrand et al., 1987; Jackson et al., 2013). The Hottah Terrane is cryptic in nature and origin, and comprises >2000 Ma basement and overlying 2000-1880 Ma plutonic rocks (Jackson et al., 2013).

The present geometry in the southern Metamorphic Internal zone reveals the metasedimentary rocks to be underlain by gneissic culminations of Archean basement, which crop out from under the Paleoproterozoic rocks in several locations (Fig. 1.2, 1.3, 1.4, 1.5; Appendix A Plates 1 & 2). The Exmouth Massif is an example of such an occurrence, where superposed folding events have resulted in the exposure of Archean basement (Fig. 1.3).

## 1.2 Geology of the Metamorphic Internal Zone

Detailed regional mapping projects conducted throughout the Metamorphic Internal zone have allowed many early workers to define the tectonic elements that comprise the Wopmay Orogen. Stratigraphy is defined and described much more extensively in the northern half of the orogen, however, as rocks are better exposed and thicker sections are abundant than in the south. To the south rocks are more ductilely deformed and, alongside structural, geochronological and geochemical studies, extrapolations and correlations have been made to define ambiguous units. Evolutionary models that were based on deformation and metamorphism observed in the north have been used to draw parallels with structures and thermal effects observed in the south (Easton, 1981; Frith, 1990, 1992; Jackson and Ootes, 2012; Nielsen, 1977, 1986; Pehrsson, 2002; St-Onge et al., 1984).

### *1.2.1 Geology of the Northern Metamorphic Internal Zone*

Field work by St-Onge (1981) in and around the Hepburn and Wentzel batholiths described the presence of three "progressive" metamorphic suites in the northern Wopmay orogen. Two of these suites are related to metamorphism associated with the intrusion of the Hepburn batholith, and the third one associated with the Wentzel Batholith. Hepburn-related plutons are dated at ca. 1890 to 1875 Ma, and have fabrics that suggest they are syn-tectonic with the first major shortening event (Jackson et al., 2013; St-Onge, 1984). The isograds mapped around the Hepburn and Wentzel Batholiths in these areas were shown to be both "inverted" and "normal" respectively (St-Onge, 1981). The dip of the isograds is attributed to the funnel-shape of the associated plutons. In the case of the Hepburn Batholith, it is thought that the present exposure represents the floor at approximately 12km depth, while the present exposure of the Wentzel Batholith shows its roof (St-Onge, 1981).

Structures and isograds are 'nicely' exposed in the north because of thermal culminations exposed in oblique section due to cross-folds (St-Onge et al., 1984). Major NE-SW cross folds and minor NNE-SSW antiform/synform pairs throughout the region expose the lower levels of the Asiak Thrust and Fold belt as well as the Archean basement. Hepburn plutons are coincident with the Calderian thermal culmination (St-Onge et al., 1984). No Hepburn intrusions are found to intrude the Coronation margin basement. Three basement-cored fold structures are mapped north of 65°, all of which are reported to preserve no Proterozoic fabrics, except at a regional scale (antiforms and synforms) (Fig. 1.2). One of three basement-cored fold structures exposed at the edge of the Slave craton at 65° N, overlain by rocks of the Coronation Supergroup, is reported to preserve Proterozoic fabric (St-Onge et al., 1984). This schistosity was documented in the Exmouth Massif (Fig. 1.3). St-Onge et al. (1984) report "inverted isograds", increasing in grade away from "cold" basement culminations.

In the northern half of the orogen many large fault and thrusts appear to have formed pre-metamorphic peak, as isograds cross the features but are not offset by them (St-Onge, 1984). The metamorphic isograds are thought to be associated with large, older foliated granites, which may represent older phases of the batholiths (St-Onge, 1981). It was once thought that intrusions associated with the Hepburn Intrusive Suite extend as far south as Arseno and Grant Lakes (Frith, 1990), however it is now known that no associated intrusions exist south of 65°N (Bennett et al., 2012; Jackson and Ootes, 2012). The Rodrigues pluton, an expansive intrusion of largely undeformed k-feldspar porphyritic granite located between Little Crapeau Lake and Brown Water Lake has a U-Pb zircon crystallization ca. 1850 Ma (Jackson et al., 2013).

### *1.2.2 Structure and Conditions of Metamorphism*

Conditions of metamorphism were studied at Hepburn Lake (St-Onge, 1981), approximately 200 km north of the area studied in this project. Having documented the reaction quartz + plagioclase + biotite + sillimanite ↔ garnet + cordierite + orthoclase + melt, the author calculated metamorphic P-T conditions around 440°C (chlorite zone) up to 727°C and 2.2-3.8 kbars. Garnet-biotite thermobarometry indicates that higher temperatures up to 560-765°C may have affected the rocks of the passive margin (St-Onge, 1984). Additionally, the pressure culmination has been estimated at 2.6-5.2 kbars using the solid-solid reaction plagioclase ↔ grossular + aluminosilicate + quartz (St-Onge, 1984). Further studies by St-Onge (1986) looking at PT paths through zoned poikiloblastic garnets through a 30 km composite transect of crust outline paths consistent with loading, uplift and erosion in "overthrust" terrains, with an average uplift rate of 1.5-2.7 mm/year. Variability in uplift rates throughout the area can be attributed to the cross-folding event noted in the northern part of the orogen (St-Onge, 1986).

In their 1987 description of a "rapidly evolving" thermo-tectonic regime, St-Onge and King (1987) describe crustal stretching and thinning, inducing the first 'stage' of metamorphism

which generated a High-T Low-P mineral assemblage. Approximately 5-10 My after stretching, and after deposition of west-facing sedimentary prism around 1.9-1.885 Ga, emplacement of a suite of plutons ca. 1896-1878 Ma occurred and was followed by subhorizontal shortening during the Calderian Orogeny. Plutons also intrude thrusted and folded syn-orogenic foredeep sedimentary rocks (St-Onge et al., 1987).

The 1st stage of metamorphism is attributed to crustal thinning and heating. The 2nd stage of metamorphism is recorded in high and intermediate structural levels in the form of syn-tectonic metamorphic mineral growths that are "spatially related" to the plutons. The 3rd stage is related to uplift and erosion of thickened and transported crust, recorded in P-T paths of post-tectonic garnets.

Hildebrand et al. (1990) mapped rocks of the Wopmay Fault zone east of Wopmay Lake (Fig. 1.3). Low-grade assemblages of metasedimentary rocks were observed here, including quartz arenite, semipelite and dolomite-argillite rhythmite, intruded by gabbro sills. They observed that most fold axes and mineral lineations in rocks in the vicinity of the Wopmay Fault zone displayed a moderate northward plunge, and dated these northerly-striking folds at 1843 Ma (Hildebrand et al., 1990). These folds postdate Great Bear magmatism, as cross-folding affects these rocks. It is thought that northwesterly-striking folds that rotate into northerly-striking folds along the fault zone are a result of strong strike-slip motion and dextral transpression during the collision of Hottah Terrane with the Slave Craton (Hildebrand et al., 1990). Northerly-striking folds in the Wopmay Lake area are re-folded by easterly-striking cross-folds (Hildebrand et al., 1990).

## 1.3 Geology of the Southern Metamorphic Internal Zone

The Southern Metamorphic Internal zone is not as well understood in the literature, due to its poor exposure and disputed stratigraphic correlations. The areas encompassing Brown Water Lake and Little Crapeau Lake have been mapped and studied by Easton (1981), Frith (1990, 1992), Nielsen (1977, 1986) and Pehrsson (2002), while extensive new mapping initiatives are underway, led by Jackson and Ootes at the NTGO (Jackson et al., 2013).

Easton (1981) mapped the geology around the Grant Lake and Four Corners Lake areas at 1:50,000 scale, and described isograds at both Grant and Little Crapeau Lakes. He attributes metamorphism of the region's Akaitcho sediments to intrusions of Hepburn and Wentzel batholiths (Easton, 1981).

### *1.3.1 Lithology, Structure and Metamorphism*

Frith (1990, 1992) produced two maps in the vicinity of Brown Water Lake. A 1:50,000 scale map at Arseno Lake placed emphasis on the structure and metamorphism around the area's Archean gneiss domes, and another at 1:125,000 scale focussed mainly on the western margin of the Slave structural Province near Indin Lake, approximately 45 km southeast of Brown Water Lake. Metasedimentary rocks at Arseno Lake were subdivided into porphyroblastic to migmatitic schist, paragneiss and migmatite, and rusty coloured subgreywacke, arkosic, sandstone, mudstone, dolomite and calc-silicate rocks (Frith, 1990). Mapping and geochronological work also confirmed the presence of the Archean cored gneiss domes throughout the map area, mantled by migmatitic paragneiss (Frith, 1974; Frith et al., 1977). For the most part, metasediments in the map area were not specifically recognized as belonging to the Proterozoic Snare Group or the 2.67 Ga Yellowknife Supergroup, as Rb-Sr whole rock isochron studies remained ambiguous (Frith, 1990; Frith and Loveridge, 1982; Nielsen, 1977).

Metamorphic isograds were documented as increasing westward, away from the Slave craton, from sub-biotite to above cordierite-garnet grade (Frith, 1990). Migmatitic banding, deformed by up to three phases of deformation, is preserved in paragneiss above the sillimanite isograd. These show thickening and thinning of compositional differences in original bedding owing to metamorphic segregation (Frith, 1990). In total, two phases of ductile deformation and two phases of brittle deformation were recognized in the area as a result of the Calderian Orogeny (Frith, 1990). The first two phases caused east-west shortening, subsequent thickening of the sedimentary prism, as well as large scale undulations which exposed various levels of the crust. The last two phases resulted in large scale dextral transpressive faulting and conjugate fault sets that crosscut local intrusions and the Slave Province, alike (Frith, 1990).

Nielsen (1977, 1986) mapped metamorphic mineral assemblages and isograds in the Proterozoic metasediments at Arseno Lake and described Abukuma facies type metamorphism. He defined six isograds with the first appearance of the following minerals: biotite; andalusite; cordierite (muscovite + chlorite out); sillimanite (andalusite out); sillimanite + K-feldspar (muscovite + quartz out); and almandine + K-feldspar ± cordierite (biotite + sillimanite + quartz out) (Nielsen, 1986). Nielsen distinguished between "remobilized Archean paragneiss" and Proterozoic sediments in the Arseno Lake area on the basis of distinguishing characteristics such as polymetamorphism, presence of high P-T relic grains, and Rb/Sr whole rock data which indicated an age of >2100 Ma for some rocks (Nielsen, 1977). Nielsen (1977) and McGlynn and Ross (1963) also noted that rocks to the east of the cordierite isograd are deformed by tight, upright, westerly-dipping $D_1$ folds trending 020°. A second deformation event, $D_2$, overprints these upright folds with gentle, open folds that trend 080°. The authors attribute porphyroblast growth on axial planar structures to the "penetrative nature" of the $D_1$ deformation (Nielsen, 1977).

### *1.3.2 Relevant Regional Geochronological Data*

As part of the larger South Wopmay mapping initiative conducted by the NTGO, a large amount of geochronological data was gathered over a period of a decade to help develop an understanding of the orogen's history (Jackson et al., 2013). Relevant to this study are the following U-Pb zircon crystallization dates (see Fig. 1.3 for selected sample locations; also see Jackson et al., 2013 for all sample locations):

1) Hepburn suite aged intrusions:

    Little Crapeau Sill (dated for this study): 1877 ± 2 Ma

2) Post-Hepburn aged intrusions:

    Deformed Zinto suite: 1867.4 ± 1 Ma

    Rebesca Lake granodiorite: 1867.7 ± 0.9 Ma

    Exmouth granodiorite: 1865.9 ± 0.8 Ma

    Blocky granite: 1862.83 ± 0.58 Ma

3) Bishop suite aged intrusions and/or post-orogenic/Great Bear magmatism age:

    Rodrigues pluton: 1849.4 ± 1.4 Ma to 1851.8 ± 3.2 Ma

    Black Lichen: 1856.78 ± 0.95 Ma

    Peri Granite: 1858 ± 4.3 Ma

While intrusions of groups 1) and 3) fall within the previously known age brackets of orogen-scale Hepburn and Bishop intrusive suites, rocks of group 2) fall somewhere in between. This indicates a separate phase of crustal heat circulation associated with a suite of intrusions that were previously unrecognized. Discussion about this is found in section 5.4.6.

## 1.4 Map Areas for this Study

The southern Metamorphic Internal zone is the focus of this study (Fig. 1.3). This area has been previously studied (Easton, 1981; Frith, 1990; Hoffman and Hall, 1993; Nielsen, 1977; Pehrsson, 2002), however new mapping and geochronological data resulting from renewed study of the orogen require further investigation to reassess the kinetic and metamorphic history of the rocks.

Two map areas were chosen to perform this investigation for this project: the Brown Water Lake area, located on NTS map sheet 086B12, and the Little Crapeau Lake area, covering sheets 086C15 and 086C16 (Fig. 1.3, 1.4, 1.5; Appendix A Plates 1 & 2). These two areas sit within the 1:150,000 scale mapping project by the Northwest Territories Geoscience Office (Fig. 1.1 c). In both areas the Paleoproterozoic metasedimentary rocks were the focus of mapping. They are sequences of multiply deformed and metamorphosed pelitic schist, semi-pelitic schist, and pelitic gneiss. They are intruded by intrusions of various ages, and overlie parautochthonous Archean basement.

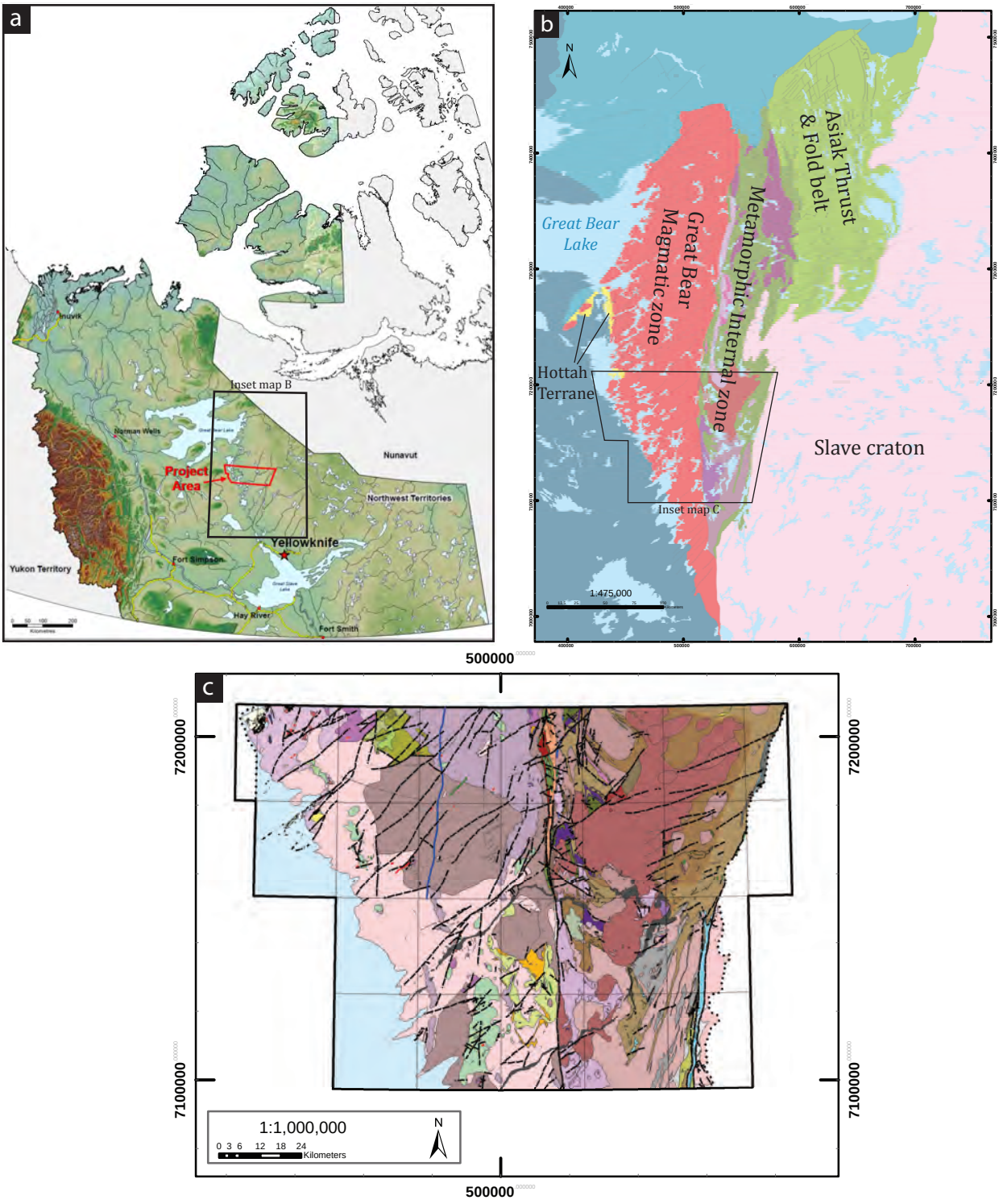


**Figure 1.1 Maps showing locations of study areas. a)** Physiographic relief map of the Northwest Territories. Red outline shows project area for the Northwest Territories Geoscience Office (NTGO) South Wopmay Phase II mapping initiative. Project area is approximately 240 km NNW of the town of Yellowknife, NT. **b)** Tectonic setting and elements of the Wopmay Orogen, west of the Archean Slave Craton. The main elements of the Wopmay Orogen are the Asiak Thrust and Fold belt (or Coronation margin), Metamorphic Internal zone (or Coronation supergroup), Great Bear magmatic zone, and Hottah Terrane. These are lie on the western margin of the Slave craton . NTGO map area is outlined by solid black line. **c)** Map produced by the NTGO Phase I and II mapping project (Jackson and Ootes, 2012). Map area is bisected by the Wopmay Fault zone, a an extensive north-south ductile and brittle fault. All maps modified from Jackson and Ootes, 2012.

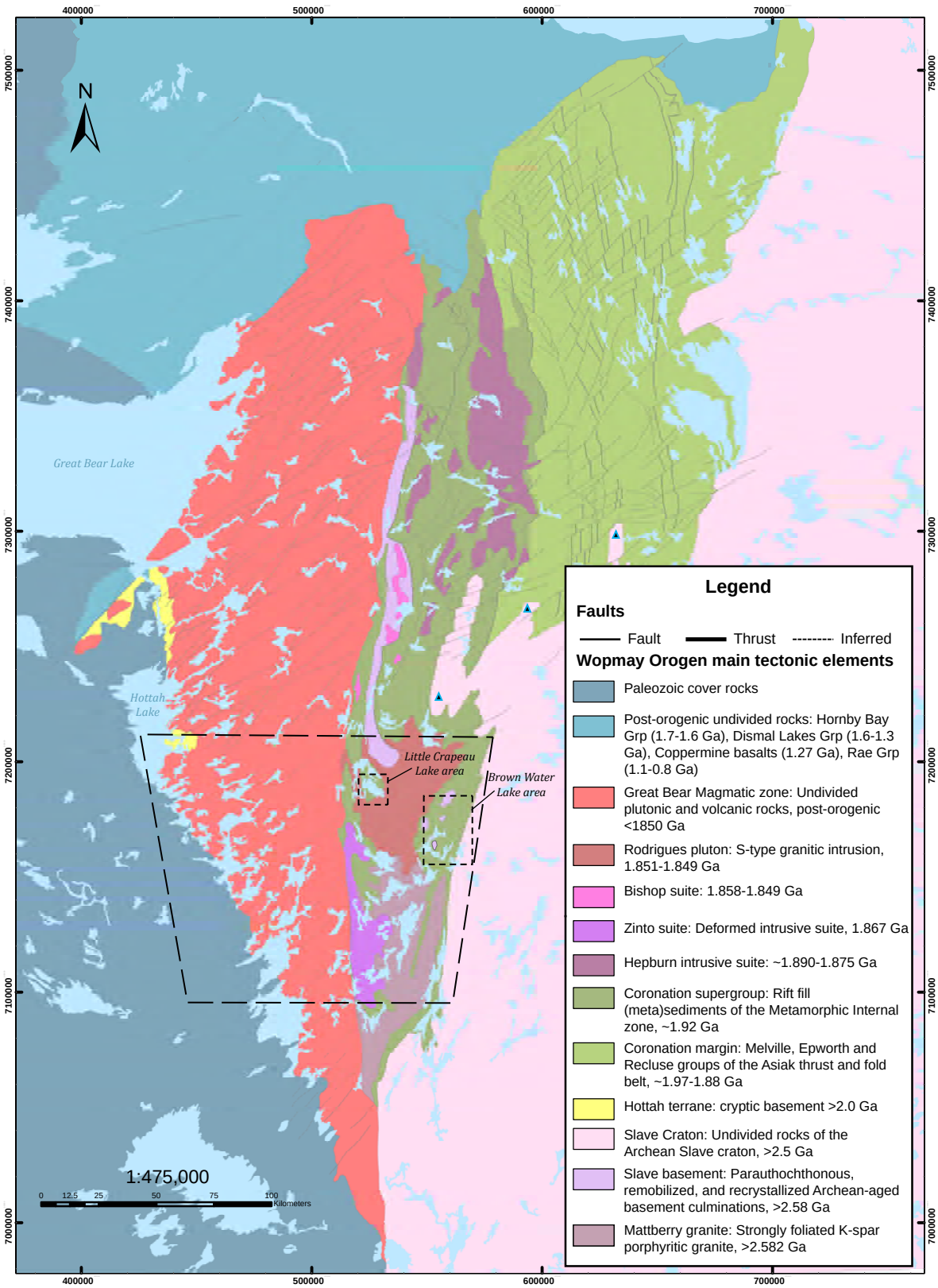


**Figure 1.2 Main tectonic elements of the Wopmay Orogen.** Simplified geology of the Wopmay Orogen, with project areas marked in dashed lines: NTGO Phase I & II mapping (long dashed lines), and two inset map areas for this study (short dashed lines) within the Metamorphic Internal zone of the Coronation Supergroup. The Wopmay Fault zone stretches for over 500 km north to south, and divides the Coronation Supergroup from the Great Bear Magmatic zone. Blue triangles show locations of three basement-cored fold structures. Modified from Cook (2011) and Jackson and Ootes (2012).

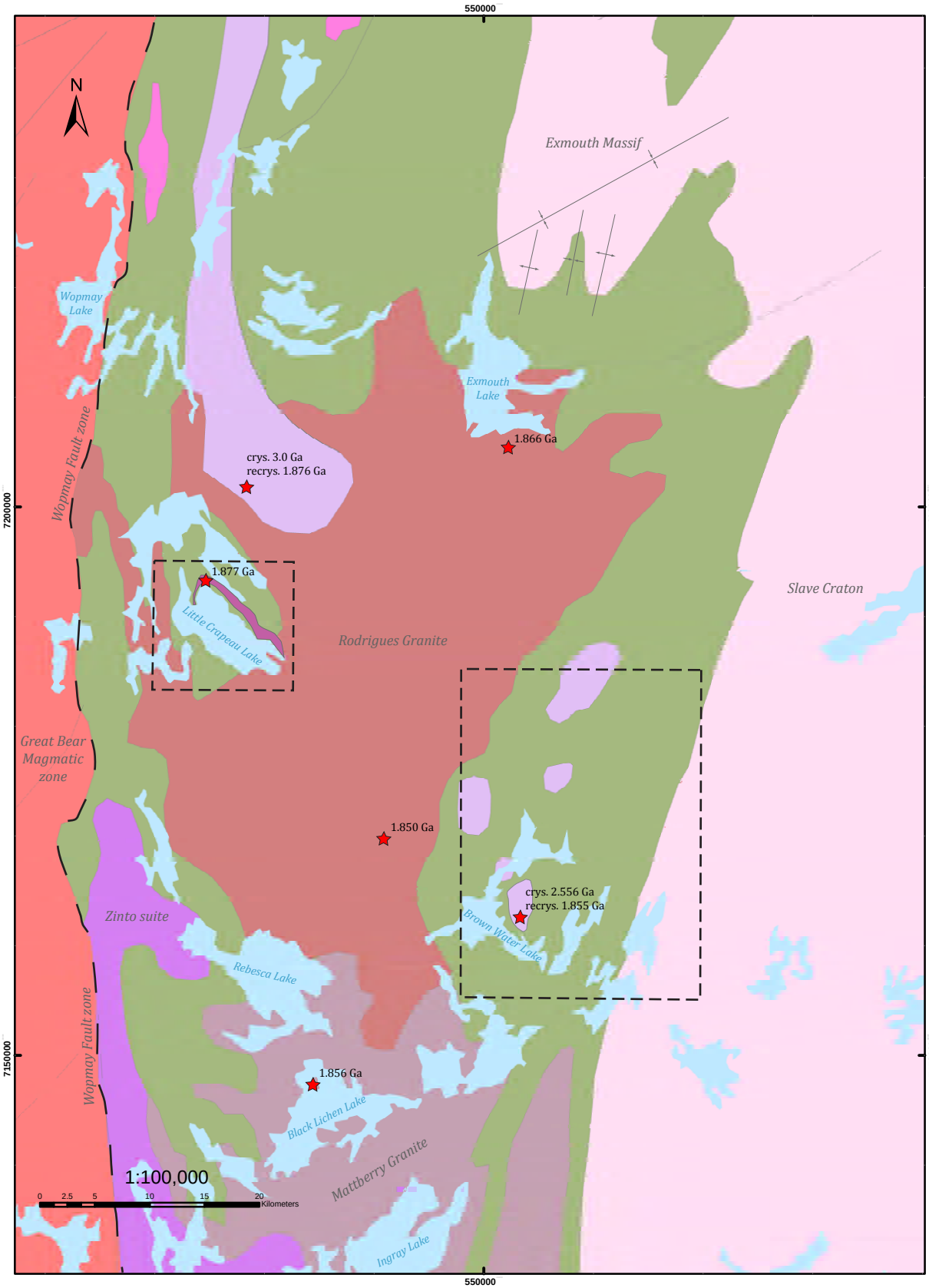


**Figure 1.3 Simplified geology of the Metamorphic Internal zone of the Southern Wopmay orogen with regional intrusive ages.** Generalized geology showing mapping areas for this sutdy. Locations of relevant intrusive age data are shown as red stars (without errors). These samples were collected, analysed and interpreted by the NTGO (Jackson et al., 2013). Not included are the locations of the Deformed Zinto suite, the Blocky granite, and Peri granite, which plot south of Ingray Lake. Modified from St-Onge et al. (1984), Cook (2011), and Jackson and Ootes (2012).

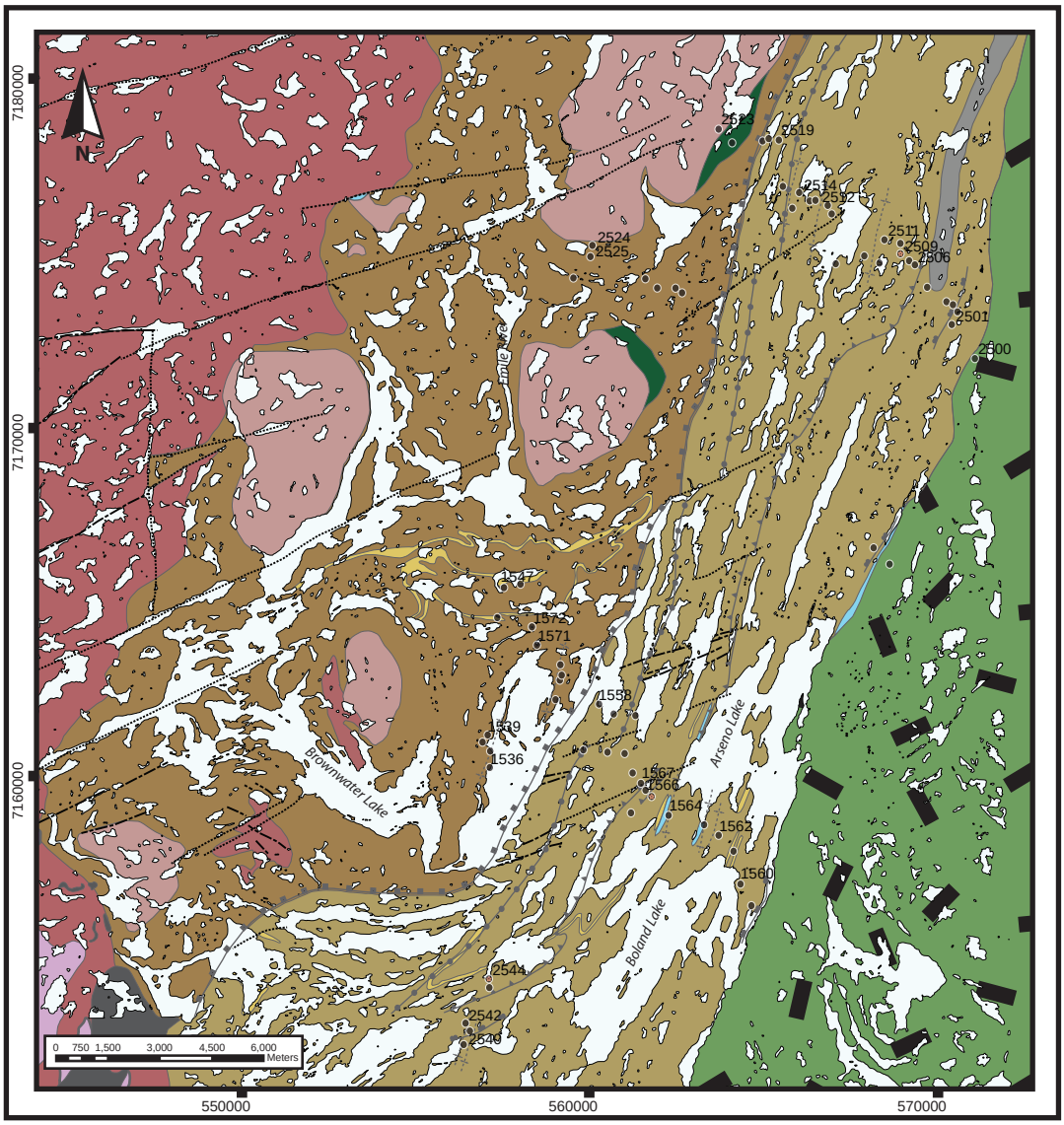


## Legend

**Lithologies**

PROTEROZOIC

- Hottah dykes and sills (ca. 780 Ma): brown-black diabase sills and dykes
- Rodrigues granite (ca. 1850 Ma): homogenous granitic body, k-feldspar megacrystic peraluminous S-type granite.
- Diorite to gabbro
- Pelitic schists of the Coronation margin (undifferentiated): Fine to medium grained, brown to rusty weathered, laminated to bedded, and stronlgy foliated. Peak metamorphic assemblage is biotite + muscovite + cordierite + andalusite ± garnet ± fibrolite
- Pelitic gneisses of the Coronation margin: Coarse grained, rusty weathered, migmatitic with melt pods. Metamorphic assemblages are k-spar + sillimanite + andalusite + cordierite ± garnet ± melt ± corundum bearing.
- Quartzite/Quartz pebble conglomerate: Coarse grained, white to gray quartzite in ~50cm thick beds. Quartz pebble conglomerate comprises pebble to cobble sized clasts in a white/gray to brown arenite matrix
- Carbonate rocks. Marbles and calc-silicates are white to gray, massive to layered and foliated.

ARCHEAN

- Biotite phyllite to schist
- Amphibolite: Dark green to brown and black, coarse grained foliated amphibolite with ~50cm thick bands of interlayered white granitic melt.
- Gneiss and migmatite (ca. 2580 to >2900 Ma): Gneissic and migmatitic Archean culmination, includes metasedimentary phases and disaggregated metamafic dykes
- Slave craton: undifferentiated units

2512
2509

Select station locations and number (shortened from "09ls1537" or "10ls2512")

Station location with star indicating the first appearance of garnet, going up metamorphic grade

1)
2)
3)
4)
5)

**Metamorphic Mineral zones** (mark on the high T side of line):
1) biotite zone (chlorite out);
2) cordierite zone;
3) andalusite±cordierite zone;
4) sillimanite zone
5) melt-in/gneiss zone

Lineament

Fault, inferred

Trace of axial plane of major antiform or synform

**Figure 1.4** Geology of Brown Water Lake

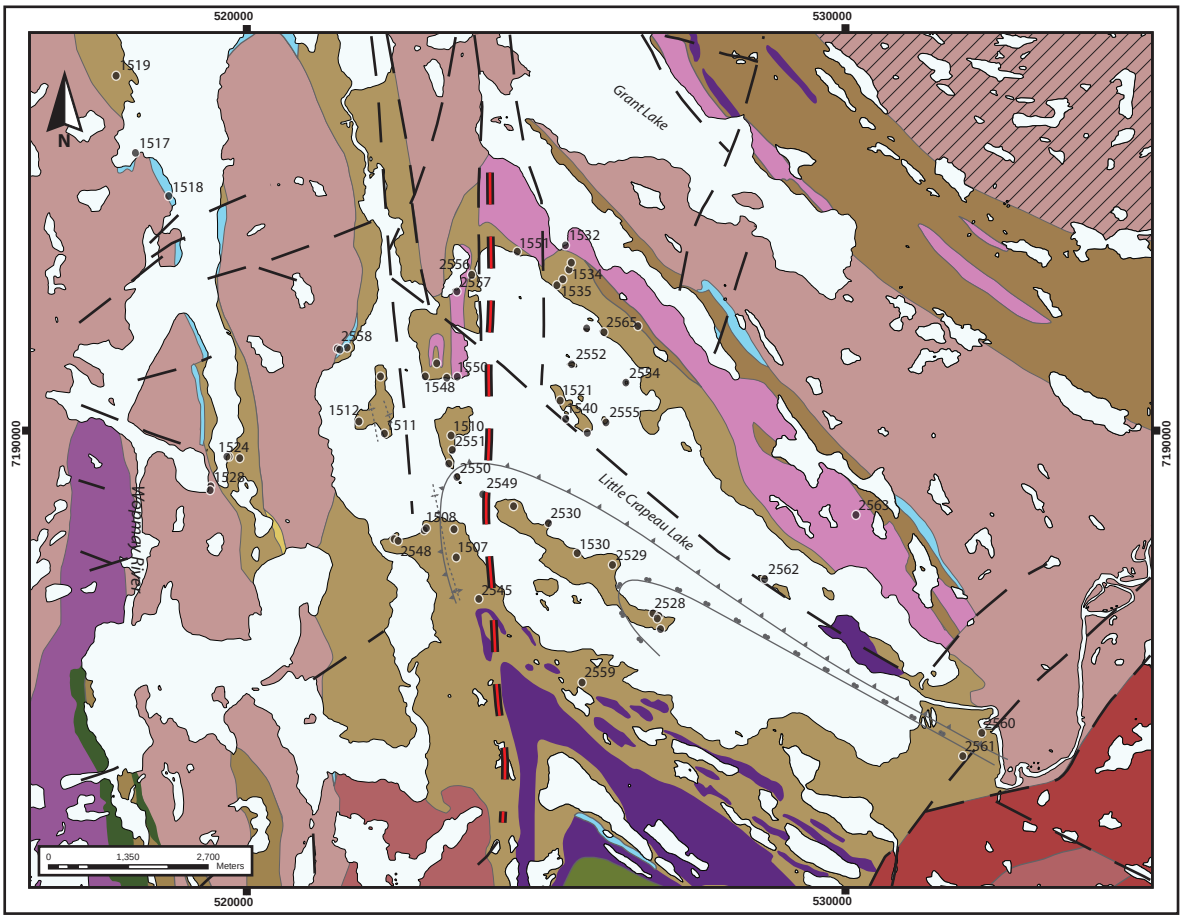


## Legend

**Lithologies**

PROTEROZOIC

- Rodrigues granite (ca. 1850-1857 Ma): pink to white, coarse grained, homogenous granitic body, k-feldspar megacrystic, peraluminous S-type granite.
- Undivided granite to granodiorite: Uncertain relationship to Rodrigues granite
- Little Crapeau Sill: Biotite muscovite ± garnet granite (ca. 1878 Ma): Medium to fine grained white to gray granite, massive to strongly foliated. Forms sills ~30 cm thick and veinlets.
- Granodiorite to diorite
- Diorite to gabrro
- Basalt to andesite: Pillowed and massive flows
- Pelitic schists of the Coronation margin (undifferentiated): Fine to medium grained, brown to rusty weathered, laminated to bedded, and stronlgy foliated. Peak metamorphic assemblage is biotite + muscovite + cordierite + andalusite ± garnet ± fibrolite
- Pelitic gneisses of the Coronation margin (undifferentiated): Coarse grained, rusty weathered, migmatitic with melt pods. Metamorphic assemblages are k-spar + sillimanite + andalusite + cordierite ± garnet ± melt
- Quartzite/Quartz pebble conglomerate: Coarse grained, white to gray quartzite in ~50cm thick beds. Quartz pebble conglomerate comprises pebble to cobble sized clasts in a white/gray to brown arenite matrix
- Carbonate rocks. Marbles and calc-silicates are white to gray, massive to layered and foliated.

ARCHEAN

- Amphibolite: Massive to banded and foliated
- Gneiss and migmatite (ca. 2580 to >2900 Ma): Gneissic and migmatitic Archean culmination, includes metasedimentary phases and disaggregated metamafic dykes
- Mesoarchean granite-gneiss (>2900 Ma): Similar to Archean gneiss and migmatite with abundant disaggregated and recrystallized mafic dykes

Fault, inferred

Trace of axial plane of major antiform or synform

Line bisecting western structural domain from eastern structural domain

1)
2)

**Metamorphic Mineral zones** (mark on the high T side of line):
1) biotite zone (chlorite out);
2) andalusite±cordierite zone

**Figure 1.5** Geology of Little Crapeau Lake area

# 2 RESEARCH PLAN & METHODS

The rocks of the Metamorphic Internal zone in the northern part of the Wopmay Orogen have been very well studied (Hoffman, 1984; King, 1985). Rocks in the southern half of the orogen, south of 65°, have been less well studied as they are not as well exposed. The focus of this study is to constrain the P-T-t-d path for the rocks of the southern MIz by comparing two contrasting locations that are geologically and metamorphically similar, yet preserve a different structural history. The metasedimentary rocks at Brown Water Lake are the main focus of the study, while the metasedimentary rocks at Little Crapeau Lake serve as a source of comparison in terms of structural geometry, kinematics, and absolute timing of deformation and metamorphism.

## 2.1 Field Data Collection

The Brown Water Lake and Little Crapeau Lake areas were mapped along several traverses that cross structural grain and previously mapped isograds (Fig. 1.4, 1.5; Appendix A Plates 1 & 2). The goal of each traverse was to document and examine progressive metamorphic mineral assemblages, as well as to observe macroscopic structural features and to collect structural data. Orthophotos and regional magnetic survey data were used to aid in structural interpretation. One or more oriented samples were collected at every outcrop so that additional structural information could be collected from the rocks. These rocks were re-oriented in the lab, using a plastic wash basin filled with clean quartz sand.

Structural data collected in the field can be found in Appendix B. All sample and station numbers mentioned within the text can be found on the maps in Plates 1 & 2 (Appendix A). In Figures 1.4 and 1.5 only select stations locations are shown.

## 2.2 Structural and Metamorphic Analysis

Oriented thin sections were cut from hand samples to obtain sections that emphasize the relationship between early, main and late-stage fabrics. A petrographic microscope was used for detailed microstructural analysis, and stereographic analysis was carried out by hand and using the stereonet plotting program GEOrient (Holcombe, 2011). For all measurements of straight and curved inclusion trails in porphyroblasts, non-rotation during formation was assumed (Bell et al., 1992).

Cross-sections were constructed from lines drawn across these transects at a high angle to the strongest deformation and steepest fabric (e.g. $S_{4B}$ at Brown Water Lake). Stereonet analysis of structural data was employed to pick out fold patterns from fabric measurements taken from outcrop and from hand samples in the lab. Structural nomenclature for lineations and fold axes was applied following the methods of Bell and Duncan (Bell and Duncan, 1978). Structural fabrics and deformational events were labeled with a subscript 'B' for Brown Water Lake and with a 'C' for Little Crapeau Lake, i.e. $S_{4B}$. Metamorphic analysis was also performed using the petrographic microscope to determine metamorphic mineral paragenesis. Peak metamorphic mineral assemblages were evaluated both in the field and petrographically to determine metamorphic grade and to assess to pressure-temperature conditions.

## 2.3 Whole Rock and Mineral Geochemistry

Whole rock geochemistry was performed with the purpose of determining the range of compositions among pelitic schists and gneisses in both study areas, and in particular to check for major lithological differences within sedimentary packages. The analysis also aimed to reveal more subtle variations in Mg and Fe that would explain differences in metamorphic mineral assemblages between similar looking rocks.

All rock samples were prepared by cutting hand samples in half and removing intensely weathered surfaces and organic material from the rocks. One half was kept, and the other half was photographed and sent to ALS Minerals Laboratories for whole rock lithium borate fusion major element lithogeochemical analysis using XRF. In total, 30 samples were sent for analysis, including two duplicate samples. From Brown Water Lake, 21 samples were submitted in total. Of these, 13 were low grade, biotite, cordierite or andalusite zone pelitic schists, and 8 were gneissic, sillimanite zone rocks. From Little Crapeau Lake, 7 representative samples were selected, all pelitic schists from the biotite, cordierite and andalusite zones. A list of these samples and the results can be found in Appendix C. In the lab, standard drying and fine crushing preparation methods were applied to analyse a pulverized split of 70% material less than 2 mm diameter. Results were returned in weight percent oxides for major elements.

Metamorphic and rock forming minerals from seven samples were analysed on the electron microprobe at the University of British Columbia. Results are tabulated in Appendix D. Selected uncovered, polished thin sections were carbon coated, and individual porphyroblasts were imaged on the scanning electron microprobe (SEM) at UBC. Priority was given to samples that contained metamorphic mineral assemblages that are representative of each metamorphic zone. Minerals analysed include: biotite, muscovite, cordierite, garnet, plagioclase, potassium feldspar and ilmenite for major element chemistry. Mineral abbreviations used herein are listed in Appendix F.

Special note was taken of the variation of Mg/Fe and Na/Ca in metamorphic minerals, particularly cordierite and plagioclase respectively. Garnet composition was also probed for Fe, Mg, Mn and Ca content.

The data were manipulated according to calculations by Vilà et al. (2007) to adjust for A, F, M values which were needed to plot AFM diagrams. Data analysis was performed by plotting

calculated values for various elements (Mg, Fe, Al, Ca, Mn) on AFM and AKF triangular plots, and by plotting calculated element indices on scatter plots using the geochemical plotting software ioGas.

## 2.4 Pressure-Temperature Determinations

To estimate P-T conditions of metamorphism at Brown Water and Little Crapeau Lakes, the software package Perple_X was used to model P-T pseudosections. Perple_X is open-sourced software designed to calculate and graphically display phase diagrams using geochemical data to pin metamorphic reactions to pressure and temperature conditions particular to each rock (Connolly and Petrini, 2002).

In addition, using the whole rock and mineral geochemistry datasets rock compositions were plotted on published P-T diagrams for the six component ideal system KFMASH to constrain metamorphic conditions (Pattison et al., 2002).

## 2.5 Geochronological Studies

To determine the age of metamorphic events within the two areas, in-situ dating of metamorphic monazite was carried out using of two geochronological methods: U-Th chemical dating on a microprobe at the University of Massachusetts at Amherst, and by U-Pb dating on the SHRIMP at the Geological Survey of Canada in Ottawa. Additional U-Pb zircon ages were obtained from granitic dykes that crosscut structure and lithology of the Little Crapeau Lake area and were also analysed at the Geological Survey of Canada in Ottawa by ID-TIMS. Further discussion of methods can be found in section 5.4. Age calculations for U-Th chemical dating were performed using Isoplot, a Microsoft Excel add-on, and are provided in Appendix E.

# 3 BROWN WATER LAKE

The Brown Water Lake area is located approximately 75 km south of the Exmouth Massif (Fig. 1.3, 1.4; Appendix A Plate 1). The Paleoproterozoic supracrustal rocks in the Brown Water Lake area (and neighbouring Arseno Lake) are classified as Snare Group sediments by previous workers, however owing to a regional reclassification of sedimentary units, they will be considered part of the broader Coronation Supergroup. They form a highly strained, poly-deformed and metamorphosed belt of interbedded pelites, semi-pelites, calc-silicate rocks, and minor amphibolite, with cross-cutting mafic and felsic dykes. The sedimentary rocks abut the Slave structural province to the east. The area also includes Archean gneissic domes (culminations) that crop out from under the Paleoproterozoic cover. They are interpreted to be exposed as a result of regional-scale cross-folds (King et al., 1987). The regionally extensive Rodrigues granite spans a large area to the west and is thought to be a sill-shaped body that intrudes and is structurally emplaced on top of the supracrustal rocks. This area was previously mapped and described by McGlynn and Ross (1963), Nielsen (1977), King (1985), and Frith (1990). Five traverses across strike of the dominant deformation fabric were completed to gather structural and metamorphic data from the supracrustal rocks in the Brown Water Lake area.

## 3.1 Lithological Units

### *3.1.1 Pelitic to Semi-pelitic Schists*

The majority of rocks in this study area are pelitic to semi-pelitic schists (Fig. 3.1, 3.2). Metamorphic grade increases laterally westward and northward, toward the locally expansive Rodrigues granite (Fig. 1.3, 1.4). A total of four metamorphic zones are recognized in the area: biotite zone; cordierite zone; andalusite zone; and sillimanite zone.

The rocks of lowest metamorphic grade are biotite zone schists located at the Archean Slave craton boundary to the east. These rocks are grey to rusty brown weathered, thinly to thickly bedded (0.5-10 cm), strongly foliated and folded slates to biotite schists (Fig 3.3, 3.4, 3.5). The typical mineral assemblage for these low grade rocks is: qtz + plg + bt ± ms ± late chl ± organic components. Porphyroblast mineralogy is controlled by the sandy versus muddy character of primary sediments. In rocks sampled for whole rock major element geochemistry, $SiO_2$ varies from 46-71 wt % (Appendix C). Interbedded with the pelitic schists are minor units of metamorphosed quartz sandstone and polymictic conglomerate (Fig 3.6). A single occurrence of the metaconglomerate is noted within 2 km of the Archean gneiss domes. It has been proposed that this unit overlies a basal conglomerate which represents an unconformity (Jackson et al., 2013).

Slates and biotite schist grade upwards to biotite porphyroblastic schist. Biotite porphyroblasts are visible in outcrop, are <1 mm in diameter, and comprise ~15-20% of the rock. In thin section, the porphyroblasts are dispersed in a matrix of very fine grained, foliated quartz and biotite. In its surface expression the biotite zone is up to 4 km wide, at which point the cordierite zone occurs.

Cordierite zone pelitic schists are defined by the first appearance of porphyroblastic cordierite. In outcrop porphyroblasts are 0.5-1 cm, white to gray, and oval shaped in brown to gray weathered, strongly foliated biotite schist. The dominant mineral assemblage is: quartz + plagioclase + biotite (biotite folia and biotite porphyroblasts) + muscovite (Fig. 3.7, 3.8). Cordierite is widely pinnitized, and is often evident only as recessed pits in outcrop. In thin section, porphyroblasts are colourless to yellow-orange and are often replaced by very fine grained muscovite + chlorite, which preserve early fabrics. Cordierite porphyroblasts overgrow

and include biotite porphyroblasts. The cordierite zone is <500 m wide in the high strain belt, and up to 1.5 km wide to the south where the sedimentary prism is less deformed.

The andalusite zone is defined by the first appearance of andalusite which occurs as small rims on cordierite initially, and then as large anhedral porphyroblasts approaching the sillimanite zone (Fig. 3.7, 3.8). In outcrop, andalusite is white to pink, anhedral knots, ~1 cm and often elongate in the plane of the dominant foliation, $S_{4B}$ (Fig. 3.9).

The biotite, cordierite and andalusite schists show very little chemically diversity (Fig. 3.1, 3.2). They are iron-rich, low-aluminum pelites. Ca-index ranges from 11-59% (Appendix C). There is a direct correlation between Fe-content and Ca-index (Fig. 3.2). Where rocks are highest in iron, they are also highest in calcium. Manganese index values are overall low (<2% MnO), with garnet-bearing schists having the highest values, up to 8% (Fig. 3.2).

### *3.1.2 Garnet Schists*

Garnet schists are rare in the sequence, and are usually interbedded with cordierite zone schists. The typical mineral assemblage of garnet schist is: Qtz + Plg + Bt + Grt ± Crd ± Ilm. Garnet porphyroblasts are 1-5 mm, often preserving inclusion trails (Qtz + Plg ± Chl) showing early fabric orientations. Garnets are sub- to anhedral, comprise 5-15% of the rock, and sit in a matrix of strongly foliated biotite and ~50% quartz. Small stubby to long need-like ilmenite can be found as inclusions within garnets and in the matrix.

Sample 2512A from the high strain zone adjacent to the Archean craton shows two distinct generations of garnet growth (Fig. 3.10). See section 3.3 for a full description of this sample, microstructural analysis and timing of growth.

Garnet-bearing schists plot near or within the low-aluminum pelite classification (Fig. 3.1). In classic pelites, the garnet isograd is largely controlled by the MnO + CaO content (Spear, 1993).

The garnet-bearing schists of the Brown Water Lake area are high-iron/low-magnesium rocks, typically having a high Mn/Ca ratio, and in some samples both Mn and Ca indices are high (Fig. 3.2; Appendix C).

### *3.1.3 Coticule Rocks*

In some pelitic units garnet growth appears to be especially compositionally controlled, as some biotite, cordierite and andalusite zone schists contain distinct garnet-bearing layers (or interbeds) (Fig. 3.11). Garnet-quartz-rich layers, thought to be coticules (Kramm, 1976), appear at intervals, and are very distinctive. Layers are bedding parallel, 0.5-2 cm thick, pink to white, and toothpaste-like, interbedded with fine grained schist. These layers consist solely of garnet, quartz, and minor biotite (~15%). Garnets are anhedral, <0.5 mm, and preserve inclusion trails defined by quartz. These coticule layers are very competent compared to the surrounding host rock. They show complex fold patterns, often buckling where the host pelite has folded passively or dissolved, and have been observed to fold ptygmatically and into sheath folds. They are only documented in 4 outcrops throughout the Brown Water traverses.

The origin of these is unknown, although it has been proposed in other localities that they may represent the metamorphosed equivalents of manganese-rich clayey to muddy sediments associated with submarine volcanism or a distal volcanic-exhalative source (Lamens et al., 1986).

Whole-rock major element geochemistry shows the coticules to be more manganiferous and calcic in composition compared to other rocks from the area (Fig. 3.1, 3.2, Appendix C).

### *3.1.4 Calc-silicates, Marbles*

Rare, massive to weakly foliated marble and calc-silicate units are interbedded with the biotite schist (Fig. 3.6, 3.12). They are usually located stratigraphically near each other along with interbedded quartzite.

Near the andalusite zone, rare calc-silicate interbeds occur more frequently and are boudinaged within the schist, parallel to the bedding plane (Fig. 3.12), and are folded on the outcrop scale. Calc-silicate boudins are white to rusty brown, ~30 cm long, and are rimmed with an amphibole-garnet-rich rind. The amphibole is aligned in the axial planar foliation, either $S_{2B}$ or $S_{4B}$.

### *3.1.5 Gneissic Rocks*

The sillimanite zone appears 6 km to the west of the Slave craton. Initially, porphyroblasts are white fibrolite bunches, about 5-10 mm, and appear aligned in the main SSW-striking foliation (Fig. 3.4 f). The melt-in zone occurs within ~1 km of the sillimanite zone, and results in significant coarsening of minerals and the formation of leucocratic pods of melted material, located within the metasedimentary rocks and around coarser porphyroblasts (Fig. 3.13, 3.14). Coarser pelites contain clear blue cordierite porphyroblasts, coarse white fibrous knots of sillimanite, and pink matrix garnets with quartz and plagioclase haloes (Fig. 3.15). Closer to the Archean gneiss domes and the locally expansive Rodrigues granite, rafts of deformed and undeformed metasedimentary bedding 'float' in paragneiss, orthogneiss and banded amphibolite that mantles/surrounds the domes (Fig. 3.13). At outcrop 1547 ~5 cm-long euhedral, tabular, bladed to fibrous porphyroblasts appear to be sillimanite pseudomorphed after kynanite (Fig. 3.14). This would indicate a higher pressure regime affecting the rocks in this area. The same rock also contains smaller, white, fibrous sillimanite porphyroblasts.

Between the Archean gneiss domes, migmatized metasediments preserve generations of fabrics differently than in the high strain belt to the east. Perhaps due to a buttressing effect of the domes, the rocks between the domes were not overprinted by the strong SSW $S_4$ foliation that dominates the pelites directly to the east. Instead they preserve a strong migmatitic fabric, representing/parallel to original bedding, and a SE-NW crenulation (in some cases strongly axial planar) interpreted as $S_{3B}$ (Fig. 3.16).

### *3.1.6 Intrusive Rocks*

The Rodrigues granite is a locally expansive, homogenous granitic body that intrudes and overlies rocks of the Brown Water Lake area. It is a coarse, k-feldspar megacrystic peraluminous S-type granite covering a large area to the west and northwest of the study area (Jackson et al., 2013). The Rodrigues granite yielded a U-Pb zircon crystallization age between 1851.8 ± 3.2 Ma and 1849.4 ± 1.4 Ma (Jackson et al., 2013). The cliff-like contact often observed between the Rodrigues granite and the migmatized pelites reveals the nature of the contact; the granite is structurally emplaced on top of the pelites rather than doming or cropping out from underneath them (Fig. 3.15 e). At the contact between the metasediments and the granite, rock are strongly melted, recrystallized and migmatized.

### *3.1.7 Archean Gneiss Domes*

Cropping out from under the Proterozoic sedimentary cover are several local Archean gneiss domes, described by Frith (1974; 1990). Gneiss domes are defined as domal structures comprising metamorphic or plutonic rocks (Fayon et al., 2004). The culminations were originally considered part of a granodioritic plutonic complex, however preserved fabrics and a number of radiogenic ages have shown these are reworked, parautochthonous Archean basement**. The domes are fringed by an apron of conglomerate, quartz arenite, carbonate, or marble that is thought to sit immediately above an unconformity (Jackson et al., 2013). A U-Pb

zircon crystallization age at 2580 ± 71 Ma, and a recrystallization age at ca. 1850 Ma have been acquired. An Rb/Sr age from the core of one of these domes yields an age of 2712 ± 89 Ma (Frith, 1992). In most instances, the culminations are flanked by migmatized metasedimentary rock, amphibolite, and leucogranitic melt (Fig. 3.13 e).

## 3.2 Structural Fabrics

Low and high grade schists of the Brown Water Lake area show evidence for multiple overprinting fabrics. In most rocks, up to five overprinting fabrics can be measured. The strongest and most consistent fabric across all areas is $S_{4B}$. This served as a point of reference and correlation between the three structural domains. In the structural analysis of outcrop, hand sample and thin section, the $S_{4B}$ fabric had an approximate orientation of 190/80. Using this foliation as a marker, all other preserved or overprinting fabrics were designated a generation that preceded or succeeded $S_{4B}$.

The Brown Water Lake area has been divided into three structural domains based on character and orientation of foliations, intersection lineations, and styles of folding. These three are: the Inter-dome area, the High Strain Belt area, and South of Brown Water Lake (Fig. 3.9, 3.17). The character and style of deformation has been preserved differently between these three areas. The High Strain Belt is dominated by a strong, steeply dipping, NNE-SSW striking grain, which is visible even in satellite imagery (Fig. 3.18). The area South of Brown Water Lake preserves the same fabrics, however these have a slightly different orientation than in the High Strain Belt. In the Inter-dome area, the effects of the strong NNE-SSW deformation are barely evident, and the dominant structural grain in Proterozoic rocks is ESE-WNW. Bedding orientation is at a 90° angle to bedding measured in the high strain zone. All structural fabrics observed at Brown Water Lake have been correlated between field measurements and microstructural

observations made from oriented hand samples and thin sections. These have been plotted on equal area stereonets in Figure 3.9.

### *3.2.1 $S_{0B}$*

Bedding in the Brown Water Lake area is preserved in all structural domains. It is observed to be folded axial planar to $S_{2B}$, $S_{3B}$ and $S_{4B}$. Poles to bedding plane measurements can be found in Figure 3.9. Throughout the High strain belt, where it is most commonly observed, it is steep and NNE-striking. In a few locations (i.e. 2516, Plate 1) it is flat-lying and deformed by open folds in a hinge zone of a large scale fold. At station 2511 (Fig. 1.4, 3.19 b, c) bedding defines upright folds with shallowly north-northeast or south-southwest plunging $F_{4B}$ fold hinges (Fig. 3.21, Appendix A Plate 1). Over the entire Brown Water Lake region, bedding is folded into $F_{4B}$ folds such as the ones seen at 2511. The High strain belt is characterized by $F_{4B}$ folds, as is the area South of Brown Water Lake. Bedding-parallel coticule layers help document early generations of deformation, preserving evidence for steep intersection lineations and sheath folds (Fig. 3.11).

The character of $S_{0B}$ changes in the Inter-dome zone. Gneissic layering, that may have formed parallel to or transposed primary compositional layering, is largely oriented with an east-west strike, dipping moderately to steeply northward (Fig. 3.9). Here it has not been overprinted by the strong $S_{4B}$ fabric.

### *3.2.2 $S_{1B}$*

The earliest fabric measured in thin section is not visible in outcrop. It is preserved in garnet porphyroblasts from sample 2512A (Fig. 3.10) in the high strain belt of rocks to the east, and as microlithons in between strongly developed folia in sample 2540 at the south end of Brown

Water Lake. It is a moderately west-dipping, N to NNW-striking foliation that shows minor variability in orientation.

Garnet cores from sample 2512A preserve $S_{1B}$ as curved inclusion trails defined by biotite and quartz grains that are finer grained than in the surrounding matrix. For each oriented section cut from the same sample (see section 3.3), an average orientation was taken for the pitch of the inclusion trail in the plane of the cut. These were all plotted on a stereonet and a maximum and minimum dip was drawn to account for the variation in pitch angles. The resulting $S_{1B}$ plane varies in dip approximately 45°, and varies in strike direction by ~20°. $S_{1B}$ is difficult to measure in outcrop in the southern structural domain. It was observed and measured in one sample (2540) in a series of oriented thin sections, and aligns with the fabric observed in the garnet cores measured in the high strain zone.

### *3.2.3 $S_{2B}$*

The $S_{2B}$ fabric is a strong, fabric that is mainly seen in thin section preserved in porphyroblasts. It is axial planar to $F_2$ folds. The fabric is overgrown by garnet rims and cordierite. In the high strain belt of metapelites adjacent to the Slave craton, $S_{2B}$ is the fabric preceding the dominant $S_{4B}$ foliation. It is defined by quartz, plagioclase, and mica inclusions.

### *3.2.4 $S_{3B}$*

The $S_{3B}$ foliation is observed in two locations in the Brown Water Lake area. It is documented between the Archean culminations as a strong foliation in pelitic gneisses (Fig. 3.14 b; 3.16 a, b). Another $S_{3B}$ fabric is observed to the south of Brown Water Lake, as an axial planar fabric to north-trending folds (Fig, 3.5 c). $S_{3B}$ is a strong, steeply dipping, SE-striking fabric that folds and deforms high metamorphic grade, coarse grained rocks in the Archean gneiss dome area. The fabric is defined by gneissic banding in this area. In rocks of the area south of Brown Water

Lake, $S_{3B}$ was observed in outcrop as a fabric that folds bedding with a more northerly-striking axial trace. $F_{4B}$ folds in the same rocks are more north-easterly-striking.

### *3.2.5 $S_{4B}$*

The $S_4$ foliation is the strongest and most pervasive throughout most rocks of the Brown Water Lake area. It is the most consistent and recognizable fabric. In all domains it is a steeply dipping, N-NNE-striking axial planar foliation. The surficial geometry of the high strain belt on the eastern side is strongly controlled by the $S_{4B}$ fabric. Only between the Archean gneiss domes does it affect the rocks much more weakly than elsewhere. The fabric is defined by a strongly developed biotite + muscovite foliation. It is also a folding event, and forms large isoclinal upright folds in rocks of the high strain belt and southern domain, that have very shallowly plunging fold hinges that trend NNE-SSW.

In between the Archean culminations the $S_{4B}$ fabric affects the coarse gneissic rocks much more weakly. It is a spaced crenulating cleavage that overprints the gneissic banding and dismembers $S_0$-parallel dykes. An often noted feature in the andalusite and sillimanite grade rocks is the presence of quartz veins that have intruded axial planar to the $S_{4B}$ fabric and are boudinaged parallel to it (Fig. 3.20 a & b).

### *3.2.6 $S_{5B}$ and Late Crenulations*

Many late crenulation generations are observed in the rocks at Brown Water Lake. They are represented on the equal-area stereonets as orange and yellow dotted great circles (Fig. 3.9). Fine grained biotite-rich schists (versus more quartz-rich schists) preserve these gently crenulating fabrics particularly well. The most prominent and well preserved late stage fabric is a SE-striking, moderately SW-dipping crenulation. It is present in most fine grained schists in

the Brown Water Lake area. The crenulation is observed mainly in thin section, and it kinks biotite and muscovite folia.

Another set of more north-striking crenulations are noted in a few locations in outcrop, although it is unclear what their temporal relationship is to the aforementioned crenulation cleavage. They affect pelitic schists in the eastern and southern structural domain and appear to strongly overprint $F_{4B}$ folds.

## 3.3 Radial Analysis of Two Phase Garnet Growth

Sample 2512A shows two distinct phases of garnet growth that clearly overgrew two progressively developing fabrics (Fig. 3.10). The sample was cut into eight oriented thin sections, six sections cut vertically, 20 to 30° apart. One section was cut at 123/63, and one horizontally. This was done according to Bell and Newman (2006), Sharib and Bell (2011), who performed a similar study on porphyroblasts to determine foliation inflection axes – the axis about which a curved foliation inside a porphyroblast will changes inflection .

Continuous curved inclusion trails show that the cores of these garnets overgrew the earliest preserved foliation, $S_{1B}$ as it was being rotated into the dominant foliation, $S_{2\text{-}4B}$. The rims of the garnets overgrow the dominant foliation, and possibly the developing crenulation that followed, $S_{4B}$ foliation and $S_{5B}$ crenulation.

## 3.4 Mesoscopic and Macroscopic Structure

$S_{4B}$ is ubiquitous and easily recognizable at all scales. Bedding to cleavage asymmetries were used to constrain the location of the axial trace of macroscopic $F_{4B}$ antiforms and synforms (Appendix A Plate 1). Earlier phases cannot be traced at the map scale with the information available.

On the outcrop scale, large amplitude (m to km scale), asymmetric open $F_{4B}$ folds with the strongly developed $S_{4B}$ axial planar foliation are the most obvious and dominant stage of deformation (Fig. 3.19). Reversals of $F_{4B}$ fold hinge plunge are often documented across the structural transects in outcrop scale folds of bedding. This can be attributed to gentle folding of the fold hinge, which may be an effect of the $S_{5B}$ crenulation cleavage superposed at a high angle to $S_{4B}$. Most of the fold axis measurements taken in the field are thought to be $F_{4B}$ generation folds. These shallowly plunging (~20-40°) folds trend NNW and SSE.

The relationship of the Proterozoic supracrustal rocks to the Slave craton to the east, as well as the Archean basement (culminations) is difficult to ascertain. This relationship is shown in schematic cross-sections in Figure 3.21. In the northern part of the orogen, workers have placed a basal décollement above an early Proterozoic, ~300 m thick section of autochthonous stratigraphy which was deposited on the Slave margin (St-Onge et al., 1984). This décollement served as the sole fault on which overlying stratigraphy was translated eastward and deformed during the Calderian orogeny. The stratigraphic section above the décollement has been folded into tight chevron folds. In the cross-sections constructed for this study, this sole thrust fault is shown to have transported Proterozoic metasedimentary rocks and remobilised Archean basement over a thin veneer of autochthonous metasedimentary rock (Fig. 3.21). Basement-cored fold structures are also noted in the north, which may be similar in nature to the Archean gneissic culminations observed in the Brown Water Lake area (Fig. 3.17, 3.21 c). The nearest occurrence of one of these basement-cored structures outside the study area is the Exmouth Massif (Fig. 1.3). St-Onge et al. (1984) documented two generations of antiforms and synforms that form a cross-fold. One set has a NNE-SSW strike, very similar to $S_{4B}$, and the second more NE-SW, which might be correlated with the $S_{2B}$ event. If parautochthonous basement exposed in the gneiss culminations at Brown Water Lake is similar in nature to the Exmouth Massif, then their exposure may be attributed to the same structural events.

More locally, Frith (1986) places a normal fault along the length of the Archean/Proterozoic boundary in the Indin Lake map area, which includes the Brown Water Lake map area. Near station 2535 (Appendix A Plate 1) the contact between the Slave craton and the Proterozoic metasedimentary rocks was observed. This area comprises a deep gully, with a steep ~20 m vertical Archean 'wall' showing possible evidence of cataclastic material. This provides supporting evidence for the placement of a fault at this contact.

## 3.5 Metamorphism

The rocks at Brown Water Lake define a prograde metamorphic sequence of aluminosilicate minerals which indicate a westward-increasing heat gradient with proximity to the Rodrigues intrusion (Appendix A Plate 1). The lowest metamorphic grade at Brown Water Lake is biotite zone schist, occurring near the contact of the Paleoproterozoic schists with the Archean Slave craton. Biotite porphyroblasts are the first to appear in all rocks at Brown Water Lake. They are wrapped by steep $S_{4B}$, and are overgrown by and are inclusions in cordierite and andalusite porphyroblasts (Fig. 3.8 a).

After the appearance of biotite porphyroblasts, the order of first appearance switches between the garnet and cordierite isograds throughout the high strain pelite belt. Where biotite schist grades westward or northwestward to garnet biotite schist, matrix garnets are mm-scale, euhedral to subhedral, and are wrapped by the strong biotite $S_{4B}$ foliation. Some garnets are confined to layers of coticule (Fig. 3.11). In other locations, garnet appears after the first appearance of cordierite. Garnet grains in coticule layers are very similar in size, shape and colour to matrix garnets in other pelites, except that they contain a higher concentration of inclusion trails. These are defined by biotite and quartz.

In the High strain belt, cordierite overgrows the $S_{4B}$ axial planar foliation, but predates any local crenulation (Fig. 3.8 a). Spatially, the first appearance of andalusite is nearly synchronous with the appearance of cordierite. Andalusite porphyroblasts overgrow the main $S_{4B}$ foliation and $S_{5B}$ crenulation, and often wrap cordierite relics in a rim-like manner.

It is difficult to constrain the timing of sillimanite. Presumably it is later or synchronous with the growth of andalusite, however textural relationships are not as obvious as with other porphyroblasts. Fibrolite appears to be aligned with the strongest fabric and sometimes kinked by a late crenulation. The timing of the growth of coarse sillimanite grains is also difficult to determine as gneissic rocks are very coarse and do not retain early fabrics. Sillimanite also does not preserve inclusion trails.

An in-depth structural study by King (1986) contains a vertical composite cross-section of the Paleoproterozoic crust of the Metamorphic Internal zone, which shows the structure, stratigraphy and metamorphism up to 30 km depth. The section shows a distinct zone of high-pressure metamorphism where kyanite was documented in the field. The location of this occurrence is approximately along strike from station 1547 (Appendix A Plate 1), where both possible kyanite relics and corundum occur in the pelitic gneisses at Brown Water Lake (Fig. 3.14 e). Further investigation may show that similar metamorphic conditions affected the rocks closest to the Archean gneiss domes, and that they were brought up from a deeper level than previously thought.

The pressure and temperature conditions of metamorphism are discussed in section 5.3.

### *3.5.1 Isograds*

The mineral paragenesis was described in the field and enhanced using detailed microscopic thin section analysis (Table 3.1). Within ~2.5-5 km of the Archean contact, garnet, cordierite

and andalusite occur as porphyroblasts, with sillimanite appearing within the next 0.6-1 km. The melt-in zone occurs within 0.3-1.2 km of the sillimanite-in isograd, and always occurs before encountering the Archean gneissic domes. Metamorphic grade increases from lower biotite to melt within 7-8 km. In the field, cordierite porphyroblasts occur prior to the appearance of andalusite, although in thin section, cordierite is typically accompanied by a rim of andalusite. With increasing metamorphic grade, cordierite porphyroblasts are pinnitized (replaced with very fine muscovite and chlorite), whereas andalusite continues to replace/grow around the porphyroblasts and grows larger as the matrix coarsens.

In thin section sillimanite always appears first as masses of brown fibrolite, growing in random orientations in the matrix. Not until coarsening of the matrix minerals and after the melt-in isograd does the sillimanite grow to become coarse, unoriented blades.

Garnet growth appears to be mainly controlled by the original composition of the pelite. Garnet porphyroblasts do not occur until the occurrence of cordierite rimmed by later andalusite, although at Brown Water Lake the rocks containing garnet do not contain cordierite or andalusite. Instead, garnet-bearing pelitic schist comprises only garnet as a porphyroblast phase in discreet layers or beds.

| Porphyroblast phase | Timing of growth |
|---|---|
| Biotite | Pre-$S_{4B}$ |
| Garnet (matrix) | Pre-$S_{4B}$ |
| Cordierite | Syn to post-$S_{4B}$ |
| Andalusite | Syn to post-$S_{5B}$ crenulation |
| Fibrolite/Sillimanite | Late (post-$S_{5B}$?) |

**Table 3.1** Summary of metamorphic mineral paragenesis

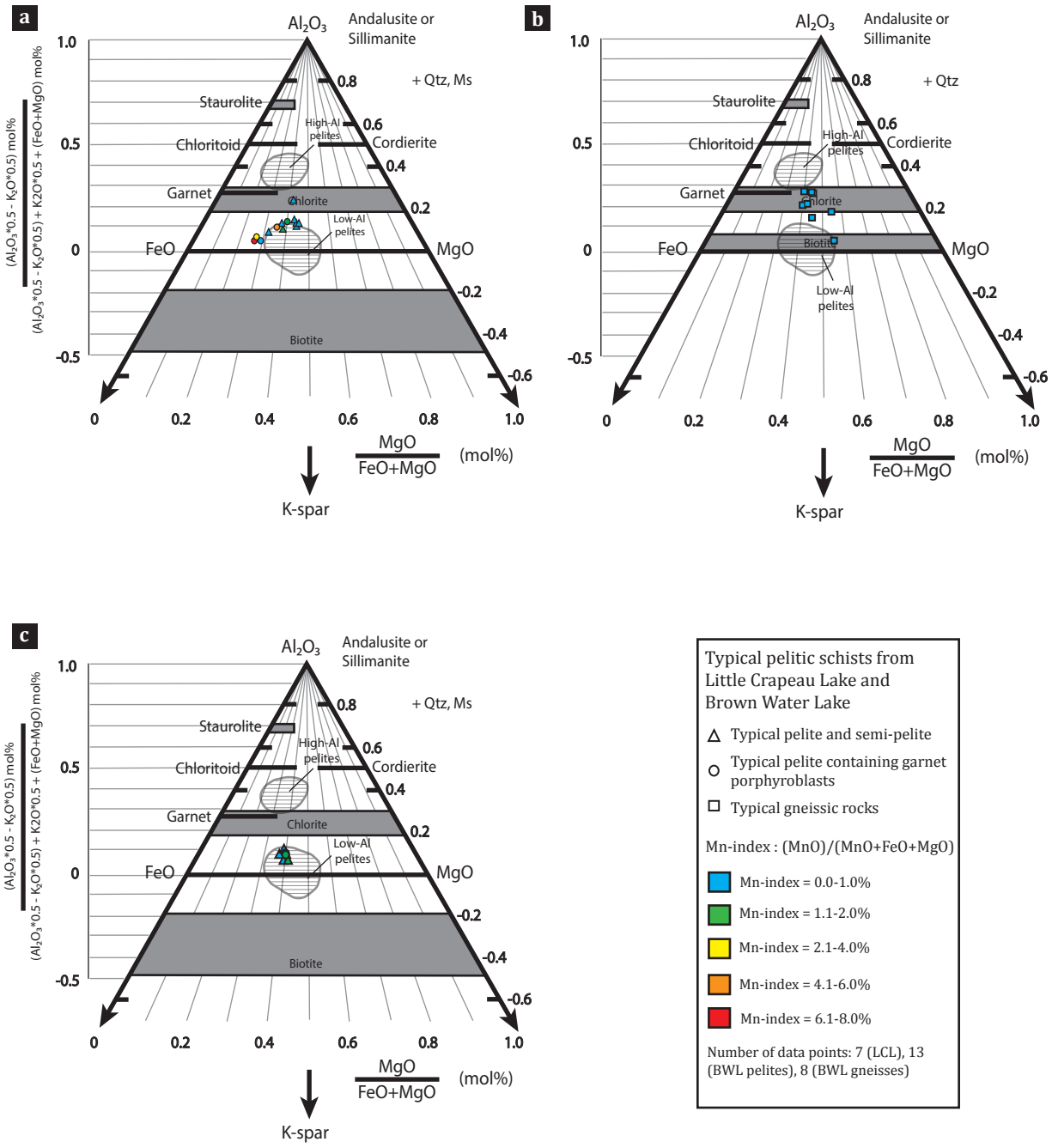


**Figure 3.1 AFM Compositional diagram for pelitic schists and gneisses from Brown Water Lake and Little Crapeau Lake. a)** Schists from Brown Water Lake are low-aluminum pelites, varying minimally in Mg value. Circles indicate schists containing garnet porphyroblasts. Some of these have a somewhat lower Mg value. Data points are coloured by manganese value. Projected from muscovite. **b)** Gneissic rocks from Brown Water Lake plot in between the low and high aluminum zones. All samples have low Mn indices. Projected from k-spar. **c)** Pelitic schists from Little Crapeau Lake clusted tightly in the low-Al field, and vary little in all components. Projected from muscovite. Calculated according to the Spear (1993) formulation. See Appendix D for MgO ratio calculations.

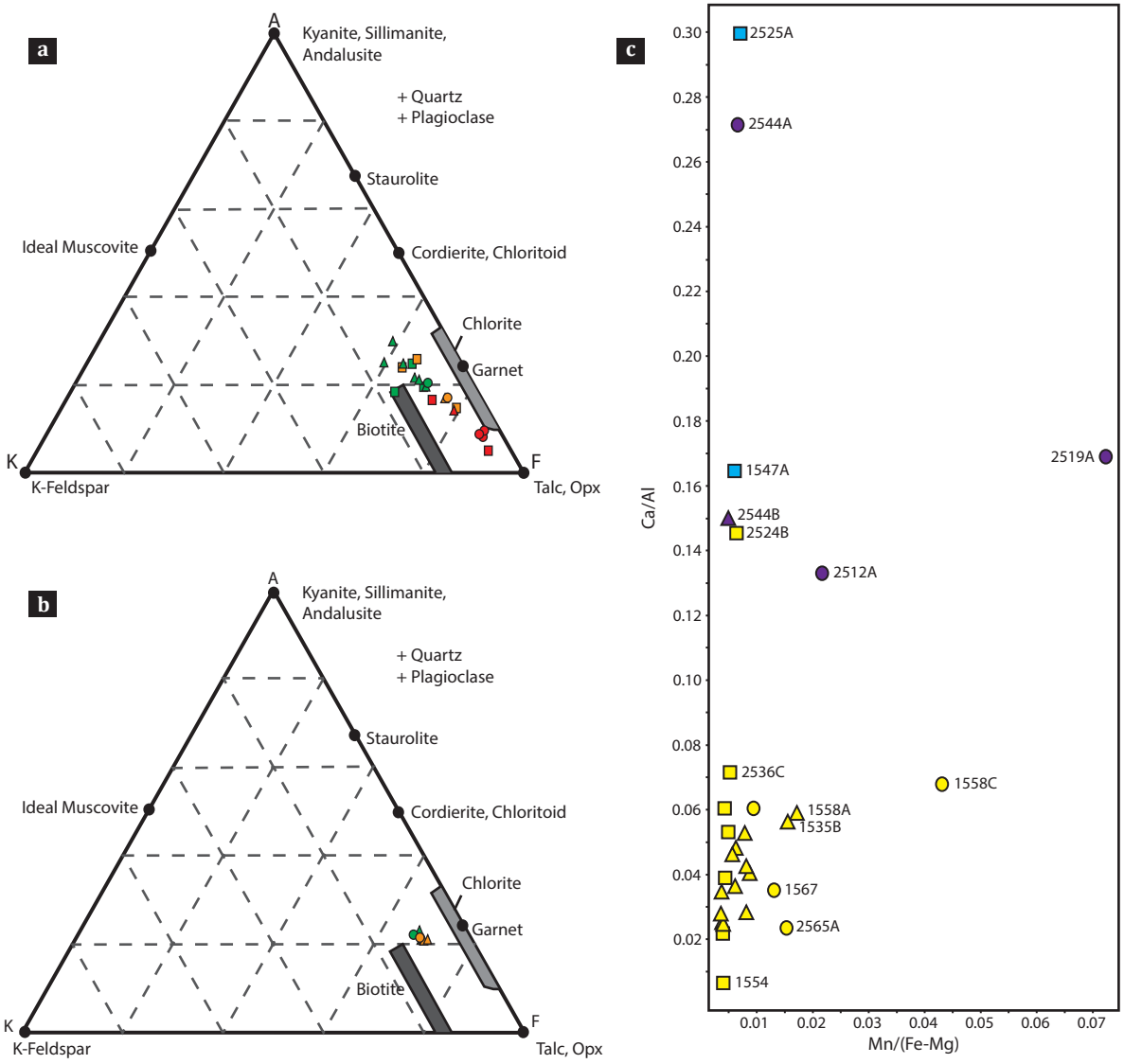


Rock types of the Brown Water Lake and Little Crapeau Lake area

- Typical pelite and semi-pelite
- Typical pelite containing garnet porphyroblasts
- Typical gneissic rocks

Ca-index : $(CaO)/(CaO+Na_2O/2+K_2O/2)$

- Ca-index = 1-20%
- Ca-index = 21-40%
- Ca-index = 41-60%

Fe Index: Fe/(Mn+Mg)

- Fe-index: 0.00 - 1.00
- Fe-index: 1.01 - 2.00
- Fe-index: 2.01 - 3.00

Number of AKF data points: 21 (BWL), 7 (LCL)

Number of Mn vs Ca data points: 30

**Figure 3.2 a) & b) AKF (aluminum-potassium-iron) compositional diagrams for pelitic schists and gneisses of Brown Water and Little Crapeau Lake (BWL, LCL). a)** Rocks from BWL show a range in aluminum content, with garnet-bearing, high-Ca samples plotting lowest on the A axis. **b)** Rocks from LCL cluster tightly in AFM space, showing a very narrow compositional range (Al, K, Fe, Ca). Pelitic schists are projected from muscovite, while gneisses are projected from K-feldspar. **c)** Mn versus Ca plot of major element geochemistry for analysed samples. This plot aims to differentiate between garnet-bearing samples and typical pelitic schists and gneisses, however only a few stsand out. The three samples with highest Mn ratio are garnet-bearing. Mn is known to stabilize the growth of garnet. Samples are coloured by Fe-index value. See Appendix D for calculations.


**Figure 3.3 Character of bedding at Brown Water Lake.** Bedding is preserved as 0.5-10 cm layers of pelitic and semi-pelitic schist. Beds gray to rusty brown, often alternating. In most outcrops it is straight and steeply dipping **(a, b)**, however it is also folded in many locations **(c)**.

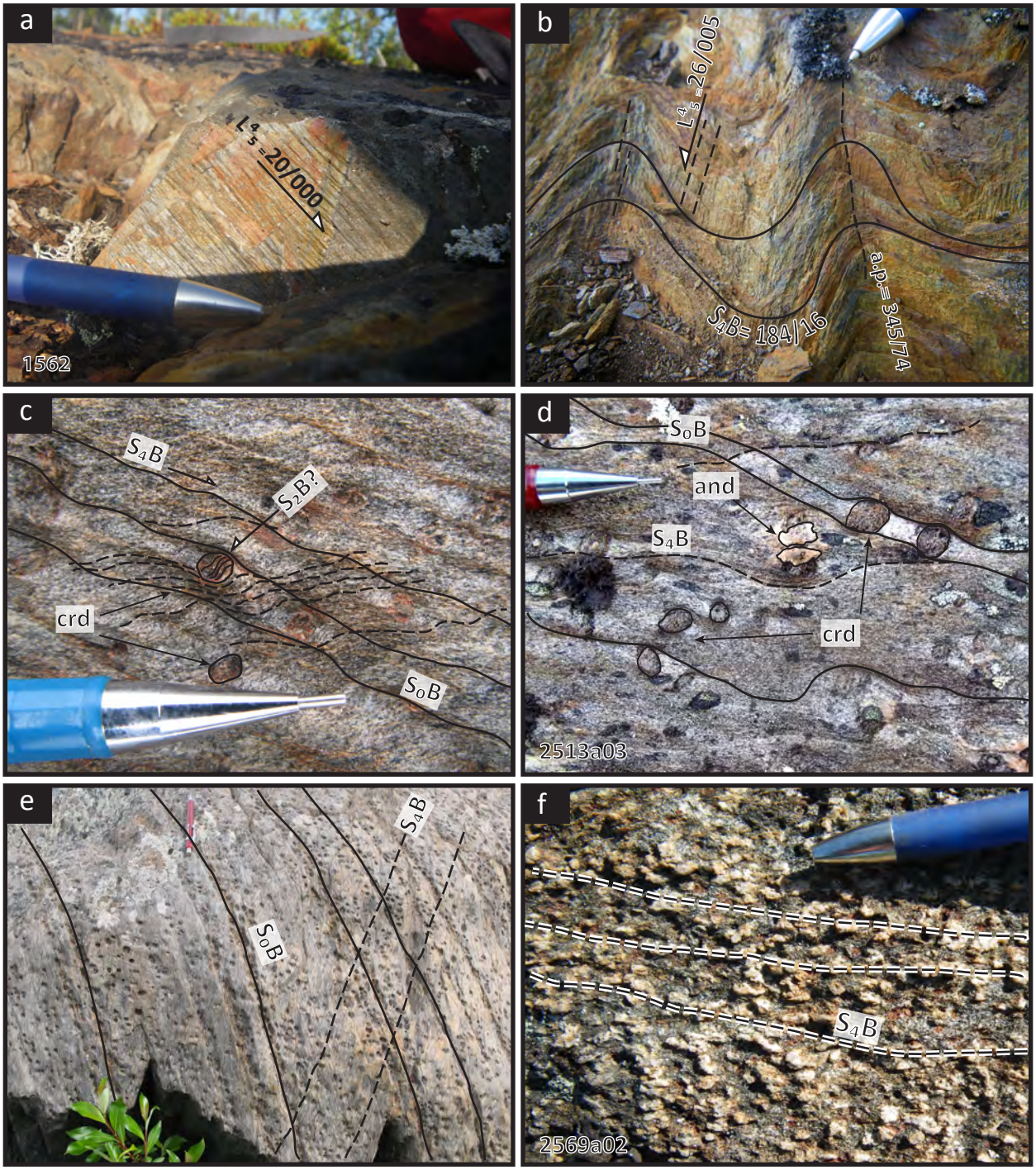


**Figure 3.4 Fabrics and porphyroblasts in schists at Brown Water Lake. a)** & **b)** Rusty brown fine grained biotite schist preserves $S_{2B}$ and $S_{4B}$ in outcrop. A crenulation lineation is visible where $S_{5B}$ intersects the $S_{4B}$ bedding-parallel schistosity. It plunges moderately to the north. $D_{4B}$ is responsible for small outcrop-scale folds and large regional-scale folding. Pen tip points North. **c)** Pinnitized cordierite porphyroblasts preserve $S_{2B}$(?) while being wraped by an $S_{4B}$ schistosity in a fine grained quartz+biotite strongly foliated matrix. Preserved $S_{0B}$ is made visible by compositional differences in bedding (quartz-rich versus biotite-rich). Pen for scale. **d)** Anhedral andalusite porphyroblasts grow amongst pinnitized cordierite porphyroblasts in a quartz biotite schist. In thin section andalusite is shown to nucleate and grow as rims on cordierite. Pen tip points North. **e)** Pits left behind by pinnitized cordierite. Outcrop preserves $S_{0B}$ which is crosscut by a strong $S_{4B}$ foliation. Pen points North. **f)** Coarse, white, fibrous sillimanite is aligned in the $S_{4B}$ fabric in a sillimanite quartz biotite schist. Pen tip points North.

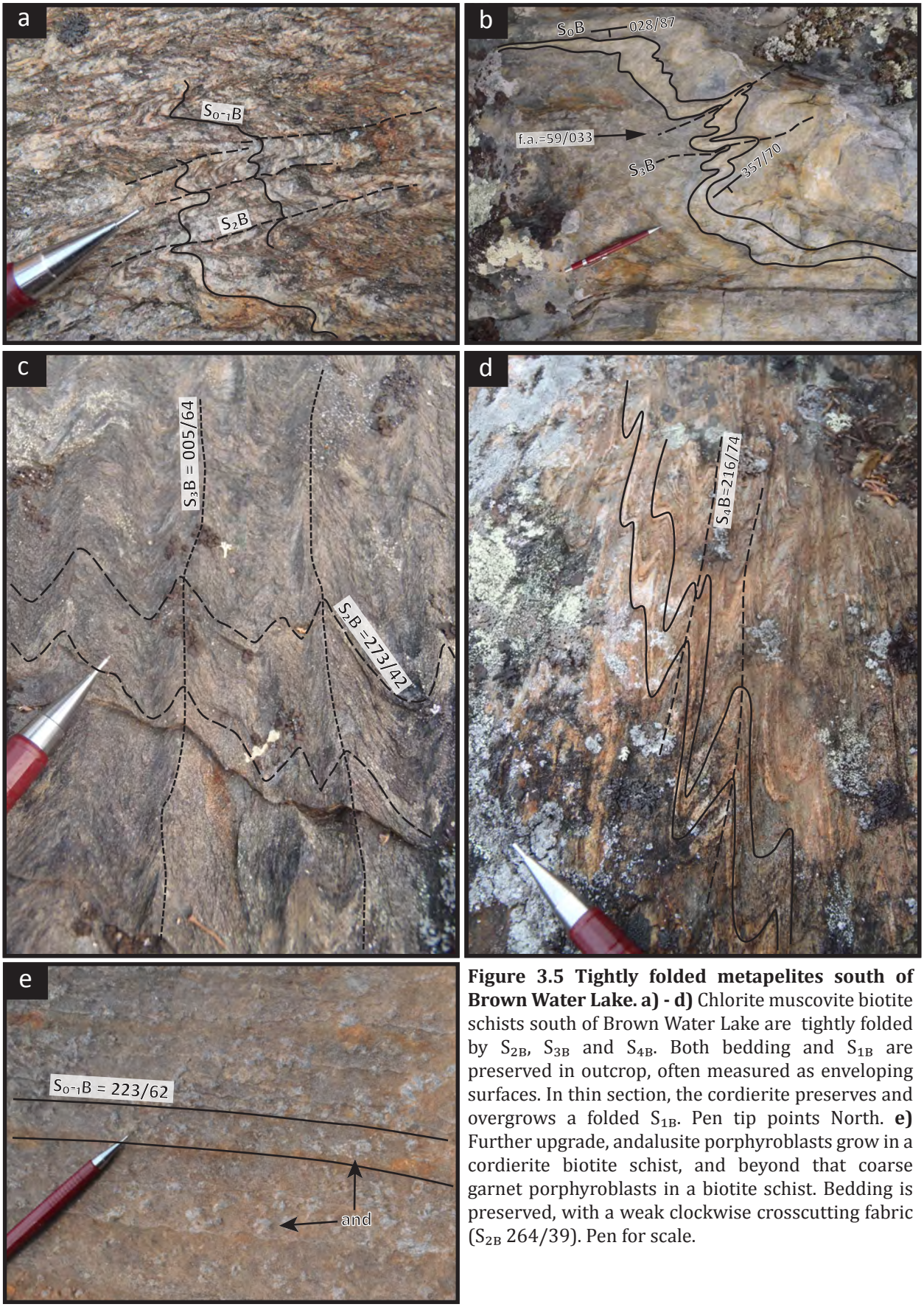


**Figure 3.5 Tightly folded metapelites south of Brown Water Lake. a) - d)** Chlorite muscovite biotite schists south of Brown Water Lake are tightly folded by $S_{2B}$, $S_{3B}$ and $S_{4B}$. Both bedding and $S_{1B}$ are preserved in outcrop, often measured as enveloping surfaces. In thin section, the cordierite preserves and overgrows a folded $S_{1B}$. Pen tip points North. **e)** Further upgrade, andalusite porphyroblasts grow in a cordierite biotite schist, and beyond that coarse garnet porphyroblasts in a biotite schist. Bedding is preserved, with a weak clockwise crosscutting fabric ($S_{2B}$ 264/39). Pen for scale.

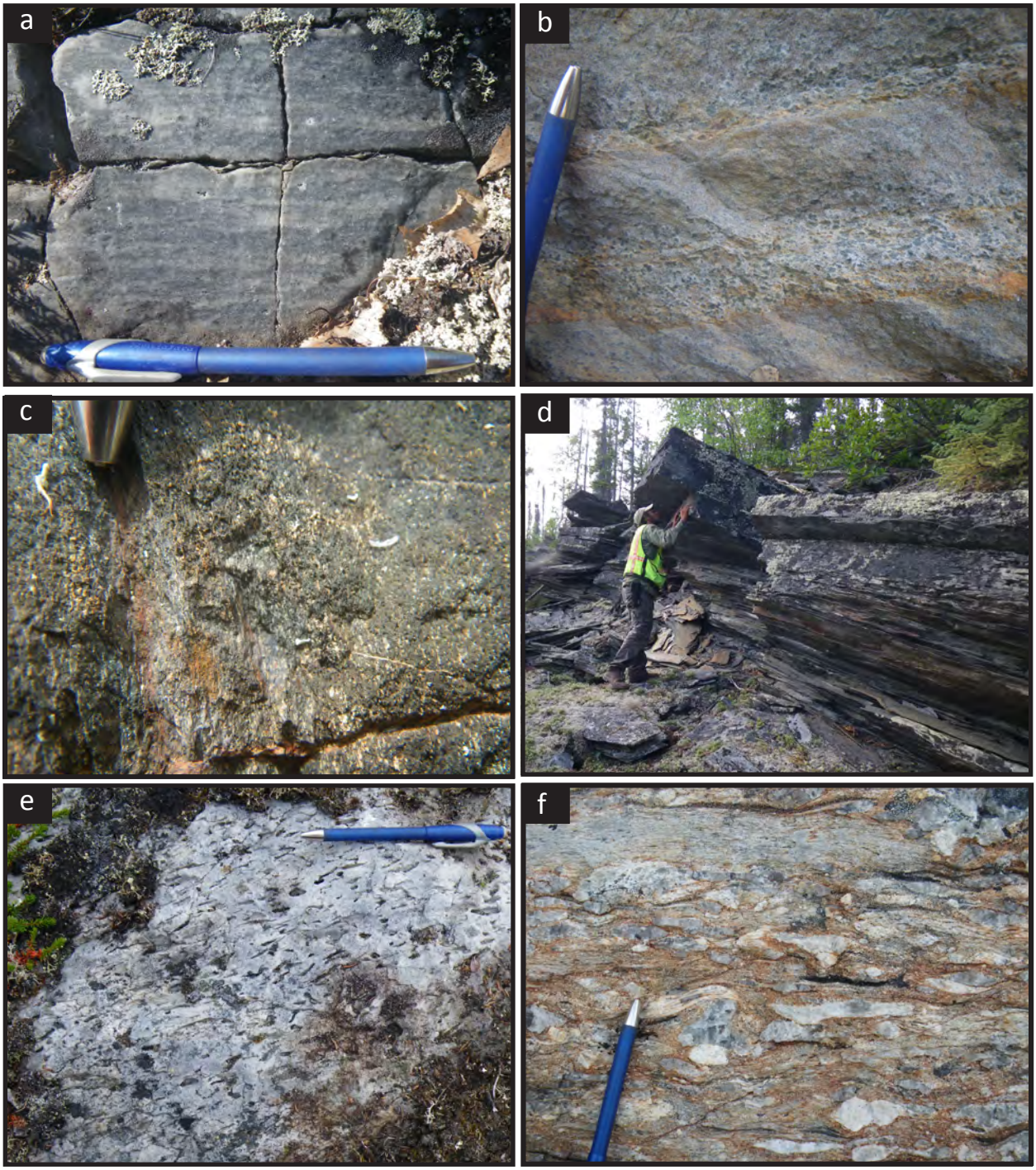


**Figure 3.6 Interbedded quartizte, calc-silicate, amphibolite, marble and conglomerate units. a)** Gray, massive to weakly foliated, bedded quartzite is noted in two different locations along the traverses that cross the highly strained metapelites of the Brown Water Lake area. Quartzite is laterally continuous and may serve as a marker unit. Pen tip points North. **b)** Gray-green, bedded calc-silicate. Porphyroblasts are amphibole, in a pelitic matrix. Pen for scale. **c)** Weakly foliated amphibolite with minor disseminated pyrite. Likely part of a mafic dyke rather than an interstratified unit. Pen tip points North. **d)** Outcrop of unusually slatey biotite schist preserves bedding and a crosscutting cleavage, with a clockwise bedding to cleavage relationship. Geologist for scale. **e)** Foliated gray-white impure marble, stratigraphically located next to quartzite and garnet-rich biotite schist to the west. Impurities may include diopside and/or epidote. Pen tip points North. **f)** Polymictic quartz pebble metaconglomerate. Clasts are largely quartz pebbles, but there are minor leucogranite clasts. The matrix is a coarse grained, brown weathered metapsammite. Pen tip points North.

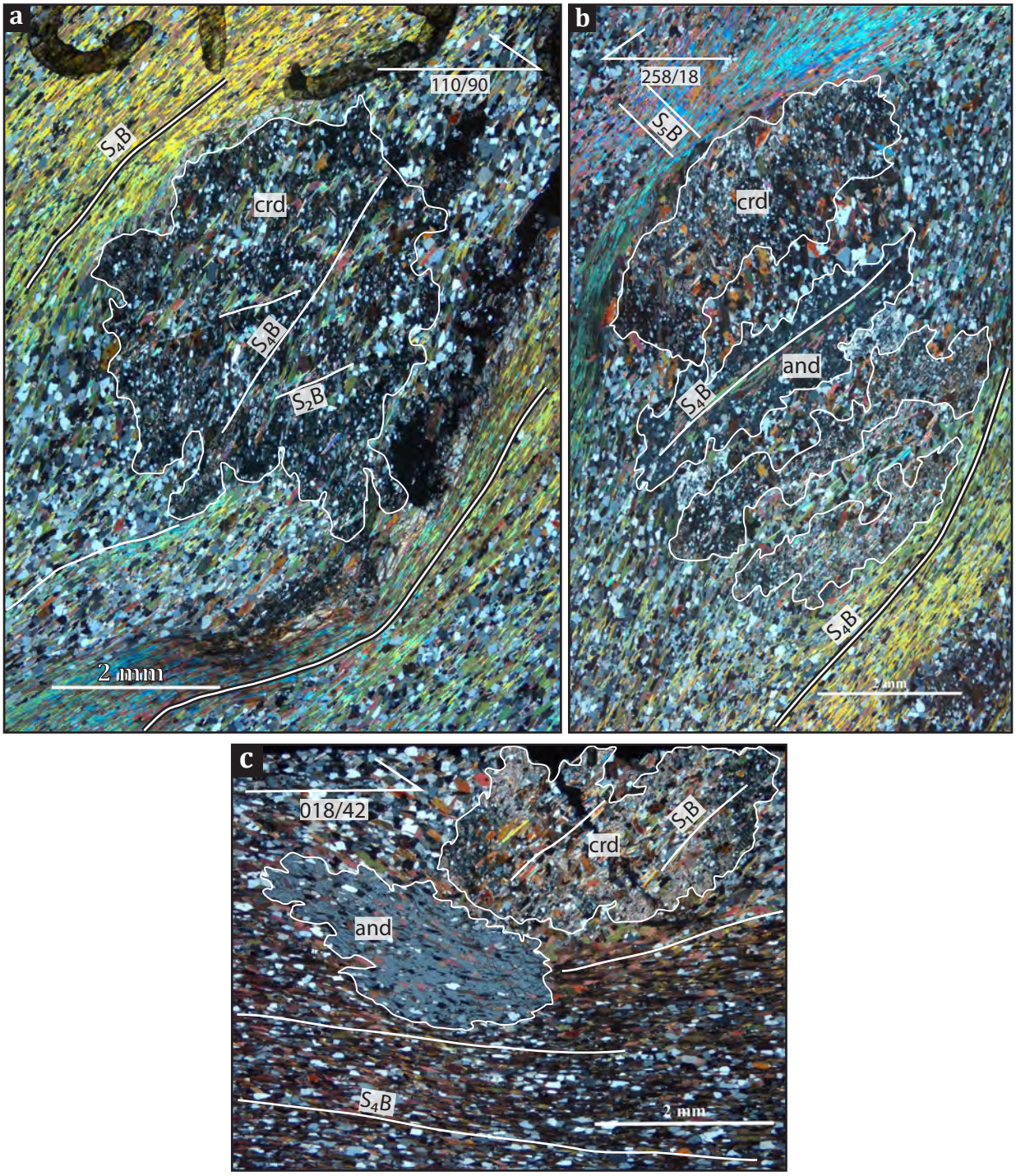


**Figure 3.7 Cordierite and anadalusite porphyroblasts from samples 2512C and 2513.** Porphyroblasts that grew in the matrix of a biotite schist from samples 2512C **(a)** and 2513 **(b, c)** overgrow $S_{1B}$, $S_{2B}$ and $S_{4B}$. Cordierite porphyroblasts' textural relationships show that it grew prior to andalusite, and that growth was initiated after the development of $S_{1B}$ **(c)**, and during the early stages of $S_{3B}$ foliation development, where $S_2B$ is still preserved in the microlithons **(a)**. Andalusite clearly overgrows the dominant foliation, $S_{4B}$ **(b, c)**, $S_{5B}$ in other rocks, and does not preserve any earlier fabrics. All rocks in this area show cordierite to be strongly replaced by biotite + muscovite + chlorite. The $S_{3B}$ foliation is not visible in these rocks, as it was likely strongly overprinted by or rotated into $S_{4B}$.

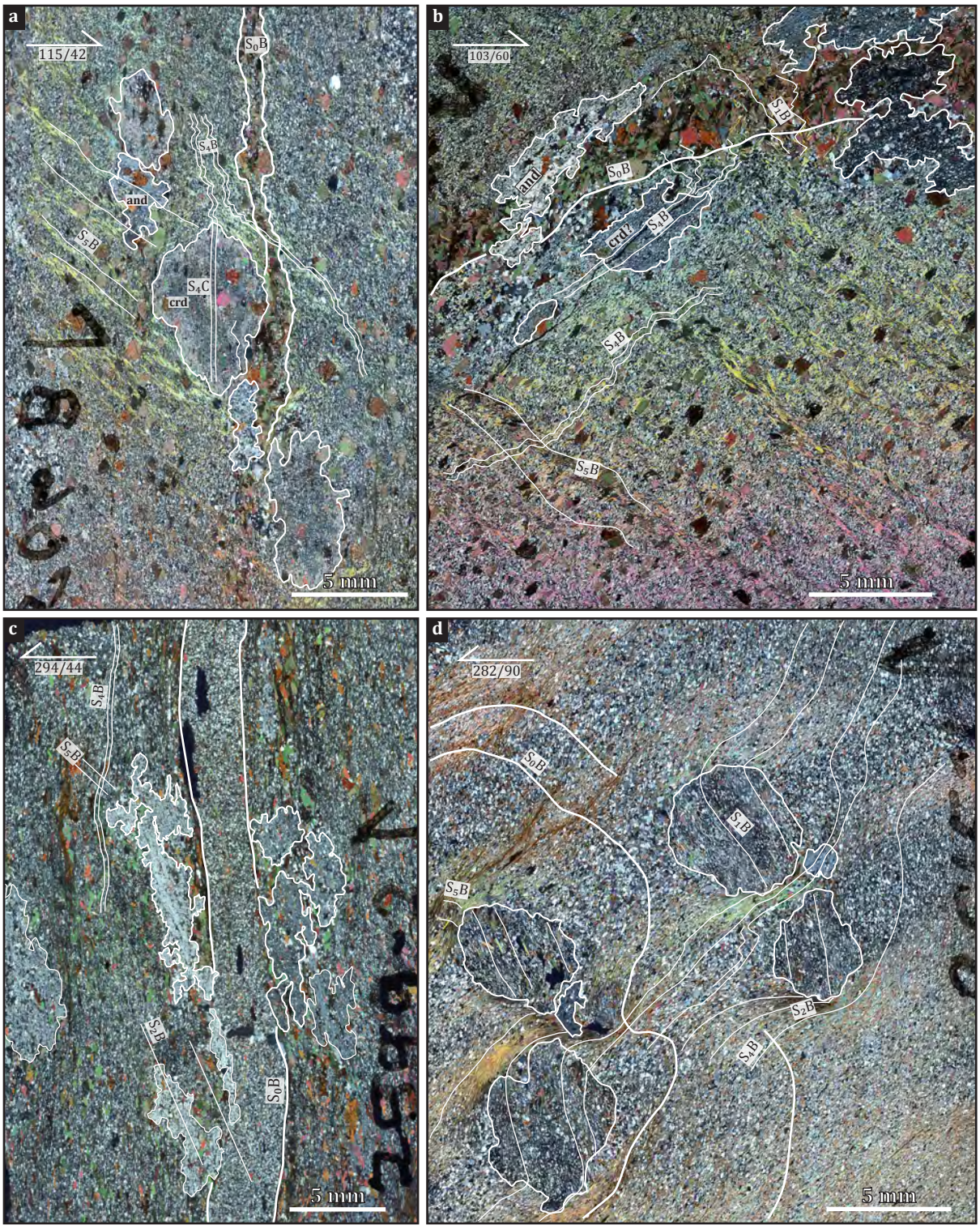


**Figure 3.8 Photomicrographs show overprinting fabrics in biotite cordierite andalusite schists from the high strain belt at Brown Water Lake.** All samples are from the northern traverse crossing the high strain belt of metapelites on the eastern side of the map area. Sample **a)** shows cordierite to have overgrown $S_{4B}$, while andalusite overgrew the $S_{4B}$ fabric crenulated by $S_{5B}$. Abundant biotite porphyroblasts are interspersed throughout the foliated matrix of all samples. **b)** Sample 2511B is from a hinge zone and shows the flattening of $S_{0B}$. Porphyroblast relationships to overprinting fabrics appear different here, however this may be an effect of transposing foliations. **c)** Cordierite is stretched and folded in the orientation of $S_{2B}$, while $S_{4B}$ wraps the porphyroblasts. Abundant biotite porphyroblasts are overgrown by all metamorphic phases. **d)** Folded bedding is preserved by concentrated bands of biotite in this sample, 2515-1. Cordierite overgrows $S_{1B}$, with curved inclusion trails showing continued growth during $S_{2B}$. $S_{4B}$ strongly transposes $S_{2B}$ into a steeper orientation and is defined by thick biotite folia. Microlithons preserve the orientation of $S_{1B}$ in cordierite strain shadows. Gray andalusite porphyroblasts overgrow $S_{4B}$.

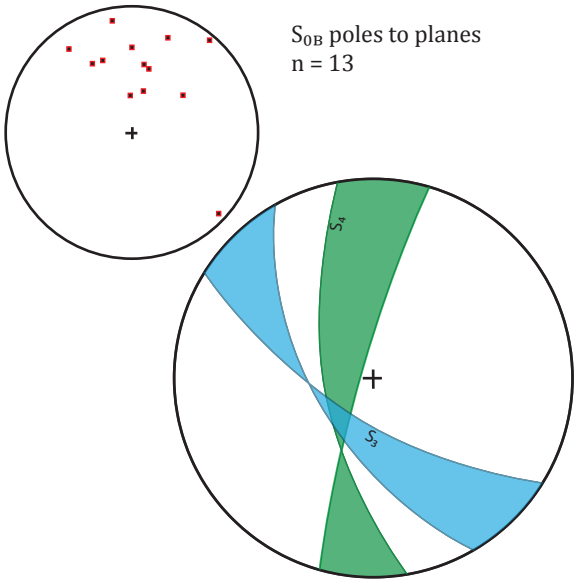


b) High strain belt

$S_{0B}$ is consistently steep and NNE-striking throughout, unless near a hinge zone, where it flattens out and is more NW-SE striking.
$S_{1B}$ is overgrown by garnet cores with varying orientations
$S_{2B}$ is overgrown by crd in 2512C-2, 2506B; crd is folded by (or after?) $S_{2B}$ in 2508B-2
$S_{3B}$ doesn't exist here or has been strongly overprinted
$S_{4B}$ is main marker fabric, overgrown by garnet rims, andalusite; garnet (2509B) is wrapped by $S_{4B}$, cren overprints the $S_{4B}$ fabric
Late crens (orange): in 2508 is overgrown by cordierite, andalusite
Late crens (yellow): measured in 2505, 2511

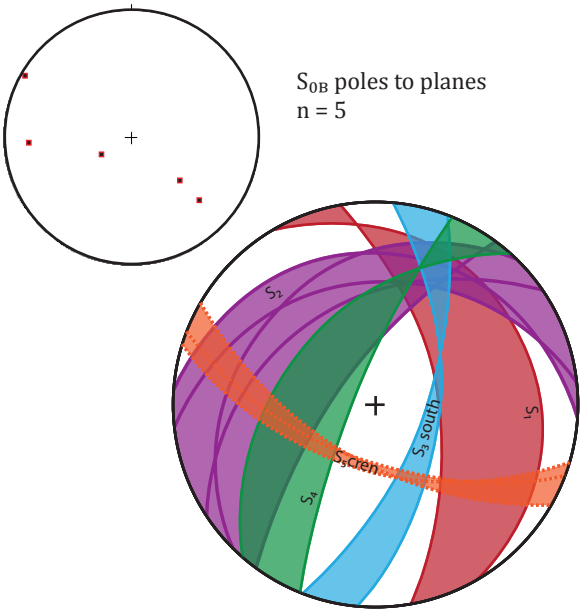


a) Between Archean Gneiss Domes

$S_{0B}$ is compositional gneissic banding and sandy layering in high grade rocks (shown as poles to planes). Approximately the same orientation as majority of bedding at Little Crapeau Lake area. Gneissic banding may be parallel to $S_{2B}$ as measured in the high strain belt.
$S_{2B}$ is probably recrystallized in any remaining porphyroblasts (crd is very coarse)
$S_{3B}$ is the main axial planar fabric in this area and it is moderately crenulated by $S_4$. $S_{3B}$ may be the same deformation event as $S_{4C}$ at Little Crapeau Lake. Here we'll call it $S_{3B}$.
$S_{4B}$ is not nearly as strong here as in the belt to the east
*The matrix of these gneissic rocks is likely too coarse and recrystallized to preserve weak, late crenulations

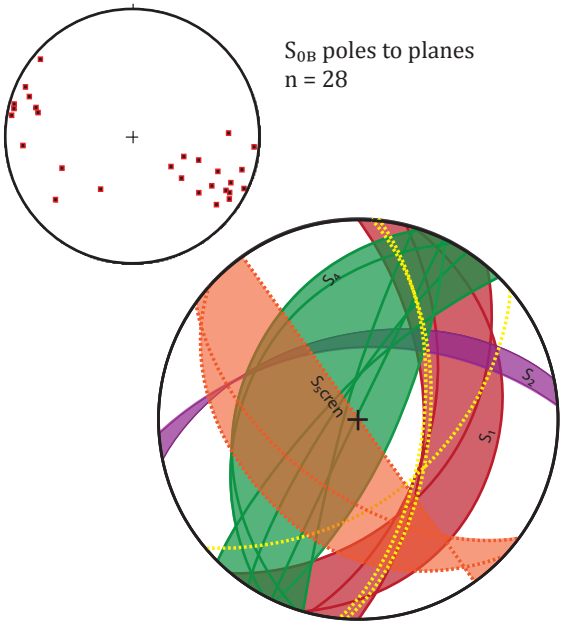


c) South end of Brownwater Lake

$S_{0B}$ is mostly measured in outcrop, in sandy and schistose beds, folded by $S_{3B}$ and $S_{4B}$.
$S_{1B}$ is preserved between folia, where dominant fabric is $S_{2B}$. Andalusite has overgrown $S_{2B}$ and late crenulation in 2543 - peak of metamorphism is syn-$S_{5B}$ crenulation
$S_{3B}$ is measured in outcrop as a fold event, not clearly marked by a foliation. $F_{3B}$ folds $S_{0B}$, and have axial traces striking ~north.
Mica-rich porphyroblast relics (crd?) in 2542 are stretched out in the orientation of $S_{4B}$ (and overgrow a crenulated $S_{1B}$). $F_{4B}$ folds strike NE. $S_{4B}$ is SW-striking and steeply dipping.
$S_{5B}$ is a crenulation noted in thin section and outcrop

**Figure 3.9 Stereonets depicting fabrics per structural zone at Brown Water Lake.** The area is divided into three structural domains, based on slight changes in styles and character of deformation.

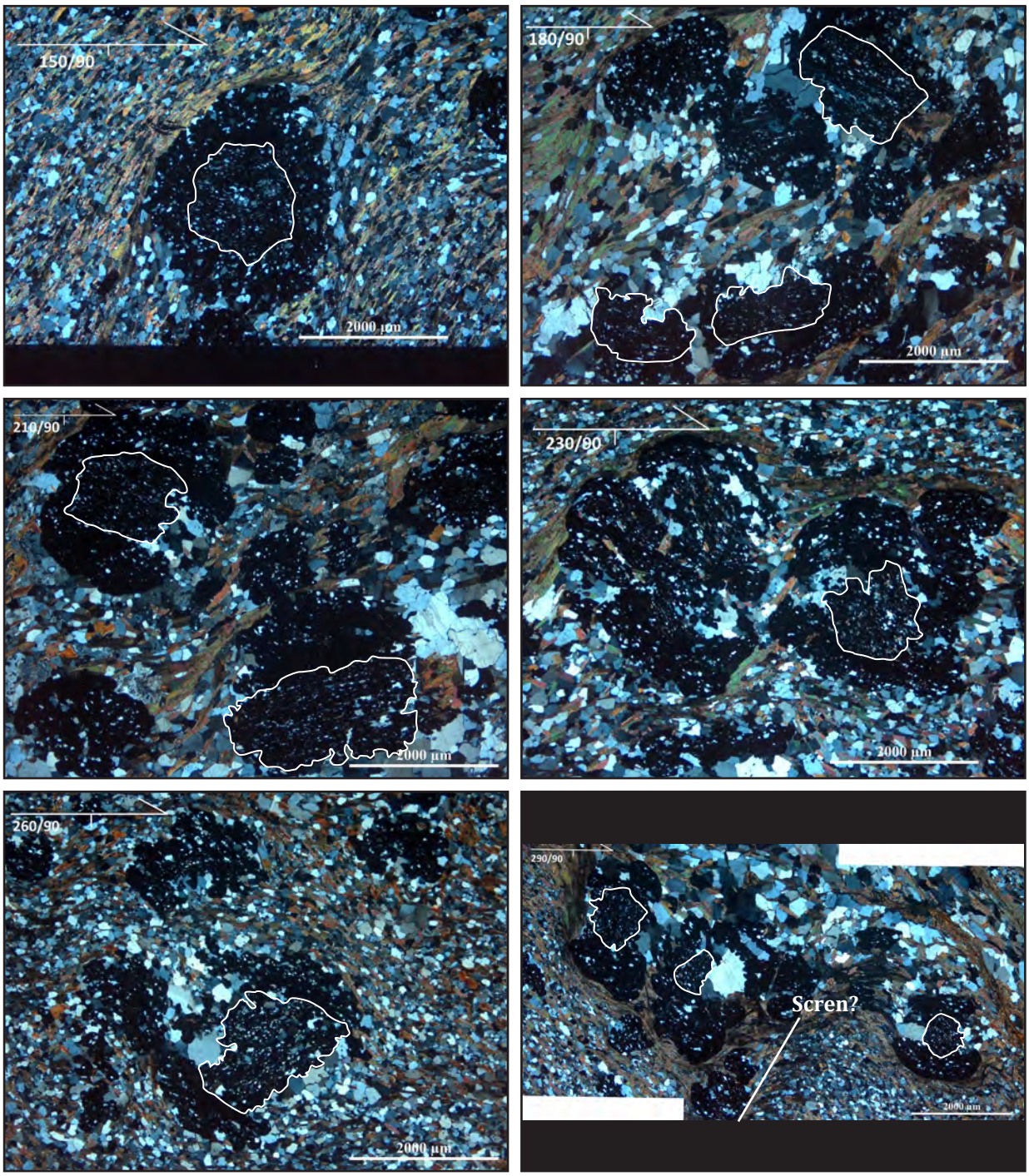


**Figure 3.10 Garnet porphyroblasts preserve two generations of deformation, from radially cut sample 2512A.** Garnet porphyroblasts in a strongly foliated biotite schist from Brown Water Lake. Cores of garnets (outlined with white) are defined by finer grained inclusions than rims. Inclusion trails are quartz, biotite and plagioclase. Coarsening of the matrix minerals during progressive metamorphism is recorded in the rims, where included grains are larger than in the core. The earliest foliation orientation measured from this rock shows a fabric with an average orientation around 032/58. Core inclusion trails show this fabric to be variably dipping ESE, and possibly somewhat rotated. Curvature in these early trails suggests that the cores were still growing as the fabric was being rotated into the now dominant orientation. The rims of the garnets overgrow the dominant foliation in the rock oriented at 205/40 ($S_{4B}$), and likely the overprinting crenulation. The dominant fabric in this rock is somewhat more shallow than the dominant foliation across the high strain belt, however is likely the same generation of deformation. The overprinting crenulation fabric crosscuts the main foliation at approximately 050/57.


**Figure 3.11 Ptygmatic folding of coticule layers in sillimanite zone pelites. a)** Garnet rich bedding-parallel layers are folded along with beds of sillimanite zone biotite quartz schist. Garnet porphyroblasts are <1mm and are limited to these layers, as none are found in the matrix of the rock. The complex fold patterns indicates that significant shortening has occured within the rocks; less competent pelitic layers likely dissolved under the shortening conditions whereas highly competent garnet-quartz coticules buckled. **b)** and **c)** show detail of folds in a). A fold resembling a hand and one that may approximate a sheath fold show the styles of folding related to the high competency contrast between adjacent pelitic beds. As measured in outcrop, fold axes are both steeply and shallowly plunging with local plunge reversals, indicating complex 3D shortening. Vertical folds (with verticallly plunging fold axes) dominate these ptygmatic (disharmonic) folds where high competency contrast has caused differences in folding style. Bedding-parallel quartz-spessartine layers, simillar to these quartz-garnet bands are discussed by Kramm (1976) and are thought to be the metamorphosed equivalent of manganese-rich sediments, derived from a cherty or clayey starting material, possibly originating from a volcanic-exhalative process (Lamens et al., 1986).


**Figure 3.12 Boudinaged and metamorphosed calc-silicate beds. a)** Calc-silicate interbeds are boudinaged parallel to the bedding plane, likely synchronous with development with $S_{1B}$, and are then folded by $F_{4B}$, displaying a strong axial planar foliation. Pen tip points North. **b)** Detail of calc-silicate boudin, showing garnet porphyroblasts in the rim, and $S_{2B}$ (or $S_{4B}$?) aligned amphibole grains in the center.

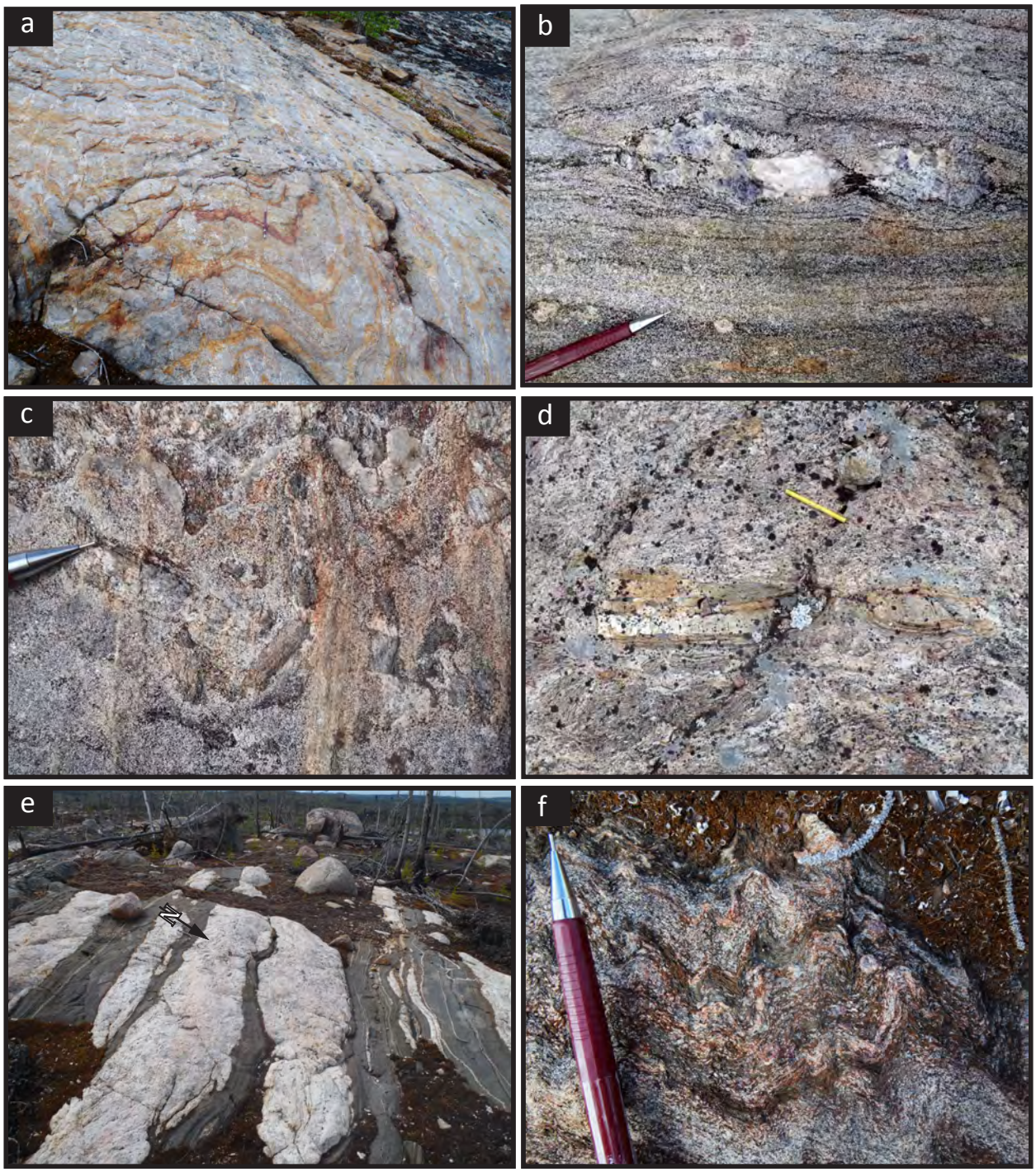


**Figure 3.13 Brown Water Lake rocks are coarser approaching Archean gneiss domes and Rodrigues granite. a)** Melt stringers follow along axial planes of $F_{4B}$ folds, shear bands and other planes of weakness in coarsening metasedimentary units. Pen tip points North. **b)** Coarser rocks contain clear, blue cordierite with quartz-rich haloes, and ~1 cm garnets porphyroblasts. Pen tip points North. **c)** Sillimanite porphyroblats grow ~2 cm in a pelitic matrix within the melt-in zone. Pen for scale. **d)** Rafts of metasedimentary bedding are set in migmatized metasediments proximal to the Rodrigues granite. Pen magnet for scale. **e)** Granitic dykes and amphibolite mantle the perimeter of the Archean gneiss domes. North arrow next to pen for scale. **f)** Coarse sillimanite biotite quartz schist shows open folds in outcrop. Compositional banding likely represents original bedding, folds are defined by coarse biotite and quartz. Main fabric in this outcrop is a shallow dipping, E-W striking foliation, strongly crenulated by a N-S striking steep fabric, likely $S_{4B}$. Pen tip points North.


**Figure 3.14 Coarse rocks in around and between Archean gneiss domes. a)** A crumbly, rusty brown, sillimanite zone gneiss displays small open upright folds in outcorp. Axial planar fabric of folds is $S_{4B}$. Hammer for scale. **b)** Between the domes different fabrics are preserved than in the high strain belt to the east. Here, $S_{4B}$ does not overprint the strong east-west as it does elsewhere. Instead, a $S_{3B}$ crenulation is superposed and is visible as offset in the $S_{2B}$-parallel quartz vein. Pen tip points North. **c) & d)** Similarly to the fabrics in b), gneissic banding and minor migmatitic melt highlights the differentiated $S_{4B}$ cleavage. Pen tip for North, and hammer for scale. **e)** Long, tabular, gray-blue porphyroblasts in a sillimanite biotite quartz schist may be pseudomorphs of sillimanite after kyanite. Pen for scale.

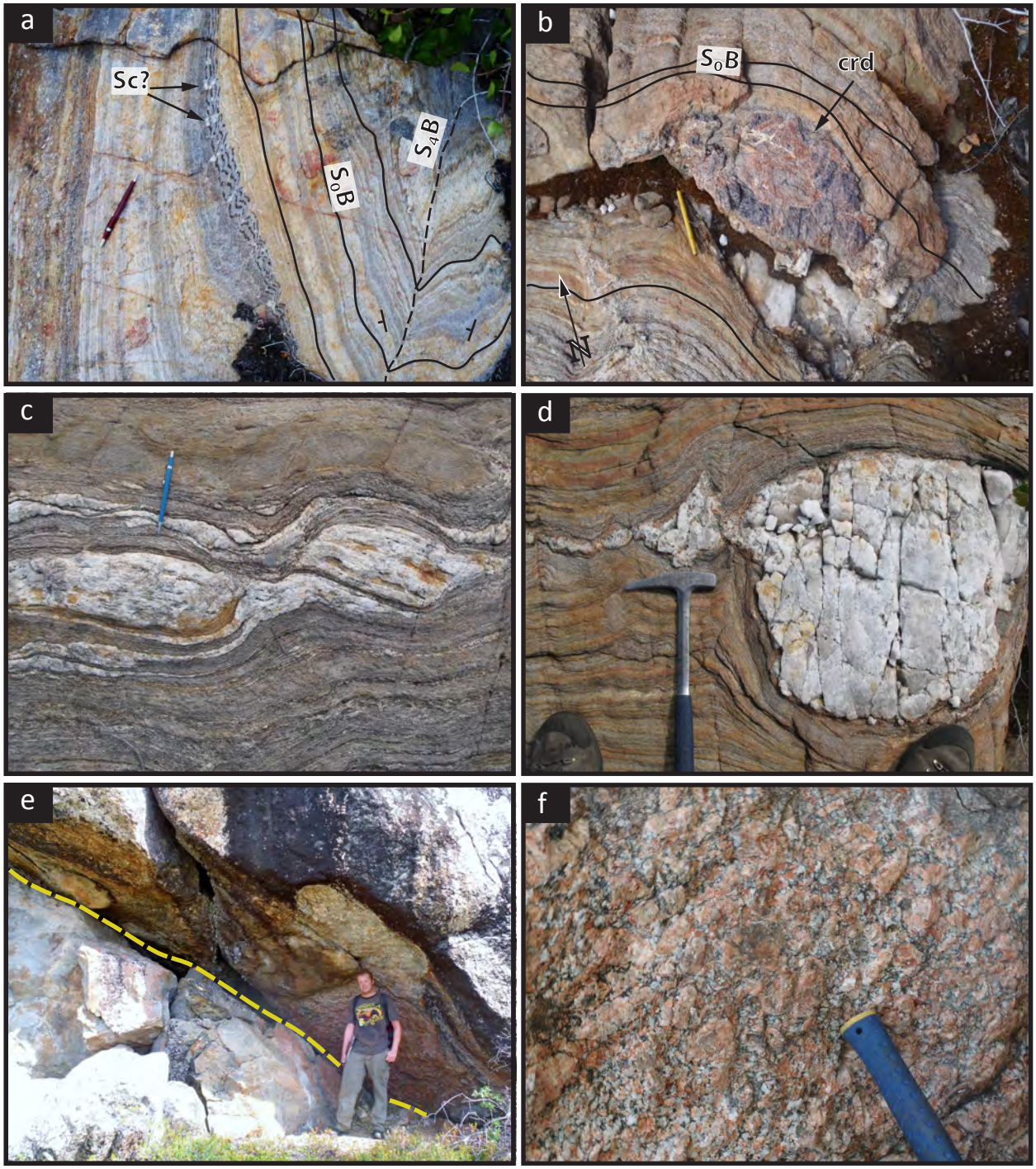


**Figure 3.15 Migmatite grade pelites and the Rodrigues granite. a)** Compositional layering is nicely preserved and folded by $S_{4B}$. Small stringers of leucocratic melt cross perpendicular to the limbs of the fold. In this area fold axes plunge steeply southwest. Pen tip points North. **b)** Migmatitic layering preserves original bedding, which wraps a ~30 cm clear blue cordierite porphyroblast. In this area cordierite and garnet porphyroblasts grow much larger than in the lower grade pelites. Pen magnet for scale. **c) & d)** Migmatized pelites are strongly layered with quartz-rich to granitic veins emplaced parallel to bedding. These are boudinaged parallel to $S_{0B}$. Pen and hammer for scale. **e)** A yellow dashed line shows the contact between the ca. 1850 Ma Rodrigues granite (hanging wall) and migmatized pelites (footwall). This type of contact with the Rodrigues is not uncommon - the intrusion is likely sill-shaped and was structurally emplaced above the metasediments. **f)** Alkali-feldspar megacrystic peraluminous Rodrigues granite. Hammer handle for scale.

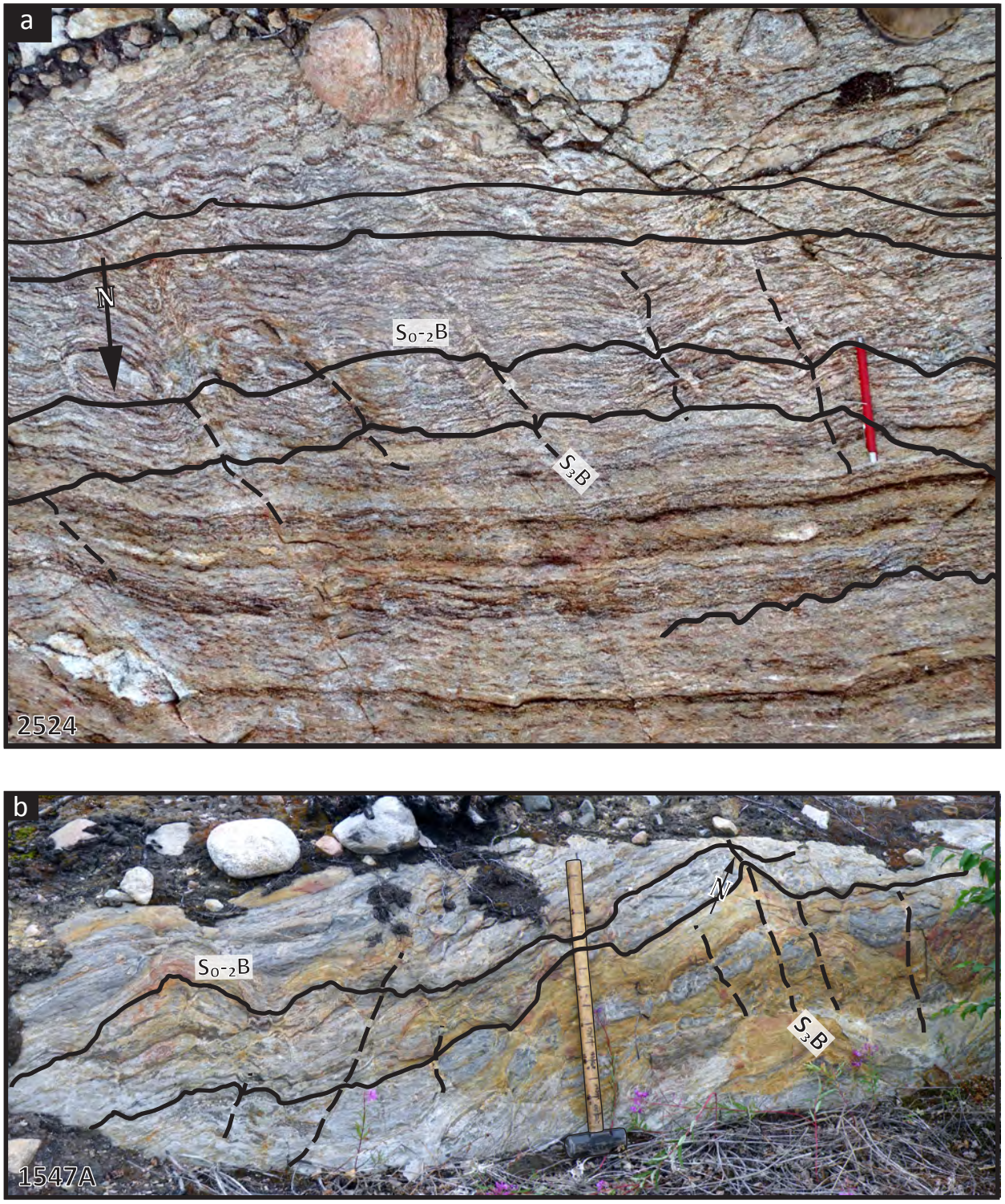


**Figure 3.16 Fabrics preserved differently between Archean gneiss domes. a)** Between the Archean gneiss domes, rusty brown migmatized cordierite biotite schist of the Brownwater Lake area preserve east-striking, moderaly dipping migmatitic layering, $S_{0B}$ and $S_{2B}$ fabrics that are also seen in the highly strained rocks of the belt directly to the east. Stringers of leucocratic melt follow a fabric, $S_{3B}$, that kinks $S_{0-2B}$. **b)** Boudinage along the $S_{0-2B}$ plane shows the same layer-parallel strain as above, with $S_{3B}$ boudinaging thick incompetent bedding. Hammer for scale.

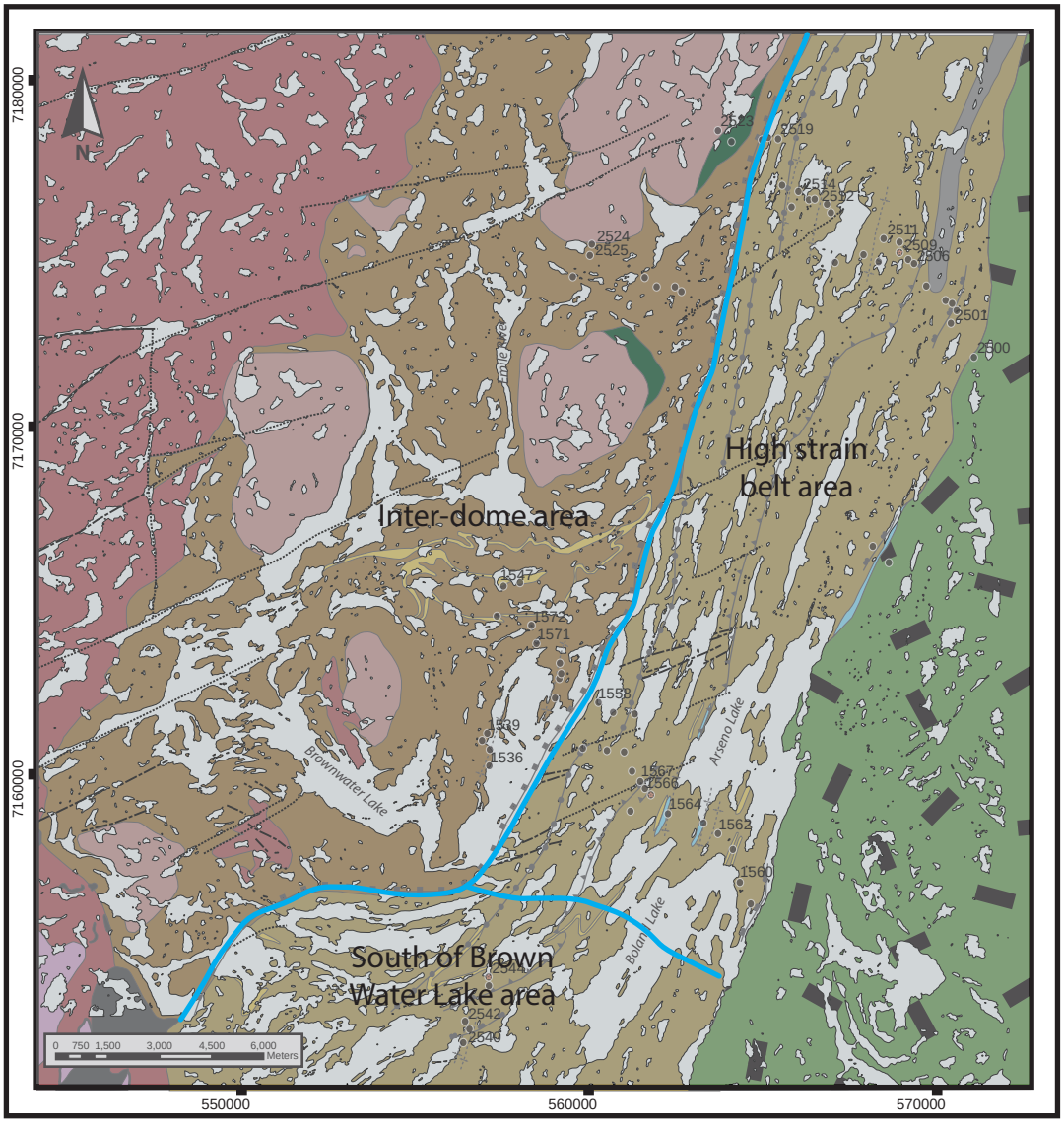


**Figure 3.17 Structural domains at Brown Water Lake.** The Brown Water Lake area is divided into three main structural domains: the Inter-dome area, the High-strain belt, and South of Brown Water. Rocks in the High strain belt and South of the lake are tightly folded, but differ in the orientation of their dominant fabrics, and in their preservations of early fabrics. Rocks belonging to the Inter-dome area are not affected as strongly by the $S_{4B}$ fabric (steep, NNW-striking foliation), and instead preserve a well-developed $S_{3B}$ gneissic fabric that is not preserved elsewhere. These rocks are also strongly recrystallized and don't preserve early fabrics.

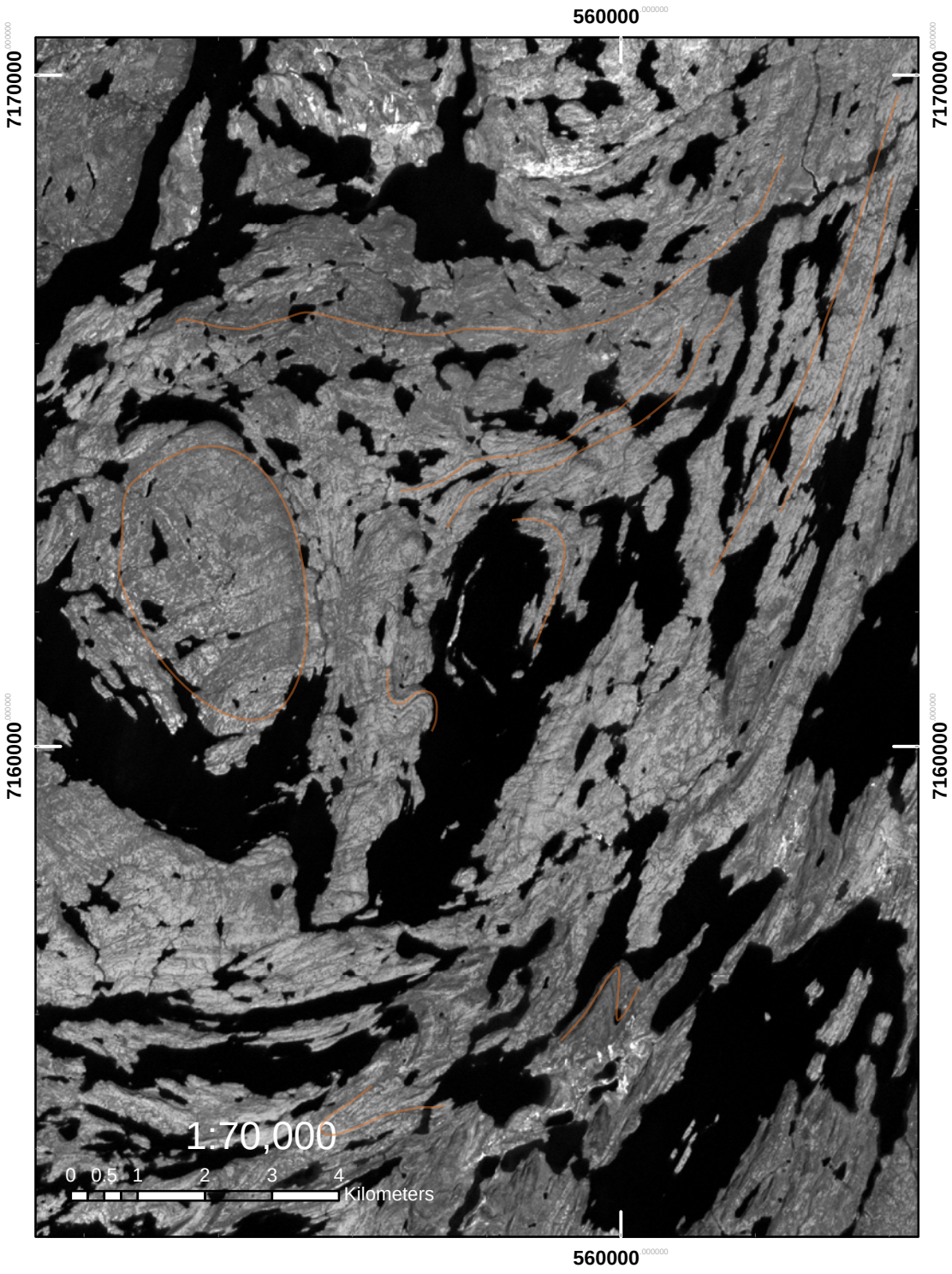


**Figure 3.18 Spot imagery for the southern extent of the Brown Water Lake map area.** Landform features in spot imagery enhance the appearance of mesoscopic geological structures. Visible at this scale (oulined in orange) are an Archean gneiss dome (circular feature to the west), east-west trending planar structural features being reoriented into NNE -SSW trending ones, and kilometre-scale folds. Stongly overprinting the landforms and geological structures are glacial striae, crossing the area from WSW to ENE.

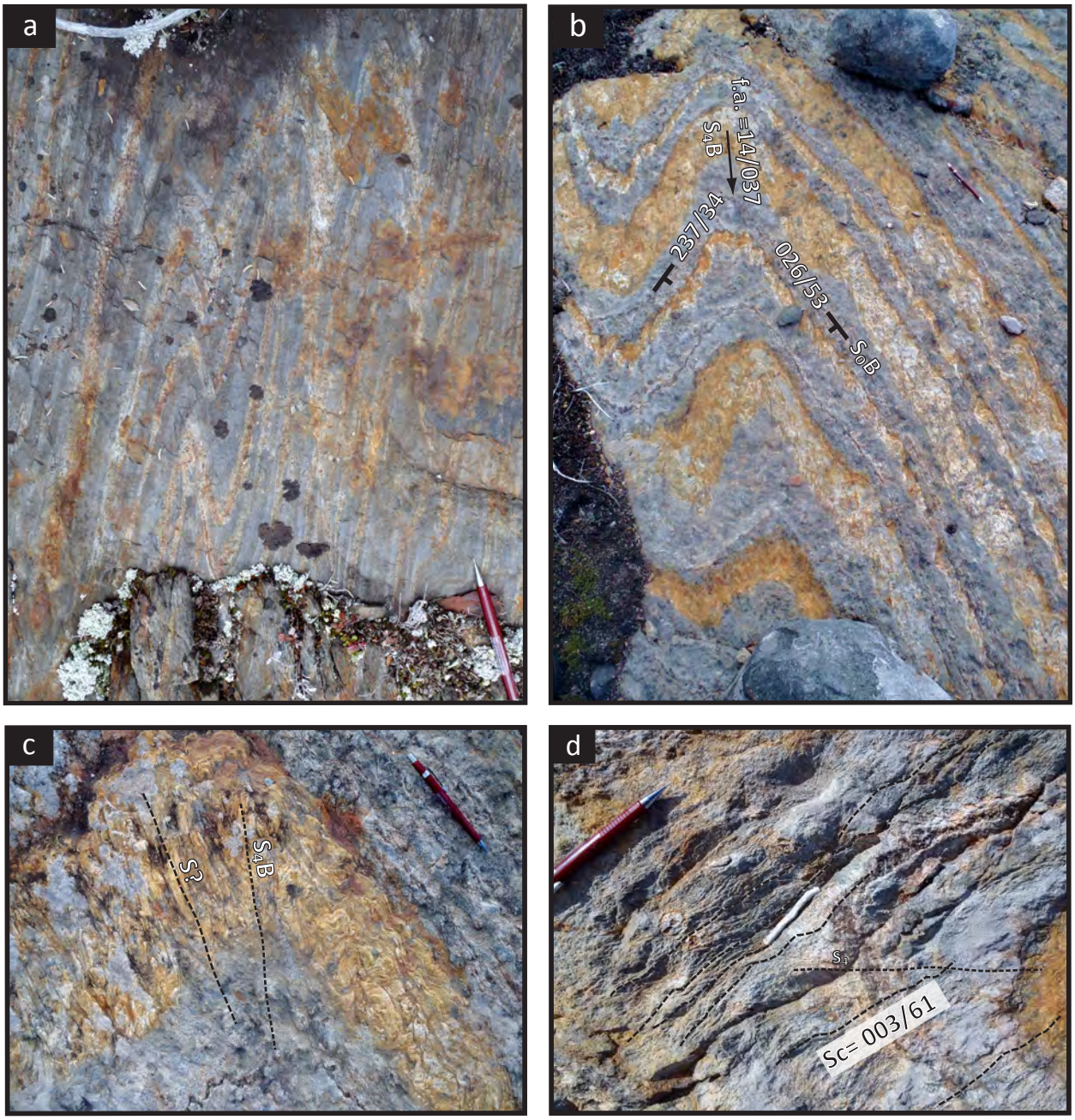


**Figure 3.19 Brownwater Lake fold patterns. a)** Bedding of greenschit grade rocks is folded, with a strong axial planar foliation striking 192/79, $S_{4B}$, and a crenulating fabric at 006/66, Sc. Pen tip points North. **b) & c)** Cordierite andalusite muscovite biotite schist shows open, upright folds in outcrop. Fold hinges dip shallowly to the NE. Beds are ~10 cm thick. Rusty brown beds show tight internal folding of an earlier fold phase than $S_{4B}$. The nearly parasitic appearance of these folds is likely a result of the shallow viewing angle of the outcrop surface. $F_{4B}$ is the major fold phase and is the axial planar foliation to folded bedding and $S_{1B}$. Pen tip points North. **d)** Detail from folds in b), shows strong, steep crenulation fabric crossing $S_{0B}$ and $S_{4B}$.

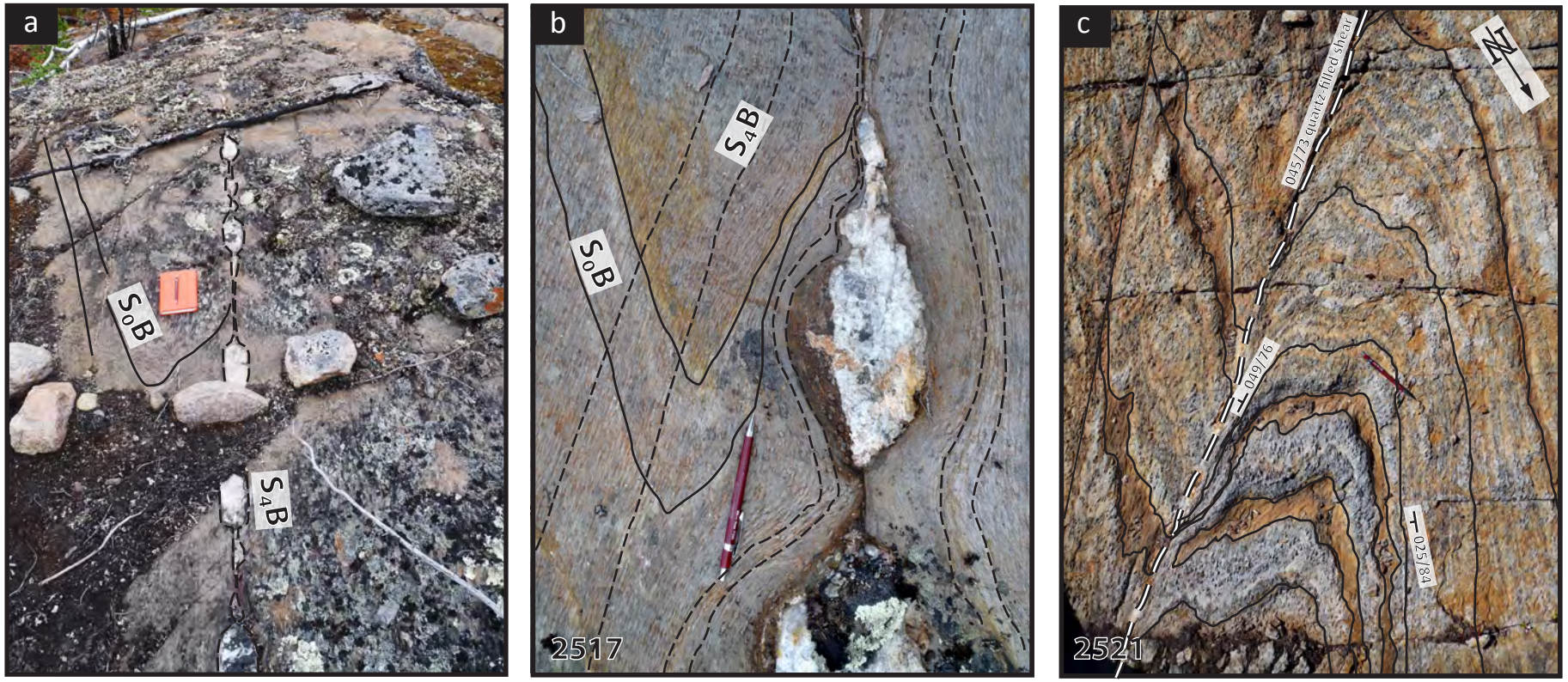


**Figure 3.20 Boudinage due to rhealogical differences: a) & b)** Quartz veins emplaced along the axial planar foliation of folded cordierite biotite quartz schist are boudinaged, likely synchronous with development of $S_4B$. The quartz boudins are mantled by a dark 'metasomatic' rim of biotite + andalusite. Pen tip points North. **c)** Folded sillimanite zone schists show folds with thin limbs, as well as boudinaging of quartz-filled ductile shears that have formed parallel to $F_4B$ limbs. This style of deformation occurs in many outcrops in the higher grade rocks of the area.

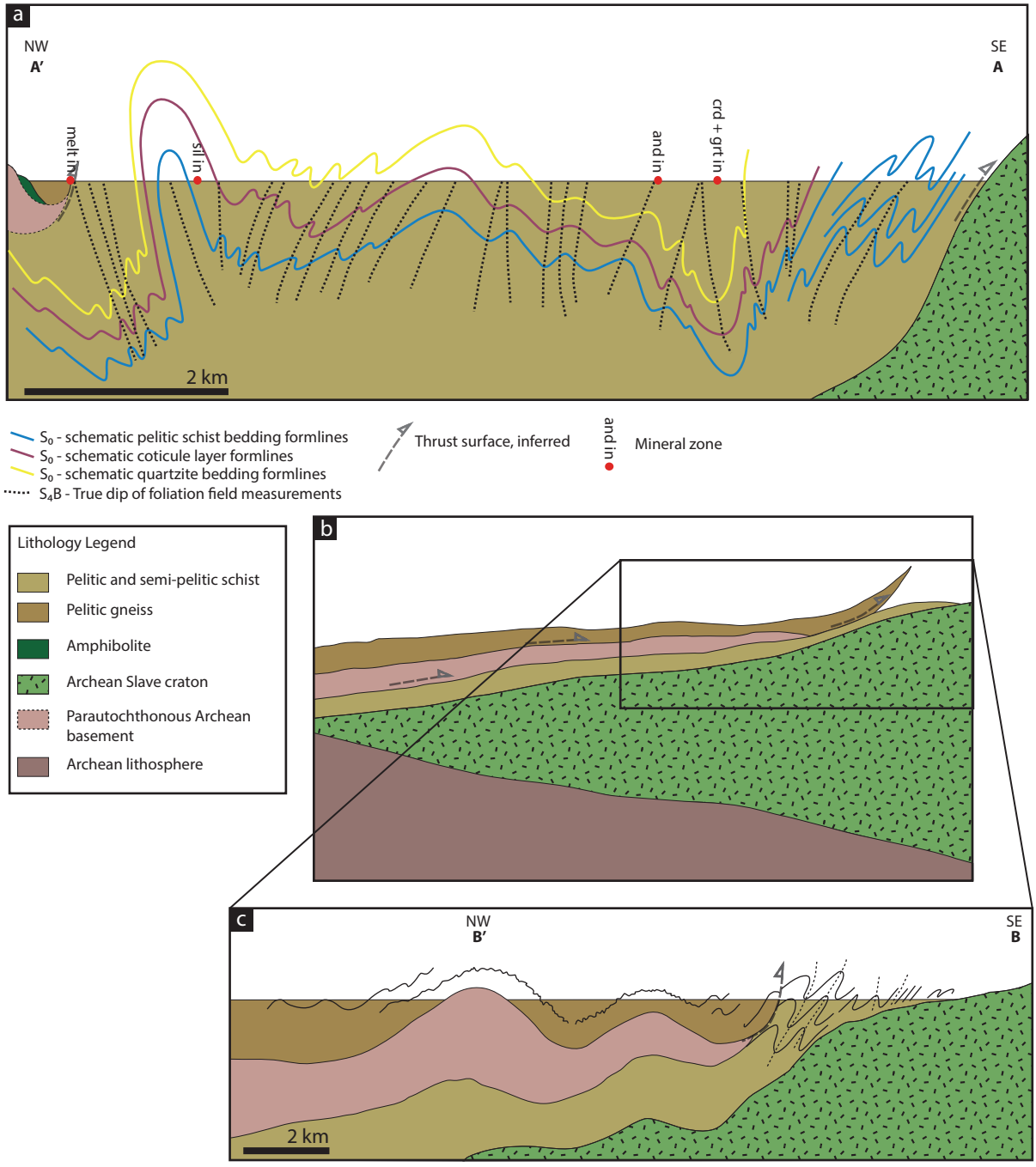


**Figure 3.21 Cross-sections at Brown Water Lake.** Refer to Plates 1 & 2 in Appendix A for cross-section locations and lengths. Sections are schematic. **a)** The northern end of the High Strain belt shows a tightly concertinaed transect of folded supracrustal rocks of the Paleoproterozoic Coronation Supergroup. The true dip of the dominant fabric, $S_{4B}$ has been traced and is axial planar to large km-scale antiforms, synforms and broad hinge zones. The contact between the Slave craton and the metasediments is hypothesized to be a thrust contact, although this is difficult to prove with the current amount of information available. At the NW side, the Archean gneiss dome is represented by a thin, folded sliver with a mantle of Archean amphibolite. Coticule and quartzite occurrences in outcrop were used as the closest approximation to marker bedding. Cross-sections **b)** and **c)** are more schematic than **a)**. A small scale interpretation of the thrust relationship is shown in b), where mobilised, parautochthonous Archean basement has been thrust eastward, back over the Slave craton with a cover of metasedimentary rocks. The inset cross-section c) shows from B to B' the detail of tight, upright to southeast-vergent folds, in contact with pelitic gneisses that may have been transported along with the thrusted Archean basement. The cross-folding effect of the $S_{3B}$ and $S_{4B}$ deformation events may have caused the observed doming of the basement. Section c) is modified from King et al. (1987)

# 4 LITTLE CRAPEAU LAKE

The Little Crapeau Lake area is located ~40 km to the northwest of the Brown Water Lake area (Fig 1.3, 1.5; Appendix A Plate 2). Stratigraphically, sedimentary rocks around Little Crapeau Lake (and neighbouring Grant Lake) are assigned to the Akaitcho group (Easton, 1981). These rocks have been further subdivided and assigned to the Grant subgroup, which correlates with the Zephyr formation and Nasittok subgroup in the northern part of the orogen. The area comprises a basal dolomite sequence, overlain by interbedded pelites, psammites, and metavolcanic rocks. The area is bordered immediately to the west by the Wopmay Fault zone (Fig. 4.1). In the northeast corner, notably between Little Crapeau and Grant Lakes, pelites are crosscut by leucogranite intrusions, collectively named the Little Crapeau sills. Nearby exposed Archean basement forms a large culmination to the northeast. On the west side of Little Crapeau Lake, close to the Wopmay Fault zone, a strongly deformed sliver of Archean granitic gneiss crops out from the basal pelitic sequence. Thick gabbro sills intrude the supracrustal rocks to the south of Little Crapeau and are folded and truncated to the west by the Wopmay Fault zone. These rocks were previously described and mapped in detail by Easton (1981).

Many islands dot the lake, making it easy to pick out punctuated changes in metamorphic grade, though making it difficult to trace a continuous set of metamorphic mineral zones across the area. Isograds drawn on the Little Crapeau Lake map in Appendix A (Plate 2) depicts these zones.

The proximity of the rocks at Little Crapeau Lake to the Wopmay Fault zone likely causes a strong influence on the structural character and deformational history. This can be seen in spot imagery and in regional magnetic survey data (Fig. 4.1, 4.2). Structures, such as the gabbro sills and the Archean culmination are pulled northward or truncated to the west of Little Crapeau Lake.

Apart from the Wopmay Fault, several significant fault structures crosscut this area and have juxtaposed units against one another. To the southeast of the area, a crustal-scsale, regionally traceable NE-SW striking fault appears to have structurally placed the Rodrigues granite against the supracrustal rocks and intrusions around Little Crapeau Lake. Other faults crisscross the area.

At Little Crapeau Lake, chemical composition of the rocks sampled is fairly consistent (Fig. 3.1; Appendix C). Therefore, the metamorphic mineral assemblage is far more dependent on actual pressure-temperature conditions than on variations in bulk composition, as it is at Brown Water Lake.

## 4.1 Lithological Units

### *4.1.1 Pelitic Schists*

The majority of rocks at Little Crapeau Lake are a chemically homogenous group of pelitic schists (Fig. 3.1, 3.2; Appendix C). The lowest grade pelitic rocks are gray to brown weathered phyllites, finely laminated to bedded (~3 cm), and are devoid of porphyroblasts (Fig. 4.3). Rare interbeds are more quartz-rich. A distinct package of the gray metasediments crops out on the northeast side of the big island, and is especially rhythmic in its bedding frequency and thickness (Fig. 4.3 a). It is traceable across a few islands, including locations 1529, 2562, and 2564 (Appendix A Plate 2). In this unit, normal grading shows younging to be upwards toward the southwest. At this low grade, bedding does not show outcrop scale folding, but consistently dips shallowly to moderately southwestward.

Beyond the central island, pelitic schists largely contain abundant andalusite porphyroblasts (Fig. 4.4). Andalusite zone schist is the next and highest grade of metasedimentary rock directly observed in the area, and is the widest. Andalusite porphyroblasts range from small (~3 mm)

and anhedral, to large (up to 4 cm) euhedral, pink to dark gray, prismatic and sometimes elongate (up to 10 cm) crystals. Chiastolite is noted in a few locations. In some samples the porphyroblast show evidence of retrograde metamorphism, by replacement with very fine grained muscovite along fractures in the grains, and of entire porphyroblasts. Matrix material is gray to brown biotite + muscovite schist. Biotite and muscovite folia are well developed along the main foliation, and often intensely crenulated and folded.

The andalusite schist often contains anhedral relicts of cordierite porphyroblasts that are replaced with cryptocrystalline aggregates of sericitic material or isotropic orange-brown discolouration (pinite). These aren't readily visible in outcrop as they are usually spatially associated (wrapped) with much larger andalusite grains, are strongly replaced by fine grained muscovite and chlorite, and are very small (<3 mm). In this map area, no distinct cordierite zone has been recognized, as cordierite appears with andalusite in all cases. However textural relationships show it to have grown before andalusite (Fig. 4.5, 4.6).

Inclusion trails in both andalusite and cordierite are defined by biotite + quartz + plagioclase. They are curved, continuous, and preserve fabrics overgrown during prograde metamorphism.

Garnet porphyroblasts are also present in some rocks or beds with slightly elevated manganese levels (Fig. 3.1, 3.2). These garnets are sub-mm, pink to red, and euhedral (Fig. 4.7). These are nearly too small to be viewed in outcrop. No garnet zone is recognized in this area. Mineral chemistry shows garnets to be slightly elevated in Fe and Mn, although bulk rock chemistry does not show much variation between rocks that have grown garnet and those that have not (Fig. 3.1; Appendix C).

Easton (1981) mapped a staurolite isograd, which has not been recognized nor observed during this study. It is not believed to exist. In the field, outcrop at station 2562 was thought to contain

staurolite showing penetration twinning, however in thin section these were found to be cordierite porphyroblasts.

Sillimanite schist was also described to the east and northwest of Little Crapeau Lake, as well as gneissic/melt-in rocks that show muscovite breakdown, and migmatitic textures (Easton, 1981). These were not directly observed in this study.

### *4.1.2 Intrusive Rocks*

Throughout the Little Crapeau Lake area, sills and dykes of various sizes intrude the metasediments and preserve pervasive fabrics that provide relative timing constraints on deformation events (Fig. 4.8, 4.9). Collectively these leucogranitic intrusions are called the Little Crapeau sill. It is a weakly foliated, medium to coarse grained, white to gray, garnet-bearing biotite muscovite granite. The granite is fairly homogenous and intrudes the metasediments to the north and east of Little Crapeau Lake. Where it is observed to intrude the metasediments, the unit forms >50 cm thick sills, and away from the main body appears as cm-scale dykelets. Minor recrystallization is seen in quartz subgrains. Biotite and muscovite are in equal abundance, and do not appear foliated in thin section. However in a few locations the dykelets do have a weak foliation defined by micas. Garnet porphyroclasts are pink, euhedral, nearly devoid of inclusions, 1.5 mm in diameter, and comprise <2% of the rock.

At the north end of the lake the Little Crapeau sill was sampled (locations 1550 and 1552, Appendix A Plate 2) for geochronological analysis and returned a U-Pb zircon crystallization age of 1877 ± 2 Ma. The sill is locally extensive, and has been intruded parallel to the second generation foliation, discussed in section 4.2. It is boudinaged in this orientation, and is folded by subsequent deformation events (Fig. 4.8 b).

Significant structural and metamorphic relationships were interpreted from the granite sills in this area, as the crystallization age and structural fabrics have enabled extrapolation of relative timing of heating and deformation events.

Large gabbro sills have been documented in the area, mainly to the southwest of the lake. These are thick, folded sequences that have been given a crystallization age of 1870 Ma, and have been correlated with the Morel sills, a mafic dyke network documented in the northern half of the orogen (Jackson et al., 2013).

#### *4.1.3 Carbonate*

A thin, basal veneer of marble has been mapped in the area, and was observed to the northwest of the lake, with interbedded serpentinite-bearing (chrysotile) layers.

#### *4.1.4 Archean Gneiss Dome*

The Archean culminations extend as far west as the Little Crapeau and Grant Lakes area. A U-Pb zircon crystallization age of 3.0 Ga was acquired for the culmination to the northeast of Grant Lake, with a U-Th recrystallization age of 1877 ± 2 Ma (Jackson et al., 2013).

## 4.2 Structural Fabrics

At Little Crapeau Lake five generations of deformation have been recognized and documented, both in outcrop, hand sample and in thin section. These have been plotted on equal area stereonets, and divided into two structural domains for the area (Fig. 4.10, 4.11, 4.12). The structural domains are the Eastern domain and Wopmay Fault high strain zone, bisecting the lake into halves. Structures and fabrics on the east side of the bisecting line (Fig. 1.5; Appendix A Plate 2) are well preserved, are both steeply and shallowly dipping, and show many generations of overprinting deformation phases. Fabrics on the western side of the lake appear

to be strongly affected by the Wopmay Fault zone, which has rotated steep fabrics into a more N-S orientation.

### *4.2.1 $S_{0C}$*

Bedding at Little Crapeau Lake is southwest dipping and southeast striking in the Eastern structural domain. It is not well constrained in the Wopmay Fault high strain zone. Younging direction has been documented in two locations, showing bedding to be upright and younging to the southwest. $S_{0C}$ was not measured as frequently at Little Crapeau Lake as at Brown Water, as it is not well preserved. The best preservation of bedding is seen in the lowest grade rocks which are located on the large central island.

### *4.2.2 $S_{1C}$*

This fabric has been observed inside cordierite and andalusite porphyroblasts, but is not seen very frequently (Fig. 4.5, 4.6). It is preserved as quartz-biotite inclusion trails inside these porphyroblasts, mainly observed in samples from the east side of Little Crapeau Lake. Where it was possible to measure $S_{1C}$, it consistently appears to be dipping shallowly to moderately in the opposite orientation to $S_{2C}$.

### *4.2.3 $S_{2C}$*

The $S_{2C}$ foliation was a steeply NNW-dipping, WSW-striking fabric, that may have transposed bedding into a steep orientation, but not likely developed parallel to it. It is observed mainly inside porphyroblasts and is preserved in strain shadows (Fig. 4.5, 4.6). It is tightly folded by a shallow, strongly crenulating $S_{3C}$. $S_{2C}$ is a well developed fabric, defined by biotite and muscovite. Granite sills and veinlets intrude parallel to $S_{2C}$ and are also folded by $S_{3C}$ (Fig. 4.9). Both meso- and macroscopically the granite deforms into large open folds. As seen in Figure 4.6, andalusite has overgrown developing $S_{1C}$ and $S_{2C}$ as the matrix grains coarsened.

#### *4.2.4 $S_{3C}$*

$S_{3C}$ is the dominant fabric at Little Crapeau Lake. It is a moderately SW-dipping cleavage. It is strongly developed and defined by biotite and muscovite. It tightly folds the preceding $S_{2C}$ fabric, and is itself steepened by a strong, NNW-striking $S_4$, but not strongly deformed by it. $S_{3C}$ folds the granite sill at all scales.

#### *4.2.5 $S_{4C}$*

This steep, NNW-striking fabric overprints $S_{3C}$ at a shallow intersection. Its strike is nearly the same orientation as $S_{3C}$, as the latter was transposed and steepened by it. Towards the west side of the lake, it is rotated slightly into a more N-S orientation. In thin section, it is defined by biotite and muscovite folia. In outcrop, it is observed as a strong cleavage, a folding event, a boudinaging event, and a crenulating phase (Fig. 4.4, 4.8).

#### *4.2.6 $S_{5C}$*

This is the final stage of strong deformation recognized at Little Crapeau Lake. It is not has pervasive and ubiquitous as $S_{4C}$, but it does form a strong $F_{5C}$ fold phase in some locations (Fig. 4.4, 4.8, 4.13). The $S_{5C}$ fabric is a steeply dipping, NNE-striking foliation.

## 4.3 Mesoscopic and Macroscopic Structure

On the regional scale, two structural domains dominate the Little Crapeau Lake area (Fig. 4.10, 4.11, 4.12). Rocks of the Eastern domain are deformed by a steeply ENE-dipping, NNW-striking fabric, $S_{4C}$, that has strongly transposed and steepened all units and preceding fabrics. The orientation of this fabric has influenced the shape and elongation of the land and islands. In this domain all five generations of deformation can be observed in outcrop, hand sample or in thin section as they are well preserved.

The Wopmay Fault high strain zone comprises rocks of the islands and mainland on the west side of the lake. The boundary of this structural domain bisects the lake and comprises rocks of the western half, truncated to the west by the Wopmay Fault zone. These rocks have been intensely affected by long-lived activity on the crustal-scale fault. Strain partitioning has ductilely reoriented $S_{4C}$ and $S_{5C}$ fabrics into a more North-South orientation (Fig. 4.11, 4.12). Intersection lineations of local foliations demonstrate this reorientation (Fig. 4.12). There is very little evidence for earlier fabrics preserved in these rocks.

The axial trace of antiforms and synforms on the western side of the lake show regional fold wavelength to be on the order of ~500 m. These were identified by inference from bedding to cleavage asymmetries. In outcrop bedding forms tight asymmetric folds, often with boudinaged limbs.

On the lake scale, bedding is shallow and folded by multiple phase of deformation, although most bedding is observed to dip shallowly to moderately SW (Fig. 4.14). Bedding is locally steep, where it is most likely steepened by $S_{4C}$ or $S_{5C}$. Toward the NNE corner of the map area, the overprinting influence of the strongest fabrics $S_{3C}$ and $S_{4C}$ is noted in the steepening of bedding and the Little Crapeau Sill dykes and dykelets. Outcrop-scale folds in pelitic schists display a complex geometry (Fig. 4.8, 4.9), where rocks of some areas (i.e. station 1540, Fig. 4.13 b) have been overprinted by the latest deformation event, $S_{5C}$, and other rocks only a few meters away have been affected only by $S_{4C}$. At station 2565 (Appendix A Plate 2) leucogranite dykelets, intruded parallel to $S_{2C}$, are folded and refolded by $S_{3C}$ and $S_{4C}$, respectively, into tight isoclinals folds (Fig. 4.8 b).

## 4.4 Metamorphism

At Little Crapeau Lake, aluminosilicate metamorphic minerals show a similar prograde sequence to rocks at Brown Water Lake over a distance of 2-3 km. Metamorphic grade ranges from chlorite zone schist, to biotite zone schist, through andalusite ± cordierite schist, with minor garnet-bearing units. The lowest grade rocks are found on a ~3 km long island in the middle of Little Crapeau Lake (at stations 2527, 2528 Appendix A Plate 2). The grade increases northward and northeast of this island, with isograds appearing folded, increasing to the highest grade rocks to the north and northeast, approaching a large Archean gneiss dome. Lithology and isograds are truncated to the west by the Wopmay Fault zone (Fig. 4.1, 4.2).

The lowest grade rocks in the sequence contain <1% chlorite in small clumps distributed in a qtz + plg + bt finely laminated matrix. Within 1.2 km of these rocks, cordierite and andalusite porphyroblasts ± garnet appear, and these are abundant in the rest of the rocks to the north and northeast.

Cordierite appears to have grown before andalusite. Grains are anhedral and pinnitized (Fig. 4.6 a). Andalusite is euhedral to subhedral and generally grows in cordierite grade rocks. Dissimilarly to rocks at Brown Water Lake, garnet also occurs in cordierite-andalusite rocks (Fig. 4.7 c). Garnets are euhedral to subhedral, pinkish red, and are <1mm in diameter. They occur scattered throughout the matrix of some rocks, and in others they are restricted to certain bedding layers (Fig. 4.7 a).

In most rocks these porphyroblasts sit in a matrix of qtz + plg + bt + ms. The micas form a strong foliation which wraps the porphyroblasts, providing evidence for timing of growth (Table 4.1).

### *4.4.1 Isograds*

The isogradic surfaces observed at Little Crapeau Lake reflect a domed/folded geometry, with lowest grade, sub-biotite zone rocks in the middle, and highest grade sillimanite zone rocks on the outer perimeter (Appendix A Plate 2). The upper boundary of the chlorite and biotite zone rocks is well defined, and grades immediately in to pelitic schists bearing large euhedral andalusite porphyroblasts. The isogradic surface representing the initiation of cordierite growth is not easily traceable, as andalusite is randomly associated with cordierite throughout the area. Metamorphic assemblages above the biotite zone appear controlled by composition and so it is difficult to draw a surface representing the cordierite-in and andalusite-in reaction. The same can be said for the garnet-in reaction – garnet porphyroblasts are found in some of the pelitic schists, but are not part of a traceable zone or package of rocks.

The isograds appear to have been folded post-$S_{2C}$, and likely syn-$S_{4C}$, a phase of strong regional folding. Peak metamorphism coincides with the growth of andalusite, and is likely post-$S_{2C}$ to syn-$S_{3C}$, and therefore the folding of the isograds must have occurred after this third deformation phase.

| **Porphyroblast phase** | **Timing of growth** |
|---|---|
| Chlorite/Biotite | |
| Garnet | Pre-cordierite(?) and pre-andalusite growth |
| Cordierite | Syn to post-$S_{1C}$, pre-$S_{2C}$ |
| Andalusite | Post-$S_{1C}$, up to syn to post-$S_{2C}$ |

**Table 4.1** Summary of metamorphic mineral paragenesis

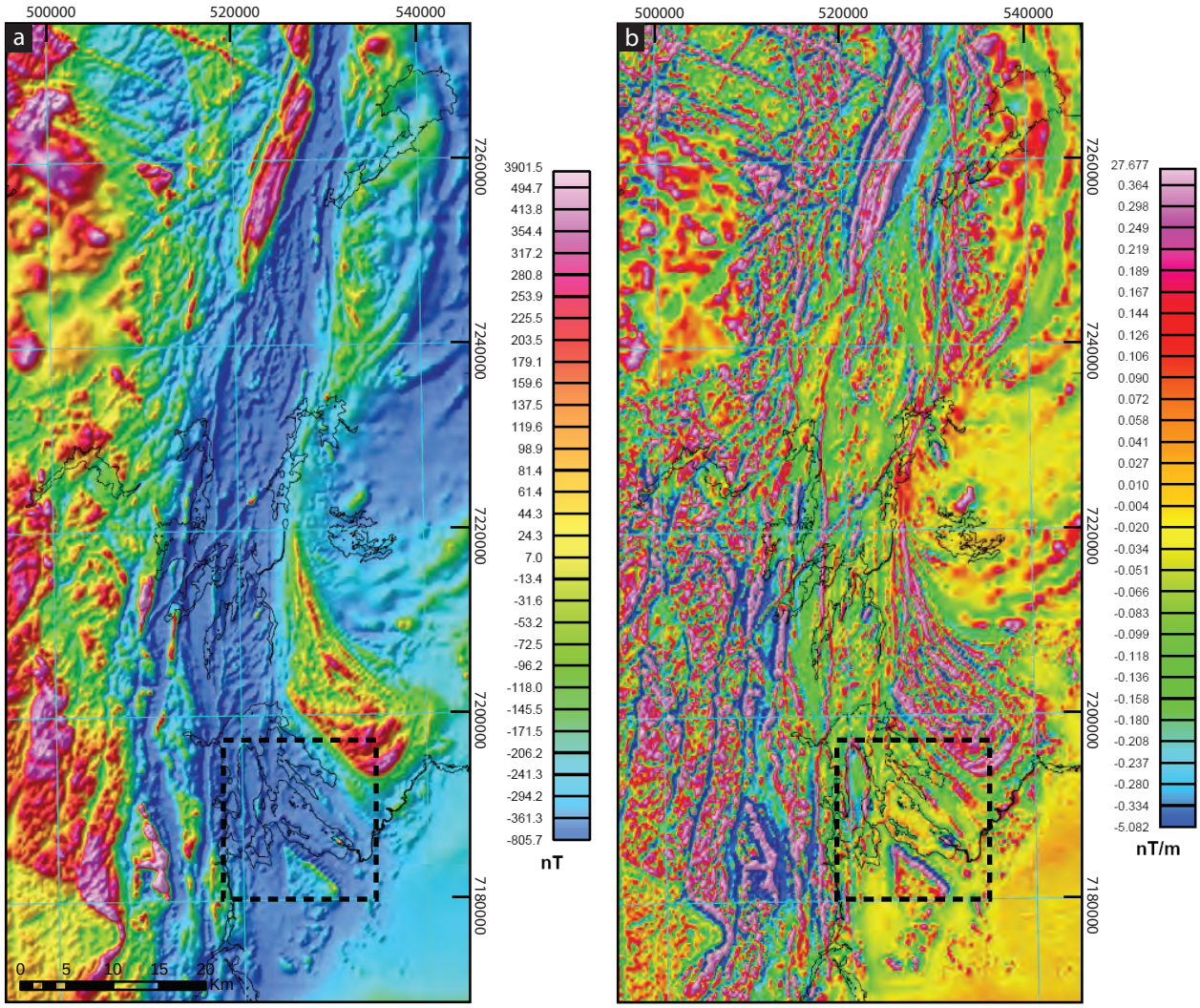


**Figure 4.1 Magnetic maps covering the western Metamorphic Internal zone at the boundary of the Wopmay Fault zone. a)** Residual total magnetic field; **b)** First vertical derivative of the magnetic field. The intense influence of the Wopmay Fault zone (north-south dark blue zone) can be seen in these airborne magnetic maps that cover the Little Crapeau Lake map area (dashed outline). The Archean basement culmination appears 'dragged' northward into the fault zone. The same strong influence is documented at the meso- and microstructural scale in metasedimentary rocks and local intrusions, where structural fabrics are steepened and reoriented into a more north-south orientation. (Hayward & Oneschuk, 2011).

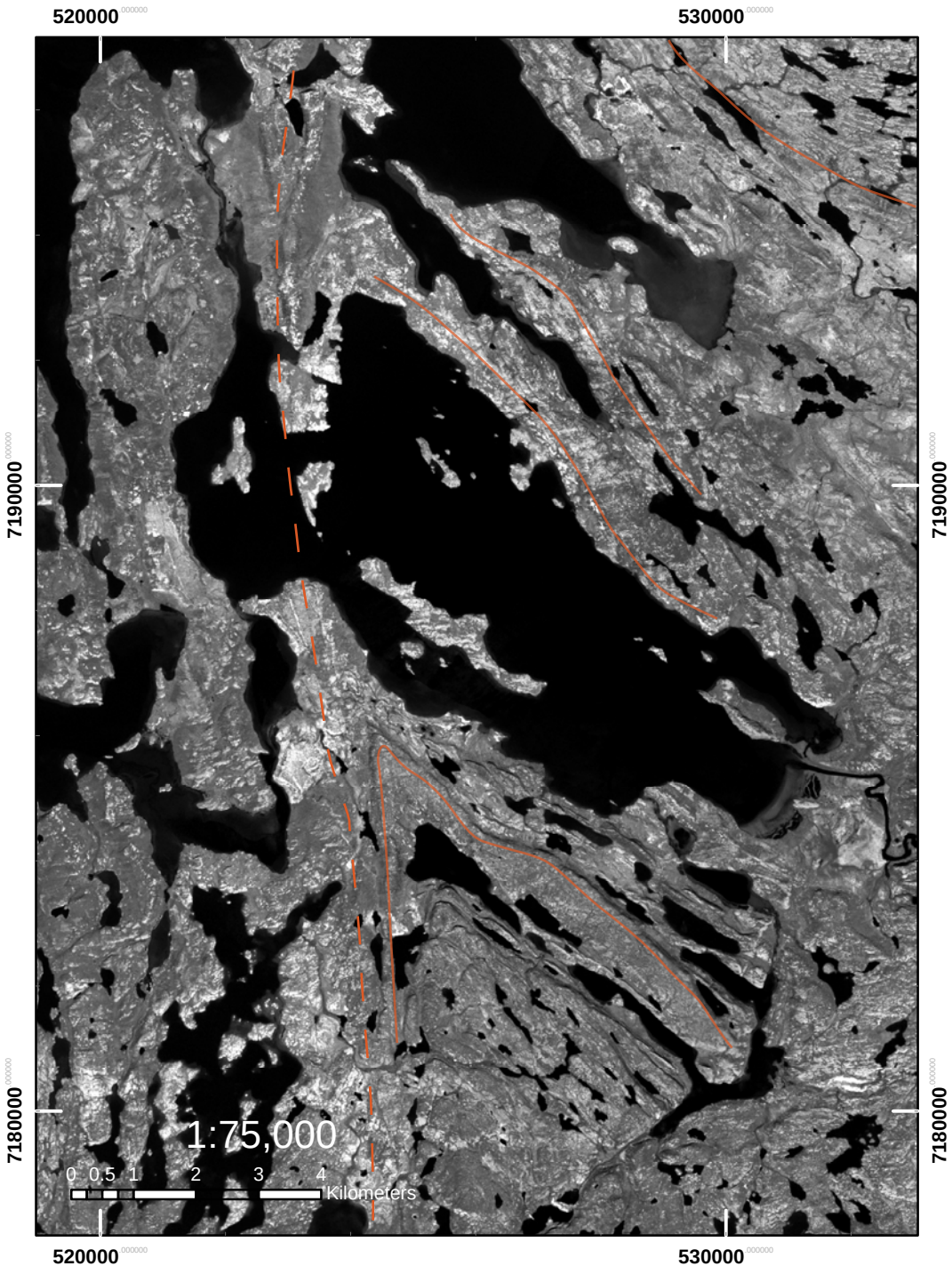


**Figure 4.2 Spot imagery for the Little Crapeau Lake map area.** The appearance of geological features are is enhanced in this image. Outlined by the solid orange line are folded gabbroic sills, which are truncated to the west by the Wopmay Fault zone (dashed orange line) and to the southeast by a late regional fault. In the northeast corner is the Archean basement culmination. In this map area, the orientation of the main kinetic structures does not allow for visible folds in plan view, with the exception of the folded gabbro sills. The dominant fabrics are NW-SE trending.


**Figure 4.3 Low grade pelitic schists from Little Crapeau Lake. a)** Rhythmic bedding shows topping direction in normal graded bedding in biotite schist. Beds dip moderately to the southwest. Magnet tip points North. **b)** Multiply-deformed biotite schist shows many generations of folding and overprinting crenulations. $S_{4C}$ is the axial planar fabric to this open fold in outcrop. **c)** Very low grade metapelite with shows alternating gray and rusty brown mm-scale bedding.

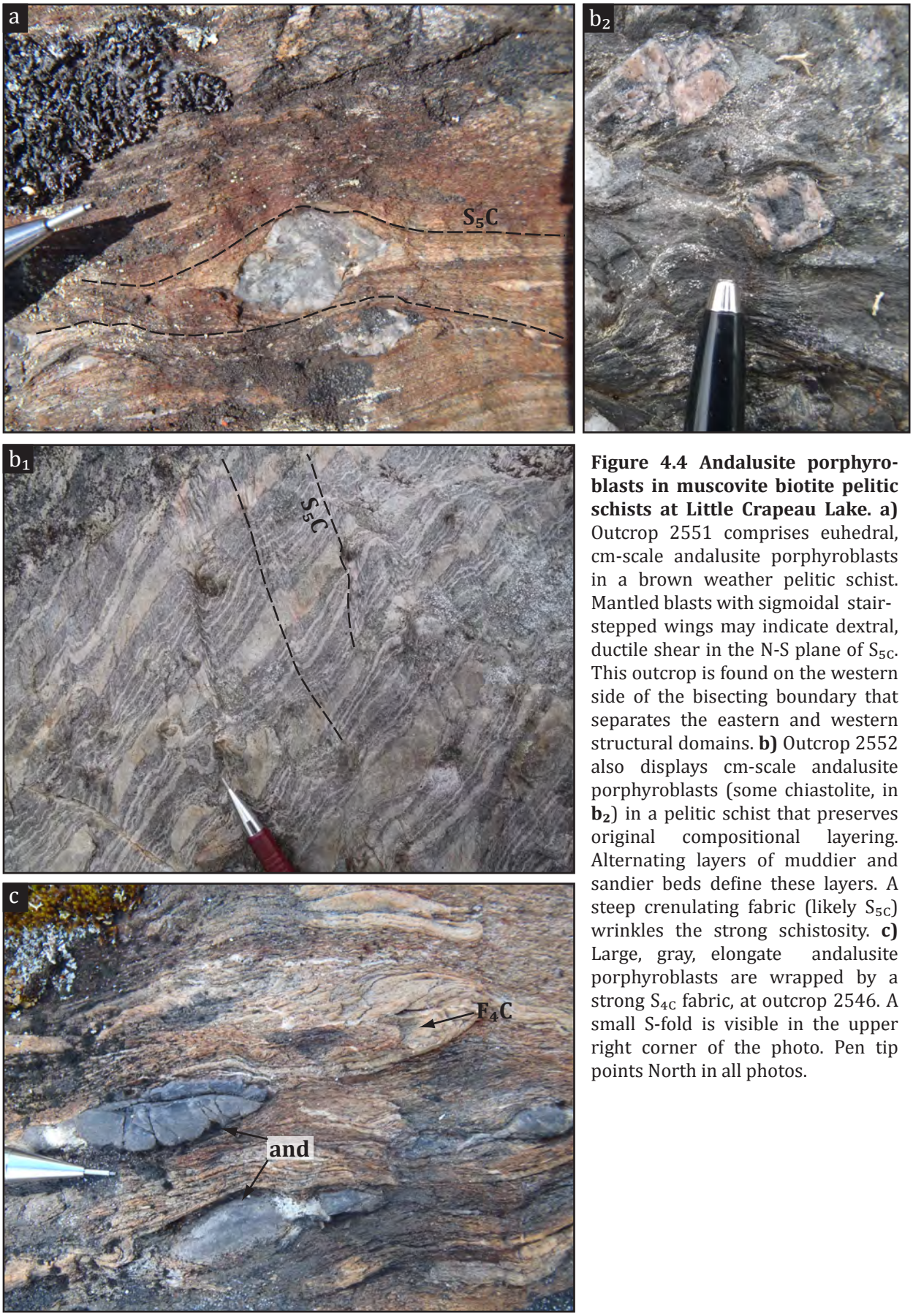


**Figure 4.4 Andalusite porphyroblasts in muscovite biotite pelitic schists at Little Crapeau Lake. a)** Outcrop 2551 comprises euhedral, cm-scale andalusite porphyroblasts in a brown weather pelitic schist. Mantled blasts with sigmoidal stair-stepped wings may indicate dextral, ductile shear in the N-S plane of $S_{5C}$. This outcrop is found on the western side of the bisecting boundary that separates the eastern and western structural domains. **b)** Outcrop 2552 also displays cm-scale andalusite porphyroblasts (some chiastolite, in **$b_2$**) in a pelitic schist that preserves original compositional layering. Alternating layers of muddier and sandier beds define these layers. A steep crenulating fabric (likely $S_{5C}$) wrinkles the strong schistosity. **c)** Large, gray, elongate andalusite porphyroblasts are wrapped by a strong $S_{4C}$ fabric, at outcrop 2546. A small S-fold is visible in the upper right corner of the photo. Pen tip points North in all photos.

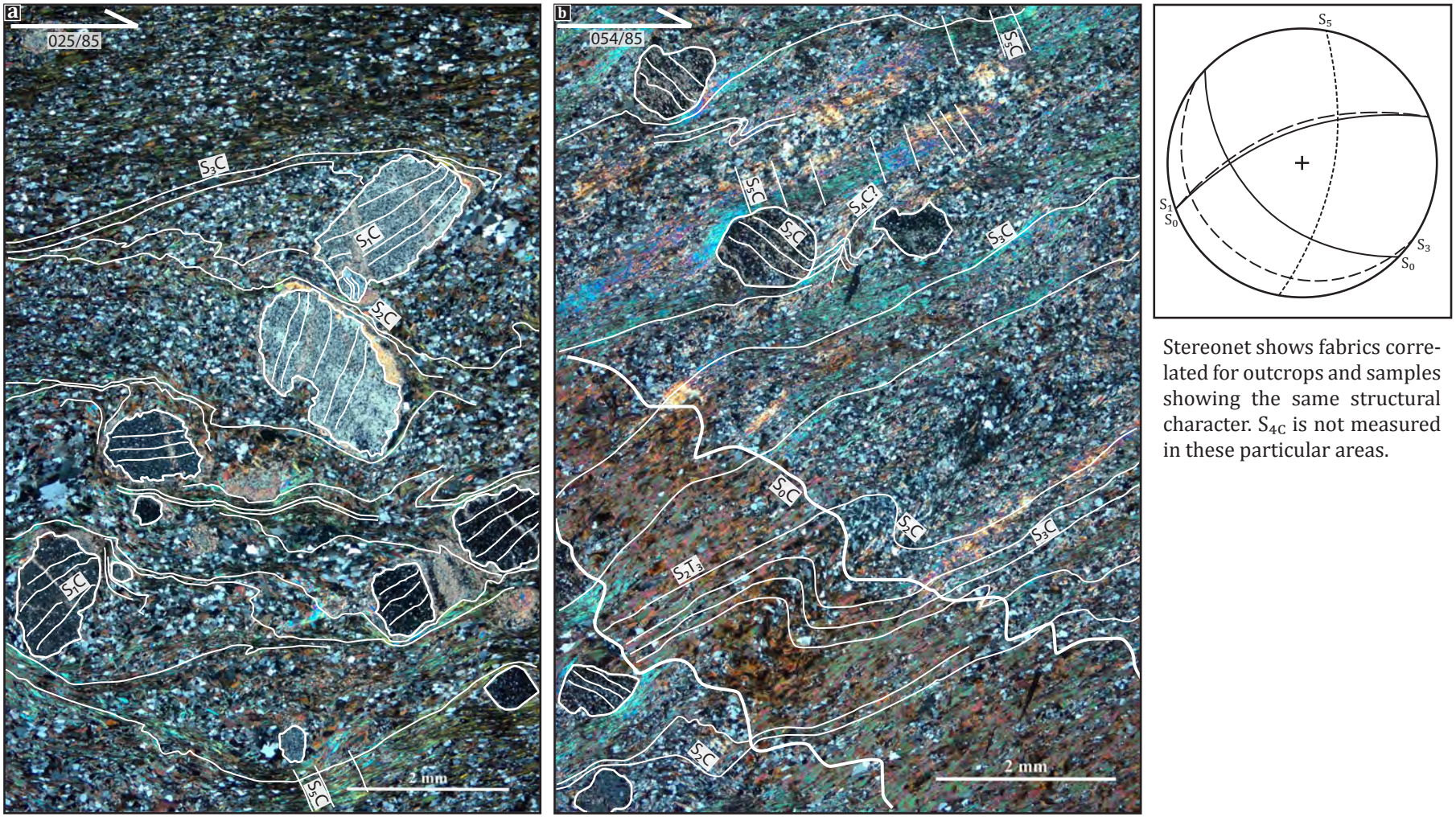


Stereonet shows fabrics correlated for outcrops and samples showing the same structural character. $S_{4C}$ is not measured in these particular areas.

**Figure 4.5 Andalusite and cordierite biotite muscovite schists from Little Crapeau Lake.** Sample 2562a **(a)** shows andalusite and cordierite porphyroblasts that overgrow and preserve $S_{1C}$ defined by straight quartz inclusion trails. $S_{2C}$ is preserved in the strain shadows around porphyroblasts, and is seen to be transposed by $S_{3C}$ into a more flat-lying orientation. Where the strongly developed $S_{3C}$ creates thick bands of biotite and muscovite folia, $S_{5C}$ can be seen overprinting it as a gentle crenulation. Bedding is preserved in sample 1540C **(b)**, defined by the thick alternating layers of biotite-rich and quartz-rich rock. $S_{2C}$ is preserved inside anhedral cordierite porphyroblasts. The $S_{3C}$ foliation is transposed and steepended into $S_{4C}$ $(S_3T_4)_,$. In some locations folded $S_{3C}$ is preserved in between $S_{4C}$ folia. Both fabrics are defined by biotite and muscovite. Cordierite porphyroblats are wrapped by the strongly developed $S_{4C}$ foliation, which is gently crenulated in some areas by the steeply west-dipping $S_{5C}$.

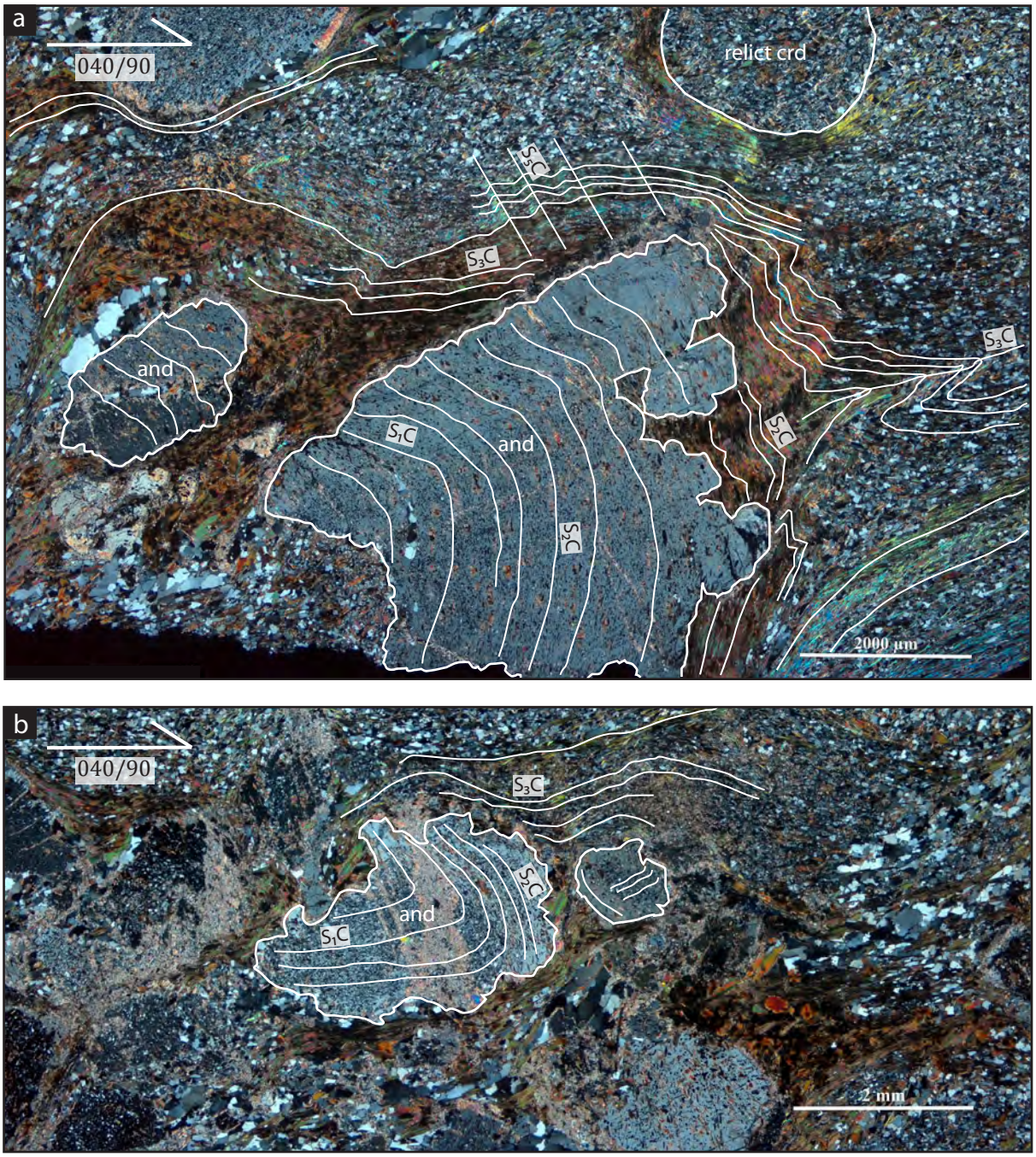


**Figure 4.6 Section 2562D shows andalusite porphyroblasts overgrowing early fabrics.** Andalusite porphyroblasts overgrow a coarsening quartz + plagioclase + biotite + muscovite matrix. $S_{1C}$ is steepened into $S_{2C}$, which is in turn flattened by SW-dipping $S_{3C}$, defined by a strong biotite muscovite foliation. $S_{5C}$ crenulations overprint the strong $S_{3C}$ folia. Andalusite likely grew after the development of $S_{1C}$, and continued during $S_{2C}$ development. In this sample and at this angle, cordierite does not preserve any fabrics.

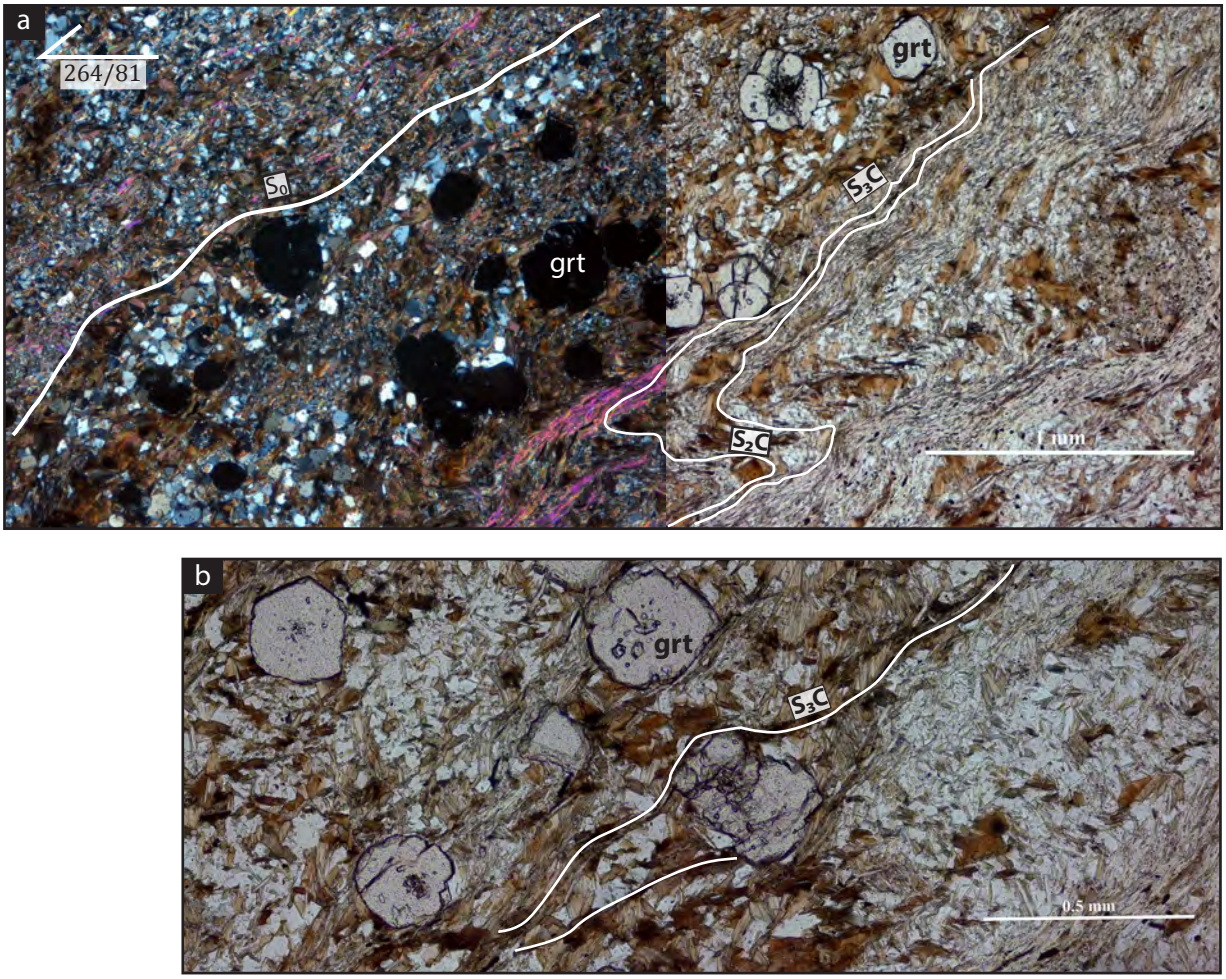


**Figure 4.7 Textural garnet relationships in biotite muscovite schist. a)** & **b)** Sample 1540D shows garnet porphyroblats confined to bedding layers and wrapped by the $S_{2C}$ fabric. This indicates that garnet grew prior to the development of $S_{3C}$. **c)** Sample 2565A shows textural relationships that suggest garnet porphyroblasts grew prior to andalusite growth. Andalusite overgrows $S_{1C}$ in nearby rocks, which indicates that garnet growth may have been quite early in the history of metamorphism (section is unoriented).

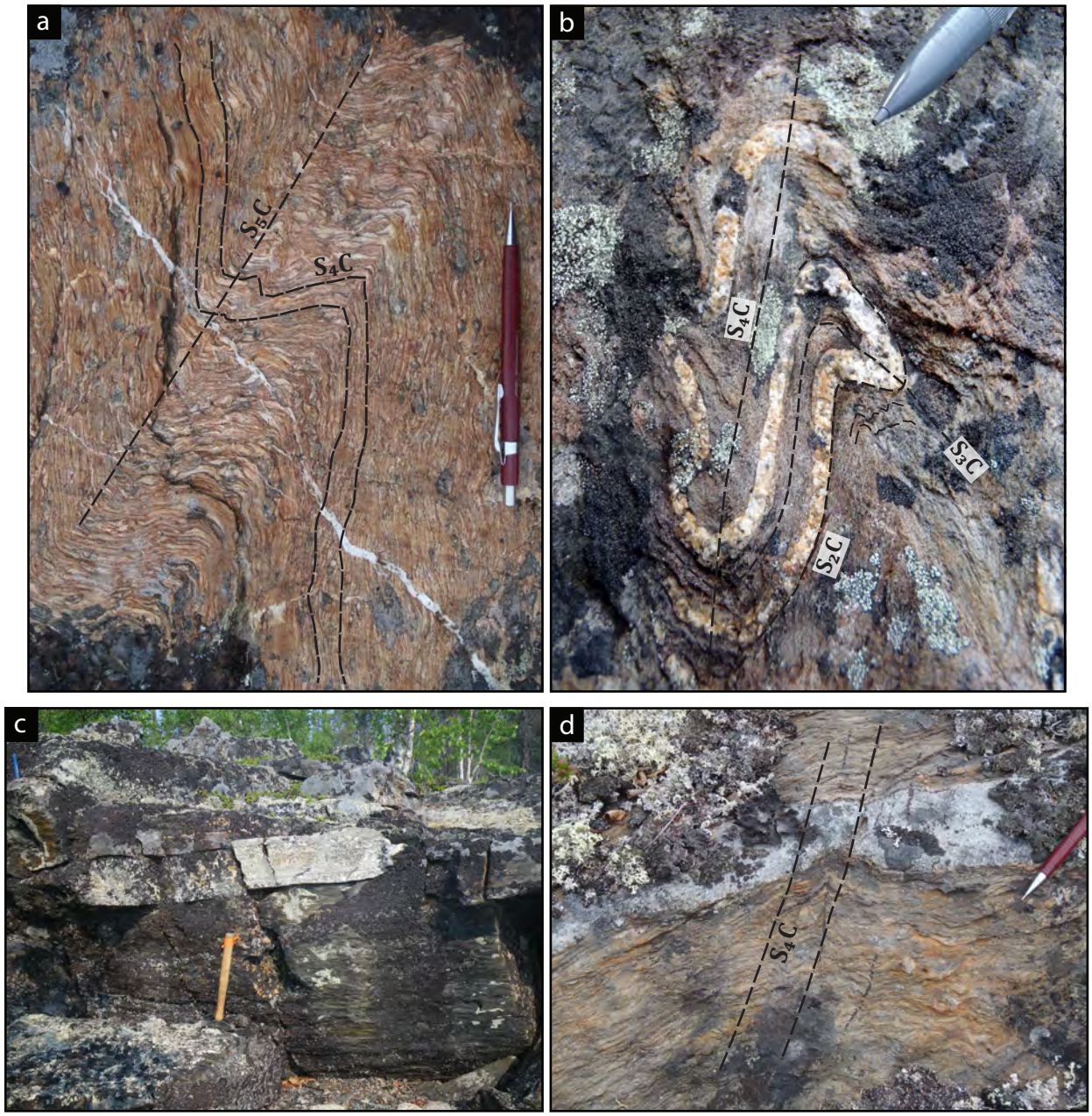


**Figure 4.8 Folds, refolded folds, and the Little Crapeau sill. a)** Low grade chlorite biotite muscovite schist at outcrop 2561 is strongly foliated by $S_{4C}$, and is overprinted by an $F_{5C}$ fold phase. The outcrop is crosscut by late quartz veins. **b)** Andalusite zone pelitic schist is intruded by leucogranite veinlets which were emplaced parallel to $S_{2C}$. These were folded and refolded by two subsequent deformation events, likely $S_{3C}$ and $S_{4C}$ in this location. **c) & d)** The biotite muscovite ± garnet granite Little Crapeau sill is folded and boudinaged at many scales. In **c)** it is flatlying, parallel to $S_{2C}$ and to $S_{3C}$. In **d)** it is crosscut by the $S_{4C}$ foliation. Hammer for scale. Pen tip points North.

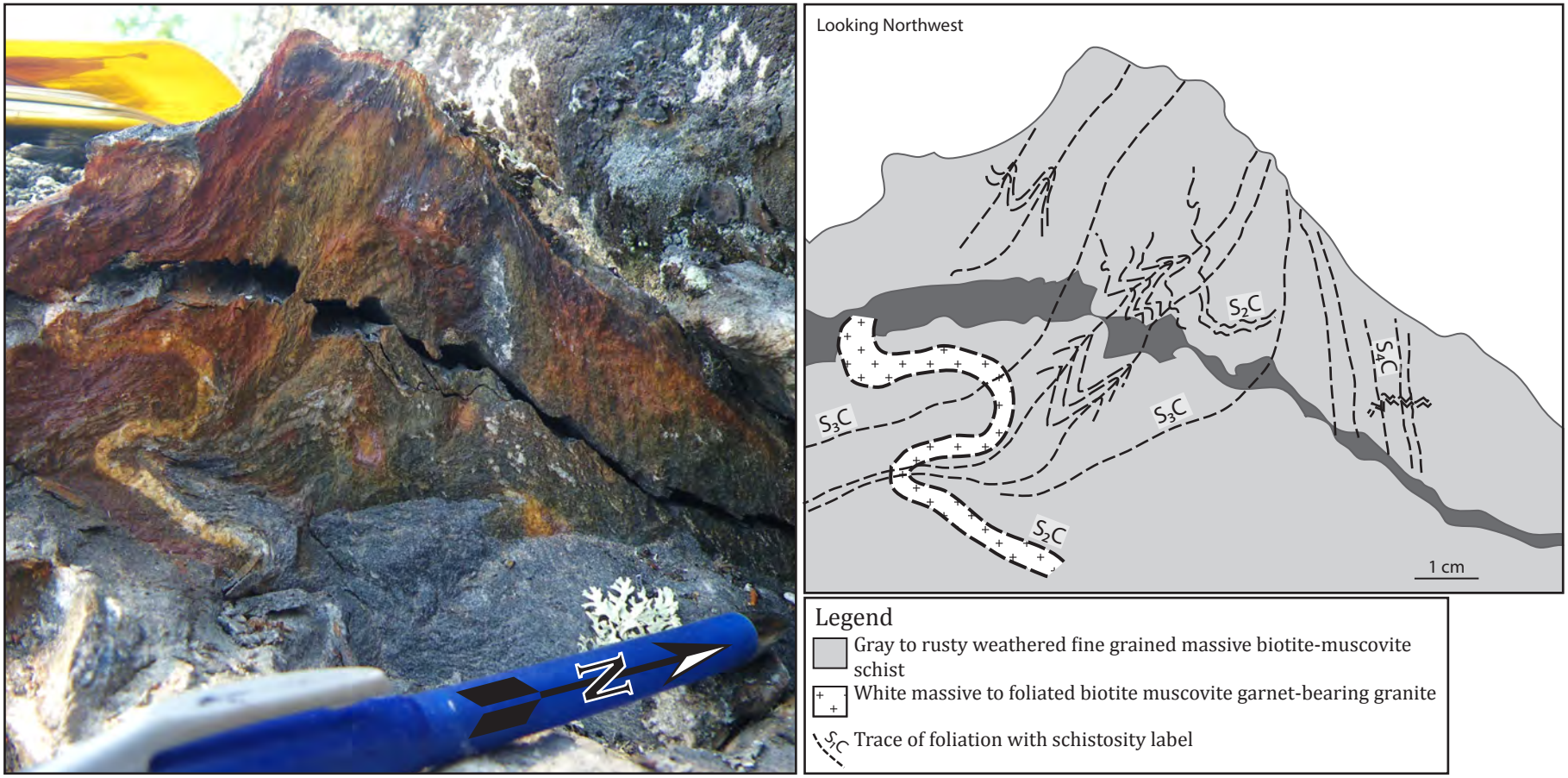


**Figure 4.9 Outcrop photo from station 1534.** A strongly developed, steeply dipping $S_{3C}$ is axial planar to tightly folded and steeply dipping to $S_{2C}$ foliation. On the regional and mesoscopic scale, leucogranite sills and dykes of varying thickness intrude parallel to $S_{2C}$ and are folded by $S_{3C}$. This granite phase has been dated at 1877 $\pm$ 2 Ma. The $S_{3C}$ foliation is anastomosing as it is steeply overprinted by $S_{4C}$ in the orientation of this photo. $S_{4C}$ is a crenulating cleavage, at times strongly developed, as on the right side of the photo where it tightly crenulates $S_{3C}$. $S_{0C}$ is not visible in this outcrop. Pen for scale, tip points north.

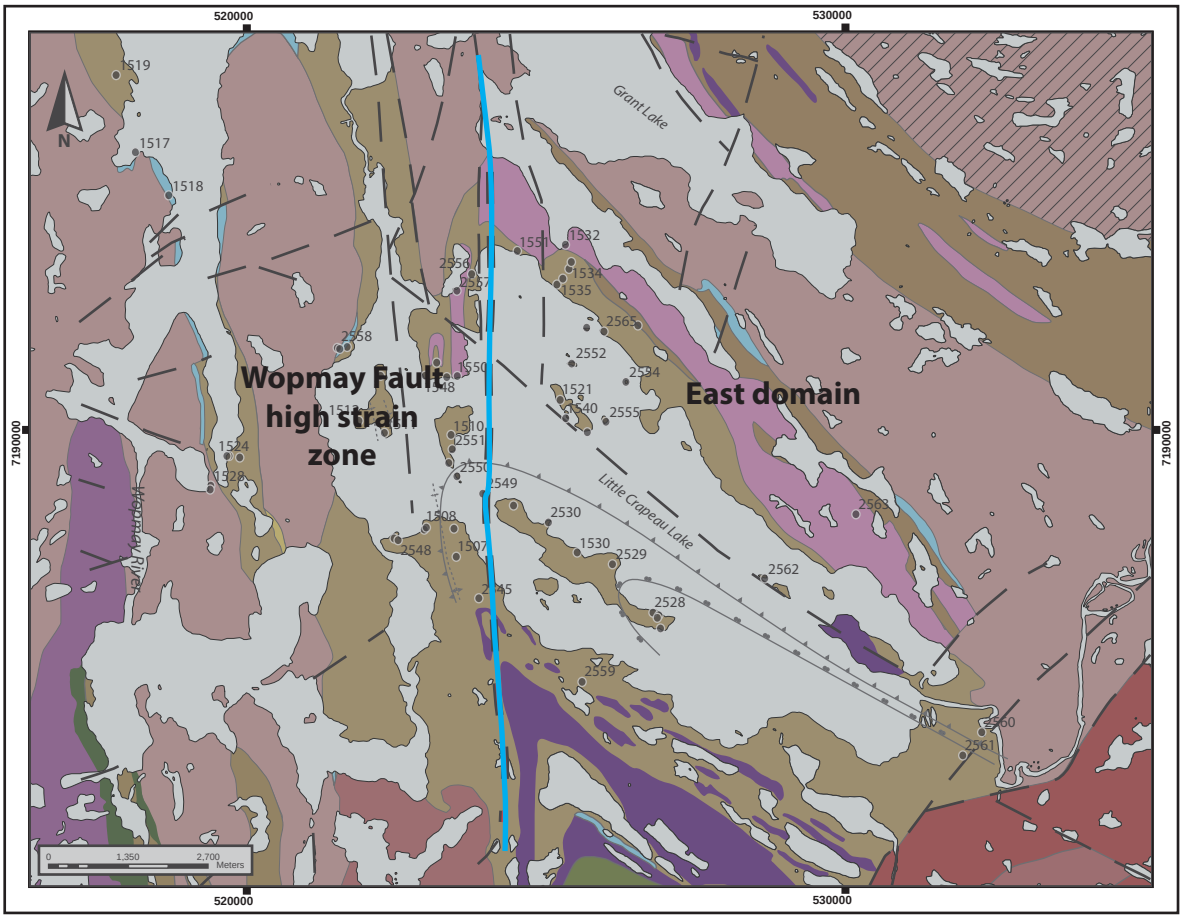


**Figure 4.10 Structural domains of Little Crapeau Lake.** The Little Crapeau Lake area can by divided into two main structural zones: East domain, and the Wopmay Fault high strain zone. Rocks in the East domain preserve many generations of deformation and early fabrics, while rocks west of the bisecting line are strongly influenced by ductile and brittle displacement that has occurred along the Wopmay Fault zone. Fabrics on the western side of the lake are steepened and dragged into a north-south orientation.

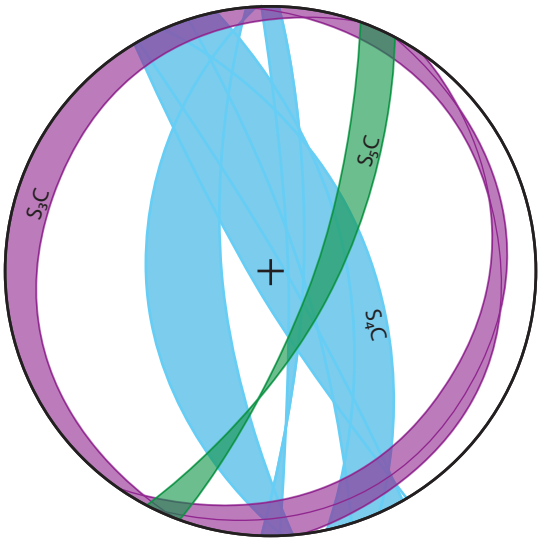


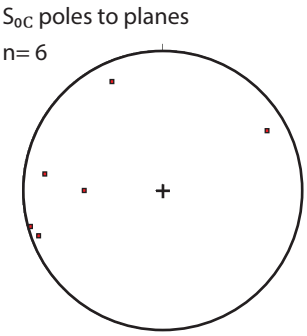


**a)** West side of Little Crapeau Lake, "Wopmay Fault High strain zone"

$S_{2C}$ was not observed in outcrop on this side of the lake. In hand sample it appears to be a moderately east-dipping enveloping surface, folded tightly by a very shallow, strong micaceous $S_{3C}$ foliation. In the western structural domain $S_{3C}$ is more of a horizontal plane than to the east. $S_{4C}$ is steep and NNW-SSE striking, folding $S_{3C}$ into gentle open folds that plunge gently SSE. $S_{5C}$ is an overprinting fabric observed less commonly. On this side of the lake, $S_{4C}$ is very strong, and slightly rotated towards the north. This is due to the influence of the Wopmay Fault zone immediately to the west.

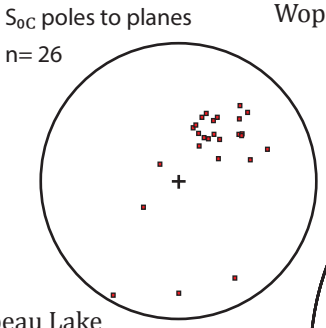


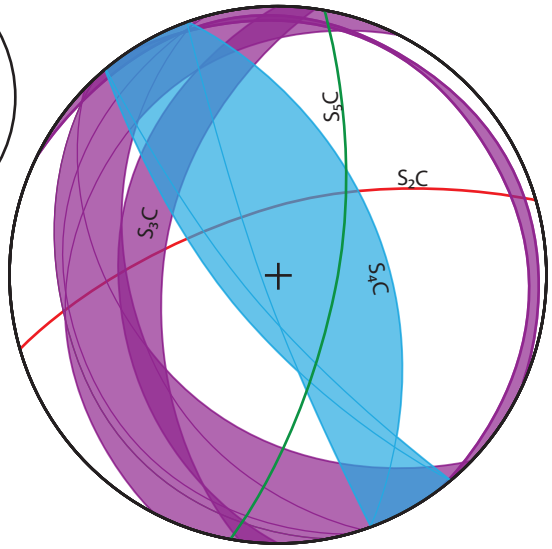


**b)** Eastearn domain of Little Crapeau Lake

$S_{1C}$ is not visible in outcrop, and barely seen in thin section. One oberserved instance from thin section 2565A shows $S_{1C}$ to be more shallow dipping than $S_{2C}$, however it needs to be measured elsewhere to be certain.

$S_{2C}$ is a steep to moderately dipping, strongly developed foliation that is visible in outcrop, and it is strongly overprinted and tightly folded by shallow $S_{3C}$. It is mainly observed and measured in thin section.

$S_{3C}$ and $S_{4C}$ ($S_{4C}$ is $S_{3C}$ transposed into a steep orientation) largely control the character of bedding - both are moderately southwest-dipping on the far east side of Little Crapeau Lake.

$S_{5C}$ is rarely observed in outcrop. At station 1540 it is axial planar to late folds.

**Figure 4.11 Stereonet zones for Little Crapeau Lake.** This area is divided into two structural domains. They are structurally very similar, however fabrics on the west side of the lake are strongly affected by the Wopmay Fault zone. $S_{3C}$ is rotated and much stronger in some outcrops than it is to the east. **a)** Depicts primary bedding measurements and overprinting fabrics in the western structural domain, while **b)** shows structures on the eastern side.

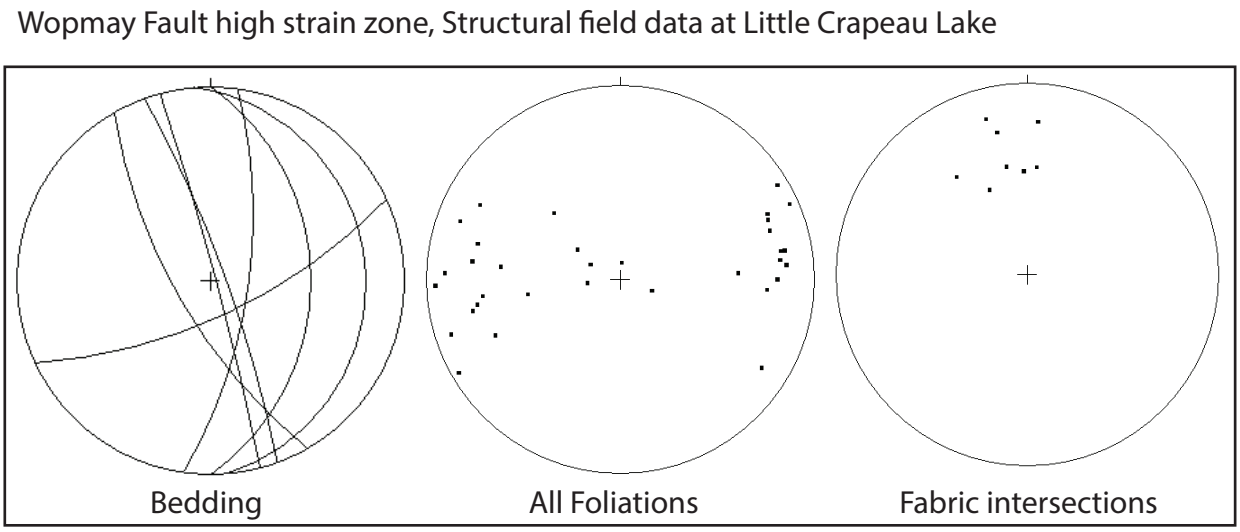


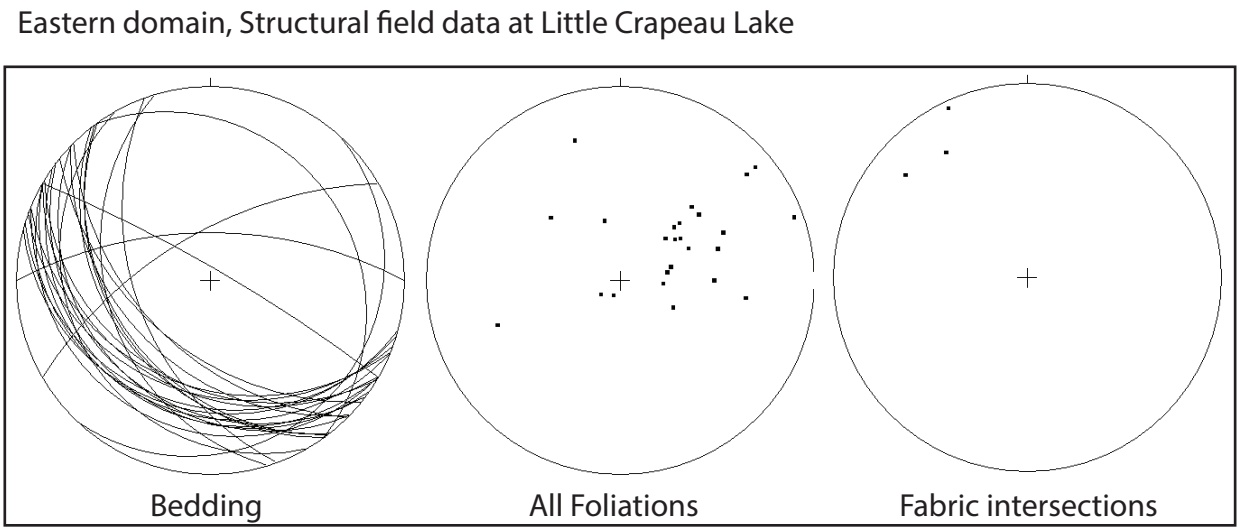


**Figure 4.12 Equal area stereographic projection of structural field data from Little Crapeau Lake.** The Little Crapeau Lake area is divided into two structural domains, approximately bissecting the lake into east and western halves. The character of bedding in the western half is poorly contrained, although appears to dip steeply to moderately eastward, whereas bedding is predominantly dipping moderately toward the SW in the eastern domain. When all foliations measured in the field are plotted (poles to planes), it is evident that in the western half foliation orientation is mainly N-S striking, and steeply dipping. In the east, however, foliations are nearly parallel with bedding. This indicates that bedding has been transposed strongly by $S_{3C}$. The $S_{1C}$ and $S_{2C}$ fabrics discernible in thin section are not commonly visible or measured in outcrop as they are preserved inside porphyroblasts and between a intensely developed $S_{3C}$. Plots showing the intersection of fabrics show the orientation of fold hinges measured in the field. In both domains folds plunge shallowly to moderately North to Northwest. Although not recognized in the field as such, these fold hinges are likely a result of the intersection of the $S_{3C}$ surface and overprinting $S_{4C}$ and $S_{5C}$, respectively. In the western structural domain, it is proposed that dominant fabrics have been rotated into a more N-S orientation due to the effects of the Wopmay Fault zone.

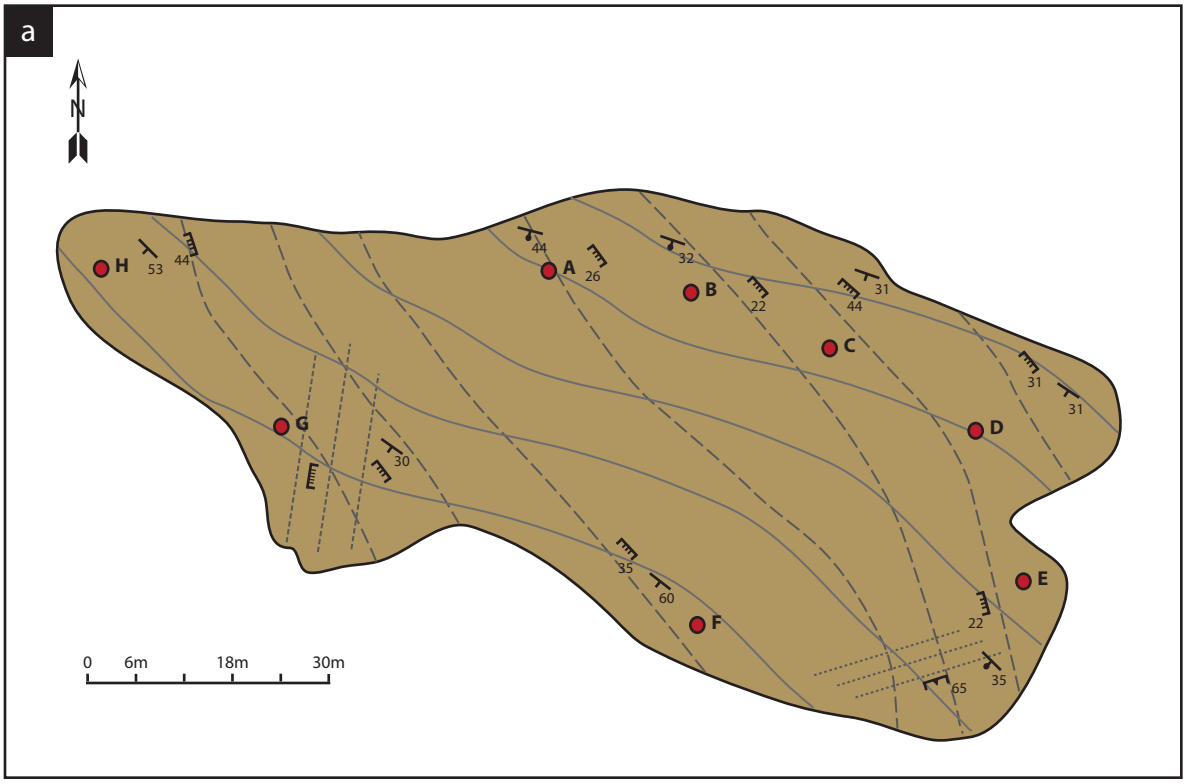


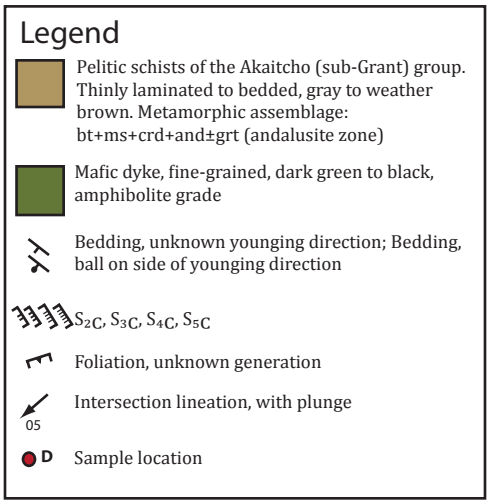


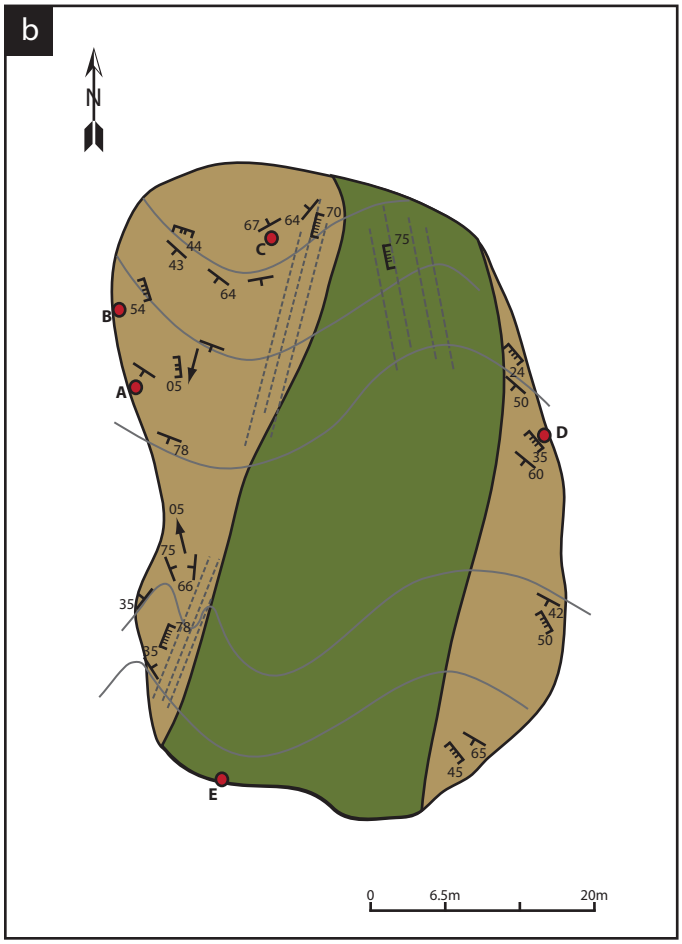


**Figure 4.13 Detailed island sketches from Little Crapeau Lake.** Stations 2562 **(a)** and 1540 **(b)** show a structural history dominated by $S_{3C}$ and overprinted by $S_{4C}$ and $S_{5C}$ transposing and crenulating events. **a)** is an island preserving one limb of an $F_{3\text{-}4C}$ fold, where bedding is more shallow than the axial planar cleavage. Island **b)** preserves the $S_{3C}$ surface folded by $S_{5C}$, with a crosscutting mafic dyke that holds a weak $S_{4C}$ foliation. Locations for these stations are found on maps in Appendix A.

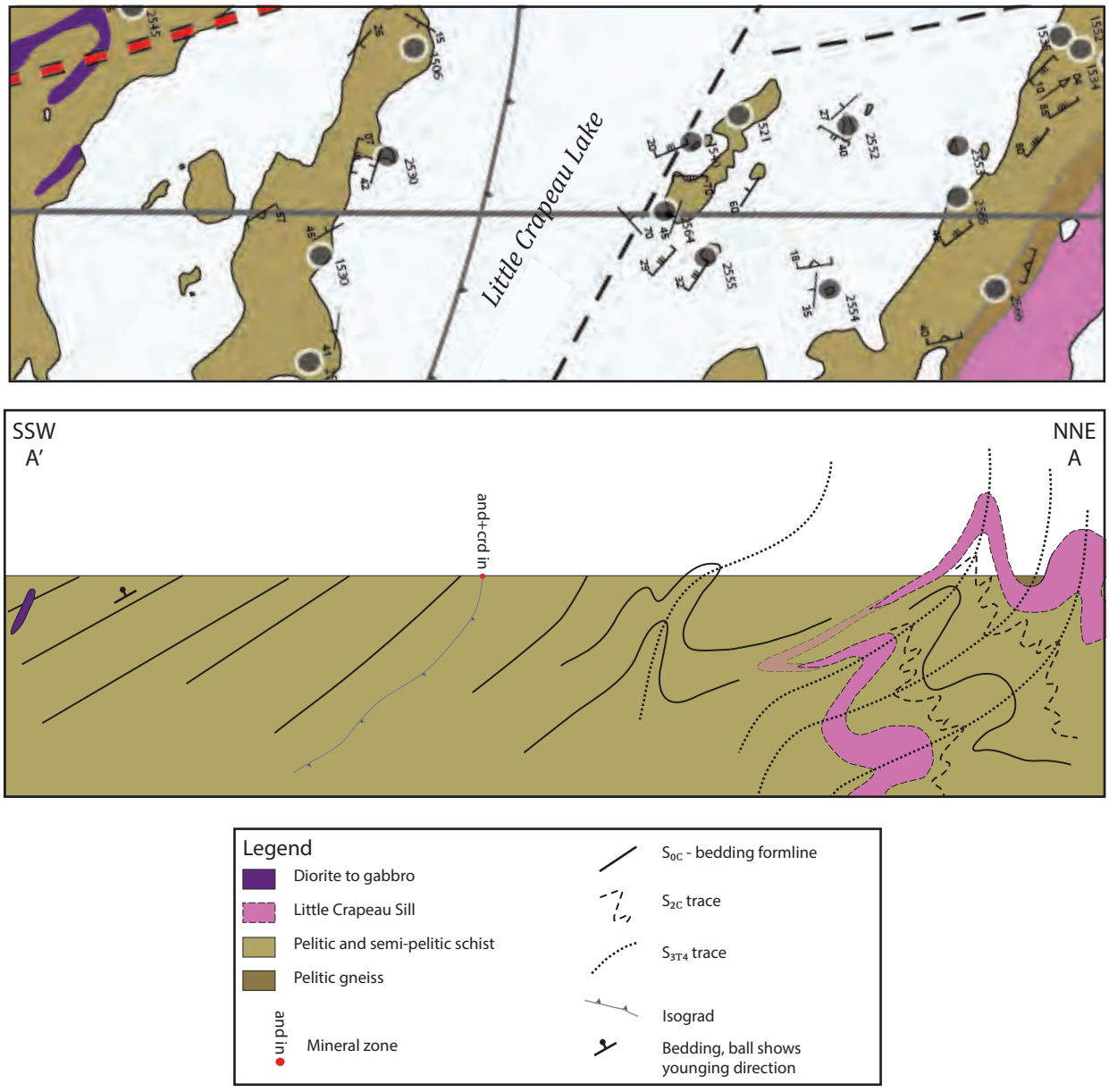


**Figure 4.14 Cross-section for Little Crapeau Lake.** A vertical transect crossing the main lithological units at Little Crapeau Lake shows bedding to be largely oriented with a south-southwest facing dip, with younging direction facing upward toward the SSW. On the NNE side of the transect, the Little Crapeau intrusion is parallel to the $S_{2C}$ fabric, which is folded axial planar to the $S_{3C}$ fabric. The $S_{3C}$ fabric has been tranposed into a steeper orientation by $S_{4C}$ ($S_{3T4}$). In outcrop, refolded dykes and dykelets of the same generation as the Little Crapeau Sill were observed (Fig. 4.8), indicating that at the regional scale the sill itself may also be refolded by the $S_{3C}$ and $S_{4C}$ deformational events, as represented by this schematic cross-section. These individual locations are not shown on the plan map as they are very minor occurrences. An isogradic surface representing the beginning of the andalusite + cordierite zone is inferred at depth, approximating the dip and shape of the local heat source, the Little Crapeau Sill. Many late faults (shown on above plan map) crosscut the units, however the dips of these are unknown.

# 5 P-T CONDITIONS OF METAMORPHISM & GEOCHRONOLOGY

## 5.1 Whole Rock Geochemistry Results

Results are tabulated in Appendix C. Duplicate samples show a small statistical variation, which may be explained by analytical error, or more likely that the samples used were not completely homogeneous. Duplicate samples were slabs cut from the original sample, which may have contained more or fewer porphyroblasts, more biotite or quartz rich layers, or any other natural variations. Discussion of the whole rock chemistries in the context of their locations is found in sections 3.0 and 4.0.

## 5.2 Metamorphic Mineral Chemistry Results

Results are tabulated in Appendix D. Three of the samples analysed for major element mineral chemistry contained garnet porphyroblasts. None of these belong to coticule layers. The garnets are all iron-rich (67-79% almandine), and the two samples from Little Crapeau Lake are manganese-rich (19-20% spessartine). Garnets in sample 2544A are slightly elevated in calcium and magnesium content (~8% grossular; 12% pyrope).

Plagioclase in all samples is largely albitic in composition. Albite composition in samples from Brown Water Lake varies between 60-86%, with similar compositions at Little Crapeau Lake at 77-85%.

Cordierite chemistry is difficult to judge from these samples. Microscope analysis revealed that cordierite porphyroblasts in samples from both Brown Water and Little Crapeau Lakes are intensely pinnitized and replaced with fine grained mica. Calculated ratios of Mg/(Mg+Fe) show no particular trend as a function of metamorphic grade, as compared to rocks from studies reported by Pattison (2002), where rocks show a moderate Mg-enrichment with increasing

grade. Matrix biotite and biotite as porphyroblasts in schist are consistently in the 0.4-0.6 range of Mg/(Mg+Fe) values for all rocks from both study areas.

## 5.3 Thermodynamic Modeling of the KFMASH System

To determine pressure and temperature conditions of metamorphism affecting the rocks in the southern Wopmay Orogen, the software package Perple_X was used in conjunction with the whole rock geochemical dataset obtained for the pelitic schists (Appendix C) to construct P-T pseudosections. The key metamorphic mineral assemblages, along with bulk rock and mineral chemistry data, were compared with and plotted on published phase diagrams which show critical reactions involved in producing characteristic low-pressure high-temperature assemblages (Pattison et al., 2002). Due to the observed metamorphic assemblages and the bulk chemistry, the model pelitic system $K_2O$-FeO-MgO-$Al_2O_3$-$SiO_2$-$H_2O$ (KFMASH) was assumed for all rocks and their reactions, and relevant P-T diagrams were used to constrain pressure and temperature conditions (Fig. 5.1).

The metamorphic assemblage Ms + Bt + Crd + And/Sil + Qtz observed in large parts of the Brown Water and Little Crapeau areas is a common assemblage in contact aureoles and low pressure metamorphism around the world, e.g. the Cooma complex in Australia, or Ballachulish aureole in Scotland (Johnson and Vernon, 1995; Pattison and Harte, 1991; Pattison et al., 2002).

Reactions dictating the prograde metamorphism of these rocks are as follows (numbered according to Pattison et al. (2002)):

2) *Muscovite + Chlorite + Quartz → Cordierite + Biotite + $H_2O$*

   Assemblage Ms + Bt + Crd + Qtz + Plg ± Grt for rocks at Little Crapeau (chlorite consumed, muscovite in excess)

1) *Muscovite + Cordierite → Biotite + $Al_2SiO_5$ + Quartz + $H_2O$*

Assemblage Bt + Ms + And/Sil + Qtz + Plg ± Grt ± Crd

5) *Muscovite + Quartz → $Al_2SiO_5$ + K-spar + $H_2O$*

Assemblage: Ms + Bt + And/Sil + Qtz + Plg ± Crd ± Grt (muscovite in excess, cordierite is eventually consumed)

7) *Muscovite + Biotite + Quartz → Cordierite + K-spar + $H_2O$*

Assemblage: Bt + Crd + Ksp + Qtz + Plg (muscovite consumed)

The shallow to moderate positive slope of reaction 1) predicted by the thermodynamic dataset by Holland and Powell (1998) and used in the Perple_X software, implies that low pressure pelites, such as the ones mapped at Brown Water and Little Crapeau Lakes, must be affected by an increase in pressure steeper than the P-T slope of reaction 1 to cross into the andalusite field from the cordierite field (Pattison et al., 2002). Pattison et al. (2002) suggest that to satisfy the textural relationships observed in porphyroblasts in their work, a reaction with a negative slope would better suit the observations, which consistently show andalusite growing after cordierite. A negative reaction slope would allow for a more isobaric heating and cooling path for rocks that see this assemblage (Pattison et al., 2002). Non-experimental support for the negative slope theory comes from observations made around contact aureoles by Pattison, where isobaric heating of rocks results in metamorphic mineral paragenesis and textures similar to the ones seen in this study, especially andalusite growing after cordierite. Since the program Perple_X uses the Holland and Powell (1998) dataset in its thermodynamic calculations, it models reaction 1 with a positive slope, which does not accurately represent the growth of andalusite after cordierite. For this reason, pseudosections produced with Perple_X were not included in this thesis.

The negative slope for reaction 1) calculated by Pattison et al. (2002) was used to estimate minimum and maximum pressures and temperatures of metamorphism for the rocks of this study. The topology of the reactions crossed by the rocks can be seen in Figure 5.1 a. The metamorphic assemblages of five rocks were plotted on the KFMASH diagram, showing a possible progression through Pattison's reactions 2, 1, and 7(5?). Rocks from Little Crapeau preserve the low grade assemblages better, while rocks from Brown Water preserve and reach higher grades.

Minimum conditions of peak metamorphism can be deduced by plotting the composition of biotite on the isopleths outlined on the P-T diagram by Pattison et al (2002), in the ideal six component system KFMASH (Fig. 5.1 b). Assuming a negative slope for reaction 1), and a Mg index Mg/(Mg+Fe) for biotite between 0.4 and 0.6 (Appendix D), rocks from Little Crapeau that have crossed reaction 2) and are (meta?)stable in reaction 1) plot below the andalusite/sillimanite transition, at ~570-630°C and 3.1-3.9 kbar. At Brown Water, the highest grade rocks reached sillimanite zone and plot in both the andalusite and sillimanite fields, at conditions between ~570-670°C (minimum) and 3.1-4.2 kbar (Fig. 5.1 b)). The temperature for rocks at Brown Water is a minimum estimate because some peak metamorphic assemblages for the highest grade rocks (e.g. sample 1547A) would plot on the higher temperature side of the reaction 5) line.

The metapelitic samples used for microprobe mineral analysis from Brown Water Lake did not contain any primary muscovite, and so the mineral was not analysed for chemistry. Most rocks of the biotite, cordierite and andalusite zone at Brown Water do however contain primary muscovite as part of the matrix foliation, so the P-T diagrams in Figure 5.1 can be used to estimate prograde metamorphic reactions. Rocks with garnet porphyroblasts do not contain primary muscovite, as aluminous phases like muscovite were likely consumed during prograde

metamorphism to produce garnet. Similarly, rocks of the sillimanite zone do not contain primary muscovite and have produced potassium feldspar as part of the reaction 5).

Nielsen (1986) estimated physical conditions of metamorphism at Brown Water Lake to be ~350°C at 2-2.5 kbar in the chlorite zone, up to ≥650°C at 3.5-4.0 kbar in the almandine + K-feldspar ± cordierite zone. These estimates are very similar to the ones calculated in this study, although no assemblages containing primary chlorite were observed.

## 5.4 Comparative Chemical and Isotopic Geochronology

Monazite, a La-Ce light rare earth phosphate ($LREEPO_4$), has long been recognized as a powerful geochronological tool in tectonic analysis, and has proven to be a reliable absolute measure of thermotectonic events (Williams et al., 1999). It is a common accessory mineral in igneous and metamorphic rocks, and can be used to date crystallization or metamorphic ages (Parrish, 1990). Certain chemical complexities can make precise dating difficult, such as monazite's preference for incorporating Th over U, leading to excess amounts of $Pb^{206}$ (Parrish, 1990). In situ dating methods are being perfected by a number of workers, and for this study two methods were undertaken to gather age data: U-Th electron microprobe (EMPA) chemical dating, and U-Pb sensitive high resolution ion microprobe (SHRIMP) isotope dating.

Chemical complexities in monazite also lead to difficulties in age interpretations. Just like zircons, monazite grains of different ages are found to coexist in metamorphic rocks (Parrish, 1990). This suggests the preservation (non-resetting) of crystallization ages despite growth of new monazite rims or entire grains during metamorphism (Parrish, 1990). Dissolution-precipitation processes and growth by coalescence (leading to morphologies like necking and irregular composite crystals) result in visually and chemically complex grains (Ayers et al.,

1999). Material precipitated on pre-existing detrital or metamorphic cores may not appear as a regular rim around a euhedral core (Fig. 5.2, 5.3).

For this study, monazite grains were analyzed in situ (contextually), in pelite and gneiss samples from both the Brown Water Lake and Little Crapeau Lake areas. Samples were selected to span the metamorphic gradient at both locations, so as to get a full representation of metamorphic ages at every stage – from biotite zone schists to gneiss. In all, 7 samples were chosen from Brown Water Lake, and 3 from Little Crapeau Lake. One of the 7 thin sections analyzed from Brown Water Lake, a garnet-bearing biotite schist (2512A), did not contain any monazite and was not used in this study.

Individual grains for analysis were chosen based on size and position in the thin section (relative to porphyroblasts and deformation fabrics). Most thin sections had very few monazite grains larger than 10 μm, and therefore selection was slim.

### *5.4.1 U-Th Electron Microprobe In-Situ Geochronology*

Thin sections were analysed on the electron probe microanalyser (EMP) at the University of Massachusetts, Amherst. Compositional analysis was performed for each carbon coated, polished thin section, mapping for Mg, Ca, Y, Zr, Ce on a Cameca SX100 Ultra-chron, with a defocused beam (ca. 30-40 μm) at 265-300 nA, 15 kV for a counting time of 25-30 microseconds/pixel, producing full-section element maps. Magnesium and cerium full-section maps were merged in an image analysis program to highlight the locations of individual monazite grains (targets with high Ce counts) in the context of the thin section. Individual cerium targets were mapped on the EMP with a focused beam (ca. 0.7-1 μm) at 250 nA, 15 kV for a counting time of 80 ms/pixel, producing high resolution chemical composition maps, showing complex domains of Y, U, Ca, Th, Nd.

High resolution grain maps were simultaneously processed in Adobe Photoshop using standardized colour levelling actions, colourizing chemical highs and lows according to measured values, so as to show all levels of each element as the same colour intensity (in each chemical map, yellow/orange/red is the same value for all analysed elements). Considering mainly the variation of Th and Ca in the high resolution grain maps, chemical homogeneities were defined and selected for U-Th dating according to size and context (e.g. rim, core).

Carbon-aluminum coated polished thin sections were submitted for multipoint background spot analysis on the EMP, with a focused microbeam at 200 nA, 15 kV for counting times detailed in Appendix E. Spot analysis was conducted for each homogeneous chemical domain, fitting as many analysis spots in each domain as possible (4-12 spots). In total, 30 grains were analysed on the EMP from 10 different thin sections. Within each grain, 1-6 chemically distinct domains were differentiated and analysed for U-Th ages. Age calculations were constrained compositionally. Domains are labelled “rim” or “core” depending on position within the grain, however in some cases “core” ages were younger then “rim” ages.

Most monazite grains detected in the thin sections are very small, between 20 and 60 μm, and the largest around 200 μm. The largest grains were found in samples 2501A and 2525A. These samples were collected closest to the Archean Slave craton, and closest to the Rodrigues granite, respectively. Monazite grains were not ideal for analysis as they do not show distinct core/rim zonation, are chemically complex, and are full of pits and inclusions (apatite) which makes large homogenous zones rare. The standards used on the microprobe at UMass were Moacyr (506 Ma), Burnet (1104 Ma), Elk Mt (1405 Ma).

### *5.4.2 U-Th Results*

The goal of this geochronological study was to constrain the timing of regional metamorphic events and relate them to recognized and documented local deformation events. To achieve this, the attempt was made to strategically select grains positioned within porphyroblasts or confined within strong foliations. The theory behind this method is that grains enclosed in porphyroblasts may yield an age of crystallization either pre- or syn- the growth of that porphyroblasts, thus providing an age of metamorphism. However, after receiving the element scans of the thin sections, no monazite grains were found within porphyroblast phases, and dating results did not yield significantly different ages between matrix grains (monazite growing in a qtz+plg-rich matrix) and foliation grains (monazite growing in dense bt+ms folia). Rather, the widest range in ages came from grains from different locations within the same map area, and from varying metamorphic grades. For example, at Brown Water Lake the lowest grade sample, 2501A, yielded grains with ages ranging from >2600 Ma to 1744 Ma, and a mean age of 1823 ± 96 Ma, whereas the highest grade sample, 2525A, yielded a very narrow range of ages with a mean of 1846.2 ± 7.9 Ma (Fig. 5.4) .

Individual grain and chemical domain analyses were evaluated independently for precision and accuracy. According to the methods practiced by workers at the University of Massachusetts at Amherst, individual domain analyses were discounted if they showed especially anomalous chemical values (i.e. very high Th values where the rest of the analyses were found to have moderate values), or if calculated errors were considerably larger than other analyses from the same chemical domain. Analyses were also discarded if total element counts were too low (<98%). The remaining ages were averaged (per chemical domain), and the standard deviations calculated to 2σ (Appendix E). The data was also processed with Isoplot, a Microsoft Excel add-on. The program produced box plot and calculated the mean of all ages yielded per

sample (Appendix E). Due to the large range of ages calculated from some grains, it is more revealing to examine grains individually (as opposed to sample averages) and their chemical domains separately.

To assess the U-Th zonation within individual grains, scatter charts plotting weight percent Th versus U were produced according to Williams (2001) to determine whether the composition of chemical domains shows any influence on chemical ages, or if composition changes with metamorphic grade (Fig. 5.5, 5.6, 5.7). Williams (2001) noted that the rocks (metapelites, metapsammites, migmatites and granodiorites from the Cooma Complex) showed Th content in monazite to become more constant with increasing grade. For this study, samples chosen from Little Crapeau Lake are cordierite-andalusite schist grade, and from Brown Water Lake span a metamorphic gradient (biotite zone through sillimanite/melt zone), When plotted in a similar fashion they show only a weak correlation between composition and metamorphic grade (or chemical age) in certain grains.

#### *5.4.2.1 Little Crapeau Lake*

Individual grains from samples at Little Crapeau Lake are anhedral to amorphous, resorbed (chemically eroded), and exhibit chemically complex zoning (Appendix E). Grain size ranges from ~10 to 120 μm. Some grains contain Ca-rich zones, which likely indicate the presence of apatite inclusions. Grain morphology is also fairly complex. Uneven grain boundaries, skeletal grains and coalescing of grains is likely a result of dissolution/precipitation mechanisms (Ayers et al., 1999). No distinct core/rim zonation is evident in the grain population, with the exception of grain m1 in sample 1535A, which preserves a euhedral low-U core, surrounded by zoned low and moderate Th rims. Two grains analysed from sample 1535A (m1 & m3, Appendix E) show a chemical distinction between “core” and “rim” zones, and fairly consistent

younging from core to rim. This zonation suggests U-enrichment and Th-depletion in newly precipitated monazite material.

Ages obtained from the rocks at Little Crapeau Lake show a distribution of crystallization ages between 1990-1832 Ma, with the mean age of 1905 Ma, and median age of 1898 Ma. Three samples were chosen for dating from this area and only two contained monazite grains large enough to provide reliable data. Grains from sample 1540D-2 were all <25 μm and highly Ca-rich, indicating abundant apatite inclusions. This sample returned the largest error. Nonetheless, ages were obtained for all samples.

#### *5.4.2.2 Brown Water Lake*

Monazite grains from samples at Brown Water Lake were overall larger than grains from Little Crapeau. Grain morphology and chemical zoning complexity are similar between the two areas (Fig. 5.2, 5.3).

Thorium versus uranium plots of chemical domains show no obvious correlations between the distribution of elements in “core” and “rim” zonations and domain age or metamorphic grade (Fig. 5.5, 5.6, 5.7).

Grains from samples 2501A and 2525A are the most intriguing of the population. They are the lowest and highest metamorphic grade, respectively. The two samples taken closest to the Archean craton and closest to the Rodrigues pluton contained the largest grains, ~60-200 μm, with the most telling history. The large grains in sample 2501A show evidence for chemical erosion on their edges, and preserve the oldest chemical domains (detrital cores) surrounded by significantly younger rim material. Grains from the highest grade sample (2525A) are entirely metamorphic material, and show a very small range in ages that coincide with the crystallization age of the Rodrigues granite around 1850 Ma (Fig. 5.2, 5.3; Appendix E).

The total spread in ages from Brown Water Lake samples is 2609 ± 104 to 1524 ± 26? Ma (1085 Ma range). The youngest age of 1524 ± 26 Ma originates from sample 10ls2506B. The grains yielded from this sample were extremely complexly zoned, packed with apatite inclusions, and had a bizarre morphology (Fig. 5.2, 5.3). It is uncertain what this age indicates or if it is statistically significant or viable.

Age data obtained from U-Th dating illustrate a long history of heating throughout the Brown Water Lake area.

### *5.4.3 SHRIMP II U-Pb Geochronology Methods*

The same polished thin sections (excluding 2544A & B) were submitted for geochronology work on the sensitive high resolution ion microprobe (SHRIMP II) at the Geological Survey of Canada (GSC) in Ottawa. In some cases, small grains that were appropriate for the size of the EMP beam (0.7-1 μm) were not large enough for the SHRIMP II beam (7 x 9 μm), in which case thin sections were scanned on the scanning electron microscope (SEM) at the GSC to locate all monazite grains and to select new, larger candidates for analysis.

Selected grains were marked on the thin sections, and disks were drilled out with a drill press and diamond drill bit hole saw. Grains were thus preserved in context, and mounted in epoxy following the preparation methods outlined in Rayner and Stern (2002). The SHRIMP mount was imaged on the SEM, producing maps of the mount, each disk individually, and of each grain to be analysed. In all, 28 disks were drilled from 7 thin sections, and from these 16 disks were chosen for mounting (Appendix E). Criteria used for choosing the best grains were size, shape, number of inclusions and context. In some cases, a larger or less inclusion-filled grain was chosen based on SEM imaging, rather than using the same grain dated with the EMP.

The epoxy mount was gold-coated, and submitted for $^{207}Pb/^{206}Pb$ isotopic geochronological analysis. Monazite grains were located with reflected light and spot analysed with the Köhler 50 SHRIMP beam, $(O_2)^{1-}$ primary beam species with an intensity of 0.25 nA, and 6 counts per spot analysis. In total, 22 grains from 5 different samples were analysed. Most grains were too small to contain more than one analysis spot; however 4 grains were large enough for 2 or 3 spot analyses, values for which were averaged for the grain. The monazite standards used for this analysis were 3345 (1821 Ma), 8153 (? Ma), and 2908 (1794 Ma).

#### *5.4.4 U-Pb Results*

To assess U-Pb isotopic ages for the monazite grains submitted for this analysis, standard Concordia ages and errors were calculated and plotted (Fig. 5.8). All analysed grains present discordant ages, which indicates some amount of Pb loss over time.

##### *5.4.4.1 Brown Water Lake*

Mean isotopic ages obtained from three rocks analysed from Brown Water Lake are 1844 ± 12 Ma, 1849.2 ± 6.6 Ma, and 1856.6 ± 8.5 Ma. These coincide with the U-Pb zircon crystallization ages of the Rodrigues granite at 1849.4 ± 1.4 Ma to 1851.8 ± 3.2 Ma.

##### *5.4.4.2 Little Crapeau Lake*

The results of U-Pb isotopic dating of two rocks from Little Crapeau Lake are two discordant ages that coincide approximately with the ID-TIMS U-Pb zircon crystallization age of the Little Crapeau sill, 1877 ± 2 Ma. Samples 1511-2 and 1535A returned mean ages of 1867.6 ± 8.9 Ma and 1879 ± 13 Ma, respectively (Fig. 5.8).

### *5.4.5 Advantages and Disadvantages to Dating Techniques, and Sources of Error*

The use of EPMA in the analysis of accessory phases such as monazite is still a technique in the testing and refining stages (Dahl et al., 2005). The science behind trace-element analysis is well understood, however complexities and inaccuracies arise in the trace-elemental analysis of REE-bearing minerals (Jercinovic and Williams, 2005). While elemental mapping of individual monazites greatly enhances the understanding of chemical complexities within a grain, it is in the analytical equipment and methods where advancements are being made to accommodate the evolving science of trace-element geochronology (Jercinovic and Williams, 2005). At UMass Amherst, Michael Williams, Michael Jercinovic and others are developing and improving techniques (i.e. multipoint background analysis) and software (i.e. DATCON III) to overcome the known problems in this field, such as large errors arising from background interference, or inaccuracy due to spatial resolution (Jercinovic et al., 2012). As a result of these issues, the U-Th age data acquired for this study should be approached with a certain degree of confidence and skepticism. One known and important issue to consider when interpreting this data is the effect of neighbouring minerals on trace-element counts. For example, rim age interpretations can be affected by incorrect counts of K due to adjacent or host K-feldspar or micas, abundant phases in metapelites, which leads to erroneous U concentrations. This effect can be felt* within 10 μm. In addition, the chemically complex nature of monazite can lead to overlapping elemental counts between domains, and difficulties in age domain interpretation.

In contrast, the theory, methods and technical protocols surrounding U-Pb isotopic geochronology have been in development for much longer, and are much more widely used. The methods are generally accepted and reliable, however in the case of monazites such as the ones used for this study, the internal heterogeneity and small size of the grains can lead to age averaging that does not properly reflect the complex history of the grain. In other comparative

methods studies, chemical ages have been compared against isotopic ages, which are represented as more reliable due to the ability of the method to discern anomalously young ages that are a result of Pb-loss (Dahl et al., 2005). Electron microprobe methods do not allow for this type of distinction using U-Pb Concordia relationships.

### *5.4.6 Discussion of Intrusive Ages*

U-Th chemical monazite ages collected from both study locations outline a continuous history of crystallization/metamorphic ages spanning from ca. 2000 Ma (excluding detrital ages from sample 2501A) to ca. 1800 Ma (Fig. 5.4). When considered together with the U-Pb zircon crystallization age data for local and regional intrusions and intrusive suites (presented in section 1.3.2), it is evident that there is a ca. 200 m.y. history of crustal heat circulation, beginning with the Hepburn-aged intrusions, which includes the Little Crapeau sill. Most of the Hepburn-aged intrusions in the Wopmay Orogen are in the northern half and have been extensively described and studied, however the Little Crapeau Sill is a new and confirmed occurrence in the southern half.

Prior to Hepburn aged intrusions there is no evidence for earlier crustal scale intrusive suites. Sedimentation of the passive margin and rift sequence is estimated at ca. 2020 Ma.

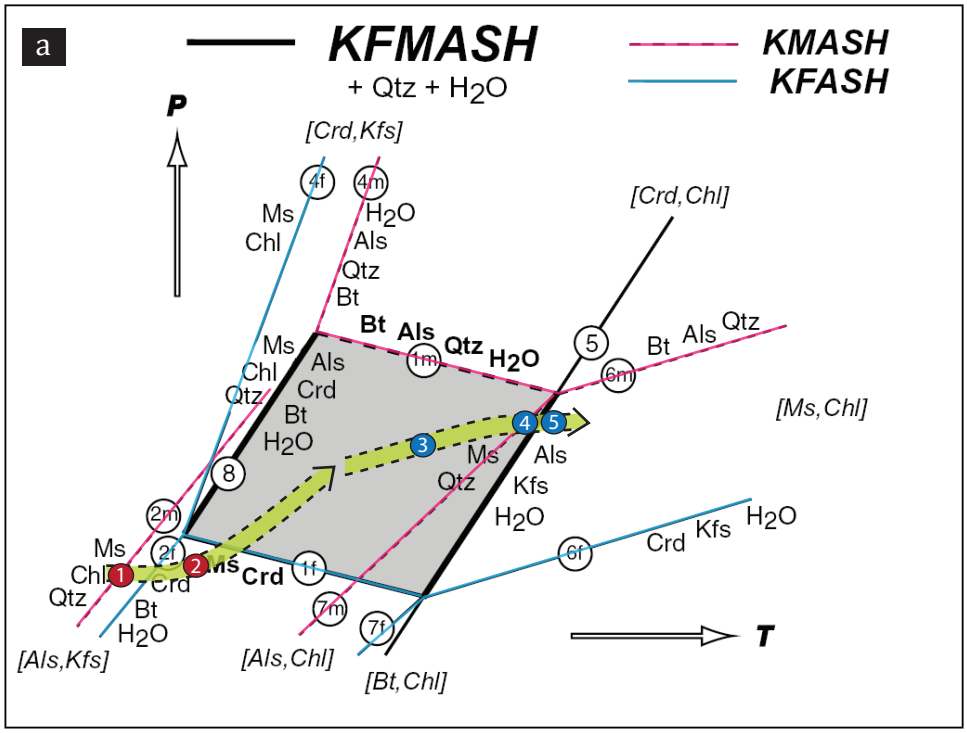


Approximate P-T path followed by pelitic schists at BWL and LCL

1 1530A: qtz+ms+chl

2 1535B: qtz+bt+ms+crd

3 2513: qtz+plg+bt+ms+crd+and

4 1567: qtz+plg+bt+ms+grt+and+relict crd

5 2520: qtz+plg+ksp+bt+sil

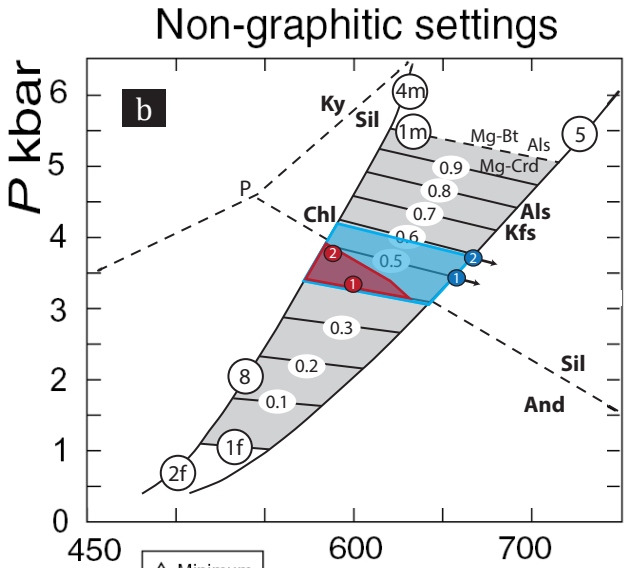


△ Minimum
◇ Defined
▽ Maximum

Ms + Qtz + H2O in excess

*P-T* region of Reaction 1 (Ms+Qtz+Crd+Als+Bt) assemblages

0.9 Isopleths of Mg/(Mg+Fe) in Bt in reaction 1

*T* (°C)

Zone for samples from Little Crapeau Lake

Zone for samples from Brownwater Lake

1 1511: 600°C, 3.3 kbar; qtz+plg+bt+ms+crd+and

2 2565A: 580°C, 3.7 kbar; qtz+plg+bt+ms+crd+grt+and

1 2518E-1: 660°C (min), 3.5 kbar; qtz+plg+bt+ksp+sil+and+crd

2 1547A: 665°C (min), 3.7 kbar; qtz+plg+bt+ksp+sil+crn

**Figure 5.1 Petrogenetic grids show reactions approximated for pelitic schists. a)** P-T diagram for the six component ideal system KFMASH, including the reaction Mu + Crd ⟶ $Al_2SiO_5$ + Bt + Qtz + $H_2O$ (1f and 1m, encompassed by the gray polygon), showing the topology of the reaction considering a negative slope for 1. Rocks at Little Crapeau Lake (LCL) crossed reactions 2 and 1, with muscovite in excess, whereas rocks at Brown Water Lake (BWL) crossed reactions 2, 1, and 7. Gneissic rocks at BWL crossed reaction 7 and grew ksp+sil. **b)** Isopleths contour the Mg/(Mg+Fe) composition of biotite (calculations shown in Appendix D). Mg index in biotite at LCL ranges from 0.43-0.47, and 0.42-0.59 at BWL, with select samples plotted accordingly. According to this phase diagram, which applies the negative slope for reaction 1, conditions of metamorphism of pelitic schists sampled at LCL were ~570-630°C and ~3.1-3.9 kbar, and ~570-670°C and ~3.1-4.2 kbar at BWL. Of the rocks mapped at LCL, none reached the sillimanite-in zone. Figures modified from Pattison et al. (2002). Triple point in phase diagram **b)** calculated by Pattison.

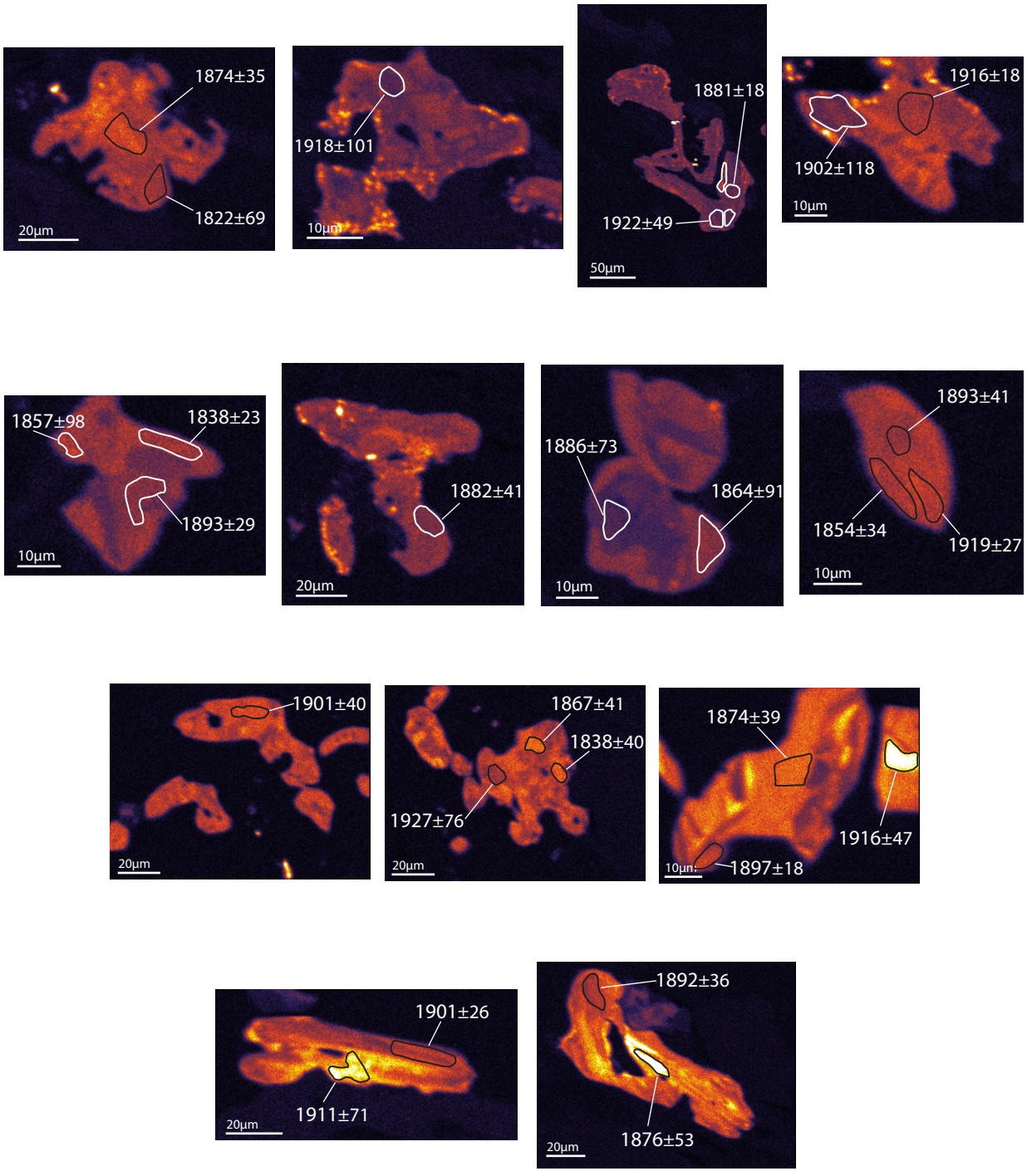


**Figure 5.2 Thorium chemical maps outlining zones analysed for monazite geochronology, for two rocks south of Brown Water Lake.** Individual monazite grains were analyzed in situ with an electron microprobe analyzer. Each **m#** denotes individual grains from the same rock. Domains for chemical analysis were chosen based on Thorium chemistry and homogeneity of zonations measured and observed in chemical imaging. Age values are given in Ma with 2σ error. Grains are amorphous with chemically complex zonations. Ages yielded from grains from these two rocks have a range of ca. 100 Ma, with the mean age for 2544A at 1880 ± 15 Ma, and 1890 ± 12 Ma for 2544B.

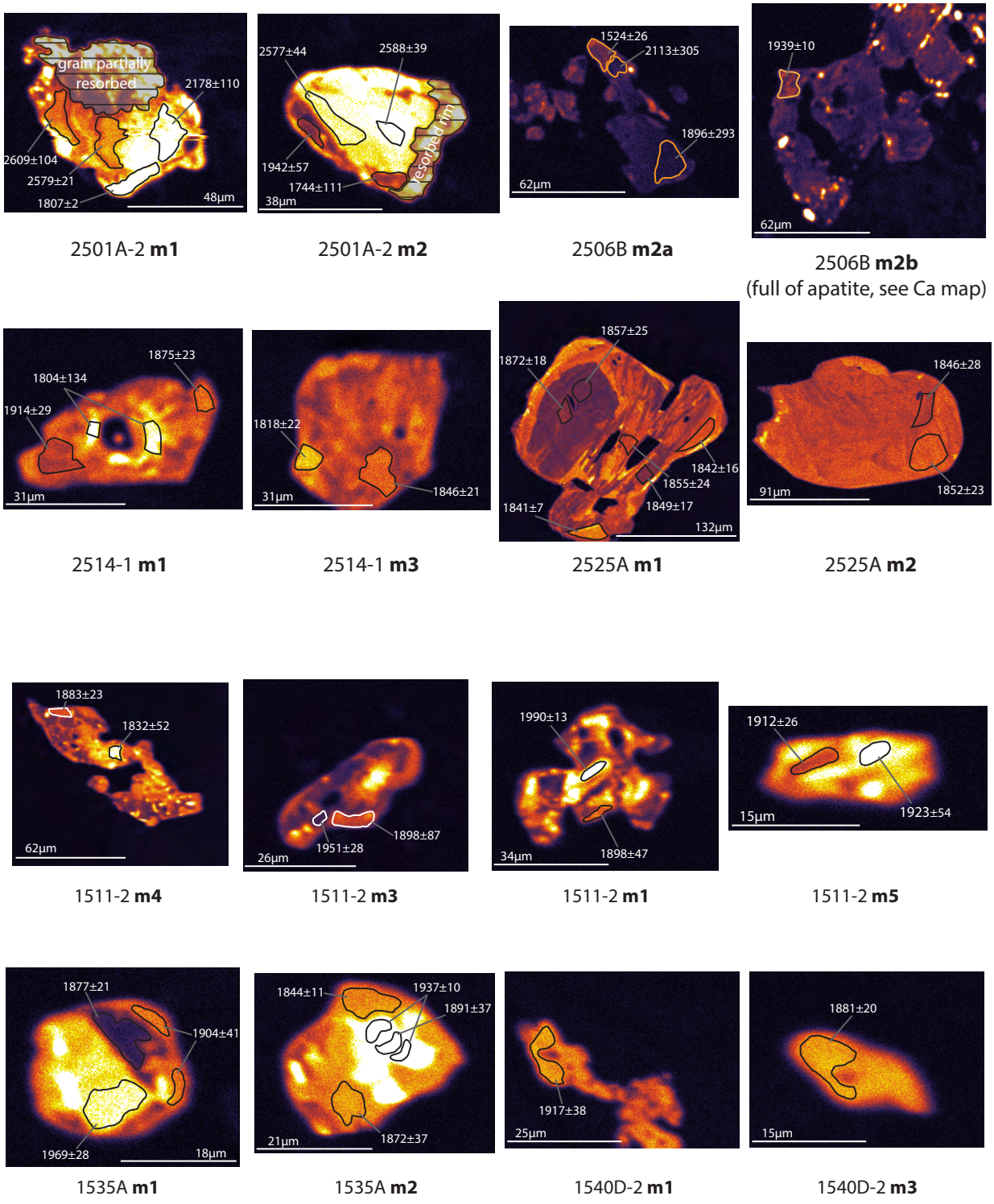


**Figure 5.3 Thorium chemical maps outlining zones analysed for monazite geochronology (cont'd).** Four samples from Brown Water Lake and three samples from Little Crapeau Lake. All monazite grains are amorphous to anhedral and have complex chemical zonation. The grains with the oldest chemical domains show evidence for chemical erosion (i.e resorbed edges in 2501A-2), indicating that these were likely detrital grains in the sedimentary sequence. Grains from sample 2506 had very low Thorium content and ages were difficult to acquire with consistency. Refer to text for discussion of all results.

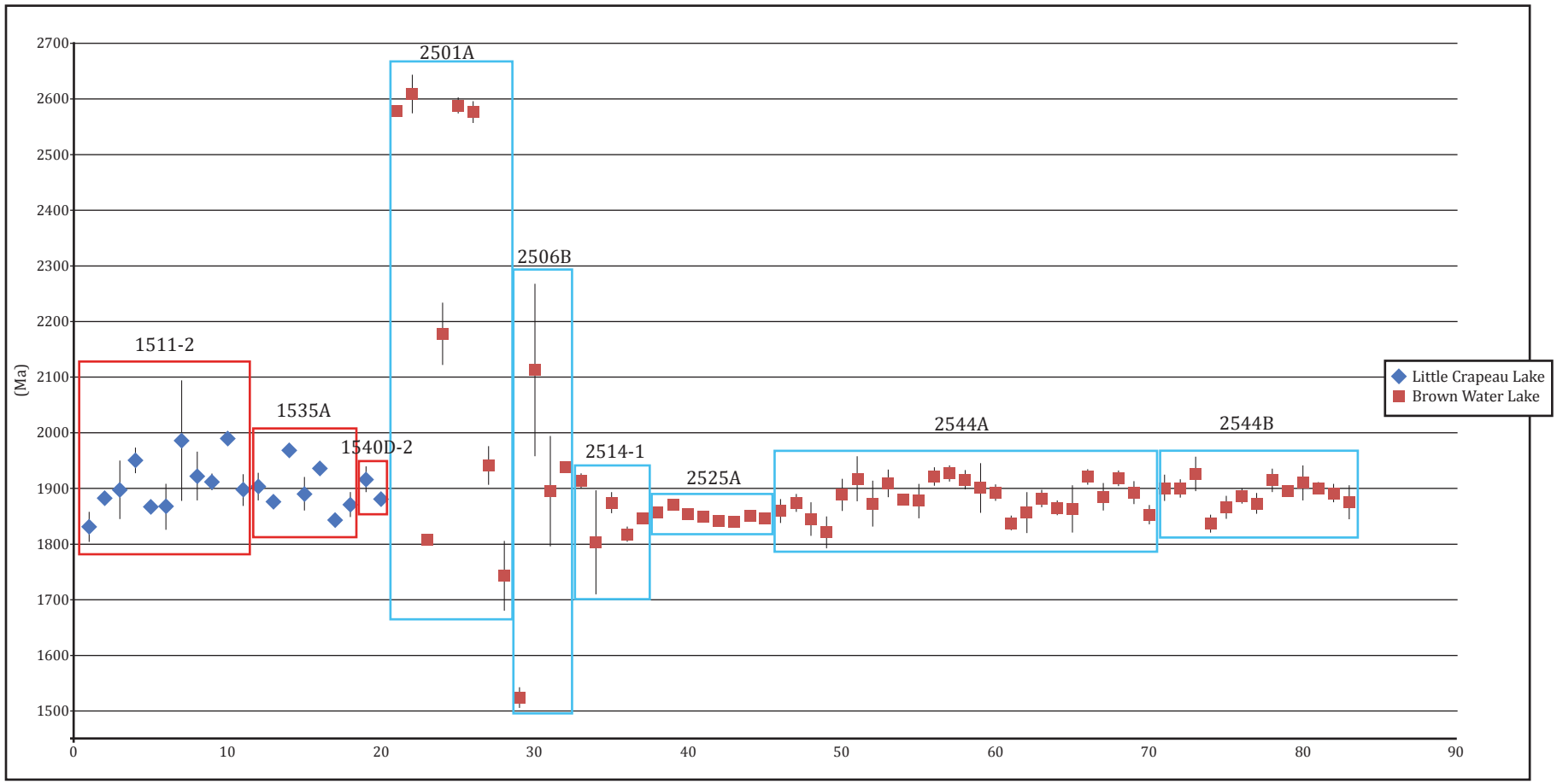


**Figure 5.4 Scatter plot showing U-Th ages calculated for all analysed monazite grains.** Each data point represents a chemical domain analysed in a monazite grain. Error bars are 1σ. Cordierite-andalusite grade samples from Little Crapeau Lake are blue diamonds boxed in red. They show a distribution in ages between 1990 and 1832 Ma, with the largest range seen in sample 1511-2. Samples from Brown Water Lake (red squares) range in grade from biotite zone (2501A) to cordierite-andalusite zone (2506A, 2514-1, 2544A & B), to gneissic (2525A). The lowest grade sample shows the largest variation in ages, preserving detrital ages ca. 2600 Ma, while the rest largely cluster between 1950-1800 Ma. The highest grade sample shows the smallest variation in age distribution, with a mean age of 1846.2 ± 7.9 Ma.

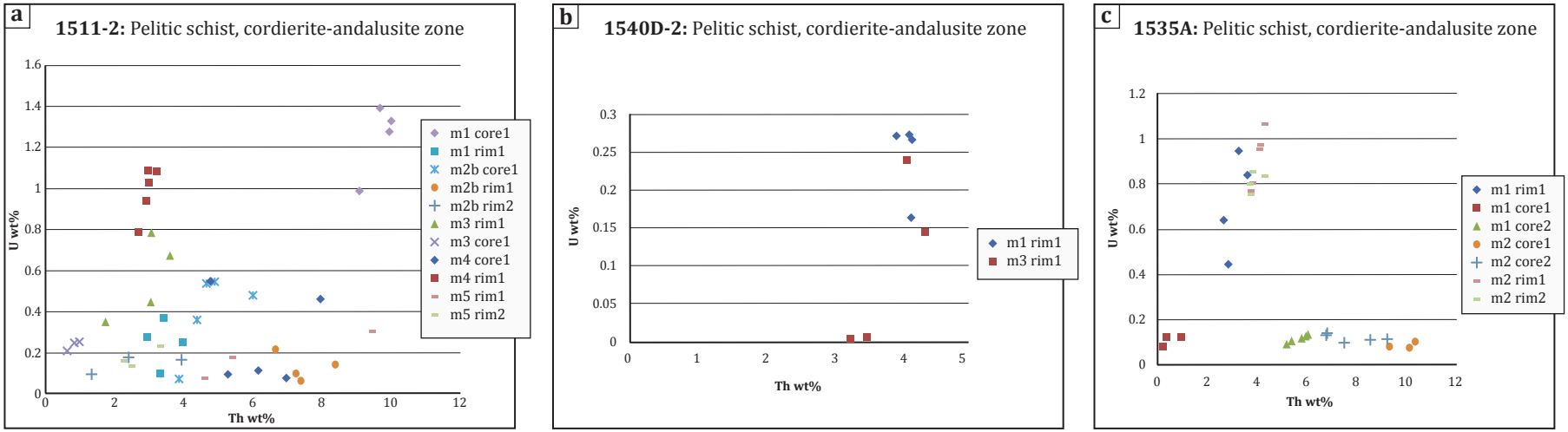


**Figure 5.5 Thorium vs Uranium scatter plots for chemical domain analyses from monazite grains in high grade metamorphic rocks from Little Crapeau Lake.** In-situ analysis of chemical zonations in monazite grains was performed with an electron microprobe, in pelitic schists from Little Crapeau Lake. The 'm' in domain names denotes individual grains (m1, m2, m2b). Results show "rim" and "core" zones to be equally variable in composition. The range in Thorium is much more variable within a rock than Uranium. No direct correlation could be made to show increasing or decreasing Th or U within a single grain with age or metamorphic grade, as has been suggested by other similar studies, such as Williams (2001). Note changes in axis values between scatter plots.

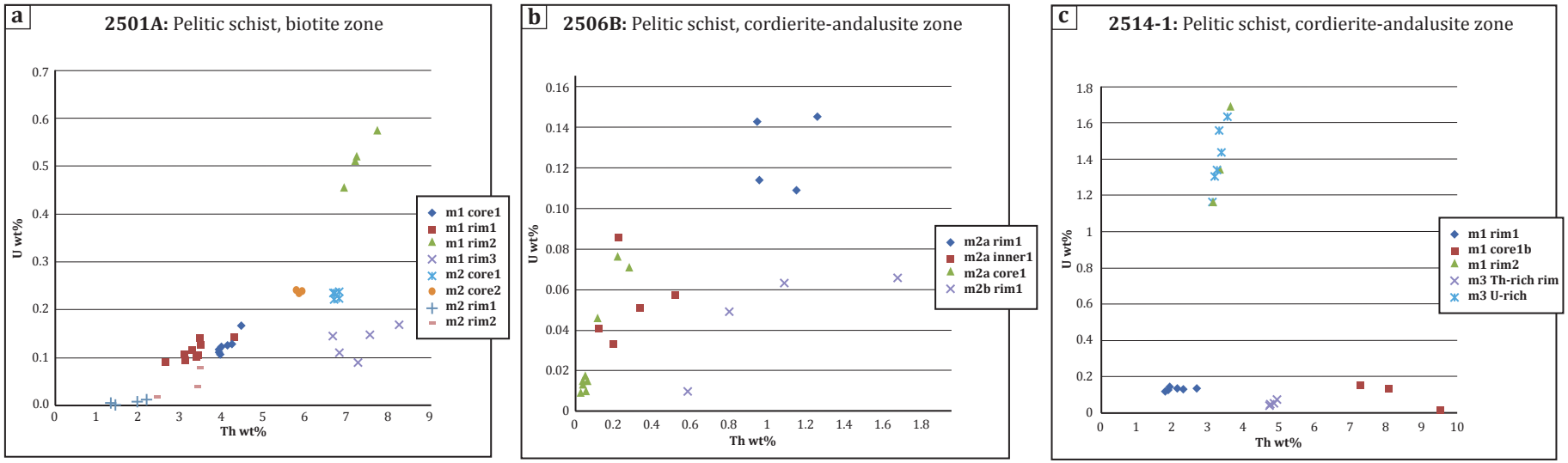


**Figure 5.6 Thorium vs Uranium scatter plots for chemical domain analyses from monazite grains metamorphic rocks from Brown Water Lake.** In-situ analysis of chemical zonations in monazite grains was performed with an electron microprobe, in pelitic schists and gneisses from Brown Water Lake. The 'm' in domain names denotes individual grains (m1, m2, m2b). Results show "rim" and "core" zones to be equally variable in composition. The range in Thorium is much more variable within a rock than Uranium. No direct correlation could be made to show increasing or decreasing Th or U within a single grain with age or metamorphic grade, as has been suggested by other similar studies, such as Williams (2001). Note changes in axis values between scatter charts.

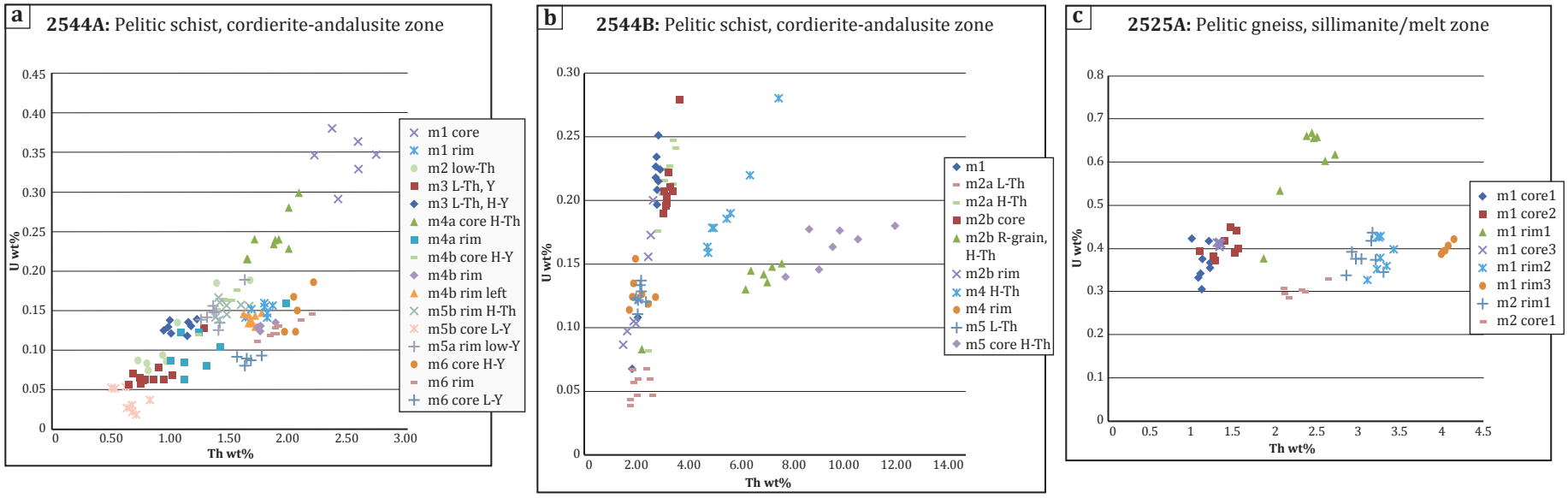


**Figure 5.7 Thorium vs Uranium scatter plots for chemical domain analyses from monazite grains in high grade metamorphic rocks from Brown Water Lake.** In-situ analysis of chemical zonations in monazite grains was performed with an electron microprobe, in pelitic schists and gneisses from Brown Water Lake. The 'm' in domain names denotes individual grains (m1, m2, m2b). Results show "rim" and "core" zones to be equally variable in composition. The range in Thorium is much more variable within a rock than Uranium. No direct correlation could be made to show increasing or decreasing Th or U within a single grain with age or metamorphic grade, as has been suggested by other similar studies, such as Williams (2001). Note changes in axis values between scatter plots.

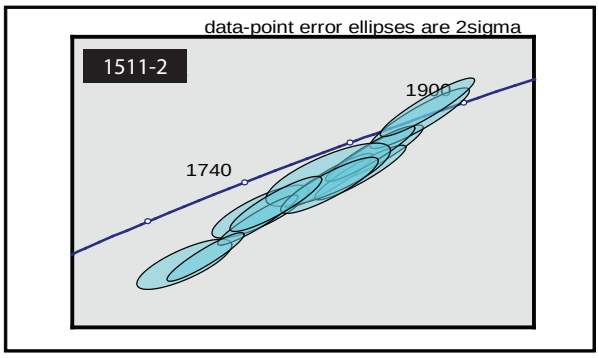


Mean = 1867.6±8.9 [0.48%] 95% conf.
Wtd by data-pt errs only, 1 of 13 rej.
MSWD = 1.20, probability = 0.28

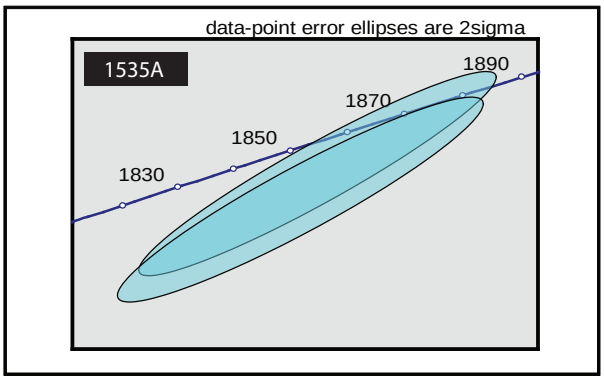


Mean = 1879±13 [0.69%] 95% conf.
Wtd by data-pt errs only, 0 of 2 rej.
MSWD = 0.52, probability = 0.47

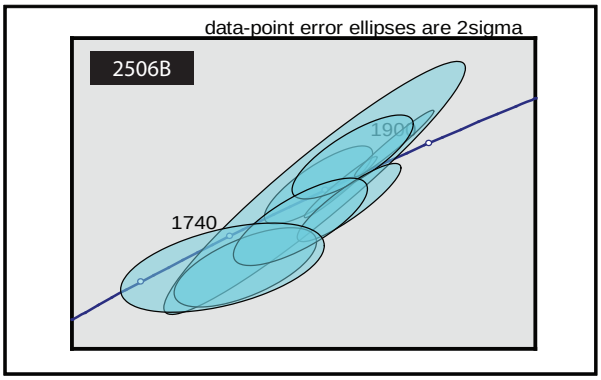


Mean = 1844±12 [0.67%] 95% conf.
Wtd by data-pt errs only, 0 of 9 rej.
MSWD = 1.9, probability = 0.054

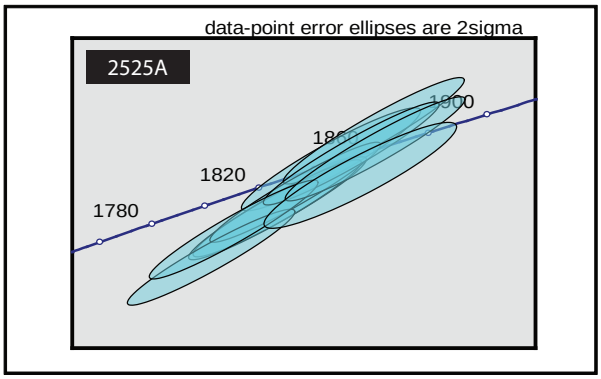


Mean = 1856.6±8.5 [0.46%] 95% conf.
Wtd by data-pt errs only, 0 of 10 rej.
MSWD = 1.9, probability = 0.049

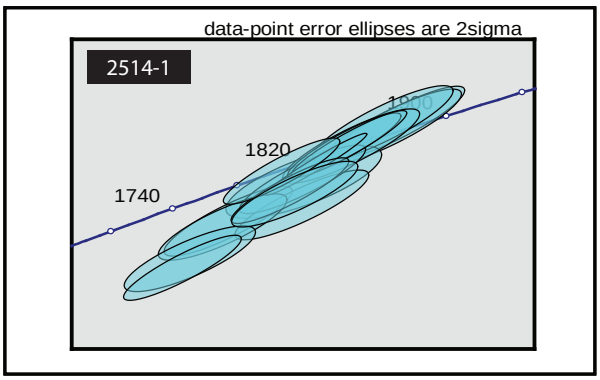


Mean = 1849.2±6.6 [0.36%] 95% conf.
Wtd by data-pt errs only, 2 of 17 rej.
MSWD = 1.03, probability = 0.41

**Figure 5.8 Concordia diagrams for U-Pb metamorphic monazite ages.** Samples from Little Crapeau Lake, 1511-2 and 1535A show a concordia mean ages in the range of ca. 1880 to 1867 Ma. This mean coincides with a known, local metamorphic event: the intrusion of the Little Crapeau sill around 1877 Ma. U-Pb ages calculated for samples from Brownwater Lake have a mean age around ca. 1850 Ma, which coincides with the U-Pb zircon crystallization age of the Rodrigues pluton ca. 1850 Ma.

# 6 INTERPRETATION AND DISCUSSION

## 6.1 P-T-t-d Summary

A schematic summary of overprinting fabrics is provided in Figure 6.1. The schematic diagram attempts to summarize and correlate all observed fabrics between Brown Water Lake and Little Crapeau Lake. The steep $S_{2C}$ fabric is the earliest fabric that can be reliably traced macroscopically at Little Crapeau Lake (Fig. 6.1 a). It is tightly folded by the NW-striking $S_{3C}$, which is steepened and transposed by the similarly oriented $S_{4C}$. These fabrics are observed in some locations to be overprinted by a NNE-striking fabric, $S_{5C.}$ Although the two areas are separated by the extensive Rodrigues granite, it may be possible to correlate the $S_{5C}$ fabric with the $S_{4B}$ fabric at Brown Water Lake, as they are approximately the same orientation, pervasiveness and intensity. Figure 6.1 shows the $S_{1B}$-$S_{2B}$ surface to be affected by $S_{3B}$ and $S_{4B}$ in a cross-folding style. This cross-folding effect may be what has caused the exposure of Archean basement culminations.

Previous workers have theorized that the doming of the Archean crust from beneath the supracrustal sequence was an effect of regional cross-folds. By the deformational numbering scheme established by this work, these folding events may have been a combination of the $D_2$ and $D_3$ or the $D_3$ and $D_4$ events in the Brown Water Lake area. This implies that peak metamorphism (syn to post-$S_{5B}$) occurred after the regional folding and doming.

The rocks at Brown Water and Little Crapeau lakes are similar in their structural styles, number of generations of deformation, and in their metamorphic styles and events. At both locations, not only does the timing of peak metamorphism coincide with major local intrusive events, but so do the strongest deformation events. This may not be coincidence; as the rocks are heated

and softened by local intrusions, they will deform and recrystallize more easily, forming strong fabrics associated with these events, i.e. the $S_{4B}$ foliation.

The two areas do differ in timing of metamorphism, and in the pressure and temperature conditions having affected the rocks during peak metamorphism (summarized in Table 6.1). Figure 6.2 provides a snapshot view at the time of peak metamorphism for both study areas. Peak metamorphic conditions for rocks of both areas were estimated by considering metamorphic mineral reactions that occurred in the rocks, and by plotting bulk rock and mineral chemical compositions on published phase diagrams. At Little Crapeau, peak conditions were reached between 3.1-3.9 kbars and 570-630°C around 1877 Ma, while P-T estimates are somewhat higher and later for rocks at Brown Water, between 3.1-4.2 kbars and 570-670°C around 1850 Ma. At Little Crapeau Lake, metamorphic mineral growth peaked after the development of the $S_{2C}$ fabric, whereas growth of these minerals at Brown Water Lake was syn- to post-$S_{4B}$ (Fig. 6.2). Metamorphic mineral paragenesis in relation to deformation stages was determined using detailed microstructural analysis. A combination of methods of analysis helped to build a strong kinetic and P-T history.

As it is presently understood, sedimentary rocks of the Coronation Supergroup were deposited as early as 2020 Ma on the western margin of the Slave Craton. U-Th in-situ dating of monazite suggests the preservation of detrital core material, with ages ranging from ~2600-2100 Ma. Through the process of dissolution and precipitation, new material nucleated on these grains, or formed new grains, during periods of crustal heating (through local intrusions) and resulting metamorphism. The most significant metamorphic events recorded in monazite at Brown Water Lake all occur after 1950 Ma (Fig. 5.4), with the most recrystallized grains (i.e. 2525A) strongly indicating an important metamorphic event ca. 1850 Ma. This coincides with the U-Pb

zircon crystallization age of the locally extensive Rodrigues granite. U-Pb zircon ages yielded from regional intrusions agree with this data.

Pelitic schists in the Brown Water Lake area record up to 5 consistently identifiable stages of deformation, with 2 or more weak, late, overprinting crenulations. The earliest documented fabric is preserved in the earliest porphyroblastic garnet phase. Cores in garnets overgrow $S_{1B}$, preserved as inclusion trails. Garnet rims preserve $S_{2B}/S_{4B}$ inclusion trails, indicating growth during and after this deformation event. The inclusion trails overgrow a late crenulation as well, providing evidence for a long period of heating which allowed for the growth of garnet in a specific bulk composition (i.e. sample 2512A). Cordierite porphyroblasts overgrow the main phase of deformation, $S_{4B}$, with some porphyroblasts preserving a gentle crenulation at the edges of grains. The late, strong $S_{5B}$ crenulation cleavage is overgrown by andalusite. On the western edge of the high strain belt at Brown Water Lake, andalusite is the highest grade porphyroblastic stage that preserves inclusion trails. With increasing metamorphic grade, sillimanite in fibrolite form is found in these pelitic schists, however it does not give good indications of growth timing in relation to deformation. It does appear to be aligned in the $S_{4B}$ fabric.

Garnet isograd controls are not obvious in the sequences of pelitic schists of the two study areas. Spear (1993) shows that rocks with high Fe/Mg are more likely to grow garnet, and added MnO increases the stability of garnet within a rock. We see this subtle chemical difference in rocks from Brown Water Lake – higher Fe and Mn ratios (Fig. 3.1). These increased elemental ratios reduce the free energy of the system, so the reaction chloritoid + biotite > garnet + chlorite happens at lower temperature conditions and higher G, expanding the stability field of garnet (Spear, 1993). Rocks with higher MnO content (Mn/(Mn+Fe+Mg)) don't need as much Fe/Mg to stabilize garnet + chlorite. Pelites will grow garnet + chlorite at

~525°C in the regular KFMASH system, whereas garnet will stabilize in the presence of MnO ~440-470°C. CaO partitions strongly into garnet (relative to chlorite, biotite, chloritoid and staurolite) and has a similar effect to MnO on the stability of garnet (Spear, 1993). The whole rock chemistry of the pelitic schists at Brown Water Lake (Appendix C) as well as garnet chemistry from both locations (Appendix D) shows garnet-bearing rocks to be strongly manganiferous and calcic. The growth of garnet in these pelites is compositionally controlled; however these controls appear to be very subtle differences in bulk rock and mineral chemistry.

Pelitic gneisses near the contact with regional Archean culminations preserve gneissic banding in the orientation of $S_{2B}$, crosscut by weak $S_{3B}$ and $S_{4B}$ shear fabrics and crenulations. Large garnet and cordierite porphyroblasts are found in these rocks, wrapped by the gneissic banding.

Coticule layers in the cordierite and andalusite zones are alternating metapelitic bedding and thin quartz-garnet layers. These layers are complexly folded, and are the only unit where both steep and shallow fold plunges have been observed (Appendix A plate 1, stations 1558 and 2519). Sheath folds, refolded folds, and brittle fractures demonstrate the complexity of the deformation. Owing to the competency difference between the schist and the coticules, folding may been preserved differently in these units than elsewhere in the belt, or deformation produced complex 3D structures.

In the Little Crapeau Lake area, deformation and metamorphism happened earlier than they did to the east. Although only separated by 40 km, and bordering both sides of the Rodrigues intrusion, the rocks of these two areas do not share the same structural or metamorphic history.

The rocks in the Little Crapeau Lake area also record 5 phases of deformation. The earliest fabric, $S_{1C}$ is rarely observed, but has been documented in rocks on the east side of the lake. It is preserved in cordierite and andalusite porphyroblasts. Undeformed $S_{2C}$ fabric is preserved by inclusion trails inside cordierite porphyroblasts. Andalusite overgrows $S_{1C}$ rotating into $S_{2C}$. Garnet porphyroblasts are found to be included inside andalusite, and are wrapped by a strong $S_{3C}$ fabric, but none have been observed to preserve inclusion trails that indicate timing of growth relative to $S_{1C}$ and $S_{2C}$. No porphyroblastic phases have been observed to overgrow any fabrics after $S_{2C}$. Therefore, peak metamorphism occurred very early in the deformational history.

The Little Crapeau sill, dated at ca. 1877 Ma, intruded parallel to $S_{2C}$ and is folded by $S_{3C}$. This is consistent with the proposed peak of metamorphism, also confirmed by U-Pb monazite ages which cluster in the range of 1880-1867 Ma. U-Th monazite mean ages are more scattered, with a range of 1925-1889 Ma.

Isogradic surfaces (or metamorphic mineral zone boundaries) are folded along a NW-trending axial plane trace. It is proposed here that they were folded by the steep $D_{4C}$ event, although it is possible that it occurred earlier during $D_{3C}$.

The large Archean culmination to the northeast of Little Crapeau Lake records a U-Th zircon recrystallization age at ca. 1876 Ma, also consistent with regional heating due to the intrusion of the Little Crapeau sill.

### *6.1.2 Regional and Orogen-Scale Interpretations and Questions*

The orientations of dominant kinetic fabrics observed, both macro and microscopically at Brown Water and Little Crapeau Lakes, are important to recognize when considering tectonic activity at the time of deformation. At Little Crapeau Lake, the $S_{3C}$ and $S_{4C}$ fabrics, whose ~NW-

SE orientation dominates the character of bedding and landforms in the area, are proposed to have developed after the intrusion of the ca. 1877 Ma Little Crapeau sill. Their orientation, if linked with continued collision during orogenesis, would suggest NE-directed basin closure or collision of a terrane. In a geologically short time thereafter, at both Little Crapeau and Brown Water Lakes, the dominant fabric development is a more SE-directed shortening event, resulting in the formation of the $S_{5C}$ and $S_{4B}$ fabrics. The $S_{4B}$ fabric is the strongest event to have affected the rocks at Brown Water Lake, occurring before the intrusion of the ca. 1850 Ma Rodrigues granite. This signifies a ~60° shift in shortening direction on a tectonic scale, within the span of ~25 m.y. As the model for the evolution of the Wopmay Orogen continues to develop, and with the aid of new geochronological data and detailed mapping, the causes for this major shift may be revealed. Until recently, the >2.0 Ga Hottah Terrane which is exposed west of the Great Bear Magmatic zone, was interpreted to be an allochthonous terrane which collided and docked during eastward directed subduction during orogenesis. Based upon new data, Jackson et al. (2013) have postulated a new origin for the terrane and its accretion with the Wopmay Orogen, and include in their hypothesis a new collision and docking direction (L. Ootes, pers. Comm.. 2013). Thus far it is not known when this collision occurred, however it may be the cause for the development of the early, strong $S_{3C}$ or $S_{4C}$ fabric.

The intrusions of post-Hepburn suite age and of Bishop suite age are all local plutons or xenoliths within plutons in the Little Crapeau and Brown Water Lake areas, whose U-Pb zircon ages validate the range in monazite ages gathered for this study. This indicates a long history (a few tens of m.y.) of crustal heating and melting that led to regional intrusive suites and resetting/dissolution of monazite material to produce a wide range of metamorphic ages in the pelitic schists. This heat circulation was likely a result of ongoing Wopmay-scale orogenesis. The Calderian orogeny is thought to have occurred ca. 1885 Ma. These new intrusive suite age dates increase the previous age range of Hepburn intrusions up to 1875 Ma and bridges the gap

that existed between the end of the Hepburn intrusive stage and the initiation of Bishop suite plutonism. This implies that heating of the crust was ongoing, and likely that the orogen was tectonically active throughout this extended time period, which agrees with the kinematic history observed in the rocks. Although, as mentioned earlier, major deformation stages appear to be focused on major intrusive events at both study locations.

In the northern half of the Wopmay Orogen, where these metasedimentary units have much greater exposure and are not as ductilely deformed, workers have been able to pick out stratigraphic marker horizons, and delineated thrusts in the sequence. In the southern half however, it is more difficult to see such features, due to exposure and degree and intensity of deformation. King et al. (1987) placed a thrust fault on the contact of the pelitic schists with the gneisses at Brown Water Lake. For this study, no definite evidence was found to warrant the placement of a thrust fault, and thus it was excluded from the map (Appendix A Plate 1). The only noteworthy difference between these rocks is the apparent sudden coarseness of the rocks heading West, with increasing metamorphic grade. Geochemically the gneisses are very similar to the pelitic rocks, although are slightly enriched in Mg and Al (Fig. 3.1). Within the pelitic sequence there is no field evidence for shear zones or sudden changes in stratigraphy to suggest that there is a thrust where King has placed it. However an argument can be made to keep this thrust and incorporate it in the structural history. It is proposed in this study that the rocks that constitute the Archean gneiss domes are reworked parautochthonous Slave material that was rifted, thinned (passive margin sedimentation happened at this time), and subsequently thrust eastward back over the Slave margin during orogenesis ($S_{3C}$ and $S_{1B}$ thrust fabrics?). If the reworked parauthochthonous material that constitutes the Archean culminations was emplaced (in its present configuration) as part of a sequence of thrust sheets, interleaved with the Paleoproterozoic sedimentary material, then a thrust surface would be

necessary. This thrust could be placed in approximately the same location as King placed hers, along the melt-in boundary, however it need not be at the same structural level (Fig. 3.21).

Additionally, it is possible that during thrusting, the supracrustal sequence deposited as part of the passive margin was incorporated with these thrusts, helping to create the geometry observed today at Brown Water Lake and at Little Crapeau.

The need for Archean basement rifting and reworking, with subsequent thrusting and interleaving, stems from the extent of deformation documented in the regional culminations, versus the lack of such deformation in the nearby cratonic rocks. The Slave craton, directly adjacent to the highly deformed rocks of the high strain belt at Brown Water Lake, shows little to no evidence for intense internal deformation, whereas Archean material in the domes is multiply deformed, and yields zircons recrystallization ages coinciding with the local intrusion ages (Rodrigues granite and Little Crapeau Sill). Rhealogically, it is difficult to explain how a thick, cold craton with a deep lithosphere (as is shown in SNORCLE transects) might deform as ductilely as rocks in the culminations show evidence for (Hoffman et al., 1988)

It is also proposed here that the original extent of the Rodrigues granite was as far east as the melt-in zone at Brown Water Lake. Rocks on either side of the melt-in boundary are geochemically similar, however appear very different in the field. While rocks of the High Strain belt are fine grained, well bedded, and preserves early fabrics and folds, rocks of the Inter-dome zone are very coarsely recrystallized and grow very large porphyroblasts (Fig. 3.15). If they are not different stratigraphic sequences, then perhaps the original extent of the Rodrigues granite was the boundary of the melt-in zone, and the Inter-dome zone rocks were much more heavily affected by contact metamorphism.

The ~30 m.y. difference in plutonic events and metamorphic ages between the Little Crapeau Lake area (1877 Ma) and Brown Water Lake area (1850 Ma) can be explained by the

association of these dates with the Hepburn and Bishop intrusive suites, which are correlated with activities associated with the Calderian orogeny (ca. 1885), and with initiation of post-orogenic, subduction-related Great Bear magmatism.

## 6.2 Summary/Conclusions

Main (dominant) deformation stage(s):

- Little Crapeau Lake
    - Two pervasive fabrics are strong and dominate the rocks: $S_{3C}$ (shallow, NW-striking "thrusting" fabric) and $S_{4C}$ (steep NW-striking fabric)
    - Little Crapeau Granite sill emplacement is syn to post-$S_{2C}$ at 1877 ± 2 Ma, deformed by $S_{3C}$
- Brown Water Lake
    - Two moderately to steeply NW-dipping fabrics: $S_{2B}$ and $S_{4B}$

Peak metamorphism:

- Little Crapeau Lake
    - Post-$S_{1C}$ (cordierite); syn-$S_{2C}$ (andalusite)
    - 3.1-3.9 kbars and 570-630°C
- Brown Water Lake
    - Post-$S_{1B}$, syn-$S_{2B}$ (garnet, cordierite); post-$S_{4B}$ to syn-$S_{5B}$ cren (cordierite, andalusite)
    - 3.1-4.2 kbars and 570-670°C

Intrusive phase responsible for peak Metamorphism:

- Little Crapeau Lake
    - Little Crapeau Sill emplacement pre-$S_{3C}$ at 1877 ± 2 Ma

- Brown Water Lake
    - Rodrigues granite emplacement at 1849.4 ± 1.4 Ma to 1851.8 ± 3.2 Ma (Jackson et al., 2013), with Zinto suite xenoliths at ca 1867.4 ± 1 Ma. This is the last phase of plutonism in the Coronation margin, which coincides with magmatism in the Great Bear Magmatic zone

### *6.2.1 Recommendations for Future Work*

- More structural mapping and microstructural analysis may add detail to the earliest events at Brown Water Lake
- Further work on crosscutting mafic and felsic dykes in both study areas can help constrain tectonic and metamorphic events, and timing of igneous activity associated with magmatism prior to initiation of the Great Bear Magmatic zone
- Better temperature constraints could be obtained using the garnet-biotite thermometer
- Dating of in-situ allanite $(Ca,REE,Y)_2(Al,Fe)_3(SiO_4)_3OH$, a metamorphic mineral that crystallizes at a lower temperature than monazite ($LREEPO_4$) may provide further information about the early thermotectonic history
- U-Pb geochronological dating of metamorphic growths (rims) on detrital zircons from pelitic schists may provide better constraints on local heat circulation in the crust
- Further probing of garnet chemistry may lead to a better understand of the coticules layers and their origin and diagenesis
- Performing whole rock geochemistry analysing for rare earth elements may add the detail needed to differentiate between lithologies – to determine whether there is more than one sedimentary package at Brown Water Lake
- Exhumation study on the Archean gneiss domes to determine their exhumation rate and the timing of their heating and ascent of original depth

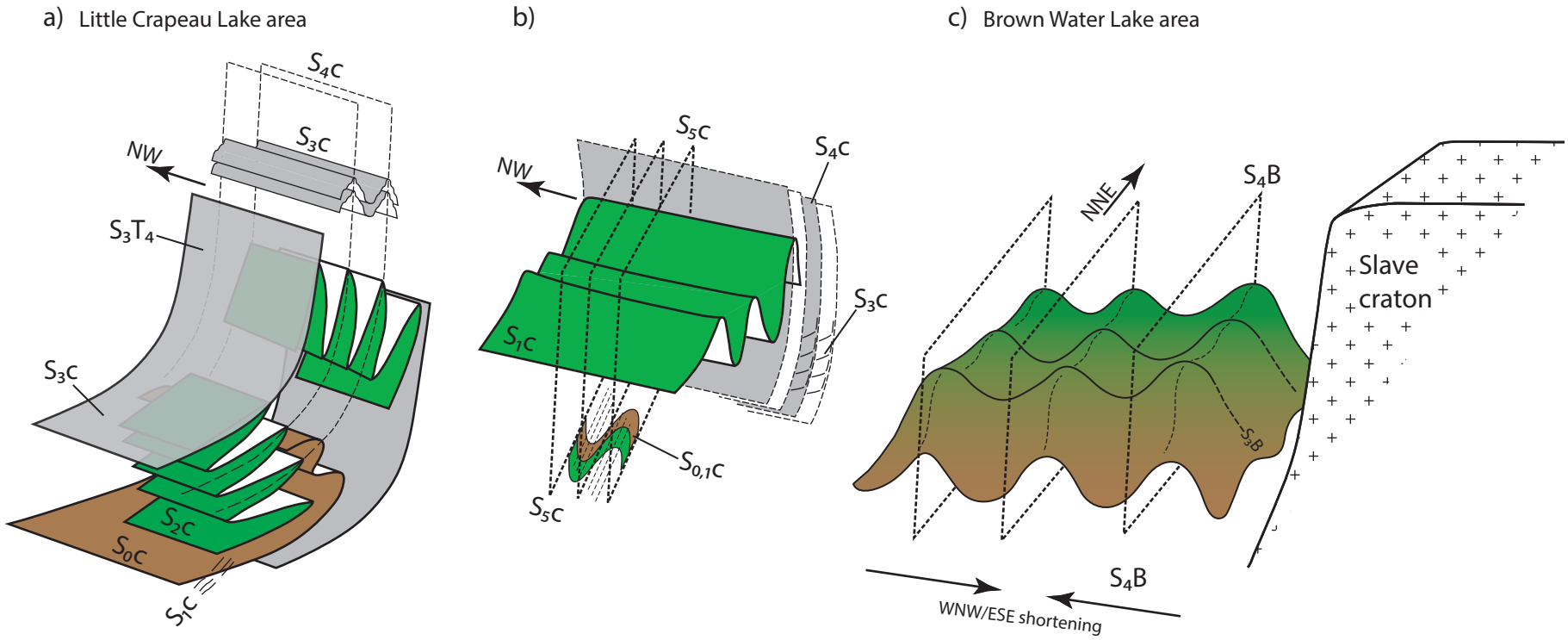


**Figure 6.1 Schematic summary of overprinting fabrics at Little Crapeau Lake and Brown Water Lake.** Rocks at Little Crapeau Lake (a) show an early, complex history of folding more clearly than rocks at Brown Water Lake (c). $S_{2C}$ was a steep, SW-dipping foliation, tightly folded by a shallow differentiated cleavage, $S_{3C}$. This shallow fabric may have developed during a fold and thrust event that resulted in the interleaving of parauthochthonous slivers of reworked Archean material and passive margin metasediments. $S_3c$ was itself subsequently steepened and transposed by $S_{4C}$ ($S_3T_4$), a steep NW-striking, differentiated cleavage. Where $S_{4C}$ is strongly developed, $S_{3C}$ is preserved as polygonal arcs (b). $S_{5C}$ is manifest in few locations at Little Crapeau, and overprints $D_{3C}$ folds with a steep, NNE-striking crenulation (b). Very little evidence exists for this $S_{4C}$ fabric being present in rocks at Brown Water Lake (c), except in between Archean culminations, where we see hints of a steep, NW-striking crenulation, $S_{3B}$ overprinting shallow, gneissic banding. A final stage of strong deformation affected the region, notably strongly affecting Brown Water Lake rocks. This final stage ($S_{4B}$ in the east, $S_{5C}$ in the west) concertinaed the rocks against the Slave craton, creating steep, tight, upright folds with gently plunging fold axes that dip shallowly NNE and SSW. The combination of $S_{3B}$ and $S_{4B}$ may be the cause for the structural uplift of the basement culminations. $S_{1C}$ is observed as inclusion trails in some andalusite and cordierite porphyroblasts at Little Crapeau Lake.

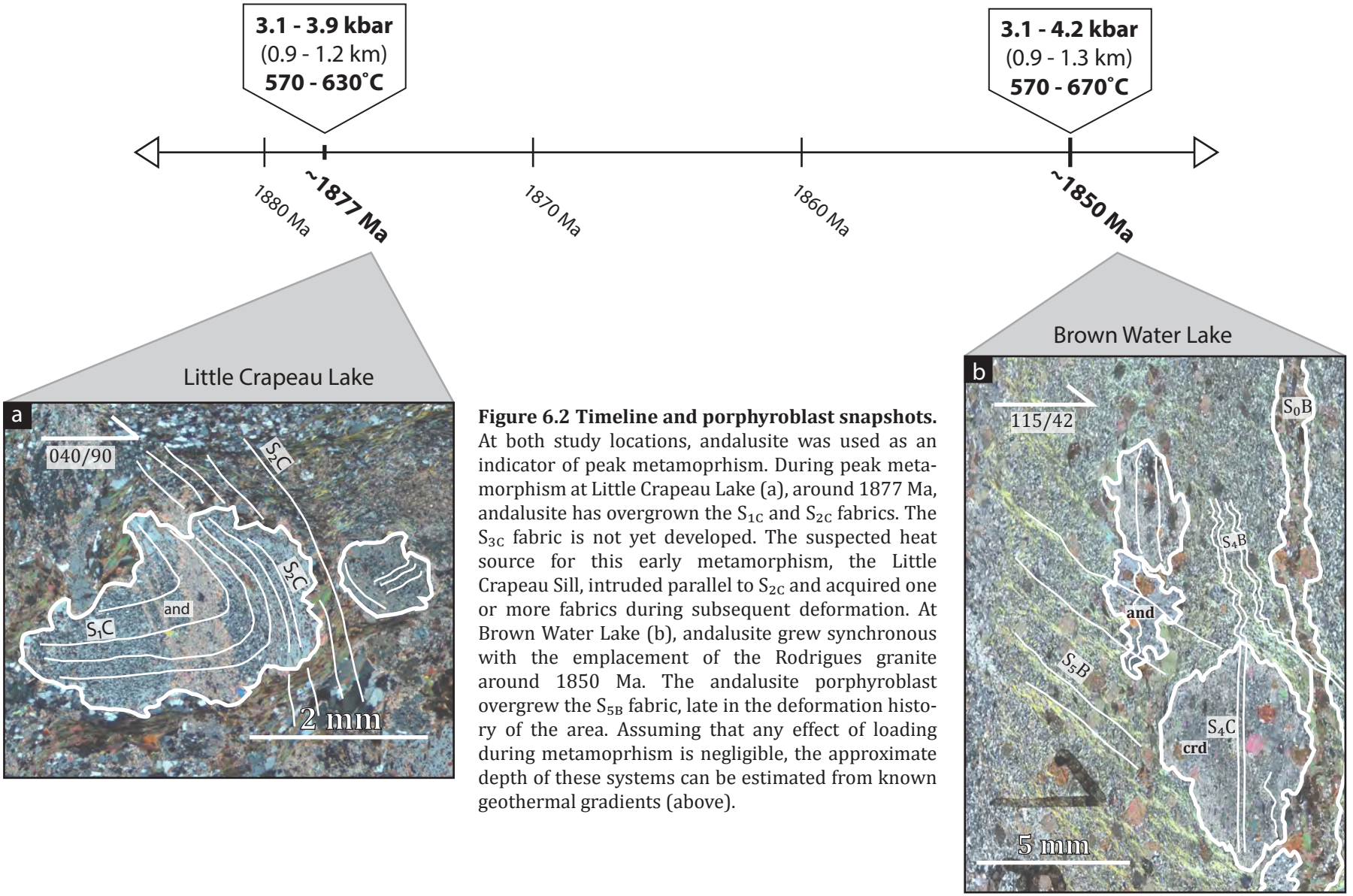


**Figure 6.2 Timeline and porphyroblast snapshots.** At both study locations, andalusite was used as an indicator of peak metamoprhism. During peak metamorphism at Little Crapeau Lake (a), around 1877 Ma, andalusite has overgrown the $S_{1C}$ and $S_{2C}$ fabrics. The $S_{3C}$ fabric is not yet developed. The suspected heat source for this early metamorphism, the Little Crapeau Sill, intruded parallel to $S_{2C}$ and acquired one or more fabrics during subsequent deformation. At Brown Water Lake (b), andalusite grew synchronous with the emplacement of the Rodrigues granite around 1850 Ma. The andalusite porphyroblast overgrew the $S_{5B}$ fabric, late in the deformation history of the area. Assuming that any effect of loading during metamoprhism is negligible, the approximate depth of these systems can be estimated from known geothermal gradients (above).

| Dominant Monazite ages | Brown Water Lake | | Little Crapeau Lake | Dominant Monazite ages |
|---|---|---|---|---|
| | | | $S_{1C}$ | |
| | $S_{1B}$ | | $S_{2C}$ | ~1877 Ma |
| | $S_{2B}$ | | $S_{3C}$ | |
| | $S_{3B}$ | = (?) | $S_{4C}$ | |
| | $S_{4B}$ | = | $S_{5C}$ | |
| 1850 Ma | $S_{5B}$ | | | |

**Table 6.1** Summary table of overprinting fabrics and metamorphic timing

# REFERENCES


Abu Sharib, A. S. A. A., and Bell, T. H., 2011, Radical changes in bulk shortening directions during orogenesis: significance for progressive development of regional folds and thrusts: Precambrian Research, v. 188, no. 1, p. 1-20.

Ayers, J. C., Miller, C., Gorisch, B., and Milleman, J., 1999, Textural development of monazite during high-grade metamorphism: Hydrothermal growth kinetics, with implications for U, Th-Pb geochronology: American Mineralogist, v. 84, p. 1766-1780.

Bell, T., and Duncan, A. C., 1978, A rationalized and unified shorthand terminology for lineations and fold axes in tectonites: Tectonophysics, v. 47, no. 1, p. T1-T5.

Bell, T. H., Forde, A., and Hayward, N., 1992, Do smoothly curving, spiral-shaped inclusion trails signify porphyroblast rotation?: Geology, v. 20, p. 59-62.

Bell, T. H., and Newman, R., 2006, Appalachian orogenesis: the role of repeated gravitational collapse: Geological Society of America, Special Papers, v. 414, p. 95.

Bennett, V., and Rivers, T., 2006, U-Pb Ages of Detrital Zircons from the Southern Wopmay Orogen, Northwest Territories: Northwest Territories Geoscience Office.

Bennett, V., Rivers, T., and Jackson, V. A., 2012, A Compilation of U-Pb Zircon Primary Crystallization and Depositional Ages from the Paleoproterozoic Southern Wopmay Orogen, Northwest Territories: Northwest Territories Geoscience Office.

Bowring, S. A., 1985, U-Pb zircon geochronology of early Proterozoic Wopmay Orogen, NWT Canada: an example of rapid crustal evolution: Kansas Univ., Lawrence (USA).

Bowring, S. A., and Grotzinger, J. P., 1992, Implications of new chronostratigraphy for tectonic evolution of Wopmay Orogen, Northwest Canadian Shield: American Journal of Science, v. 292, p. 1-20.

Connolly, J. A. D., and Petrini, K., 2002, An automated strategy for calculation of phase diagram sections and retrieval of rock properties as a function of physical conditions: Journal of Metamorphic Geology, v. 20, no. 7, p. 697-708.

Cook, F. A., 2011, Multiple arc development in the Paleoproterozoic Wopmay Orogen, northwest Canada: Arc-Continent Collision, p. 403-427.

Dahl, P. S., Hamilton, M. A., Jercinovic, M. J., Terry, M. P., Williams, M. L., and Frei, R., 2005, Comparative isotopic and chemical geochronometry of monazite, with implications for U-Th-Pb dating by electron microprobe: An example from metamorphic rocks of the eastern Wyoming Craton (USA): American Mineralogist, v. 90, no. 4, p. 619-638.

Davis, W., Hoffman, P. F., Bowring, S. A., Buchwaldt, R., and Hildebrand, R. S., 2011, Birthdate for the Coronation paleocean: age of initial rifting in Wopmay orogen, CanadaThis article is one of a series of papers published in this Special Issue on the theme ofGeochronologyin honour of Tom Krogh: Canadian Journal of Earth Sciences, v. 48, no. 2, p. 281-293.

Easton, R. M., 1981, Geology of Grant Lake and Four Corners Lake Map Areas, Wopmay Orogen, District of Mackenzie: Current Research, Part B, Geological Survey of Canada, v. Paper 81-1B, p. 83-94.

Fayon, A. K., Whitney, D. L., and Teyssier, C., 2004, Exhumation oforogenic crust: Diapiric ascent versus low-angle normal faulting: Gneiss Domes in Orogeny, no. 380, p. 129.

Frith, R., 1974, Rb-Sr geochronological study of rocks of the Bear and Slave Provinces, Northwest Territories: McGill University.

Frith, R., Frith, R. A., and Doig, R., 1977, The geochronology of the granitic rocks along the Bear-Slave Structural Province boundary, northwest Canadian Shield: Canadian Journal of Earth Sciences, v. 14, no. 6, p. 1356-1373.

Frith, R. A., 1986, Precambrian Geology of the Indin Lake map area: Geological Survey of Canada, Open File Report 1243.

-, 1990, Precambrian Geology of the Arseno Lake map area, District of Mackenzie, Northwest Territories, Ottawa, ON, Geological Survey of Canada.
-, 1992, Precambrian geology of the Indin Lake map area, district of Mackenzie, Northwest Territories, Ottawa, ON, Geological Survey of Canada, v. 424.
Frith, R. A., and Loveridge, W. D., 1982, Ages of Yellowknife deposition, granitoid intrusion and regional metamorphism in the northeastern Slave Structural Province: Geological Survey of Canada; Paper 82-1A, p. p. 225-237.
Gandhi, S. S., Mortensen, J. K., Prasad, N., and van Breemen, O., 2001, Magmatic evolution of the southern Great Bear continental arc, northwestern Canadian Shield: geochronological constraints: Canadian Journal of Earth Sciences, v. 38, no. 5, p. 767-785.
Grotzinger, J., and Hoffman, P., 1983, Aspects of the Rocknest Formation, Asiak thrust-fold belt, Wopmay orogen, District of Mackenzie: Current Research, Part B: Geological Survey of Canada Paper, p. 83-92.
Hayward, N., and Oneschuk, D., 2011, Regional Geophysical Compilation Project, Great Bear Magmatic Zone, Northwest Territories and Nunavut, NTS 85 M and N, and 86 C, D, E, F, K and L: Northwest Territories Geoscience Office, scale 1:500 000 scale.
Hildebrand, R., Bowring, S., and Housh, T., 1990, The medial zone of Wopmay orogen, District of Mackenzie: Current research, part C, p. 167-176.
Hildebrand, R. S., and Bowring, S. A., 1984, Continental intra-arc depressions: A nonextensional model for their origin, with a Proterozoic example from Wopmay orogen: Geology, v. 12, p. 73-77.
Hildebrand, R. S., Hoffman, P. F., and Bowring, S. A., 1987, Tectono-magmatic evolution of the 1.9-Ga Great Bear magmatic zone, Wopmay Orogen, northwestern Canada: Journal of Volcanology and Geothermal Research, v. 32, no. 1, p. 99-118.
-, 2010, The Calderian orogeny in Wopmay orogen (1.9 Ga), northwestern Canadian Shield: Geological Society of America Bulletin, v. 122, no. 5-6, p. 794-814.
Hildebrand, R. S., Paul, D., Pietikainen, P., Hoffman, P. F., Bowring, S. A., and Housh, T., 1991, New geological developments in the internal zone of Wopmay orogen, District of Mackenzie, Current Research, Part C, Volume Paper 91-1C, Geological Survey of Canada, p. 157-164.
Hoffman, P., Tirrul, R., King, J., St-Onge, M., and Lucas, S., 1988, Axial projections and modes of crustal thickening, eastern Wopmay orogen, northwest Canadian shield: Processes in continental lithospheric deformation; Geological Society of America Special Paper, v. 218, p. 1-29.
Hoffman, P. F., 1980, Wopmay Orogen: A Wilson cycle of Early Proterozoic age in the Northwest of the Canadian Shield, *in* Strangway, D. W., ed., The Continental Crust and its Mineral Deposits, Volume Special Paper 20: Ottawa, Geological Survey of Canada.
-, 1984, Geology, northern Internides of Wopmay Orogen, District of Mackenzie, Northwest Territories: Geological Survey of Canada.
Hoffman, P. F., and Bowring, S. A., 1984, Short-lived 1.9 Ga continental margin and its destruction, Wopmay orogen, northwest Canada: Geology, v. 12, p. 68-72.
Hoffman, P. F., Bowring, S. A., Buchwaldt, R., and Hildebrand, R. S., 2011, Birthdate for the Coronation paleocean: age of initial rifting in Wopmay Orogen, Canada: Canadian Journal of Earth Sciences, v. 48, p. 281-293.
Hoffman, P. F., and Hall, L., 1993, Geology, Slave craton and environs, District of Mackenzie, Northwest Territories: Geological Survey of Canada, scale 1:1,000,000.
Holcombe, R., 2011, GEOrient ver 9.5.0.
Holland, T. J. B., and Powell, R., 1998, An internally consistent thermodynamic data set for phases of petrological interest: Journal of Metamorphic Geology, v. 16, no. 3, p. 309-343.

Jackson, V. A., and Ootes, L., 2012, Preliminary Geologic Map of the South-Central Wopmay Orogen (parts of NTS 86B, 86C, and 86D); results from 2009 to 2011: Northwest Territories Geoscience Office, scale 1:100,000.

Jackson, V. A., Van Breemen, O., Ootes, L., Bleeker, W., Bennett, V., Davis, W. D., Ketchum, J., and Smar, L., 2013, U-Pb zircon ages and field relationships of Archean basement and Proterozoic intrusions, south-central Wopmay Orogen, NWT: implications for tectonic assignments.: Canadian Journal of Earth Sciences, no. 50, p. 979-1006.

Janots, E., Engi, M., Rubatto, D., Berger, A., Gregory, C., and Rahn, M., 2009, Metamorphic rates in collisional orogeny from in situ allanite and monazite dating: Geology, v. 37, no. 1, p. 11-14.

Jercinovic, M., Williams, M., Allaz, J., and Donovan, J., Trace analysis in EPMA, *in* Proceedings IOP Conference Series: Materials Science and Engineering2012, Volume 32, IOP Publishing, p. 012012.

Jercinovic, M. J., and Williams, M. L., 2005, Analytical perils (and progress) in electron microprobe trace element analysis applied to geochronology: Background acquisition, interferences, and beam irradiation effects: American Mineralogist, v. 90, p. 526-546.

Johnson, S., and Vernon, R., 1995, Stepping stones and pitfalls in the determination of an anticlockwise P-T-t-deformation path: the low-P, high-T Cooma Complex, Australia: Journal of Metamorphic Geology, v. 13, no. 2, p. 165-183.

King, J. E., 1985, Structure of the metamorphic-internal zone, northern Wopmay Orogen, Northwest Territories, Canada [Ph.D.: Queen's University, 208 p.

King, J. E., 1986, The Metamorphic Internal Zone of Wopmay Orogen (Early Proterozoic), Canada: 30 km of Structural Relief in a Composite Section Based on Plunge Projection: Tectonics, v. 5, no. 7, p. 973-&.

King, J. E., Barrette, P. D., and Relf, C. D., 1987, Contrasting styles of basement deformation and longitudinal extension in the metamorphic-internal zone of Wopmay Orogen, N.W.T., Current Research, Part A, Volume Paper 87-1A, Geological Survey of Canada, p. 515-531.

Kramm, U., 1976, The Coticule Rocks (Spessartine Quartzites) of the Venn-Stavelot Massif, Ardennes, a Volcaniclastic Metasediment?: Contributions to Mineralogy and Petrology, v. 56, p. 135-155.

Lalonde, A. E., 1989, Hepburn Intrusive Suite - Peraluminous Plutonism within a Closing Back-Arc Basin, Wopmay Orogen, Canada: Geology, v. 17, no. 3, p. 261-264.

Lamens, J., Geukens, F., and Viaene, W., 1986, Geological Setting and Genesis of Coticules (Spessartine Metapelites) in the Lower Ordovician of the Stavelot Massif, Belgium: Journal of the Geological Society, v. 143, p. 253-258.

McGlynn, J., and Ross, J. V., 1963, Arseno Lake Map-area, District of MacKenzie 86 B/12, Geological Survey of Canada, Department of Mines and Technical Surveys.

Murphy, J. B., and Nance, R. D., 1991, Supercontinent model for the contrasting character of Late Proterozoic orogenic belts: Geology, v. 19, no. 5, p. 469-472.

Nielsen, P. A., 1977, Metamorphic Petrology and Mineralogy of the Arseno Lake Area, NWT [Ph.D.: University of Alberta.

-, 1986, Metamorphism of the Arseno Lake area, N.W.T., Canada: an Abukuma facies series of Aphebian age: Canadian Journal of Earth Sciences, v. 23, no. 5, p. 646-669.

Parrish, R. R., 1990, U-Pb dating of monazite and its application to geological problems: Canadian Journal of Earth Sciences, v. 27, no. 11, p. 1431-1450.

Pattison, D., and Harte, B., 1991, Petrography and mineral chemistry of pelites, Equilibrium and Kinetics in Contact Metamorphism, Springer, p. 135-179.

Pattison, D. R. M., Spear, F. S., Debuhr, C. L., Cheney, J. T., and Guidotti, C. V., 2002, Thermodynamic modeling of the reaction muscovite + cordierite > Al2SiO5 + biotite +

quartz + H2O: constraints from natural assemblages and implications for the metapelitic petrogenetic grid: Journal of Metamorphic Geology, v. 20, p. 99-118.
Pehrsson, S. J., 2002, Geology, Indin Lake, Northwest Territories: Geological Survey of Canada, scale 1:125,000.
Rayner, N. M., and Stern, R. A., 2002, Improved sample preparation method for SHRIMP analysis of delicate mineral grains exposed in thin sections; Radiogenic Age and Isotopic Studies, Geological Survey of Canada, Current Research 2002-F10: Ottawa, Geological Survey of Canada, p. 3.
Spear, F. S., 1993, Metamorphic Phase Equilibria and Pressure-Temperature-Time Paths, Washington, D. C., Mineralogical Society of America, 799 p.:
St-Onge, M. R., 1981, "Normal" and "Inverted" Metamorphic isograds and their relation to syntectonic Proterozoic batholiths in the Wopmay Orogen, Northwest Territories, Canada: Tectonophysics, v. 76, p. 295-316.
-, 1984, Geothermometry and Geobarometry in Pelitic Rocks of North-Central Wopmay Orogen (Early Proterozoic), Northwest-Territories, Canada: Geological Society of America Bulletin, v. 95, no. 2, p. 196-208.
-, 1986, Zoned Poikiloblastic Garnets: P-T paths and syn-metamorphic uplift through 30 km of structural depth, Wopmay Orogen, Canada: Journal of Petrology, v. 28, no. Part 1, p. 1-21.
St-Onge, M. R., King, J. E., and Dalziel, I. W. D., 1987, Evolution of Regional Metamorphism during Back-Arc Stretching and Subsequent Crustal Shortening in the 1.9 Ga Wopmay Orogen, Canada: Philosophical Transactions of the Royal Society of London., v. A321, no. 1557, p. 199-219.
St-Onge, M. R., King, J. E., and Lalonde, A. E., 1984, Deformation and metamorphism of the Coronation Supergroup and its basement in the Hepburn metamorphic-plutonic zone of Wopmay orogen: Redrock Lake and the eastern portion of the Calder River map areas, District of Mackenzie, in Current Research, Part A: District of Mackenzie: Geological Survey of Canada Paper, p. 171-180.
Thompson, A., Ridley, J., and Mason, R., 1987, Pressure--Temperature--Time (P--T--t) Histories of Orogenic Belts [and Discussion]: Philosophical Transactions of the Royal Society of London. Series A, Mathematical and Physical Sciences, v. 321, no. 1557, p. 27-45.
Tirrul, R., 1982, Frontal thrust zone of Wopmay Orogen: Takijuq map area, District of Mackenzie: Geological Survey of Canada Current Research, Part A, Paper, p. 119-122.
-, 1983, Structure cross-sections across Asiak foreland thrust and fold belt, Wopmay orogen, District of Mackenzie: Current Research, Part A: Geological Survey of Canada Paper, p. 253-260.
Vilà, M., Pin, C., Liesa, M., and Enrique, P., 2007, LPHT metamorphism in a late orogenic transpressional setting, Albera Massif, NE Iberia: implications for the geodynamic evolution of the Variscan Pyrenees: Journal of Metamorphic Geology, v. 25, no. 3, p. 321-347.
Williams, I., 2001, Response of detrital zircon and monazite, and their U–Pb isotopic systems, to regional metamorphism and host-rock partial melting, Cooma Complex, southeastern Australia*: Australian Journal of Earth Sciences, v. 48, no. 4, p. 557-580.
Williams, M. L., Jercinovic, M. J., and Terry, M. P., 1999, Age mapping and dating of monazite on the electron microprobe: Deconvoluting multistage tectonic histories: Geology, v. 27, no. 11, p. 1023-1026.
Zhao, G., Cawood, P. A., Wilde, S. A., and Sun, M., 2002, Review of global 2.1–1.8 Ga orogens: implications for a pre-Rodinia supercontinent: Earth-Science Reviews, v. 59, no. 1, p. 125-162.

Zhao, G., Sun, M., Wilde, S. A., and Li, S., 2004, A Paleo-Mesoproterozoic supercontinent: assembly, growth and breakup: Earth-Science Reviews, v. 67, no. 1, p. 91-123.

# APPENDICES

# APPENDIX A

# Geology of Brown Water Lake
# 1:150,000

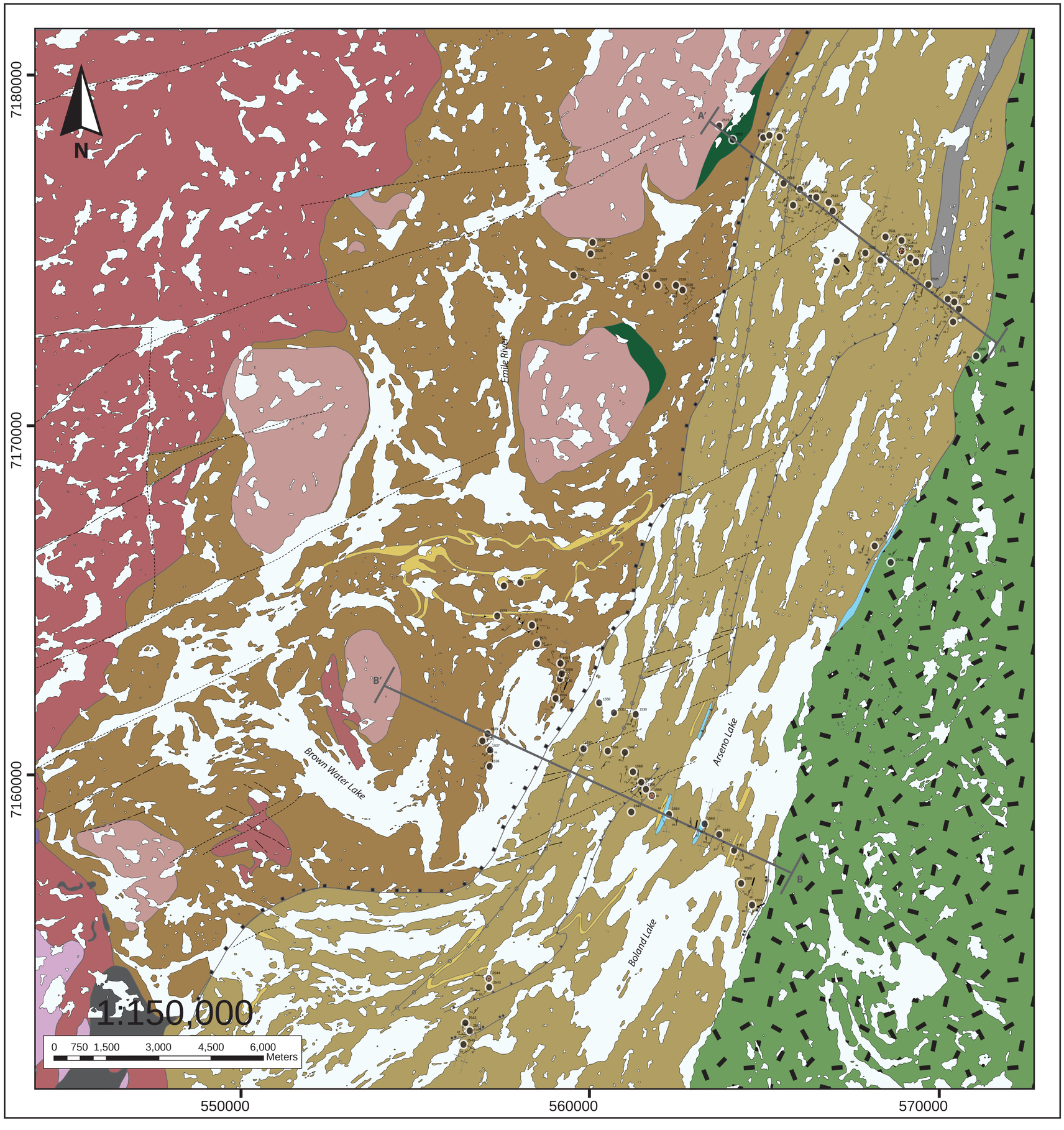


## Legend

### Lithologies

PROTEROZOIC

- Hottah dykes and sills (ca. 780 Ma): brown-black diabase sills and dykes
- Rodrigues granite (ca. 1850 Ma): homogenous granitic body, k-feldspar megacrystic peraluminous S-type granite.
- Diorite to gabbro
- Pelitic schists of the Coronation margin (undifferentiated): Fine to medium grained, brown to rusty weathered, laminated to bedded, and stronlgy foliated. Peak metamorphic assemblage is biotite + muscovite + cordierite + andalusite ± garnet ± fibrolite
- Pelitic gneisses of the Coronation margin: Coarse grained, rusty weathered, migmatitic with melt pods. Metamorphic assemblages are k-spar + sillimanite + andalusite + cordierite ± garnet ± melt ± corundum bearing.
- Quartzite/Quartz pebble conglomerate: Coarse grained, white to gray quartzite in ~50cm thick beds. Quartz pebble conglomerate comprises pebble to cobble sized clasts in a white/gray to brown arenite matrix
- Carbonate rocks. Marbles and calc-silicates are white to gray, massive to layered and foliated.

ARCHEAN

- Biotite phyllite to schist
- Amphibolite: Dark green to brown and black, coarse grained foliated amphibolite with ~50cm thick bands of interlayered white granitic melt.
- Gneiss and migmatite (ca. 2580 to >2900 Ma): Gneissic and migmatitic Archean culmination, includes metasedimentary phases and disaggregated metamafic dykes
- Slave craton: undifferentiated units

2512
2509

Station locations and number (shortened from "09ls1537" or "10ls2512")

Station location with pink star indicates the first appearance of garnet, increasing in metamorphic grade

Lineament

Fault, inferred

Trace of axial plane of major antiform or synform

### Structural Measurements

- Bedding: Younging direction unknown, younging direction upright
- Foliation: Main or unknown generation
- Foliation: 1st, 2nd, 3rd and 4th generation
- Crenulation fabric
- Migmatitic Layering: Main generation
- Gneissosity: Injection layering (granite into seds)
- Dyke, Vein
- Axial Plane
- Ductile Shear: Unknown sense, Sinistral sense
- Mineral Lineation: 1st generation
- Intersection Lineation: Unknown generation
- Fold Hinge
- Z-Fold Hinge: Unknown generation, 1st generation
- S-Fold Hinge: 1st generation
- Cross-section line (A′ – A)

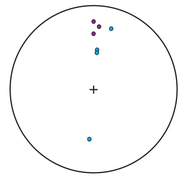

**Lineations plotted on equal area stereonet:** Crenulation lineations are shallow to moderately plunging northward (purple). One fold axis measurement plunges moderately southward, while the others plunge moderately toward the north to northeast (blue).

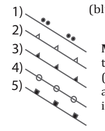


**Metamorphic Mineral zones** (mark on the high-T side of line): 1) biotite zone (chlorite out); 2) cordierite zone; 3) andalusite±cordierite zone; 4) sillimanite zone 5) melt-in/gneiss zone

NTS Map sheet covered by this area: 086B12
Datum: NAD 83, UTM Zone 11N
Scale: 1:150,000

Map is a compilation of work by Frith (1990), Hoffman and Hall (1993), Jackson and Ootes (2012), including work done by this author over the summers of 2009 and 2010. Undifferentiated units of the Slave craton are mapped and described in details by Pehrsson (2002). Lithologies that have not been directly observed for this study are simply named in the legend, without a complete description. These have been named and described by Jackson and Ootes (2012).

Inset map, at right, is a clip of the 1:150,000 scale Southern Wopmay Orogen mapping project by Jackson and Ootes (2012). The area shown comprises intrusive and metasedimentary units of the Metamorphic Internal zone and the eastern margin of the Great Bear magmatic zone. The Brown Water Lake map area is outlined by the dashed line.

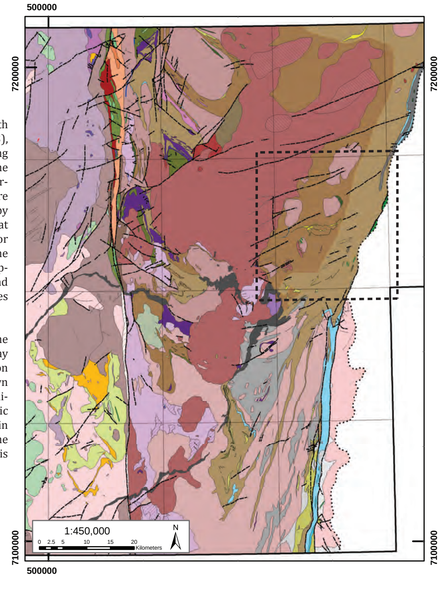



References
Frith, R. A., 1990, Precambrian Geology of the Arseno Lake map area, District of Mackenzie, Northwest Territories, Ottawa, ON, Geological Survey of Canada.
Hoffman, P. F., and Hall, L., 1993, Geology, Slave craton and environs, District of Mackenzie, Northwest Territories: Geological Survey of Canada, Open File 2559, scale 1:1,000,000.
Jackson, V. A., and Ootes, L., 2012, Preliminary Geologic Map of the South-Central Wopmay Orogen (parts of NTS 86B, 86C, and 86D); results from 2009 to 2011: Northwest Territories Geoscience Office, scale 1:100,000.
Pehrsson, S. J., 2002, Geology, Indin Lake, Northwest Territories: Geological Survey of Canada, scale 1:125,000.

# Geology of Little Crapeau Lake area
# 1:75,000

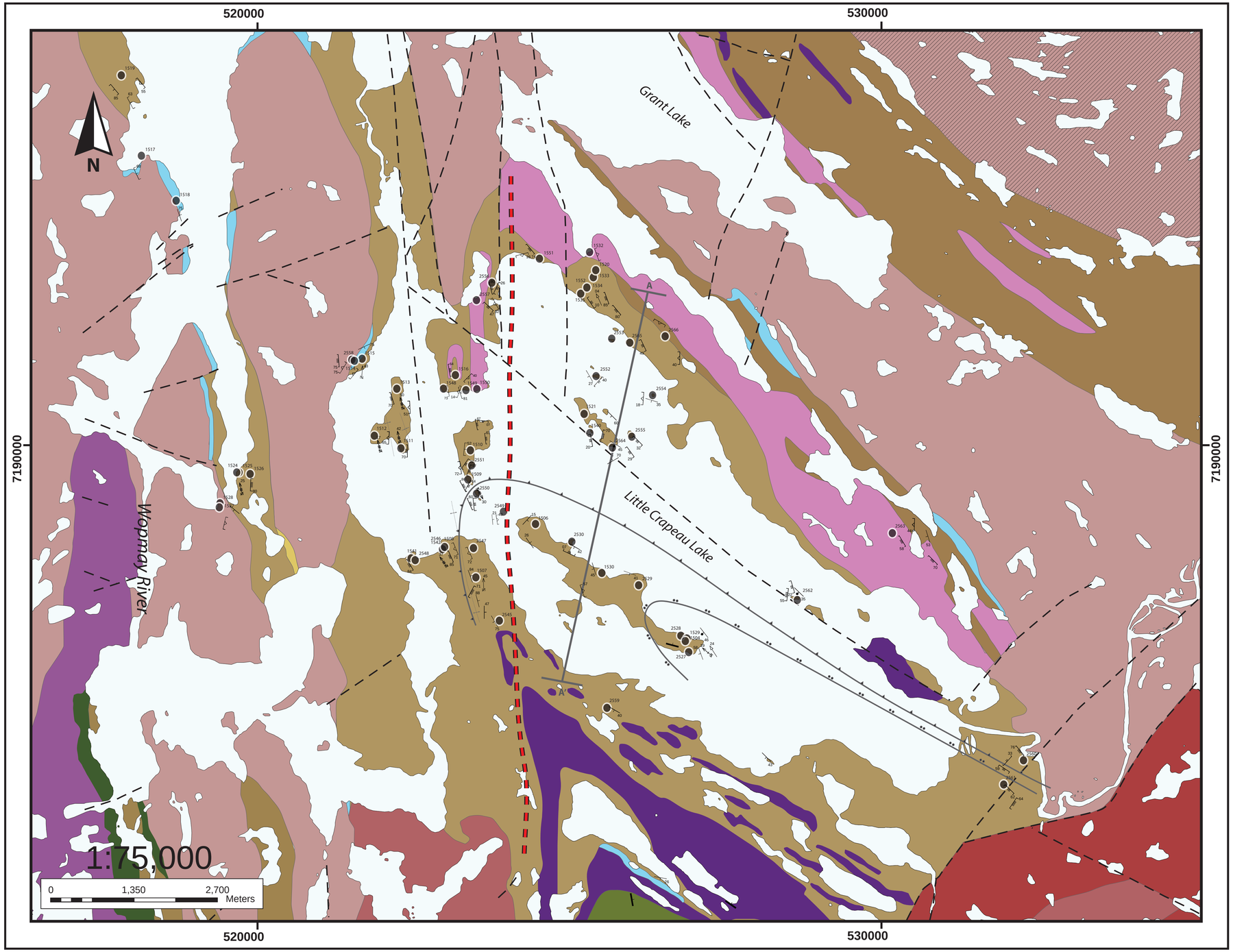


## Legend

### Lithologies

PROTEROZOIC

- Rodrigues granite (ca. 1850-1857 Ma): pink to white, coarse grained, homogenous granitic body, k-feldspar megacrystic, peraluminous S-type granite.
- Undivided granite to granodiorite: Uncertain relationship to Rodrigues granite
- Little Crapeau Sill: Biotite muscovite ± garnet granite (ca. 1878 Ma): Medium to fine grained white to gray granite, massive to strongly foliated. Forms sills ~30 cm thick and veinlets.
- Granodiorite to diorite
- Diorite to gabbro
- Basalt to andesite: Pillowed and massive flows
- Pelitic schists of the Coronation margin (undifferentiated): Fine to medium grained, brown to rusty weathered, laminated to bedded, and stronlgy foliated. Peak metamorphic assemblage is biotite + muscovite + cordierite + andalusite ± garnet ± fibrolite
- Pelitic gneisses of the Coronation margin (undifferentiated): Coarse grained, rusty weathered, migmatitic with melt pods. Metamorphic assemblages are k-spar + sillimanite + andalusite + cordierite ± garnet ± melt ± corundum bearing.
- Quartzite/Quartz pebble conglomerate: Coarse grained, white to gray quartzite in ~50cm thick beds. Quartz pebble conglomerate comprises pebble to cobble sized clasts in a white/gray to brown arenite matrix
- Carbonate rocks. Marbles and calc-silicates are white to gray, massive to layered and foliated.

ARCHEAN

- Amphibolite: Massive to banded and foliated
- Gneiss and migmatite (ca. 2580 to >2900 Ma): Gneissic and migmatitic Archean culmination, includes metasedimentary phases and disaggregated metamafic dykes
- Mesoarchean granite-gneiss (>2900 Ma): Similar to Archean gneiss and migmatite with abundant disaggregated and recrystallized mafic dykes

- Fault, inferred
- Trace of axial plane of major antiform or synform
- Line bisecting western structural domain from eastern structural domain. Wopmay Fault zone comprises area west of this line.

### Structural Measurements

- Bedding: Younging direction unknown, younging direction upright
- Foliation: Main or unknown generation
- Foliation: 1st, 2nd, 3rd, 4th, 5th generation
- Crenulation fabric
- Migmatitic Layering: Main generation
- Gneissosity: Injection layering (granite into seds)
- Dyke, Vein
- Axial Plane
- Ductile Shear: Unknown sense, Sinistral sense
- Mineral Lineation: 1st generation
- Intersection Lineation: Unknown generation
- Fold Hinge
- Z-Fold Hinge: Unknown generation, 4th generation
- S-Fold Hinge: Unknown generation, 4th generation
- Cross-section line

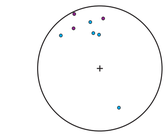

**Lineations plotted on equal area stereonet:** Crenulation lineations plunge shallowly to moderately north and northwest (purple). One fold axis plunges moderately to the southeast, while the rest plunge moderately north to northwest (blue).

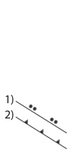


**Metamorphic Mineral zones** (mark on the high T side of line): 1) biotite zone (chlorite out); 2) andalusite±cordierite zone

NTS Map sheet covered by this area: 086B12
Datum: NAD 83, UTM Zone 11N
Scale: 1:150,000

Map is a compilation of work by Easton (1981), Hoffman and Hall (1993), Jackson and Ootes (2012), including work done by this author over the summers of 2009 and 2010. Undifferentiated units of the Slave craton are mapped and described in details by Pehrsson (2002). Lithologies that have not been directly observed for this study are simply named in the legend, without a complete description. These have been named and described by Jackson and Ootes (2012).

Inset map, at right, is a clip of the 1:150,000 scale Southern Wopmay Orogen mapping project by Jackson and Ootes (2012). The area shown comprises intrusive and metasedimentary units of the Metamorphic Internal zone and the eastern margin of the Great Bear magmatic zone. The Little Crapeau Lake map area is outlined by the dashed line.

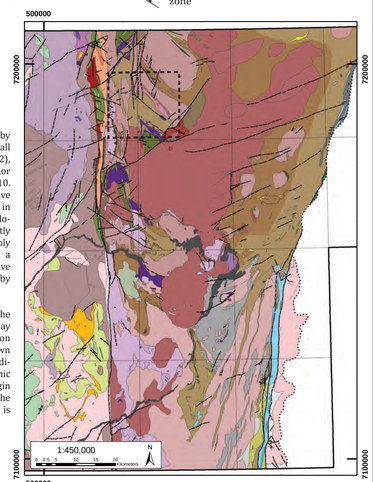



References
Easton, R. M., 1981, Geology of Grant Lake and Four Corners Lake Map Areas, Wopmay Orogen, District of Mackenzie: Current Research, Part B, Geological Survey of Canada, v. Paper 81-1B, p. 83-94.
Hoffman, P. F, and Hall, L., 1993, Geology, Slave craton and environs, District of Mackenzie, Northwest Territories: Geological Survey of Canada, Open File 2559, scale 1:1,000,000.
Jackson, V. A., and Ootes, L., 2012, Preliminary Geologic Map of the South-Central Wopmay Orogen (parts of NTS 86B, 86C, and 86D); results from 2009 to 2011: Northwest Territories Geoscience Office, scale 1:100,000.
Pehrsson, S. J., 2002, Geology, Indin Lake, Northwest Territories: Geological Survey of Canada, scale 1:125,000.

# APPENDIX B

Appendix B

| YEAR | STATNUM | FEATURE | DIP | STRIKE | LITHOLOGY | COMMENTS | EASTING | NORTHING |
|---|---|---|---|---|---|---|---|---|
| 2009 | 1500 | Fold hinge, first gen | 11 | 345 | S - Argillite | trend and plunge of fold hinge in metaseds. | 522031 | 7201319 |
| 2009 | 1500 | Intersection lineation, unknown gen | 20 | 20 | S - Argillite | unsure what type of lineation, on cleavage plane where micaceous. | 522186 | 7201691 |
| 2009 | 1500 | Bedding, younging direction unknown | 40 | 219 | S - Argillite | bedding with parallel cleavage, thin siltstone and mudstone | 522031 | 7201324 |
| 2009 | 1500 | Bedding, younging direction unknown | 46 | 190 | S - Argillite | moving eastward, bedding/cleavage rotating | 522031 | 7201344 |
| 2009 | 1500 | Bedding, younging direction unknown | 59 | 185 | S - Argillite | thin siltstone and mudstone bedding, rotating | 522062 | 7201344 |
| 2009 | 1500 | Bedding, younging direction unknown | 72 | 210 | S - Argillite | bedding/cleavage of thin meta-siltstone mudstone | 522108 | 7201500 |
| 2009 | 1500 | Bedding, younging direction unknown | 84 | 184 | S - Argillite | same as previous, thin bedded siltstone mudstone | 522144 | 7201593 |
| 2009 | 1501 | Bedding, younging direction unknown | 66 | 180 | S - Arkose | thinly bedded siltstone and mudstone. cleavage parallel to beds. | 522487 | 7202282 |
| 2009 | 1502 | Foliation, first gen | 61 | 173 | M - Pelitic Schist | foliation/cleavage is intense appears to follow bedding, but difficult to tell. mica defines the planes. | 522631 | 7202356 |
| 2009 | 1502 | Foliation, first gen | 67 | 180 | M - Pelitic Schist | parallel with cleavage and probably original bedding. defined by compositional banding. | 522758 | 7202394 |
| 2009 | 1503 | Mineral lineation, first gen | 35 | 325 | M - Pelitic Schist | lineation on cleavage plane, as previous. | 522590 | 7202757 |
| 2009 | 1503 | Gneissosity | 52 | 188 | M - Felsic Gneiss | gneissic banding in felsic gneiss | 522795 | 7202474 |
| 2009 | 1503 | Bedding, younging direction unknown | 74 | 174 | S - Argillite | bedding/cleavage in slate | 522475 | 7202889 |
| 2009 | 1503 | Bedding, younging direction unknown | 70 | 178 | S - Argillite | very fine bedding, siltstone and mudstone | 522447 | 7203190 |

Appendix B

| YEAR | STATNUM | FEATURE | DIP | STRIKE | LITHOLOGY | COMMENTS | EASTING | NORTHING |
|---|---|---|---|---|---|---|---|---|
| 2009 | 1504 | S-fold hinge, 1st gen | 19 | 310 | S - Argillite | s-fold in thinly bedded siltstone/argillite | 526850 | 7186901 |
| 2009 | 1504 | Bedding, younging direction unknown | 46 | 142 | S - Argillite | thin ~1cm size bedding in argillite | 526867 | 7186944 |
| 2009 | 1504 | Bedding, younging direction unknown | 33 | 105 | S - Argillite | thin bedding in siltstone, thick bedding in sandstone [upto 50cm] | 526798 | 7186660 |
| 2009 | 1504 | Bedding, younging direction unknown | 24 | 120 | S - Argillite | biotite grade siltstone and sandstone | 526867 | 7186651 |
| 2009 | 1505 | Bedding, younging direction overturned | 48 | 143 | S - Siltstone | thinly bedded siltstone and mudstone | 525508 | 7187970 |
| 2009 | 1505 | Foliation, unknown gen | 57 | 340 | S - Siltstone | unknown gen, moderate to strong cleavage crosscutting siltstone bedding | 525280 | 7187605 |
| 2009 | 1506 | Bedding, younging direction unknown | 26 | 324 | S - Siltstone | bedding changes orientation on west Side of island | 524278 | 7188612 |
| 2009 | 1506 | Bedding, younging direction unknown | 15 | 43 | S - Siltstone | siltstone bedding | 524429 | 7188777 |
| 2009 | 1506 | Bedding, younging direction unknown | 91 | 115 | S - Siltstone | perhaps nearing nose of fold, siltstone bedding changes orientation | 524342 | 7188711 |
| 2009 | 1506 | Bedding, younging direction unknown | 21 | 355 | S - Siltstone | schistose/phyllic bedding, intense cleavage | 523979 | 7188919 |
| 2009 | 1507 | S-fold hinge, 1st gen | 45 | 358 | S - Siltstone | s fold in bedded siltstone. intense cleavage, poor exposure. | 523612 | 7187766 |
| 2009 | 1507 | Bedding, younging direction unknown | 84 | 340 | S - Siltstone | finely laminated siltstone, deformed, strong cleavage | 523536 | 7187881 |
| 2009 | 1508 | Z-fold, first gen | 37 | 324 | M - Pelitic Schist | z folds in bt-musc-staurolite grade metased | 523098 | 7188394 |
| 2009 | 1508 | Foliation, first gen | 71 | 158 | M - Pelitic Schist | highly strained meta seds, have reached bt/musc/staurolite grade | 523070 | 7188387 |
| 2009 | 1509 | Foliation, first gen | 72 | 173 | S - Siltstone | foliation in highly strained metasediments | 523399 | 7189496 |

Appendix B

| YEAR | STATNUM | FEATURE | DIP | STRIKE | LITHOLOGY | COMMENTS | EASTING | NORTHING |
|---|---|---|---|---|---|---|---|---|
| 2009 | 1509 | Foliation, first gen | 61 | 353 | S - Siltstone | intense foliation with strained qtz lenses, oriented counterclockwise to bedding/foliation. | 523606 | 7190209 |
| 2009 | 1509 | Foliation, first gen | 65 | 14 | M - Pelitic Schist | foliated, highly strained with staurolite porphyroblasts | 523521 | 7190073 |
| 2009 | 1510 | Foliation, first gen | 52 | 6 | M - Pelitic Schist | intense foliation in metasediments containing staurolite porphyroblasts | 523421 | 7189902 |
| 2009 | 1511 | S-fold hinge, 1st gen | 42 | 349 | M - Pelitic Schist | hinge of tight isoclinal[?] fold. see photo | 522363 | 7189922 |
| 2009 | 1511 | Foliation, first gen | 70 | 180 | M - Pelitic Schist | intense foliation in highly strained metasediments. original bedding not visible . | 522310 | 7189949 |
| 2009 | 1511 | Foliation, first gen | 75 | 170 | M - Pelitic Schist | highly strained metasediments, strong foliation | 522319 | 7189949 |
| 2009 | 1512 | Z-fold, first gen | 17 | 345 | M - Pelitic Schist | tight v-shaped fold, likely a z-fold but difficult to see [other folds around are Z] | 521945 | 7190215 |
| 2009 | 1512 | Foliation, first gen | 65 | 184 | M - Pelitic Schist | very strong foliation in highly strained metasediments | 521937 | 7190189 |
| 2009 | 1513 | Z-fold, first gen | 50 | 336 | M - Pelitic Schist | small z folds in highly strained metasediments, andalusite | 522310 | 7190882 |
| 2009 | 1513 | Foliation, first gen | 70 | 162 | M - Pelitic Schist | intense foliation in highly strained metasediments | 522265 | 7190891 |
| 2009 | 1514 | Z-fold, unknown gen | 43 | 5 | M - Granitic Gneiss | z folds in leucogranite unit. | 521662 | 7191303 |
| 2009 | 1514 | Foliation, unknown gen | 91 | 220 | M - Granitic Gneiss | general foliation direction in leucogranite. no dip measured. | 521600 | 7191303 |
| 2009 | 1515 | Bedding, younging direction unknown | 75 | 65 | M - Amphibolite | ap-ears to be bedding, but may not be. see photos. | 521731 | 7191364 |
| 2009 | 1516 | Foliation, first gen | 64 | 350 | M - Pelitic Schist | intense folfoliation in highly strained metasediments, andalusite grade | 523211 | 7191166 |

Appendix B

| YEAR | STATNUM | FEATURE | DIP | STRIKE | LITHOLOGY | COMMENTS | EASTING | NORTHING |
|---|---|---|---|---|---|---|---|---|
| 2009 | 1517 | Foliation, first gen | 55 | 320 | M - Felsic Gneiss | intense foliation in mylonite | 518262 | 7194536 |
| 2009 | 1517 | Foliation, first gen | 68 | 335 | M - Felsic Gneiss | intense foliation in highly strained metasediments, with bt, musc, chl. | 518114 | 7194245 |
| 2009 | 1518 | Bedding, younging direction unknown | 81 | 150 | S - Argillite | very difficult to see bedding tops, very messy. | 518767 | 7193857 |
| 2009 | 1518 | Bedding, younging direction unknown | 75 | 340 | M - Felsic Gneiss | highly strained metasediments, foliation appears parallel to original bedding | 518605 | 7193728 |
| 2009 | 1519 | Foliation, first gen | 63 | 332 | M - Pelitic Schist | intenseense foliation in highly strained metasediments. cannot see bedding. | 517925 | 7195833 |
| 2009 | 1519 | Foliation, first gen | 85 | 140 | M - Pelitic Schist | intense foliation in highly strained metasediments, bt, musc, andalusite | 517731 | 7195756 |
| 2009 | 1519 | Foliation, unknown gen | 55 | 140 | M - Pelitic Schist | same intense foliation, but opposite dip in same outcrop | 517912 | 7195833 |
| 2009 | 1520 | Foliation, unknown gen | 91 | 340 | P - Granite | foliated leucogranite | 525340 | 7193032 |
| 2009 | 1521 | Bedding, younging direction unknown | 85 | 300 | M - Pelitic Schist | staurolite porphyroblasts in metaseds | 525470 | 7190069 |
| 2009 | 1521 | Bedding, younging direction unknown | 60 | 135 | M - Pelitic Schist | staurolite porphyroblasts in highly strained metasediments | 525724 | 7189996 |
| 2009 | 1521 | Bedding, younging direction unknown | 70 | 270 | M - Pelitic Schist | staurolite porphyroblasts in highly strained metasediments | 525595 | 7190042 |
| 2009 | 1521 | Bedding, younging direction unknown | 70 | 240 | M - Pelitic Schist | staurolite porphyroblasts in highly strained metasediments | 525633 | 7190047 |
| 2009 | 1521 | Foliation, unknown gen | 20 | 170 | M - Pelitic Schist | staurolite porphyroblasts in highly strained metasediments | 525491 | 7190061 |
| 2009 | 1521 | Foliation, unknown gen | 32 | 155 | M - Pelitic Schist | staurolite porphyroblasts in highly strained metasediments | 525737 | 7190026 |
| 2009 | 1524 | S-fold hinge, 1st gen | 25 | 348 | M - Metaseds <30% Melt | tight rounded s-fold hinge in metaseds | 519732 | 7189525 |

Appendix B

| YEAR | STATNUM | FEATURE | DIP | STRIKE | LITHOLOGY | COMMENTS | EASTING | NORTHING |
|---|---|---|---|---|---|---|---|---|
| 2009 | 1524 | Foliation, first gen | 80 | 2 | M - Metaseds <30% Melt | intense foliation in highly strained metasediments | 519796 | 7189530 |
| 2009 | 1525 | Foliation, first gen | 85 | 358 | M - Metaseds <30% Melt | intense anastamosing foliation in bt,musc, sil +/- crd schist | 519810 | 7189566 |
| 2009 | 1526 | Foliation, first gen | 66 | 7 | M - Metaseds <30% Melt | intense anastamosing foliation | 519959 | 7189552 |
| 2009 | 1527 | Mineral lineation, first gen | 21 | 4 | P - Tonalite | qtz and plag define lineation | 519454 | 7188990 |
| 2009 | 1527 | Foliation, first gen | 91 | 13 | P - Tonalite | almost gneissic banding but very poorly exposed | 519352 | 7188787 |
| 2009 | 1527 | Bedding, younging direction unknown | 91 | 130 | S - Argillite | weak thick siltstone beds | 519508 | 7189021 |
| 2009 | 1529 | Intersection lineation, unknown gen | 24 | 327 | S - Argillite | crenulation lineation. intersection between s1 and s2? | 526865 | 7186892 |
| 2009 | 1529 | Bedding, younging direction unknown | 58 | 160 | S - Argillite | slatey bedding in metaseds | 526844 | 7186906 |
| 2009 | 1530 | Bedding, younging direction unknown | 85 | 190 | M - Pelitic Schist | subvertical bedding in garnet bt schist | 561217 | 7161613 |
| 2009 | 1530 | Foliation, unknown gen | 65 | 198 | M - Pelitic Schist | strong cleavage in bt garnet schist, defined by bt and porph alignment | 561220 | 7161613 |
| 2009 | 1534 | Intersection lineation, unknown gen | 4 | 335 | M - Pelitic Schist | Crenulated/folded intersection of S1 & S2 | 525289 | 7192476 |
| 2009 | 1534 | Foliation, first gen | 10 | 325 | M - Metaseds <30% Melt | enveloping surface of metaseds and parallel leucogranite sill | 525271 | 7192477 |
| 2009 | 1534 | Foliation, first gen | 10 | 325 | M - Pelitic Schist | enveloping surface, metaseds parallel to leucogran sill | 525275 | 7192476 |
| 2009 | 1534 | Foliation, second gen | 85 | 160 | M - Pelitic Schist | diff. locations of same S2 fold event, other is 140/80 | 525289 | 7192476 |

Appendix B

| YEAR | STATNUM | FEATURE | DIP | STRIKE | LITHOLOGY | COMMENTS | EASTING | NORTHING |
|---|---|---|---|---|---|---|---|---|
| 2009 | 1534 | Foliation, second gen | 80 | 140 | M - Pelitic Schist | diff. locations of same S2 fold event, other is 160/85 | 525295 | 7192455 |
| 2009 | 1536 | Gneissosity | 58 | 205 | M - Paragneiss | strong gneissosity/cleavage, folded with larger fold. | 557137 | 7160233 |
| 2009 | 1537 | Foliation, unknown gen | 45 | 225 | M - Paragneiss | measured on long limb of s-fold, limb on west side of antiform on larger east limb | 557170 | 7160625 |
| 2009 | 1537 | Foliation, unknown gen | 66 | 15 | M - Paragneiss | measured on short limb [east] of large east limb | 557204 | 7160612 |
| 2009 | 1538 | Bedding, younging direction unknown | 34 | 60 | M - Quartzite | 5-10cm bedding in gulley quartzite | 556914 | 7160894 |
| 2009 | 1538 | Foliation, unknown gen | 71 | 220 | M - Quartzite | oblique foliation in bedded quartzite | 556941 | 7160894 |
| 2009 | 1539 | Bedding, younging direction unknown | 35 | 68 | M - Paragneiss | compositional sandy,qtz layering on short limb. oblique foliation to bedding | 556821 | 7160836 |
| 2009 | 1542 | Foliation, unknown gen | 51 | 177 | M - Pelitic Schist | foliation near oriented sample location. folds tightly, in compositional banding. | 522257 | 7190769 |
| 2009 | 1543 | Foliation, unknown gen | 81 | 200 | M - Pelitic Schist | main cleavage in grt, crd, and, bt schist. | 560914 | 7160553 |
| 2009 | 1548 | Foliation, second gen | 81 | 342 | M - Pelitic Schist | steep crenulating fabric, S2? | 523123 | 7190924 |
| 2009 | 1548 | Foliation, unknown gen | 73 | 170 | M - Pelitic Schist | main fol is strong, crosscut by another fol'n at med-high angle. creates kinks in fabric. | 522999 | 7190909 |
| 2009 | 1548 | Foliation, unknown gen | 14 | 200 | M - Pelitic Schist | flat lying, S1? | 523120 | 7190930 |
| 2009 | 1549 | Foliation, unknown gen | 40 | 45 | M - Pelitic Schist | main foliation [s1?] looks like it contains compositional banding, lkely parallel to s0. | 523372 | 7190863 |

Appendix B

| YEAR | STATNUM | FEATURE | DIP | STRIKE | LITHOLOGY | COMMENTS | EASTING | NORTHING |
|---|---|---|---|---|---|---|---|---|
| 2009 | 1550 | Foliation, unknown gen | 91 | 350 | P - Tonalite | weak foliation in tonalite | 523537 | 7190894 |
| 2009 | 1551 | Foliation, second gen | 74 | 140 | M - Pelitic Schist | steep foliation that folds shallow crenulated surface, s2? | 524532 | 7192947 |
| 2009 | 1551 | Foliation, unknown gen | 26 | 75 | M - Pelitic Schist | flatlying foliation that is folded by upright/steep foliation. | 524520 | 7192947 |
| 2009 | 1554 | Dyke | 61 | 202 | P - Diabase | mafic fine grained dyke, not foliated. contact with metaseds at 202 deg. | 559227 | 7162694 |
| 2009 | 1554 | Fold hinge, first gen | 51 | 5 | M - Metaseds <30% Melt | folded bedding, antiform plunging northward | 559171 | 7162583 |
| 2009 | 1554 | Foliation, second gen | 91 | 225 | M - Metaseds <30% Melt | foliation that crosscuts main stronger one, clockwise | 559023 | 7162130 |
| 2009 | 1554 | Foliation, second gen | 75 | 220 | M - Metaseds <30% Melt | bt foliation crosscutting main cleavage. fol itself is crenulated | 559067 | 7162391 |
| 2009 | 1554 | Bedding, younging direction unknown | 84 | 190 | M - Metaseds <30% Melt | compositional layering in metaseds, strong | 559021 | 7162127 |
| 2009 | 1554 | Bedding, younging direction unknown | 84 | 199 | M - Metaseds <30% Melt | bedding/compositional layering in bt,sil,musc metaseds with minor melt | 559093 | 7162427 |
| 2009 | 1555 | Bedding, younging direction unknown | 69 | 3 | M - Metaseds <30% Melt | compositional layering of metaseds, grt,bt | 559196 | 7162789 |
| 2009 | 1555 | Bedding, younging direction unknown | 86 | 350 | M - Pelitic Schist | compositional layering in grt,bt metaseds | 559202 | 7162817 |
| 2009 | 1555 | Foliation, unknown gen | 34 | 12 | M - Metaseds <30% Melt | unknown, shallow, flatlying foliation on top of near vertical comp layering. | 559219 | 7162785 |
| 2009 | 1556 | Bedding, younging direction unknown | 85 | 191 | M - Pelitic Schist | grt metaseds, nearly vertical bedding beside sample location. thick, coarse grained | 559221 | 7162840 |
| 2009 | 1556 | Bedding, younging direction unknown | 75 | 190 | M - Pelitic Schist | highly strained metasediments, parallel to bedding | 559117 | 7163005 |
| 2009 | 1556 | Bedding, younging direction unknown | 54 | 309 | M - Pelitic Schist | 90deg swing in bedding direction | 559134 | 7163069 |

Appendix B

| YEAR | STATNUM | FEATURE | DIP | STRIKE | LITHOLOGY | COMMENTS | EASTING | NORTHING |
|---|---|---|---|---|---|---|---|---|
| 2009 | 1557 | Axial plane, 1st gen | 76 | 205 | M - Pelitic Schist | tight v-fold folds beds of bt metased | 559159 | 7163151 |
| 2009 | 1557 | Fold hinge, first gen | 54 | 5 | M - Pelitic Schist | folding bedding, tight v-folds | 559151 | 7163155 |
| 2009 | 1557 | Bedding, younging direction unknown | 56 | 300 | M - Pelitic Schist | garnetiferous metasediments, main cleavage likely parallel to bedding. | 559118 | 7163128 |
| 2009 | 1557 | Bedding, younging direction unknown | 60 | 325 | M - Pelitic Schist | main enveloping surface of m-folds, defined by bedding | 559045 | 7163187 |
| 2009 | 1557 | Bedding, younging direction unknown | 78 | 340 | M - Pelitic Schist | bedding swinging around hinge zone | 559064 | 7163256 |
| 2009 | 1559 | Dyke | 91 | 245 | P - Gabbro | mafic dyke, gabbro intrudes and crosscuts metaseds | 564752 | 7156263 |
| 2009 | 1559 | Dyke | 91 | 250 | P - Diabase | weakly metamorphosed mafic dyke with moderate foliation. mostly obscured by moss. crosscuts metaseds. foliation at ~230. | 564517 | 7156937 |
| 2009 | 1559 | Bedding, younging direction unknown | 65 | 178 | S - Siltstone | siltstone/slatey bedding, laminae up to ~4cm thick. strong foliation parallel. | 564708 | 7156266 |
| 2009 | 1559 | Foliation, unknown gen | 46 | 189 | S - Siltstone | main cleavage, very strong in slatey metaseds | 564736 | 7156148 |
| 2009 | 1559 | Foliation, unknown gen | 70 | 205 | S - Siltstone | bedding not visible here, strong cleavage dominant. | 564628 | 7156479 |
| 2009 | 1559 | Foliation, unknown gen | 85 | 184 | S - Siltstone | strong cleavage in slatey, rusty bt metaseds | 564628 | 7156635 |
| 2009 | 1559 | Vein | 51 | 240 | S - Siltstone | pink mineral infilled tension fractures/gashes. may be stained qtz. | 564755 | 7156150 |
| 2009 | 1560 | Dyke | 91 | 196 | P - Diabase | mafic, amphibolitic dyke with disseminated sulphides, magnetic | 564304 | 7156976 |
| 2009 | 1560 | Foliation, first gen | 85 | 185 | P - Diabase | foliation in mafic dyke, moderate | 564313 | 7156925 |
| 2009 | 1560 | Bedding, younging direction unknown | 74 | 205 | S - Argillite | good visible bedding in slatey bt metaseds. gentle s-fold kinks. | 564295 | 7157605 |

Appendix B

| YEAR | STATNUM | FEATURE | DIP | STRIKE | LITHOLOGY | COMMENTS | EASTING | NORTHING |
|---|---|---|---|---|---|---|---|---|
| 2009 | 1560 | Foliation, unknown gen | 90 | 4 | S - Argillite | very strong cleavage in slatey metaseds. anastomosing vertically. | 564336 | 7156994 |
| 2009 | 1560 | Foliation, unknown gen | 68 | 185 | S - Argillite | main strong cleavage in slatey metaseds | 564401 | 7157380 |
| 2009 | 1560 | Foliation, unknown gen | 85 | 173 | S - Argillite | steep foliation crosscutting bedding, counterclockwise. recorded by few layers, see photo. | 564314 | 7157603 |
| 2009 | 1560 | Vein | 88 | 235 | S - Argillite | qtz filled veinlets, look like tension gashes, see photo. | 564370 | 7157275 |
| 2009 | 1560 | Vein | 71 | 243 | S - Argillite | tension gashes infilled with qtz, crosscutting seds. | 564410 | 7157385 |
| 2009 | 1561 | Bedding, younging direction unknown | 62 | 202 | S - Arenite | bedding and laminae visible | 564191 | 7157742 |
| 2009 | 1561 | Vein | 51 | 324 | X _Quartz Vein | crosscutting qtz veins in qtzite | 564177 | 7157789 |
| 2009 | 1562 | Axial plane, unknown gen | 74 | 345 | S - Argillite | axial plane of folded flatlying cleavage | 563697 | 7158206 |
| 2009 | 1562 | Intersection lineation, unknown gen | 20 | 360 | S - Argillite | intersection lineation on main cleavage plane | 563782 | 7158249 |
| 2009 | 1562 | Intersection lineation, unknown gen | 26 | 5 | S - Argillite | crenulation lineation on surface of flatlying cleavage | 563695 | 7158204 |
| 2009 | 1562 | Foliation, second gen | 67 | 346 | S - Argillite | foliation is counterclockwise, likely comes after a foliation parallel to bedding | 563702 | 7158394 |
| 2009 | 1562 | Foliation, second gen | 78 | 180 | S - Argillite | foliation crosscutting bedding, probably postdates bedding-parallel cleavage | 563576 | 7158523 |
| 2009 | 1562 | Bedding, younging direction unknown | 87 | 10 | S - Argillite | good bedding, see photo | 563693 | 7158223 |

Appendix B

| YEAR | STATNUM | FEATURE | DIP | STRIKE | LITHOLOGY | COMMENTS | EASTING | NORTHING |
|---|---|---|---|---|---|---|---|---|
| 2009 | 1562 | Bedding, younging direction unknown | 87 | 205 | S - Argillite | clear bedding in argillite | 563698 | 7158396 |
| 2009 | 1562 | Bedding, younging direction unknown | 79 | 197 | S - Argillite | bedding in slatey bt metaseds | 563580 | 7158523 |
| 2009 | 1562 | Foliation, unknown gen | 65 | 207 | S - Argillite | foliation folds bedding | 563820 | 7158228 |
| 2009 | 1563 | Dyke | 91 | 155 | P - Gabbro | narrow gabbroic dyke with disseminated pyrite | 563349 | 7158536 |
| 2009 | 1563 | Dyke | 91 | 192 | P - Gabbro | gabbroic dyke with weak foliation | 562990 | 7158561 |
| 2009 | 1563 | Bedding, younging direction unknown | 86 | 185 | S - Argillite | mafic porphyroblasts along bedding enhance visibility. | 563319 | 7158540 |
| 2009 | 1563 | Foliation, unknown gen | 58 | 205 | S - Argillite | bedding not visible here, strongest visible foliation | 563375 | 7158545 |
| 2009 | 1563 | Foliation, unknown gen | 77 | 178 | P - Gabbro | amphibolitic dyke is very wide [~100m?], with weak foliation | 562948 | 7158552 |
| 2009 | 1564 | Foliation, second gen | 85 | 189 | S - Argillite | foliation crosscuts bedding clockwise, likely postdates cleavage parallel to bedding. | 562355 | 7158781 |
| 2009 | 1564 | Bedding, younging direction unknown | 51 | 336 | S - Argillite | 1-3cm thick bedding in slatey bt metaseds | 562329 | 7158789 |
| 2009 | 1564 | Bedding, younging direction unknown | 63 | 212 | S - Argillite | good bedding in bt porphyroblastic metased | 562061 | 7159125 |
| 2009 | 1565 | Bedding, younging direction unknown | 69 | 16 | S - Argillite | bedding in bt,grt metaseds | 561769 | 7159350 |
| 2009 | 1566 | Bedding, younging direction unknown | 40 | 301 | S - Argillite | weak bedding at high angle to cleavage, probably hinge | 561472 | 7159736 |
| 2009 | 1566 | Bedding, younging direction unknown | 67 | 320 | S - Argillite | 3meters to west of last bedding measurement, b-c clockwise | 561463 | 7159742 |
| 2009 | 1566 | Foliation, unknown gen | 59 | 214 | S - Argillite | main cleavage in slatey metaseds | 561498 | 7159673 |

Appendix B

| YEAR | STATNUM | FEATURE | DIP | STRIKE | LITHOLOGY | COMMENTS | EASTING | NORTHING |
|---|---|---|---|---|---|---|---|---|
| 2009 | 1566 | Foliation, unknown gen | 49 | 225 | S - Argillite | main cleavage at high angle to bedding, in slatey grt,crd? metaseds | 561479 | 7159740 |
| 2009 | 1566 | Ductile shear, unknown sense | 55 | 332 | S - Argillite | shear band? created vertical and horizontal kinks | 561546 | 7159665 |
| 2009 | 1567 | Bedding, younging direction unknown | 74 | 219 | M - Pelitic Schist | grt rich bedding in schistose metaseds | 561253 | 7160043 |
| 2009 | 1567 | Foliation, unknown gen | 59 | 244 | M - Pelitic Schist | strong cleavage at sample location | 561373 | 7159784 |
| 2009 | 1567 | Foliation, unknown gen | 85 | 181 | M - Pelitic Schist | foliation, b-c counterclockwise. | 561257 | 7160043 |
| 2009 | 1568 | Axial plane, 1st gen | 91 | 191 | M - Pelitic Schist | axial plane, no dip. folds grt rich bedding | 561070 | 7160118 |
| 2009 | 1568 | Fold hinge, first gen | 26 | 16 | M - Pelitic Schist | hinge folds garnet rich bedding | 561088 | 7160136 |
| 2009 | 1568 | Bedding, younging direction unknown | 66 | 14 | M - Pelitic Schist | east limb of synform that plunges north | 561122 | 7160127 |
| 2009 | 1568 | Bedding, younging direction unknown | 91 | 299 | M - Pelitic Schist | bedding in nose of fold, estimate without dip | 561101 | 7160173 |
| 2009 | 1568 | Bedding, younging direction unknown | 91 | 75 | M - Pelitic Schist | estimate on poorly exposed bedding, folds around outcrop | 560637 | 7160517 |
| 2009 | 1568 | Foliation, unknown gen | 70 | 16 | M - Pelitic Schist | main cleavage axial planar to folding | 561045 | 7160147 |
| 2009 | 1568 | Foliation, unknown gen | 77 | 37 | M - Pelitic Schist | foliation crosscuts bedding, b-c counterclockwise | 560606 | 7160487 |
| 2009 | 1569 | Axial plane, 1st gen | 91 | 195 | M - Pelitic Schist | folded grt/and rich beds in schistose metased. no dip. | 560538 | 7160605 |
| 2009 | 1569 | Foliation, unknown gen | 75 | 216 | M - Pelitic Schist | main cleavage across folded grt,and schistose metased | 560554 | 7160595 |
| 2009 | 1570 | Bedding, younging direction unknown | 84 | 40 | M - Pelitic Schist | cm scale bedding in bt,and schistose metaseds. get cleavage from sample. | 559802 | 7160667 |
| 2009 | 1570 | Bedding, younging direction unknown | 74 | 210 | M - Pelitic Schist | thick ~10cm bedding in bt,and schistose metaseds | 559706 | 7160704 |

Appendix B

| YEAR | STATNUM | FEATURE | DIP | STRIKE | LITHOLOGY | COMMENTS | EASTING | NORTHING |
|---|---|---|---|---|---|---|---|---|
| 2009 | 1571 | Bedding, younging direction unknown | 57 | 94 | M - Metaseds <30% Melt | comp layering in migmatized sediments. now dipping opposite way than previously | 558503 | 7164192 |
| 2009 | 1571 | Foliation, unknown gen | 54 | 264 | M - Metaseds <30% Melt | migmatite comp layering in bt,sil metaseds. varying orientation throughout outcrop. | 558546 | 7163771 |
| 2009 | 1572 | Migmatitic Layering | 71 | 105 | M - Metaseds <30% Melt | felsic banding and melting in bt,sil metaseds | 558337 | 7164248 |
| 2009 | 1572 | Ductile shear, unknown sense | 91 | 4 | M - Metaseds <30% Melt | melted shear in metaseds, between 004-030 deg. | 558352 | 7164272 |
| 2009 | 1572 | Ductile shear, unknown sense | 91 | 25 | M - Metaseds <30% Melt | dip unknown, see photo. | 557908 | 7164414 |
| 2009 | 1573 | Migmatitic Layering | 91 | 265 | M - Metaseds <30% Melt | comp layering in melted sediments | 557367 | 7164568 |
| 2009 | 1573 | Bedding, younging direction unknown | 83 | 226 | M - Metaseds <30% Melt | metased bedding, no melt, just rusty | 557541 | 7164251 |
| 2009 | 1573 | Ductile shear, sinistral sense | 72 | 205 | M - Metaseds <30% Melt | beautiful shear banding in migmatized sediments | 557938 | 7164235 |
| 2010 | 2500 | Foliation, second gen | 66 | 301 | V - Mafic Volcanic Rock | folds first/main foliation at high angle. axial plane is high angle/steep. | 571058 | 7172026 |
| 2010 | 2500 | Foliation, unknown gen | 80 | 36 | V - Mafic Volcanic Rock | main fol with crossing later crenulation cleavage(s). | 571019 | 7171989 |
| 2010 | 2501 | Foliation, second gen | 24 | 187 | M - Pelitic Schist | fabric that folds the main foln and creates crenulation | 570408 | 7172938 |
| 2010 | 2501 | Foliation, unknown gen | 81 | 34 | M - Pelitic Schist | main schistosity | 570373 | 7172944 |
| 2010 | 2506 | Foliation, second gen | 74 | 20 | M - Metaseds <30% Melt | s2 crosscutting cleavage, ccw to bedding | 569321 | 7174620 |
| 2010 | 2506 | Bedding, younging direction unknown | 80 | 213 | M - Metaseds <30% Melt | metaseds bedding with bt porphs | 569304 | 7174660 |

Appendix B

| YEAR | STATNUM | FEATURE | DIP | STRIKE | LITHOLOGY | COMMENTS | EASTING | NORTHING |
|---|---|---|---|---|---|---|---|---|
| 2010 | 2515 | Bedding, younging direction unknown | 46 | 200 | M - Metaseds <30% Melt | well defined bedding in pelitic crd-and metaseds | 566280 | 7176433 |
| 2010 | 2515 | Foliation, unknown gen | 77 | 198 | M - Metaseds <30% Melt | main foliation is...s2 or s1? schistose and wraps around crd | 566289 | 7176441 |
| 2010 | 2518 | Dyke | 91 | 45 | M - Amphibolite | set of foliated amphibolitized mf dykes, very rusty in spots | 565513 | 7177429 |
| 2010 | 2518 | Foliation, second gen | 71 | 226 | M - Metaseds <30% Melt | main foliation, axial planar to folds, contains main porphs, CW to bedding | 565497 | 7177666 |
| 2010 | 2518 | Bedding, younging direction unknown | 84 | 13 | M - Metaseds <30% Melt | well defined bedding in crd-and-grt schist [diff met mins in diff adjacent layers | 564572 | 7177365 |
| 2010 | 2518 | Bedding, younging direction unknown | 76 | 21 | M - Metaseds <30% Melt | evident bedding in crd-and/sil next to sample E location. beds are mm scale to 2cm | 565396 | 7178238 |
| 2010 | 2520 | Foliation, unknown gen | 82 | 24 | M - Metaseds <30% Melt | likely S2 foliation, also follows bedding plane | 565135 | 7178321 |
| 2010 | 2521 | Foliation, second gen | 85 | 18 | M - Metaseds <30% Melt | s2 | 565043 | 7178310 |
| 2010 | 2521 | Bedding, younging direction unknown | 84 | 13 | M - Metaseds <30% Melt | bedding | 565028 | 7178279 |
| 2010 | 2524 | Gneissosity | 53 | 60 | M - Mafic Agmatite <30% Melt | bedding | 559963 | 7175140 |
| 2010 | 2524 | Bedding, younging direction unknown | 57 | 90 | M - Metaseds <30% Melt | migmatite | 560004 | 7175003 |
| 2010 | 2525 | Bedding, younging direction unknown | 69 | 111 | M - Metaseds <30% Melt | melty | 559494 | 7174260 |
| 2010 | 2527 | Dyke | 91 | 285 | P - Gabbro | dolerite dyke crosscuts sediments | 526882 | 7186627 |
| 2010 | 2527 | Bedding, younging direction unknown | 35 | 127 | S - Argillite | bedding in sediments, cleavage is cryptic | 526912 | 7186612 |

Appendix B

| YEAR | STATNUM | FEATURE | DIP | STRIKE | LITHOLOGY | COMMENTS | EASTING | NORTHING |
|---|---|---|---|---|---|---|---|---|
| 2010 | 2528 | Bedding, younging direction unknown | 47 | 144 | S - Argillite | main/long limb of open folds in finely bedded sediments +/- chlorite sheen | 526759 | 7186987 |
| 2010 | 2529 | Bedding, younging direction unknown | 41 | 110 | S - Siltstone | siltstone bedding, varies slightly, swinging around gentle folding | 526084 | 7187790 |
| 2010 | 2529 | Bedding, younging direction unknown | 45 | 163 | S - Siltstone | siltstone bedding | 525309 | 7188012 |
| 2010 | 2530 | Foliation, first gen | 7 | 295 | S - Siltstone | cleavage xcutting siltstone | 525008 | 7188465 |
| 2010 | 2530 | Bedding, younging direction unknown | 42 | 120 | S - Siltstone | siltstone with xcutting cleavage, very shallow | 524999 | 7188474 |
| 2010 | 2531 | Foliation, second gen | 54 | 153 | M - Metaseds <30% Melt | 2nd gen? not main. main cleavage is subparallel to bedding, cw | 568296 | 7174731 |
| 2010 | 2531 | Bedding, younging direction unknown | 75 | 355 | M - Metaseds <30% Melt | bedding in metaseds | 568286 | 7174731 |
| 2010 | 2532 | Z-fold, first gen | 20 | 350 | M - Quartzite | qtzite and calc-silicate interbeds, z-folded plunging gently north | 567842 | 7174844 |
| 2010 | 2532 | Dyke | 70 | 140 | P - Pegmatite | pegmatite dyke cross-cutting mafic dyke [sample] and likely qtzite underneath | 567322 | 7174666 |
| 2010 | 2532 | Bedding, younging direction unknown | 42 | 220 | M - Quartzite | folded interbeds of qtzite and calc-silicate | 567816 | 7174844 |
| 2010 | 2532 | Bedding, younging direction unknown | 32 | 218 | M - Quartzite | bedded qtzite OR | 567397 | 7174669 |
| 2010 | 2532 | Bedding, younging direction unknown | 36 | 201 | M - Quartzite | qtzite bedding | 567262 | 7174626 |
| 2010 | 2534 | Foliation, unknown gen | 84 | 215 | M - Metagabbro | main foliation in metabasites with clasts | 568613 | 7166207 |
| 2010 | 2535 | Bedding, younging direction unknown | 54 | 185 | M - Metaseds <30% Melt | metaseds with mm-scale bedding and CW xcutting cleavage | 568270 | 7166538 |
| 2010 | 2535 | Foliation, unknown gen | 78 | 196 | M - Metaseds <30% Melt | strong foliation, low grade met in bedded metased | 568264 | 7166544 |

Appendix B

| YEAR | STATNUM | FEATURE | DIP | STRIKE | LITHOLOGY | COMMENTS | EASTING | NORTHING |
|---|---|---|---|---|---|---|---|---|
| 2010 | 2536 | Foliation, second gen | 70 | 170 | M - Metagabbro | crenulating cleavage in metagabbro. qtz vein cuts gabbro and is shear by this cleav | 561498 | 7174180 |
| 2010 | 2536 | Bedding, younging direction unknown | 85 | 130 | M - Metaseds <30% Melt | bedding in sandy bt+/-crd migmatized metaseds | 561504 | 7174187 |
| 2010 | 2536 | Foliation, unknown gen | 73 | 122 | M - Metagabbro | main fol'n in metagabbro, defined by hbl,bt | 561493 | 7174184 |
| 2010 | 2538 | Foliation, second gen | 65 | 150 | M - Metaseds <30% Melt | qtz-filled shear bands in migmatized seds with micas+sil+relict crd | 561957 | 7174068 |
| 2010 | 2538 | Foliation, unknown gen | 78 | 185 | M - Metaseds <30% Melt | main fabric in migmatized seds. maybe this is where fabric changes to N-S instead od E-W. | 562439 | 7173885 |
| 2010 | 2539 | Axial plane, 1st gen | 84 | 196 | M - Metaseds <30% Melt | foliation that folds beds. may be 1st gen, unless there's an earlier tight fold gen | 562652 | 7173802 |
| 2010 | 2539 | Bedding, younging direction unknown | 84 | 223 | M - Metaseds <30% Melt | long limb of folded seds | 562641 | 7173770 |
| 2010 | 2539 | Bedding, younging direction unknown | 42 | 144 | M - Metaseds <30% Melt | short limb of folded beds | 562635 | 7173767 |
| 2010 | 2541 | Foliation, second gen | 42 | 273 | M - Metaseds <30% Melt | may be 1st gen, hard to tell. can't see bedding here | 556527 | 7152554 |
| 2010 | 2541 | Foliation, third gen | 64 | 5 | M - Metaseds <30% Melt | crenulation cleavage, folding previous foliation into chevrons | 556551 | 7152542 |
| 2010 | 2542 | Foliation, second gen | 74 | 216 | M - Metaseds <30% Melt | calling this cleavage S2. axial planar to tightly folded bedding | 556425 | 7152833 |
| 2010 | 2545 | Bedding, younging direction unknown | 75 | 150 | M - Mafic Agmatite <30% Melt | bedding | 523824 | 7187234 |
| 2010 | 2545 | Bedding, younging direction unknown | 47 | 360 | M - Mafic Agmatite <30% Melt | bedding | 523699 | 7187271 |

Appendix B

| YEAR | STATNUM | FEATURE | DIP | STRIKE | LITHOLOGY | COMMENTS | EASTING | NORTHING |
|---|---|---|---|---|---|---|---|---|
| 2010 | 2545 | Bedding, younging direction unknown | 88 | 345 | M - Mafic Agmatite <30% Melt | bedding | 523603 | 7187394 |
| 2010 | 2545 | Bedding, younging direction unknown | 74 | 8 | M - Metaseds <30% Melt | bedding | 523551 | 7187599 |
| 2010 | 2545 | Foliation, unknown gen | 71 | 28 | M - Metaseds <30% Melt | oblique to bedding bedding to cleavage is clockwise | 523541 | 7187368 |
| 2010 | 2545 | Shear band | 91 | 280 | M - Metaseds <30% Melt | shear band strike | 523533 | 7187581 |
| 2010 | 2546 | Foliation, unknown gen | 85 | 156 | M - Metaseds <30% Melt | cleavage | 522985 | 7188365 |
| 2010 | 2547 | Foliation, unknown gen | 72 | 156 | M - Metaseds <30% Melt | subparallel to bedding | 523476 | 7188371 |
| 2010 | 2547 | Shear band | 91 | 240 | M - Metaseds <30% Melt | shear band | 523476 | 7188371 |
| 2010 | 2548 | Foliation, unknown gen | 84 | 149 | M - Metaseds <30% Melt | anastomosing cleavage in biotite | 522503 | 7188203 |
| 2010 | 2549 | Foliation, unknown gen | 40 | 351 | M - Metaseds <30% Melt | cleavage subparallel to bedding, [clock wise ti bedding ?] | 523957 | 7188933 |
| 2010 | 2550 | Foliation, first gen | 14 | 354 | M - Metaseds <30% Melt | enveloping surface | 523536 | 7189229 |
| 2010 | 2550 | Foliation, second gen | 60 | 336 | M - Metaseds <30% Melt | cren cleavage of s1 | 523540 | 7189225 |
| 2010 | 2551 | Foliation, first gen | 22 | 35 | M - Metaseds <30% Melt | andalusite porphs long axis in plane | 523422 | 7189635 |
| 2010 | 2551 | Foliation, first gen | 14 | 27 | M - Metaseds <30% Melt | micas cleavage | 523422 | 7189443 |
| 2010 | 2551 | Foliation, first gen | 67 | 348 | M - Metaseds <30% Melt | steep S1 foliation overprinted by shallow S2 cren cleavage | 523522 | 7190313 |
| 2010 | 2551 | Foliation, second gen | 77 | 20 | M - Metaseds <30% Melt | cren cleavage | 523443 | 7189622 |

Appendix B

| YEAR | STATNUM | FEATURE | DIP | STRIKE | LITHOLOGY | COMMENTS | EASTING | NORTHING |
|---|---|---|---|---|---|---|---|---|
| 2010 | 2551 | Foliation, second gen | 86 | 330 | M - Metaseds <30% Melt | cren cleavage | 523415 | 7189443 |
| 2010 | 2551 | Foliation, second gen | 7 | 95 | M - Metaseds <30% Melt | steep S1 foliation overprinted by shallow S2 cren cleavage | 523542 | 7190309 |
| 2010 | 2552 | Foliation, second gen | 40 | 42 | M - Metaseds <30% Melt | cren cleavage of s1 | 525372 | 7191070 |
| 2010 | 2552 | Bedding, younging direction unknown | 27 | 150 | M - Metaseds <30% Melt | bedding | 525408 | 7191057 |
| 2010 | 2554 | Foliation, first gen | 18 | 184 | M - Metaseds <30% Melt | crenulated by s2 | 526296 | 7190792 |
| 2010 | 2554 | Bedding, younging direction unknown | 35 | 107 | M - Metaseds <30% Melt | bedding | 526319 | 7190779 |
| 2010 | 2554 | Foliation, unknown gen | 25 | 207 | M - Metaseds <30% Melt | cross cuts bedding at a high angle | 526326 | 7190775 |
| 2010 | 2555 | Foliation, first gen | 32 | 135 | M - Metagabbro | mica plane cleavage | 525980 | 7190120 |
| 2010 | 2556 | Foliation, first gen | 26 | 25 | M - Metaseds <30% Melt | mica cleavage plane | 523787 | 7192533 |
| 2010 | 2556 | Foliation, first gen | 47 | 133 | M - Metaseds <30% Melt | mica cleavage , s plane | 523747 | 7192357 |
| 2010 | 2556 | Foliation, second gen | 80 | 345 | M - Metaseds <30% Melt | cren cleavage of s1 | 523792 | 7192559 |
| 2010 | 2556 | Foliation, second gen | 32 | 153 | M - Metaseds <30% Melt | c' cren cleavage | 523752 | 7192357 |
| 2010 | 2558 | Foliation, first gen | 75 | 212 | M - Granitic Gneiss | mylonite fabric | 521524 | 7191312 |
| 2010 | 2558 | Foliation, second gen | 75 | 175 | M - Metaseds <30% Melt | shear fabric crenulation | 521512 | 7191312 |
| 2010 | 2559 | Bedding, younging direction unknown | 40 | 120 | M - Metaseds <30% Melt | bedding | 525557 | 7185811 |
| 2010 | 2559 | Bedding, younging direction unknown | 43 | 135 | M - Metaseds <30% Melt | low grade seds. no apparent fabric | 528178 | 7184961 |

Appendix B

| YEAR | STATNUM | FEATURE | DIP | STRIKE | LITHOLOGY | COMMENTS | EASTING | NORTHING |
|---|---|---|---|---|---|---|---|---|
| 2010 | 2560 | Foliation, first gen | 76 | 140 | M - Metaseds <30% Melt | mica cleavage plane with andalusite porphs aligned within plane | 532075 | 7185005 |
| 2010 | 2560 | Foliation, first gen | 59 | 124 | M - Metaseds <30% Melt | mica cleavage plane | 531900 | 7184799 |
| 2010 | 2560 | Foliation, second gen | 33 | 222 | M - Metaseds <30% Melt | crenulation cleavage | 531900 | 7184847 |
| 2010 | 2561 | Foliation, second gen | 64 | 34 | M - Metaseds <30% Melt | shear plane crenulation cleavage, best guess | 531879 | 7184623 |
| 2010 | 2561 | Foliation, unknown gen | 62 | 135 | M - Metaseds <30% Melt | prolly s1, mica cleavage plane with andalusite porphs aligned within plane | 531859 | 7184630 |
| 2010 | 2562 | Bedding, younging direction unknown | 44 | 112 | M - Metaseds <30% Melt | tops determined by porph concentration in silty layering | 528599 | 7187550 |
| 2010 | 2562 | Bedding, younging direction unknown | 31 | 125 | M - Metaseds <30% Melt | porph concentration in silty layering | 528664 | 7187527 |
| 2010 | 2562 | Bedding, younging direction unknown | 35 | 134 | M - Metaseds <30% Melt | s0 | 528652 | 7187501 |
| 2010 | 2562 | Foliation, first gen | 26 | 137 | M - Metaseds <30% Melt | mica cleavage plane clockwise to bedding | 528605 | 7187541 |
| 2010 | 2562 | Foliation, first gen | 44 | 134 | M - Metaseds <30% Melt | mica cleavage plane | 528653 | 7187529 |
| 2010 | 2562 | Foliation, first gen | 31 | 145 | M - Metaseds <30% Melt | mica cleavage plane | 528667 | 7187525 |
| 2010 | 2562 | Foliation, first gen | 22 | 165 | M - Metaseds <30% Melt | s1 mica cleavage plane | 528650 | 7187504 |
| 2010 | 2562 | Foliation, first gen | 35 | 136 | M - Metaseds <30% Melt | folds s0[bedding ]into s folds | 528625 | 7187506 |
| 2010 | 2562 | Foliation, first gen | 44 | 140 | M - Metaseds <30% Melt | s folds of bedding | 528573 | 7187522 |
| 2010 | 2562 | Foliation, first gen | 44 | 162 | M - Metaseds <30% Melt | mica cleavage plane | 528541 | 7187539 |

Appendix B

| YEAR | STATNUM | FEATURE | DIP | STRIKE | LITHOLOGY | COMMENTS | EASTING | NORTHING |
|---|---|---|---|---|---|---|---|---|
| 2010 | 2562 | Foliation, second gen | 65 | 72 | M - Metaseds <30% Melt | maybe s2 cren | 528654 | 7187494 |
| 2010 | 2562 | Foliation, second gen | 55 | 188 | M - Metaseds <30% Melt | cren cleavage | 528573 | 7187523 |
| 2010 | 2562 | Bedding, younging direction unknown | 31 | 112 | M - Metaseds <30% Melt | s0 | 528655 | 7187529 |
| 2010 | 2562 | Bedding, younging direction unknown | 60 | 129 | M - Metaseds <30% Melt | bedding | 528623 | 7187496 |
| 2010 | 2562 | Bedding, younging direction unknown | 30 | 120 | M - Metaseds <30% Melt | bedding | 528571 | 7187524 |
| 2010 | 2562 | Bedding, younging direction unknown | 53 | 134 | M - Metaseds <30% Melt | bedding | 528543 | 7187540 |
| 2010 | 2563 | Bedding, younging direction unknown | 53 | 162 | M - Metaseds <30% Melt | bedding | 530713 | 7188575 |
| 2010 | 2563 | Foliation, unknown gen | 58 | 150 | M - Metaseds <30% Melt | mica cleavage plane | 530102 | 7188599 |
| 2010 | 2563 | Foliation, unknown gen | 44 | 182 | M - Metaseds <30% Melt | mica cleavage plane | 530370 | 7188720 |
| 2010 | 2563 | Foliation, unknown gen | 70 | 135 | P - Granite | mica foliation | 530806 | 7188252 |
| 2010 | 2564 | Bedding, younging direction unknown | 45 | 121 | M - Metaseds <30% Melt | bedding silty layering | 525677 | 7189954 |
| 2010 | 2564 | Foliation, first gen | 29 | 143 | M - Metaseds <30% Melt | mica cleavage plane | 525686 | 7189955 |
| 2010 | 2565 | Foliation, first gen | 49 | 155 | M - Metaseds <30% Melt | main generation of strong foliation in metaseds, contains aligned andalusite porphs, cren'd by S2 but hard to measure | 526042 | 7191671 |
| 2010 | 2565 | Foliation, unknown gen | 91 | 120 | M - Metaseds <30% Melt | main/first generation of foliation trends ~120, anastomosing | 526477 | 7191758 |

Appendix B

| YEAR | STATNUM | FEATURE | DIP | STRIKE | LITHOLOGY | COMMENTS | EASTING | NORTHING |
|---|---|---|---|---|---|---|---|---|
| 2010 | 2566 | Foliation, unknown gen | 40 | 180 | M - Metaseds <30% Melt | main foliation, may be 2nd...or 1st folded by 2nd. Appears to contain and porphs | 526670 | 7191344 |

APPENDIX C

## Appendix C. Representative major element whole-rock analyses of metamorphic rocks

**Brown Water Lake**

| **Sample:** | 1560A | 2501A | 2508A | 2531-1 | 1567 | 2512A | 2513 | 2544A | 2544B | 1558A | 1558C | 2518E -1 | 2519A (coticules) | 1554 | 2520 | 1537 | 2536B | 2536C (dupe) | 1571 | 1547A | 2524B | 2525A |
|---|---|---|---|---|---|---|---|---|---|---|---|---|---|---|---|---|---|---|---|---|---|---|
| **Rock type:** increasing grade left to right | metapelite | metapelite | pelitic schist | pelitic schist | pelitic schist | pelitic schist | pelitic schist | pelitic schist | pelitic schist | pelitic schist | pelitic schist | pelitic schist | pelitic schist | gneiss | gneiss | gneiss | gneiss | gneiss | gneiss | gneiss | gneiss | gneiss |
| **Met. Zone:** | Bt | Bt | And | And | And | Crd | And | And | And | Sil | Sil | Sil | Sil | Sil | Sil | Sil | Sil | Sil | Sil | Sil | Sil | Sil |
| **Assemblage:** | qtz+plg+bt+organics | qtz+plg+ms+bt | qtz+plg+ms+bt+and | qtz+plg+ms+bt+and | qtz+plg+bt+ms+grt+and+ late chl,ms | qtz+plg+bt+grt+late chl | qtz+plg+bt+mu+crd+and+ late ms | qtz+plg+bt+grt+ilm | qtz+plg+bt+and | qtz+plg+bt+and+fib+relic crd | qtz+plg+bt+grt+crd+ late ms | qtz+plg+bt+and+fib+ksp+late ms | qtz+bt+grt | qtz+plg+bt+mu+sil+rutile+late ms, chl | qtz+plag+ksp+bt+fib+and+new ms | qtz+ksp+bt+fib+sil+and+ms+relic crd | qtz+plg+ksp+bt+pyr+late ms | qtz+plg+ksp+bt+pyr+late ms | qtz+bt+ms+crd+sil | qtz+bt+plag+ksp+fib+ crn+ melt, late ms | qtz+plg+bt+ crd relics | qtz+plg+bt+sil |
| wt% | | | | | | | | | | | | | | | | | | | | | | |
| $SiO_2$ | 71.32 | 61.64 | 64.78 | 62.13 | 63.99 | 59.25 | 64.05 | 53.33 | 58.43 | 61.30 | 64.76 | 63.99 | 57.38 | 62.44 | 60.86 | 59.62 | 65.56 | 65.99 | 63.82 | 46.36 | 62.19 | 49.20 |
| $TiO_2$ | 0.75 | 0.75 | 0.67 | 0.72 | 0.62 | 0.51 | 0.68 | 3.12 | 1.90 | 0.86 | 0.67 | 0.73 | 0.55 | 0.89 | 0.73 | 0.74 | 0.63 | 0.62 | 0.69 | 0.98 | 0.71 | 0.75 |
| $Al_2O_3$ | 12.53 | 18.63 | 18.59 | 18.85 | 16.60 | 12.71 | 17.56 | 14.67 | 16.29 | 16.89 | 15.22 | 16.74 | 13.48 | 16.11 | 19.53 | 20.51 | 16.49 | 16.54 | 17.48 | 25.40 | 16.99 | 17.30 |
| $FeO_T$ | 5.16 | 4.75 | 4.72 | 5.88 | 7.42 | 16.66 | 5.84 | 14.15 | 11.17 | 9.08 | 8.39 | 6.65 | 15.94 | 7.53 | 5.30 | 7.02 | 4.73 | 4.47 | 5.71 | 7.10 | 7.02 | 11.61 |
| MnO | 0.03 | 0.03 | 0.03 | 0.04 | 0.16 | 0.49 | 0.06 | 0.13 | 0.08 | 0.25 | 0.55 | 0.07 | 1.54 | 0.05 | 0.04 | 0.05 | 0.04 | 0.04 | 0.04 | 0.09 | 0.08 | 0.18 |
| MgO | 1.72 | 2.12 | 1.89 | 2.46 | 2.77 | 3.53 | 2.73 | 3.28 | 2.96 | 3.17 | 2.50 | 2.95 | 3.16 | 2.86 | 2.41 | 2.67 | 1.95 | 1.92 | 2.54 | 4.59 | 3.27 | 8.09 |
| CaO | 0.17 | 0.28 | 0.35 | 0.25 | 0.32 | 0.93 | 0.44 | 2.19 | 1.34 | 0.54 | 0.57 | 0.33 | 1.25 | 0.06 | 0.65 | 0.44 | 0.48 | 0.65 | 0.21 | 2.30 | 1.36 | 2.85 |
| $Na_2O$ | 0.55 | 0.98 | 1.10 | 0.97 | 0.85 | 0.94 | 1.64 | 1.64 | 0.81 | 1.51 | 1.68 | 1.26 | 1.09 | 0.50 | 1.59 | 1.35 | 1.75 | 2.05 | 0.96 | 3.11 | 2.93 | 2.56 |
| $K_2O$ | 3.57 | 5.88 | 4.14 | 5.05 | 4.14 | 2.10 | 4.36 | 2.61 | 3.93 | 3.82 | 3.00 | 4.34 | 2.98 | 4.78 | 5.06 | 4.01 | 5.71 | 5.36 | 4.09 | 6.05 | 2.73 | 3.71 |
| $P_2O_5$ | 0.06 | 0.09 | 0.07 | 0.08 | 0.08 | 0.11 | 0.09 | 0.19 | 0.23 | 0.10 | 0.10 | 0.12 | 0.16 | 0.06 | 0.07 | 0.06 | 0.06 | 0.06 | 0.05 | 0.08 | 0.11 | 0.13 |
| SrO | 0.02 | 0.03 | 0.03 | 0.02 | 0.03 | 0.02 | 0.03 | 0.02 | 0.02 | 0.03 | 0.03 | 0.03 | 0.02 | 0.02 | 0.03 | 0.03 | 0.03 | 0.03 | 0.03 | 0.03 | 0.04 | 0.03 |
| BaO | 0.04 | 0.08 | 0.07 | 0.06 | 0.06 | 0.03 | 0.06 | 0.03 | 0.05 | 0.06 | 0.04 | 0.07 | 0.04 | 0.05 | 0.07 | 0.06 | 0.09 | 0.09 | 0.07 | 0.13 | 0.06 | 0.05 |
| LOI | 3.37 | 3.56 | 2.91 | 2.84 | 2.11 | 0.94 | 1.90 | 3.05 | 1.62 | 1.43 | 1.40 | 1.85 | 0.54 | 3.66 | 2.90 | 2.61 | 1.84 | 1.77 | 3.23 | 1.92 | 1.71 | 1.78 |
| Total | 99.29 | 98.82 | 99.35 | 99.35 | 99.16 | 98.21 | 99.44 | 98.42 | 98.83 | 99.04 | 98.91 | 99.13 | 98.13 | 99.01 | 99.24 | 99.17 | 99.36 | 99.59 | 98.92 | 98.14 | 99.20 | 98.24 |
| **mol.% normalized (anhydrous)** | | | | | | | | | | | | | | | | | | | | | | |
| $SiO_2$ | 79.96 | 72.19 | 74.34 | 71.52 | 72.26 | 65.82 | 72.13 | 61.41 | 66.32 | 68.91 | 72.25 | 72.05 | 64.15 | 71.91 | 70.38 | 68.91 | 74.05 | 74.17 | 73.33 | 55.00 | 69.38 | 54.77 |
| $TiO_2$ | 0.63 | 0.66 | 0.58 | 0.62 | 0.53 | 0.43 | 0.58 | 2.70 | 1.62 | 0.73 | 0.56 | 0.62 | 0.46 | 0.77 | 0.64 | 0.64 | 0.54 | 0.52 | 0.60 | 0.87 | 0.60 | 0.63 |
| $Al_2O_3$ | 8.28 | 12.86 | 12.57 | 12.79 | 11.05 | 8.32 | 11.65 | 9.96 | 10.90 | 11.19 | 10.01 | 11.11 | 8.88 | 10.93 | 13.31 | 13.97 | 10.98 | 10.96 | 11.84 | 17.76 | 11.17 | 11.35 |
| $FeO_T$ | 4.83 | 4.65 | 4.53 | 5.67 | 7.01 | 15.47 | 5.50 | 13.63 | 10.60 | 8.54 | 7.82 | 6.26 | 14.90 | 7.25 | 5.13 | 6.78 | 4.47 | 4.20 | 5.49 | 7.04 | 6.55 | 10.81 |
| MnO | 0.03 | 0.03 | 0.03 | 0.04 | 0.15 | 0.46 | 0.06 | 0.13 | 0.08 | 0.24 | 0.52 | 0.07 | 1.46 | 0.05 | 0.04 | 0.05 | 0.04 | 0.04 | 0.04 | 0.09 | 0.08 | 0.17 |
| MgO | 2.87 | 3.70 | 3.23 | 4.22 | 4.66 | 5.85 | 4.58 | 5.63 | 5.01 | 5.31 | 4.16 | 4.95 | 5.27 | 4.91 | 4.15 | 4.60 | 3.28 | 3.22 | 4.35 | 8.12 | 5.44 | 13.42 |
| CaO | 0.20 | 0.35 | 0.43 | 0.31 | 0.39 | 1.11 | 0.53 | 2.70 | 1.63 | 0.65 | 0.68 | 0.40 | 1.50 | 0.07 | 0.81 | 0.54 | 0.58 | 0.78 | 0.26 | 2.92 | 1.63 | 3.40 |
| $Na_2O$ | 0.60 | 1.11 | 1.22 | 1.08 | 0.93 | 1.01 | 1.79 | 1.83 | 0.89 | 1.65 | 1.82 | 1.38 | 1.18 | 0.56 | 1.78 | 1.51 | 1.92 | 2.23 | 1.07 | 3.58 | 3.17 | 2.76 |
| $K_2O$ | 2.55 | 4.39 | 3.03 | 3.71 | 2.98 | 1.49 | 3.13 | 1.92 | 2.85 | 2.74 | 2.13 | 3.12 | 2.13 | 3.51 | 3.73 | 2.96 | 4.11 | 3.84 | 3.00 | 4.58 | 1.94 | 2.63 |
| $P_2O_5$ | 0.03 | 0.04 | 0.03 | 0.04 | 0.04 | 0.05 | 0.04 | 0.09 | 0.11 | 0.05 | 0.05 | 0.06 | 0.08 | 0.03 | 0.03 | 0.03 | 0.03 | 0.03 | 0.02 | 0.04 | 0.05 | 0.06 |
| Total | 100.00 | 100.00 | 100.00 | 100.00 | 100.00 | 100.00 | 100.00 | 100.00 | 100.00 | 100.00 | 100.00 | 100.00 | 100.00 | 100.00 | 100.00 | 100.00 | 100.00 | 100.00 | 100.00 | 100.00 | 100.00 | 100.00 |
| **mol.% normalized NCKFMAS** | | | | | | | | | | | | | | | | | | | | | | |
| S | 80.52 | 72.73 | 74.82 | 72.03 | 72.78 | 66.44 | 72.62 | 63.26 | 67.54 | 69.62 | 73.07 | 72.59 | 65.46 | 72.52 | 70.88 | 69.41 | 74.50 | 74.61 | 73.82 | 55.56 | 69.89 | 55.24 |
| A | 8.34 | 0.67 | 0.58 | 0.63 | 0.53 | 0.43 | 0.58 | 2.78 | 1.65 | 0.73 | 0.57 | 0.62 | 0.47 | 0.78 | 0.64 | 0.65 | 0.54 | 0.53 | 0.60 | 0.88 | 0.60 | 0.63 |
| F | 4.87 | 12.95 | 12.65 | 12.88 | 11.13 | 8.40 | 11.73 | 10.26 | 11.10 | 11.30 | 10.12 | 11.19 | 9.06 | 11.03 | 13.41 | 14.07 | 11.04 | 11.02 | 11.92 | 17.94 | 11.25 | 11.45 |
| M | 2.89 | 4.69 | 4.56 | 5.71 | 7.06 | 15.62 | 5.54 | 14.04 | 10.80 | 8.62 | 7.91 | 6.31 | 15.20 | 7.32 | 5.16 | 6.83 | 4.50 | 4.23 | 5.53 | 7.12 | 6.60 | 10.90 |
| C | 0.21 | 0.03 | 0.03 | 0.04 | 0.15 | 0.47 | 0.06 | 0.13 | 0.08 | 0.24 | 0.53 | 0.07 | 1.49 | 0.05 | 0.04 | 0.05 | 0.04 | 0.04 | 0.04 | 0.09 | 0.08 | 0.17 |
| N | 0.60 | 3.73 | 3.25 | 4.25 | 4.70 | 5.90 | 4.61 | 5.80 | 5.10 | 5.37 | 4.21 | 4.99 | 5.37 | 4.95 | 4.18 | 4.63 | 3.30 | 3.24 | 4.38 | 8.20 | 5.48 | 13.54 |
| K | 2.57 | 0.35 | 0.43 | 0.31 | 0.39 | 1.12 | 0.53 | 2.78 | 1.66 | 0.66 | 0.69 | 0.40 | 1.53 | 0.07 | 0.81 | 0.55 | 0.58 | 0.79 | 0.26 | 2.95 | 1.64 | 3.43 |
| A/CNK | 2.33 | 2.07 | 2.46 | 2.36 | 2.36 | 1.77 | 1.95 | 1.09 | 1.56 | 1.97 | 1.88 | 2.10 | 1.41 | 2.59 | 1.87 | 2.51 | 1.53 | 1.43 | 2.58 | 1.27 | 1.34 | 0.93 |
| A | 0.074 | -0.037 | 0.309 | 0.144 | 0.153 | 0.153 | 0.183 | 0.179 | 0.131 | 0.177 | 0.231 | 0.135 | 0.111 | 0.032 | 0.185 | 0.309 | -0.150 | -0.072 | 0.224 | 0.210 | 0.308 | 0.125 |
| A' - musc rocks[1] | 0.003 | -0.146 | 0.225 | 0.055 | 0.091 | 0.118 | 0.044 | 0.110 | 0.086 | 0.087 | 0.130 | 0.033 | 0.062 | - | - | - | - | - | - | - | - | - |
| A' - kspar rocks[2] | - | - | - | - | - | - | - | - | - | - | - | - | - | 0.361 | 0.457 | 0.455 | 0.389 | 0.397 | 0.441 | 0.388 | 0.336 | 0.197 |
| Mg# [MgO/(FeO+MgO)] | 0.37 | 0.44 | 0.42 | 0.43 | 0.40 | 0.27 | 0.45 | 0.29 | 0.32 | 0.38 | 0.35 | 0.44 | 0.26 | 0.40 | 0.45 | 0.40 | 0.42 | 0.43 | 0.44 | 0.54 | 0.45 | 0.55 |
| CaO/(CaO+$Na_2O$/2+$K_2O$/2) | 0.11 | 0.11 | 0.17 | 0.11 | 0.17 | 0.47 | 0.18 | 0.59 | 0.47 | 0.23 | 0.26 | 0.15 | 0.48 | 0.04 | 0.23 | 0.20 | 0.16 | 0.20 | 0.11 | 0.42 | 0.39 | 0.56 |

[1] A' = ($Al_2O_3$ - $Na_2O$ - 3·$K_2O$)/[(abs·$Al_2O_3$ - $Na_2O$ - 3·$K_2O$) + FeO + MgO]

[2] A' = ($Al_2O_3$ - $Na_2O$ - $K_2O$)/[(abs·$Al_2O_3$ - $Na_2O$ - $K_2O$) + FeO + MgO]

## Appendix C. Representative major element whole-rock analyses of metamorphic rocks

**Little Crapeau Lake**

| **Sample:** | 1530A | 1508 | 1508B (dupe) | 1535B | 1511 | 1540D | 2562B | 2565A |
|---|---|---|---|---|---|---|---|---|
| **Rock type:** increasing grade left to right | pelitic schist | pelitic schist | pelitic schist | pelitic schist | pelitic schist | pelitic schist | pelitic schist | pelitic schist |
| **Met. Zone:** | Bt | Bt | Bt | Crd | And | And | And | And |
| **Assemblage:** | qtz+ms+chl | qtz+plg+ms+bt+chl | qtz+plg+ms+bt+chl | qtz+bt+ms+crd | qtz+bt+ms+and+crd | qtz+ms+bt+and+crd+ late chl | qtz+bt+ms+crd+and | qtz+plg+bt+ms+and+grt |
| wt% | | | | | | | | |
| $SiO_2$ | 61.52 | 64.66 | 65.41 | 62.16 | 59.03 | 57.76 | 61.31 | 61.03 |
| $TiO_2$ | 0.75 | 0.63 | 0.64 | 0.70 | 0.67 | 0.69 | 0.69 | 0.66 |
| $Al_2O_3$ | 18.03 | 16.40 | 15.97 | 17.96 | 19.74 | 20.21 | 17.72 | 18.54 |
| $FeO_T$ | 7.23 | 6.34 | 6.03 | 6.96 | 7.82 | 7.68 | 6.97 | 7.23 |
| MnO | 0.07 | 0.09 | 0.08 | 0.18 | 0.10 | 0.12 | 0.09 | 0.18 |
| MgO | 2.39 | 2.27 | 2.13 | 2.66 | 2.65 | 2.90 | 2.62 | 2.69 |
| CaO | 0.47 | 0.36 | 0.37 | 0.55 | 0.30 | 0.67 | 0.51 | 0.24 |
| $Na_2O$ | 1.64 | 1.51 | 1.58 | 1.49 | 1.30 | 1.26 | 1.67 | 0.72 |
| $K_2O$ | 4.36 | 4.10 | 4.07 | 4.38 | 4.69 | 5.14 | 3.98 | 5.25 |
| $P_2O_5$ | 0.06 | 0.07 | 0.08 | 0.09 | 0.06 | 0.07 | 0.08 | 0.06 |
| SrO | 0.03 | 0.03 | 0.03 | 0.03 | 0.02 | 0.02 | 0.03 | 0.02 |
| BaO | 0.08 | 0.06 | 0.06 | 0.06 | 0.07 | 0.09 | 0.06 | 0.08 |
| LOI | 2.36 | 2.70 | 2.65 | 1.65 | 2.59 | 2.31 | 2.45 | 2.33 |
| Total | 98.99 | 99.23 | 99.10 | 98.87 | 99.04 | 98.91 | 98.18 | 99.03 |
| **mol.% normalized (anhydrous)** | | | | | | | | |
| $SiO_2$ | 70.49 | 73.43 | 74.21 | 70.58 | 68.37 | 66.94 | 70.61 | 70.16 |
| $TiO_2$ | 0.65 | 0.54 | 0.55 | 0.60 | 0.58 | 0.60 | 0.60 | 0.57 |
| $Al_2O_3$ | 12.18 | 10.98 | 10.68 | 12.02 | 13.47 | 13.80 | 12.03 | 12.56 |
| $FeO_T$ | 6.92 | 6.02 | 5.72 | 6.60 | 7.57 | 7.44 | 6.72 | 6.95 |
| MnO | 0.07 | 0.09 | 0.08 | 0.17 | 0.10 | 0.12 | 0.09 | 0.18 |
| MgO | 4.08 | 3.84 | 3.60 | 4.50 | 4.58 | 5.01 | 4.50 | 4.61 |
| CaO | 0.58 | 0.44 | 0.45 | 0.67 | 0.37 | 0.83 | 0.63 | 0.30 |
| $Na_2O$ | 1.82 | 1.66 | 1.74 | 1.64 | 1.46 | 1.42 | 1.86 | 0.80 |
| $K_2O$ | 3.19 | 2.97 | 2.95 | 3.17 | 3.46 | 3.80 | 2.92 | 3.85 |
| $P_2O_5$ | 0.03 | 0.04 | 0.04 | 0.04 | 0.03 | 0.03 | 0.04 | 0.03 |
| Total | 100.00 | 100.00 | 100.00 | 100.00 | 100.00 | 100.00 | 100.00 | 100.00 |
| **mol.% normalized NCKFMAS** | | | | | | | | |
| S | 71.02 | 73.91 | 74.70 | 71.16 | 68.86 | 67.45 | 71.13 | 70.71 |
| A | 0.65 | 0.54 | 0.55 | 0.60 | 0.59 | 0.61 | 0.60 | 0.58 |
| F | 12.27 | 11.05 | 10.75 | 12.12 | 13.57 | 13.91 | 12.12 | 12.66 |
| M | 6.98 | 6.06 | 5.76 | 6.66 | 7.63 | 7.50 | 6.77 | 7.00 |
| C | 0.07 | 0.09 | 0.08 | 0.17 | 0.10 | 0.12 | 0.09 | 0.18 |
| N | 4.11 | 3.87 | 3.63 | 4.54 | 4.61 | 5.05 | 4.53 | 4.65 |
| K | 0.58 | 0.44 | 0.45 | 0.67 | 0.37 | 0.84 | 0.63 | 0.30 |
| A/CNK | 1.98 | 1.99 | 1.91 | 1.95 | 2.38 | 2.01 | 1.99 | 2.40 |
| A | 0.192 | 0.173 | 0.165 | 0.184 | 0.202 | 0.162 | 0.225 | 0.080 |
| A' - musc rocks[1] | 0.067 | 0.039 | 0.011 | 0.072 | 0.118 | 0.074 | 0.110 | 0.018 |
| A' - kspar rocks[2] | - | - | - | - | - | - | - | - |
| Mg# [MgO/(FeO+MgO)] | 0.37 | 0.39 | 0.39 | 0.41 | 0.38 | 0.40 | 0.40 | 0.40 |
| $CaO/(CaO+Na_2O/2+K_2O/2)$ | 0.19 | 0.16 | 0.16 | 0.22 | 0.13 | 0.24 | 0.21 | 0.11 |

[1] $A' = (Al_2O_3 - Na_2O - 3{\cdot}K_2O)/[(abs{\cdot}Al_2O_3 - Na_2O - 3{\cdot}K_2O) + FeO + MgO]$

[2] $A' = (Al_2O_3 - Na_2O - K_2O)/[(abs{\cdot}Al_2O_3 - Na_2O - K_2O) + FeO + MgO]$

APPENDIX D

| Sample | 10ls2544A | 09ls1558C | 10ls2518E-1 | 09ls1537 | 09ls1547A | 09ls1511 | 10ls2565A |
|---|---|---|---|---|---|---|---|
| Area: | BWL | BWL | BWL | BWL | BWL | LCL | LCL |
| Assemblage: | qtz+plg+bt+grt+ilm | qtz+plg+bt+grt+crd+late ms | qtz+plg+bt+ksp+sil+and+crd+late ms | qtz+bt+ksp+sil+and+crd+ilm +late ms | qtz+plg+bt+ksp+sil+crn+late ms | qtz+bt+ms+crd+plg+and | qtz+bt+ms+crd+plg+grt+and |
| Biotite | | | | | | | |
| Si | 1.23 | 1.24 | 1.27 | 1.26 | 1.25 | 1.21 | 1.24 |
| Al | 0.68 | 0.75 | 0.75 | 0.73 | 0.75 | 0.75 | 0.72 |
| Ti | 0.02 | 0.06 | 0.04 | 0.06 | 0.06 | 0.03 | 0.04 |
| Fe | 0.40 | 0.40 | 0.36 | 0.36 | 0.31 | 0.42 | 0.38 |
| Mn | 0.00 | 0.00 | 0.00 | 0.00 | 0.00 | 0.00 | 0.00 |
| Mg | 0.45 | 0.29 | 0.36 | 0.35 | 0.44 | 0.32 | 0.35 |
| Ca | 0.00 | 0.00 | 0.00 | 0.00 | 0.00 | 0.00 | 0.00 |
| Na | 0.01 | 0.01 | 0.01 | 0.01 | 0.01 | 0.01 | 0.01 |
| K | 0.17 | 0.24 | 0.24 | 0.25 | 0.26 | 0.20 | 0.23 |
| F | 0.02 | 0.02 | 0.02 | 0.04 | 0.01 | 0.02 | 0.03 |
| Cr | 0.00 | 0.00 | 0.00 | 0.00 | 0.00 | 0.00 | 0.00 |
| Cl | 0.00 | 0.00 | 0.00 | 0.00 | 0.00 | 0.00 | 0.00 |
| Mg/(Mg+Fe) | 0.53 | 0.42 | 0.50 | 0.50 | 0.59 | 0.43 | 0.47 |
| Muscovite | | | | | | | |
| Si | - | - | - | - | - | 1.65 | 1.65 |
| Al | - | - | - | - | - | 1.33 | 1.33 |
| Ti | - | - | - | - | - | 0.01 | 0.01 |
| Fe | - | - | - | - | - | 0.02 | 0.02 |
| Mn | - | - | - | - | - | 0.00 | 0.00 |
| Mg | - | - | - | - | - | 0.02 | 0.03 |
| Ca | - | - | - | - | - | 0.00 | 0.00 |
| Na | - | - | - | - | - | 0.03 | 0.04 |
| K | - | - | - | - | - | 0.27 | 0.26 |
| F | - | - | - | - | - | 0.01 | 0.01 |
| Cr | - | - | - | - | - | 0.00 | 0.00 |
| Cl | - | - | - | - | - | 0.00 | 0.00 |
| Cordierite | | | | | | | |
| Si | - | 1.72 | 1.73 | 1.71 | - | dna | dna |
| Ti | - | 0.00 | 0.00 | 0.00 | - | dna | dna |
| Al | - | 1.19 | 1.02 | 1.18 | - | dna | dna |
| Fe | - | 0.20 | 0.17 | 0.16 | - | dna | dna |
| Mn | - | 0.01 | 0.00 | 0.00 | - | dna | dna |
| Mg | - | 0.26 | 0.13 | 0.27 | - | dna | dna |
| Ca | - | 0.00 | 0.02 | 0.00 | - | dna | dna |
| Na | - | 0.01 | 0.02 | 0.01 | - | dna | dna |
| K | - | 0.00 | 0.05 | 0.04 | - | dna | dna |
| Cr | - | 0.00 | 0.00 | 0.00 | - | dna | dna |
| Mg/(Mg+Fe) | | 0.42 | 0.43 | 0.64 | | dna | dna |

*Values reported in Moles

$FeO_T$ denotes total Fe measured in the sample, without differentiation between $Fe^{3+}$ and $Fe^{2+}$

Some samples list muscovite in their assemblage, however only primary muscovite was probed for composition

**dna** denotes samples containing cordierite, where the mineral was too pinnitized to analyse

| Sample | 10ls2544A | 09ls1558C | 10ls2518E-1 | 09ls1537 | 09ls1547A | 09ls1511 | 10ls2565A |
|---|---|---|---|---|---|---|---|
| Area: | BWL | BWL | BWL | BWL | BWL | LCL | LCL |
| Assemblage: | qtz+plg+bt +grt+ilm | qtz+plg+bt +grt+crd+la te ms | qtz+plg+bt+k sp+sil+and+c rd+late ms | qtz+bt+ksp +sil+and+cr d+ilm +late ms | qtz+plg+bt+ ksp+sil+crn +late ms | qtz+bt+ms+ crd+plg+an d | qtz+bt+ms+ crd+plg+grt +and |
| Garnet | | | | | | | |
| Si | 1.31 | 1.30 | - | - | - | - | 1.30 |
| Al | 0.81 | 0.79 | - | - | - | - | 0.79 |
| Fe | 0.64 | 0.57 | - | - | - | - | 0.53 |
| Cr | 0.00 | 0.00 | - | - | - | - | 0.00 |
| Ti | 0.00 | 0.00 | - | - | - | - | 0.00 |
| Mg | 0.12 | 0.08 | - | - | - | - | 0.09 |
| Mn | 0.01 | 0.15 | - | - | - | - | 0.16 |
| Ca | 0.06 | 0.01 | - | - | - | - | 0.03 |
| Na | 0.00 | 0.00 | - | - | - | - | 0.00 |
| Fe/(Fe+Mg) | 0.92 | 0.94 | | | | | 0.93 |
| ı/(Mn+Fe+Mg) | 0.02 | 0.20 | | | | | 0.22 |
| Plagioclase | | | | | | | |
| Si | 2.09 | 2.31 | 2.33 | - | 2.14 | 2.31 | 2.22 |
| Al | 0.98 | 0.83 | 0.82 | - | 0.94 | 0.82 | 0.88 |
| Fe | 0.00 | 0.00 | 0.00 | - | 0.00 | 0.00 | 0.00 |
| Mg | 0.00 | 0.00 | 0.00 | - | 0.00 | 0.00 | 0.00 |
| Na | 0.30 | 0.42 | 0.42 | - | 0.33 | 0.43 | 0.39 |
| Ca | 0.20 | 0.08 | 0.07 | - | 0.17 | 0.06 | 0.11 |
| K | 0.00 | 0.00 | 0.00 | - | 0.00 | 0.01 | 0.00 |
| Na/(Na+Ca) | 0.46 | 0.75 | 0.78 | - | 0.52 | 0.79 | 0.66 |
| Potassium feldspar | | | | | | | |
| Si | - | - | - | 2.31 | 2.28 | - | - |
| Al | - | - | - | 0.70 | 0.70 | - | - |
| Fe | - | - | - | 0.00 | 0.00 | - | - |
| Mg | - | - | - | 0.00 | 0.00 | - | - |
| Mn | - | - | - | 0.00 | 0.00 | - | - |
| Na | - | - | - | 0.06 | 0.04 | - | - |
| Ca | - | - | - | 0.00 | 0.00 | - | - |
| K | - | - | - | 0.38 | 0.40 | - | - |
| Ilmenite | | | | | | | |
| Si | 0.00 | - | - | 0.00 | - | - | - |
| Ti | 1.10 | - | - | 1.10 | - | - | - |
| Fe | 0.84 | - | - | 0.80 | - | - | - |
| Cr | 0.00 | - | - | 0.00 | - | - | - |
| Al | 0.00 | - | - | 0.00 | - | - | - |
| Mg | 0.00 | - | - | 0.00 | - | - | - |
| Ca | 0.00 | - | - | 0.00 | - | - | - |
| Mn | 0.00 | - | - | 0.02 | - | - | - |
| Nb | 0.00 | - | - | 0.00 | - | - | - |

*Values reported in Moles

$FeO_T$ denotes total Fe measured in the sample, without differentiation between $Fe^{3+}$ and $Fe^{2+}$

Some samples list muscovite in their assemblage, however only primary muscovite was probed for composition

# APPENDIX E

1511-2

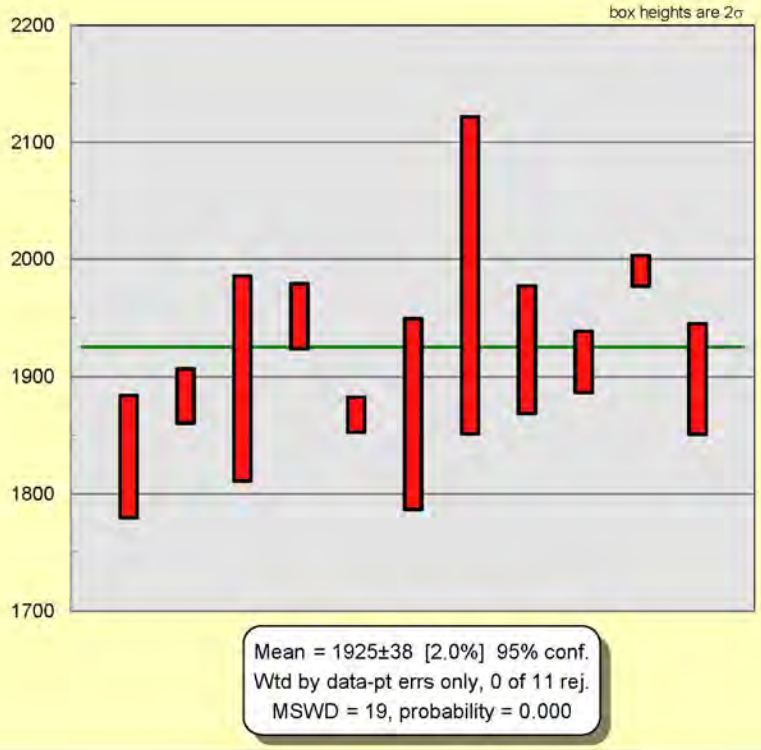
box heights are 2σ
2200
2100
2000
1900
1800
1700
Mean = 1925±38 [2.0%] 95% conf.
Wtd by data-pt errs only, 0 of 11 rej.
MSWD = 19, probability = 0.000

1535A


box heights are 2σ
2000
1960
1920
1880
1840
1800
Mean = 1897±44 [2.3%] 95% conf.
Wtd by data-pt errs only, 0 of 7 rej.
MSWD = 33, probability = 0.000

1540D


Mean = 1889±190 [10%] 95% conf.
Wtd by data-pt errs only, 0 of 2 rej.
MSWD = 2.8, probability = 0.094

2501A


Mean = 1823±96 [5.3%] 95% conf.
Wtd by data-pt errs only, 0 of 8 rej.
MSWD = 1215, probability = 0.000

2514-1


Mean = 1856±46 [2.5%] 95% conf.
Wtd by data-pt errs only, 0 of 5 rej.
MSWD = 8.1, probability = 0.000

2525A

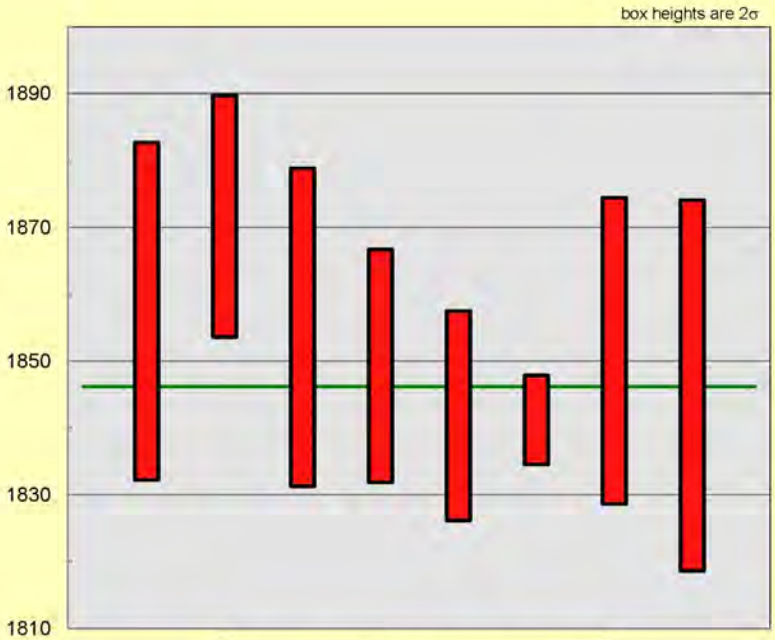


Mean = 1846.2±7.9 [0.43%] 95% conf.
Wtd by data-pt errs only, 0 of 8 rej.
MSWD = 1.7, probability = 0.094

2544A

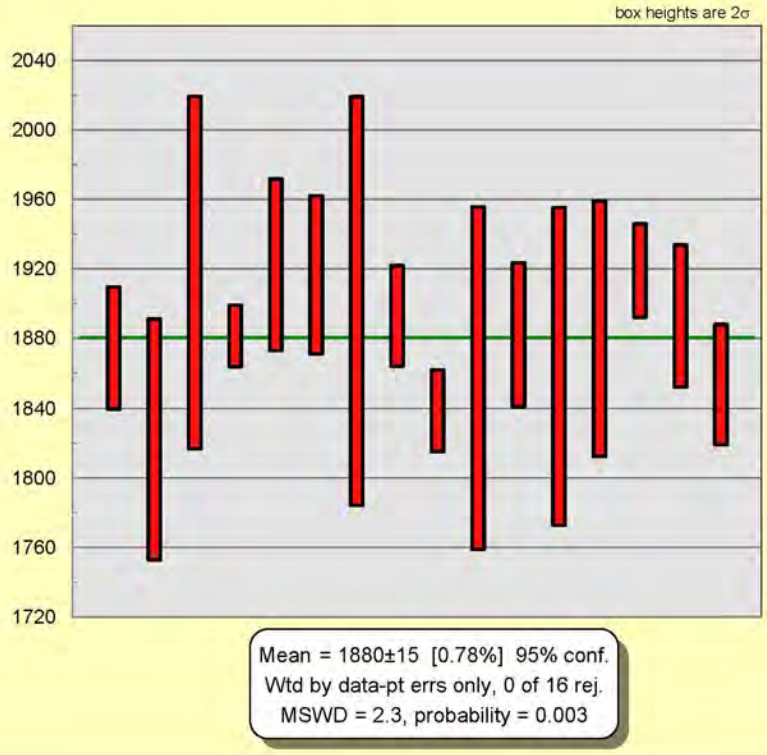
box heights are 2σ
2040
2000
1960
1920
1880
1840
1800
1760
1720
Mean = 1880±15 [0.78%] 95% conf.
Wtd by data-pt errs only, 0 of 16 rej.
MSWD = 2.3, probability = 0.003

2544B

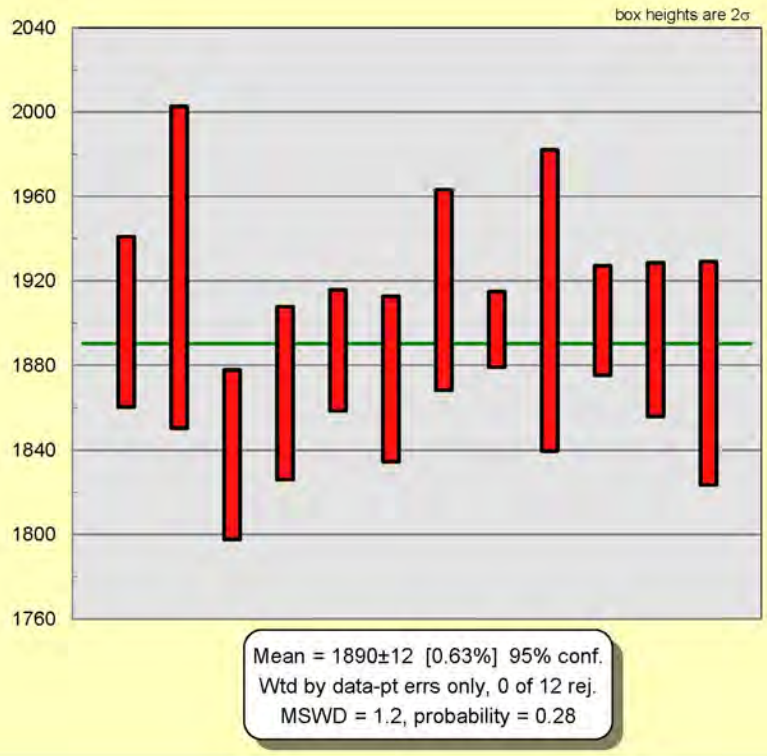
box heights are 2σ
2040
2000
1960
1920
1880
1840
1800
1760
Mean = 1890±12 [0.63%] 95% conf.
Wtd by data-pt errs only, 0 of 12 rej.
MSWD = 1.2, probability = 0.28

# 1511-2 mnz maps

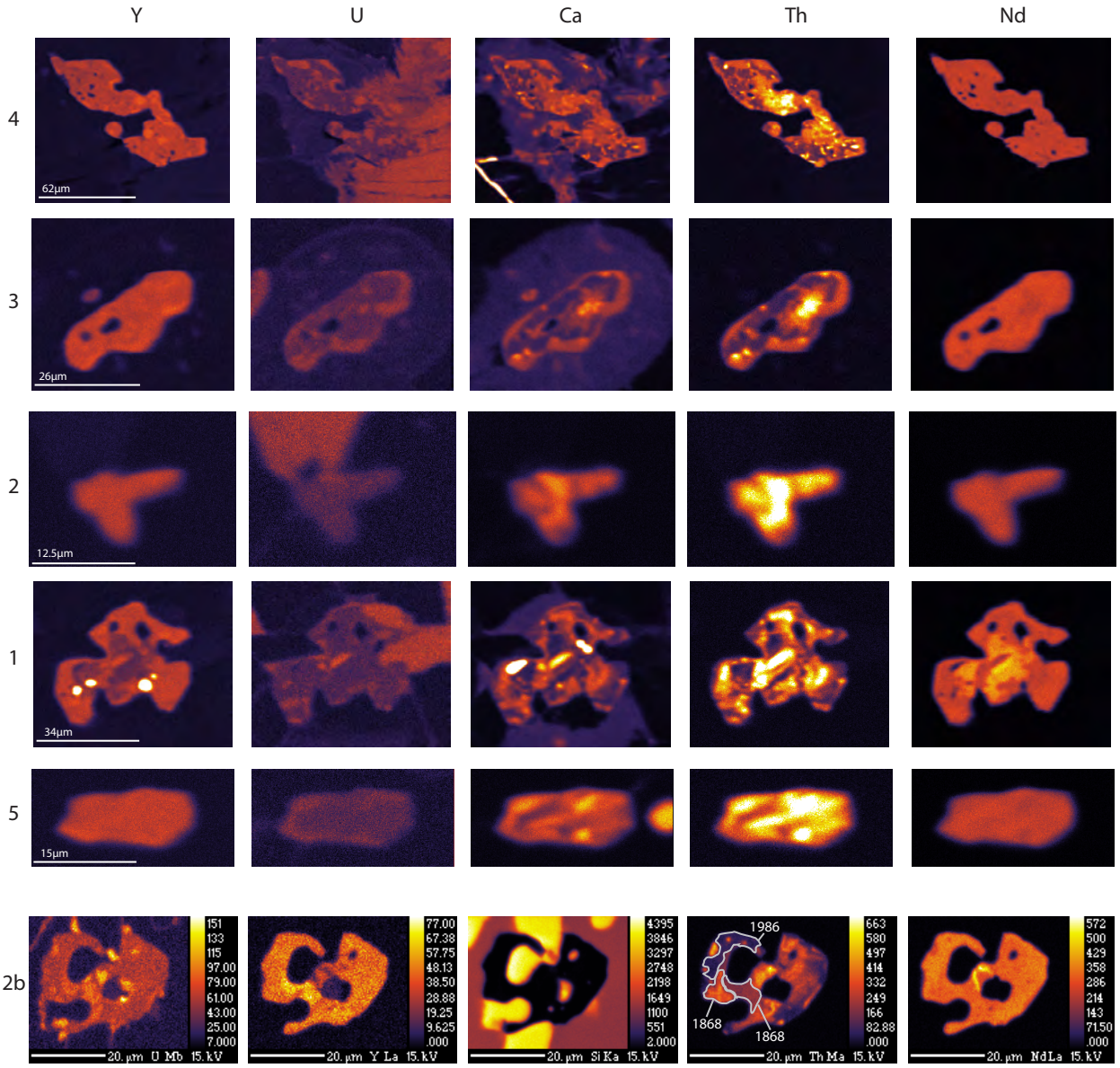

1535A mnz maps

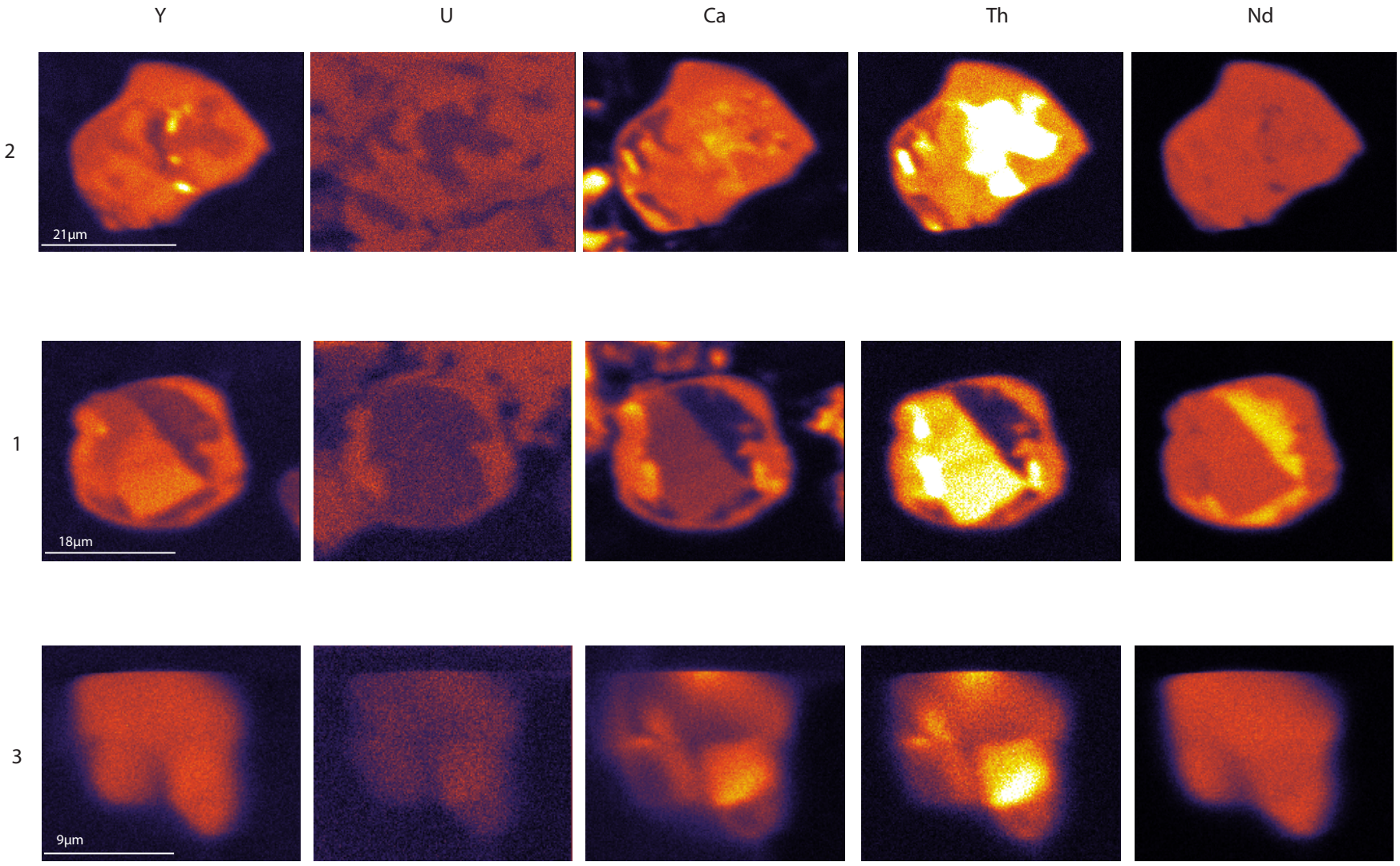

1540D-2 mnz maps

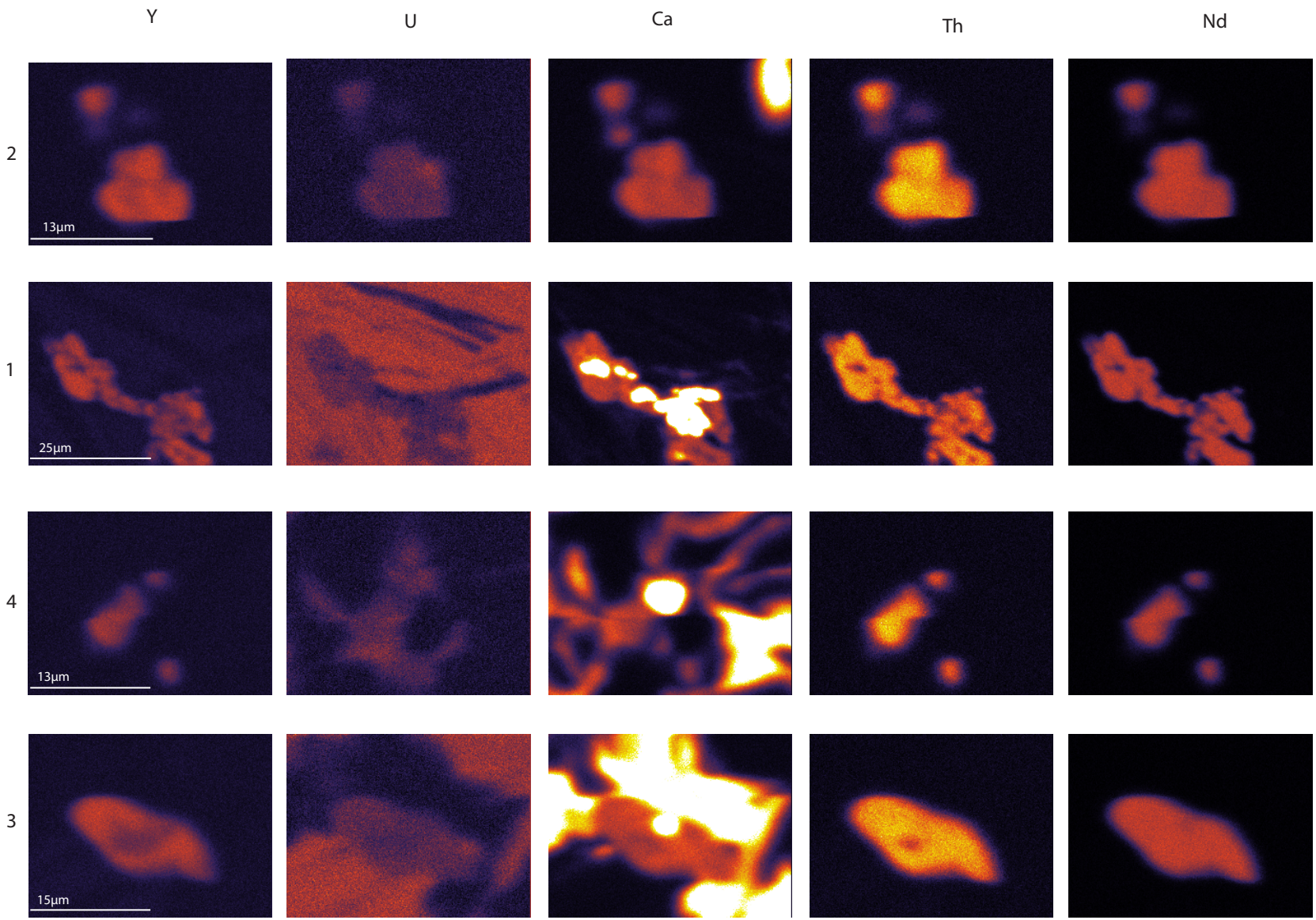

2501A mnz maps

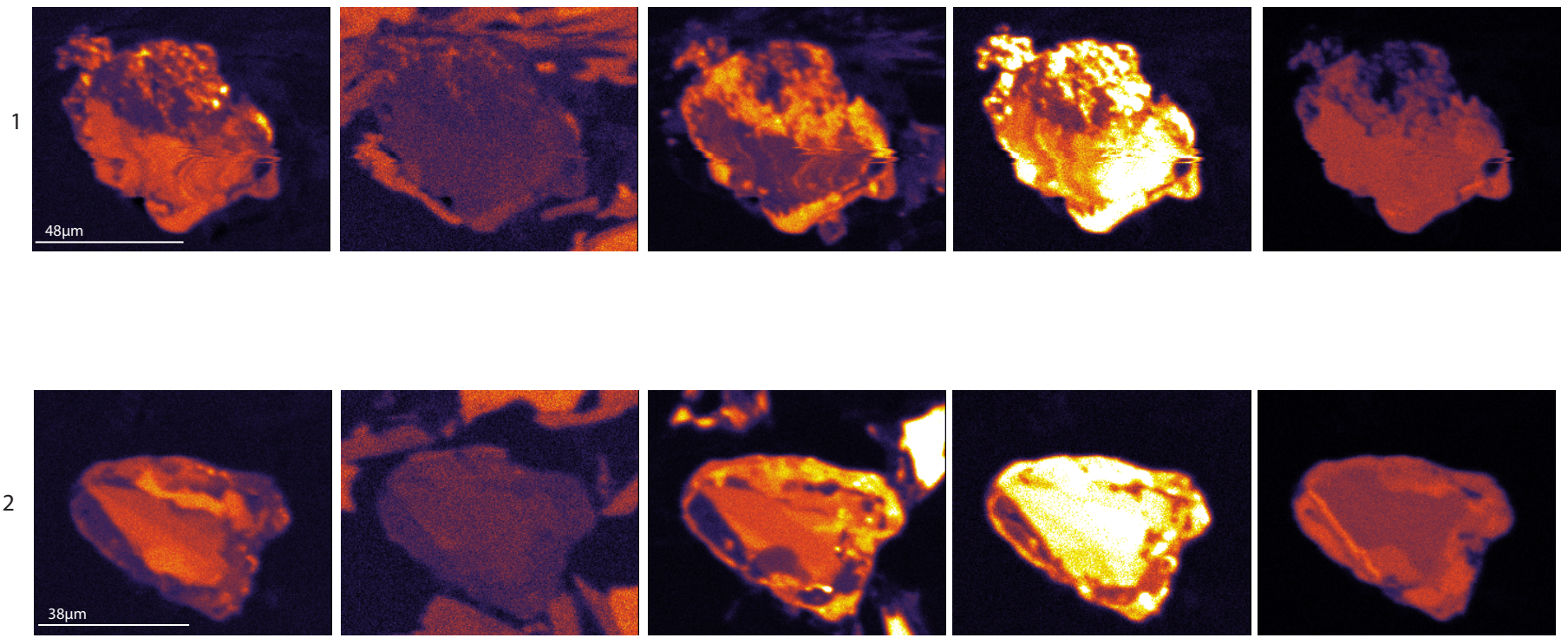

AF4 2506B mnz maps

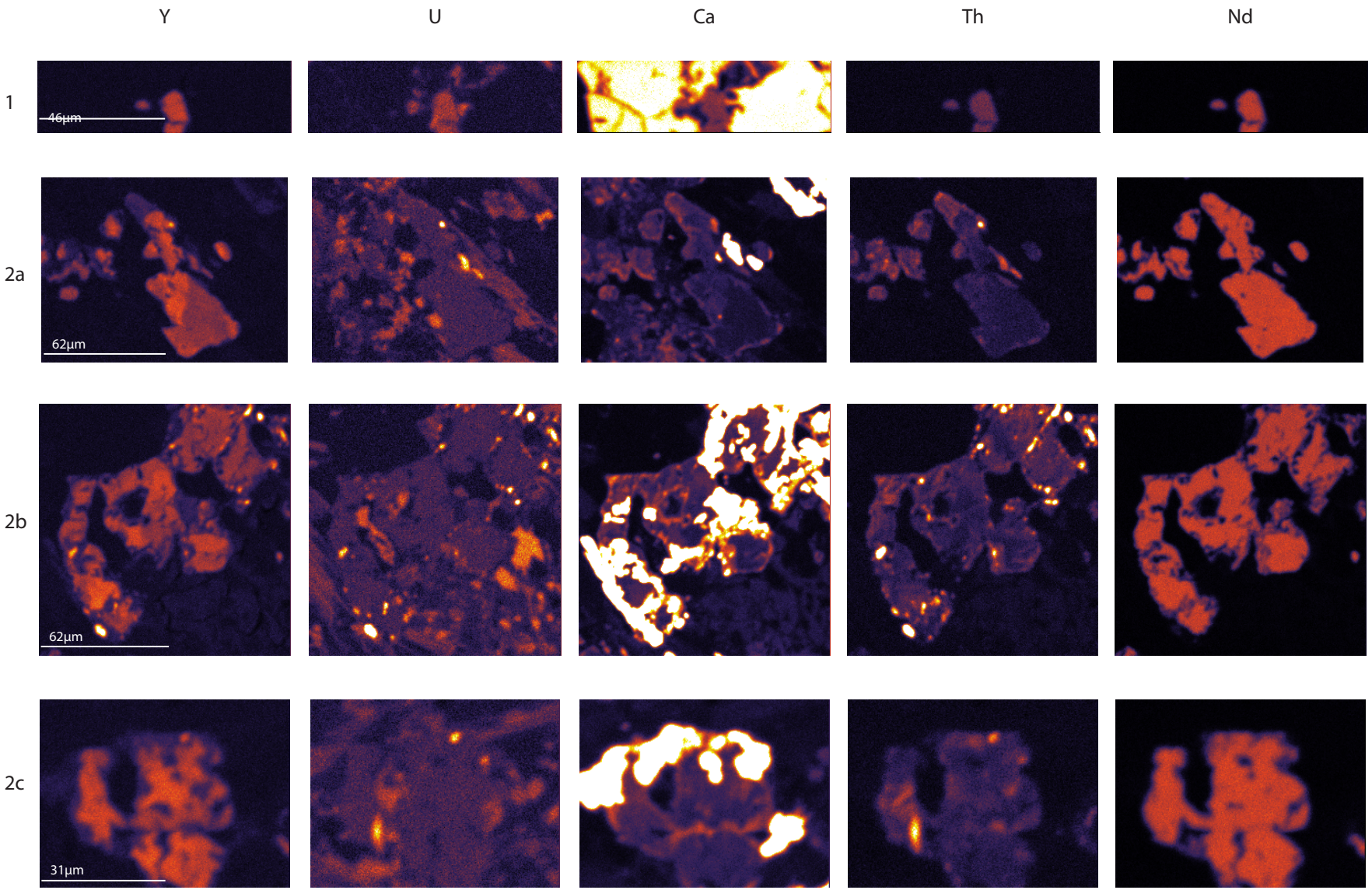

AF6 2514-1 mnz maps

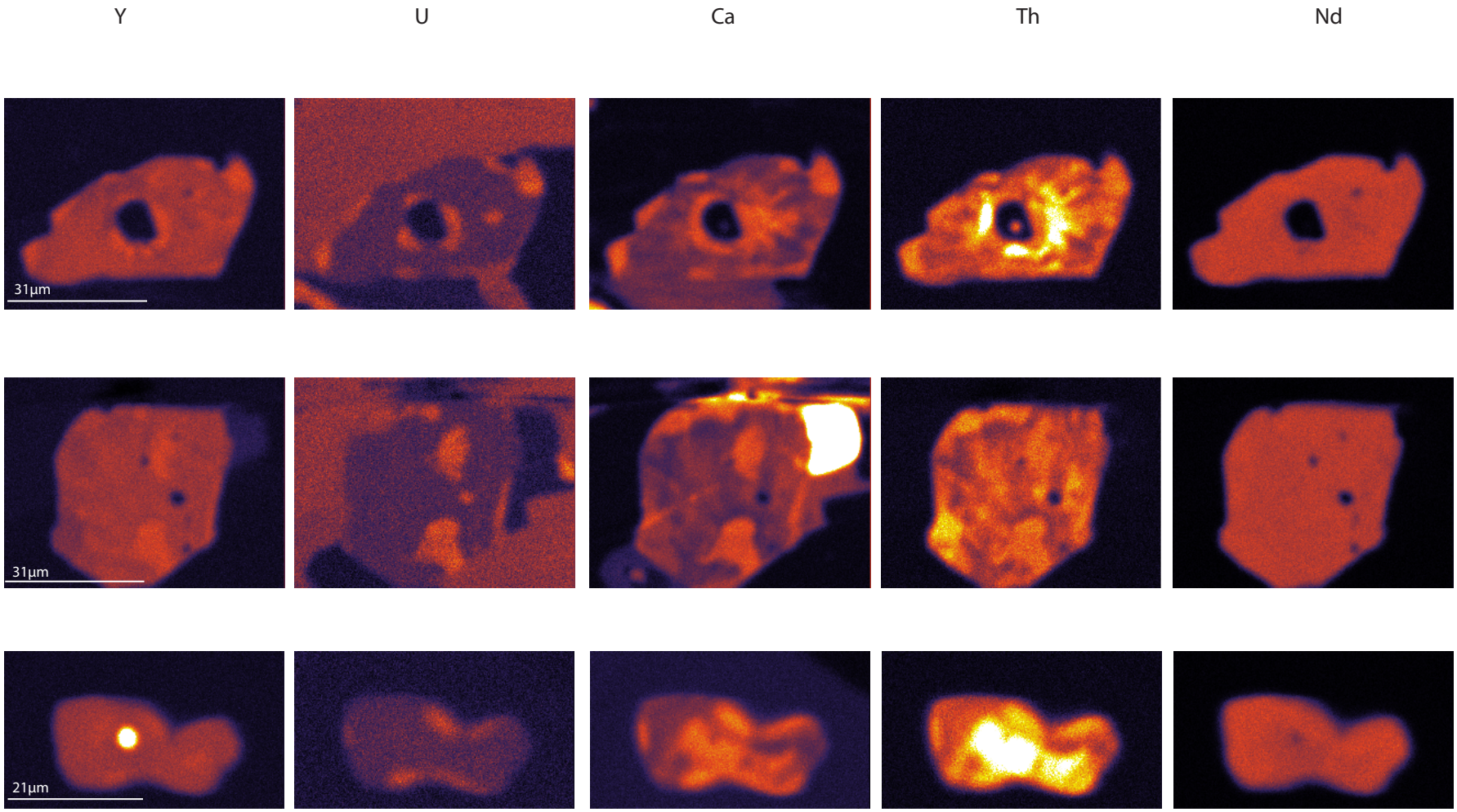

2525A mnz maps

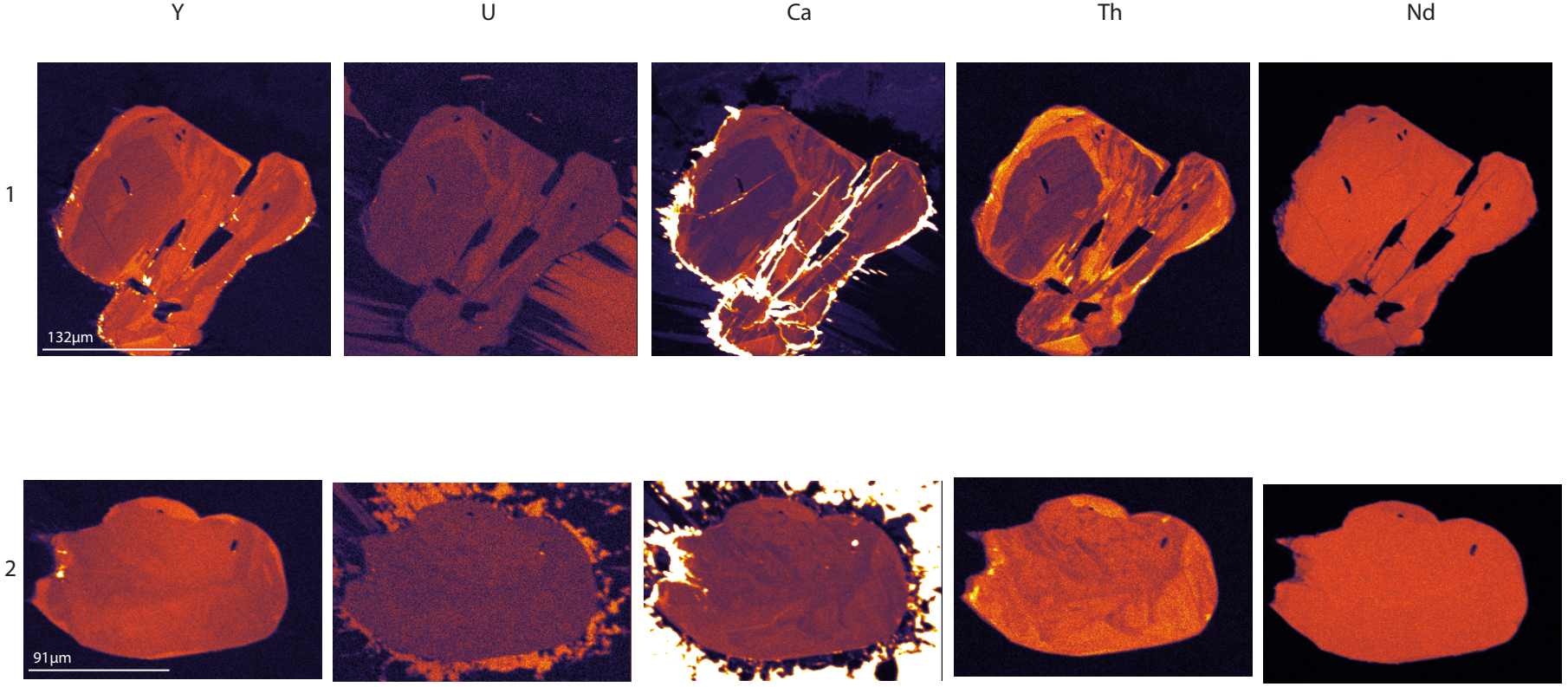

# 10ls2544A mnz maps

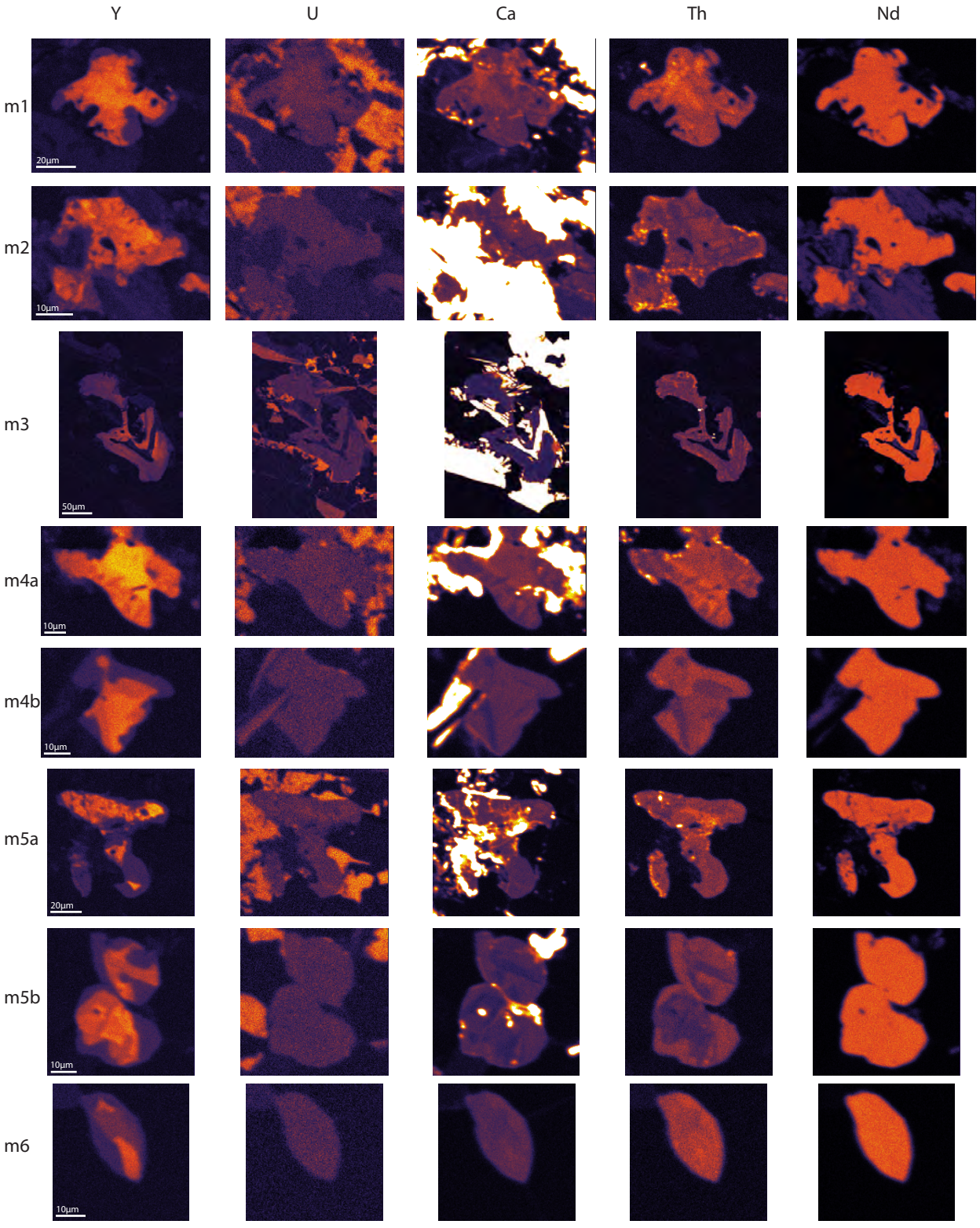

## 2544B mnz maps

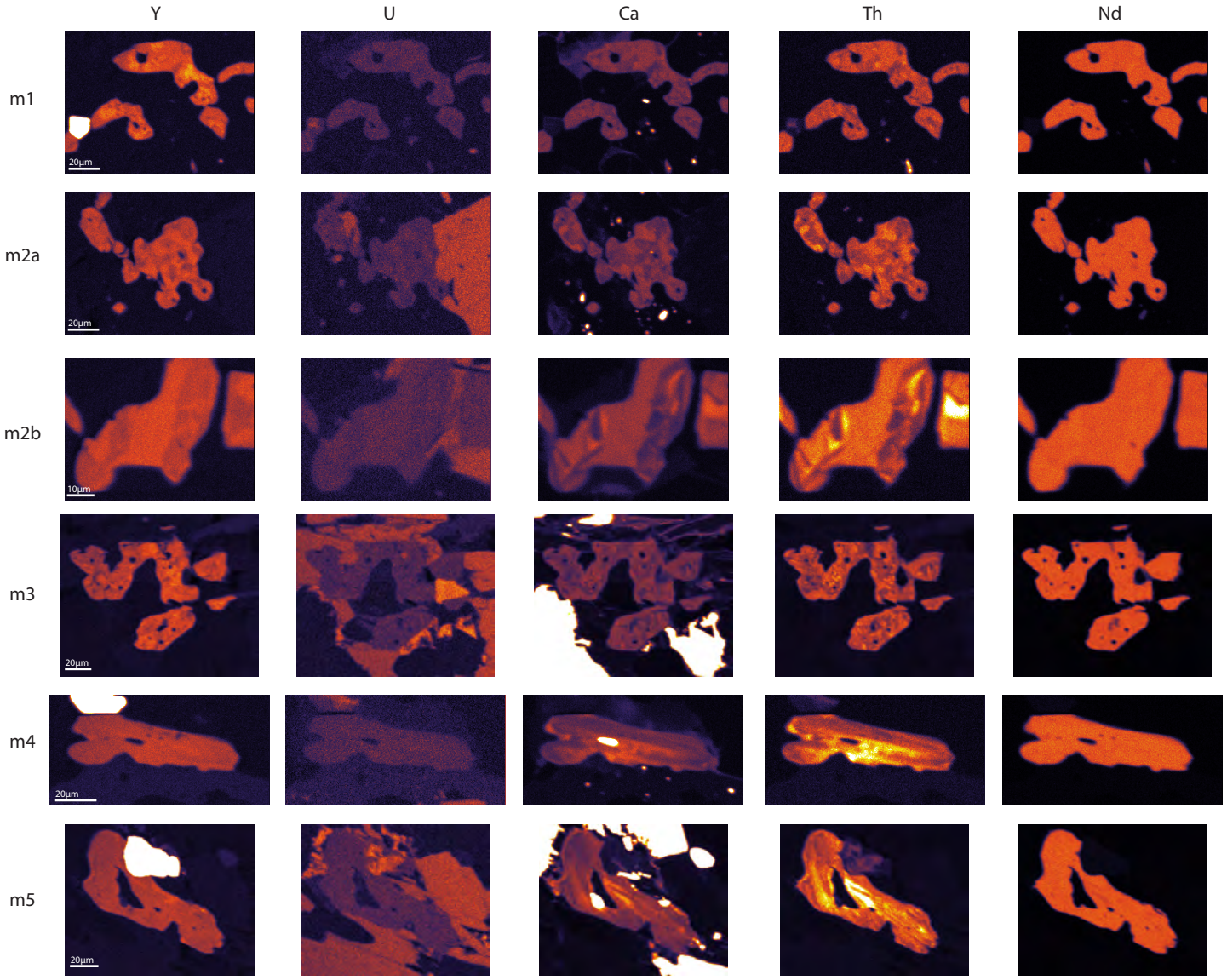

Appendix E

| SP | El. | Line | Standard | Time | | Time (long) | | Bkg | Peak | Monazite | |
|---|---|---|---|---|---|---|---|---|---|---|---|
| | | | | Peak | Bkg (each) | Peak | Bkg (each) | Type | $10^5$ sinq | Low | High |
| 1 | U | Mb | UO2 | 400 | 80 | 600 | 100 | Exp. | 42450 | Multipoint | |
| 1 | K | Kb | Microcline | 100 | 50 | 100 | 50 | Lin. | 39460 | -200 | 900 |
| 2 | Th | Ma | Cheralite CaTh(PO4)2 | 250 | 70 | 400 | 100 | Exp. | 47265 | Multipoint | |
| 2 | Ca | Ka | Wilberforce apatite | 20 | 10 | 20 | 10 | Lin. | 38390 | -500 | 500 |
| 2 | S | Ka | FeS2 | 20 | 10 | 20 | 10 | Exp. | 61390 | -5860 | 1530 |
| 2 | P | Ka | CePO4 | 20 | 10 | 20 | 10 | Lin. | 70350 | -1000 | 1000 |
| 2 | Y | La | YAG (Y-garnet) | 100 | 50 | 100 | 50 | Lin. | 73700 | -1090 | 1000 |
| 2 | Sr | La | SrF2 | 20 | 10 | 20 | 10 | Lin. | 78450 | -500 | 350 |
| 2 | Si | Ka | Microcline | 20 | 10 | 20 | 10 | Lin. | 81455 | -1170 | 850 |
| 3 | Pb | Ma | Pyromorphite | 500 | 100 | 700 | 100 | Exp. | 60385 | Multipoint | |
| 4 | Pb | Ma | (chlorophosphate) | 500 | 100 | 700 | 100 | Exp. | 60360 | Multipoint | |
| 5 | La | La | LaPO4 | 20 | 10 | 30 | 15 | Lin. | 66140 | -600 | 600 |
| 5 | Ce | La | CePO4 | 20 | 10 | 30 | 15 | Lin. | 63560 | -1000 | 1000 |
| 5 | Nd | La | NdPO4 | 20 | 10 | 30 | 15 | Lin. | 58835 | -1000 | 600 |
| 5 | Pr | Lb | PrPO4 | 20 | 10 | 30 | 15 | Lin. | 56075 | -370 | 470 |
| 5 | Eu | La | EuPO4 | 36 | 18 | 50 | 25 | Lin. | 52665 | -890 | 800 |
| 5 | Sm | Lb | SmPO4 | 36 | 18 | 50 | 25 | Lin. | 49620 | -1190 | 805 |
| 5 | Tb | La | TbPO4 | 36 | 18 | 50 | 25 | Lin. | 49065 | -1210 | 330 |
| 5 | Dy | La | DyPO4 | 36 | 18 | 50 | 25 | Lin. | 47400 | -1120 | 410 |
| 5 | Er | La | Er | 36 | 18 | 50 | 25 | Lin. | 44315 | -350 | 1080 |
| 5 | Gd | Lb2,15 | GdPO4 | 36 | 18 | 50 | 25 | Lin. | 43355 | -1320 | 1550 |
| 5 | Tm | La | Tm | 36 | 18 | 50 | 25 | Lin. | 42885 | -755 | 815 |
| 5 | Yb | La | Yb | 36 | 18 | 50 | 25 | Lin. | 41520 | -1640 | 590 |
| 5 | Ho | Lb | HoPO4 | 36 | 18 | 50 | 25 | Lin. | 40905 | -200 | 790 |
| 5 | As | Ka | GaAs | 36 | 18 | 50 | 25 | Lin. | 29190 | -375 | 340 |

Data obtained from the University of Massachussetts Amherst

Appendix E

| | Std to | Interfering element | | | To analyze | | Background | | Intensity |
|---|---|---|---|---|---|---|---|---|---|
| SP | analyze | El. | Line | Order | El. | Line | Low | High | cps/nA |
| 1 | | | Mg | I | U | Mb | -1365 | 1380 | 1.34 |
| 3 | Brab. | Th | Mz | I | Pb | Ma | -2665 | 1630 | 0.42 |
| 4 | | | Mz | I | Pb | Ma | -2665 | 1630 | 0.39 |
| 1 | Microcl. | K | Ka | I | U | Mb | -1100 | 1335 | 2.71 |
| 3 | YPO4 | Y | Lg3 | I | Pb | Ma | -2665 | 1630 | 0.97 |
| 4 | | | Lg3 | I | Pb | Ma | -2665 | 1630 | 0.84 |
| 3 | LaPO4 | La | La | II | Pb | Ma | -1490 | 2580 | 0.02 |
| 4 | | | La | II | Pb | Ma | -1490 | 2580 | 0.06 |
| 5 | PrPO4 | Pr | Lb2 | I | Eu | La | -1200 | 900 | 26.43 |
| 5 | | | Lg1 | I | Tb | La | -1250 | 600 | 0.34 |
| 5 | CePO4 | Ce | SLg10 | I | Tb | La | -1250 | 700 | 0.19 |
| 5 | | | Lb1 | I | Nd | La | -2600 | 850 | 1.2 |
| 5 | EuPO4 | Eu | Lb1 | I | Dy | La | -1500 | 1500 | 2.42 |
| 5 | | | Lg1 | I | Tm | La | -700 | 1700 | 17.34 |
| 5 | SmPO4 | Sm | Lb3 | I | Tb | La | -1150 | 1700 | 0.81 |
| 5 | | | Lg3 | I | Yb | La | -1100 | 550 | 0.56 |
| 5 | | | SLb2 | I | Sm | Lb | -700 | 1900 | 0.12 |
| 5 | NdPO4 | Nd | Lb3 | I | Eu | La | -900 | 2100 | 1.8 |
| 5 | | | Ll | I | La | La | -900 | 1200 | 0.25 |

Data obtained from the University of Massachussetts Amherst

Appendix E

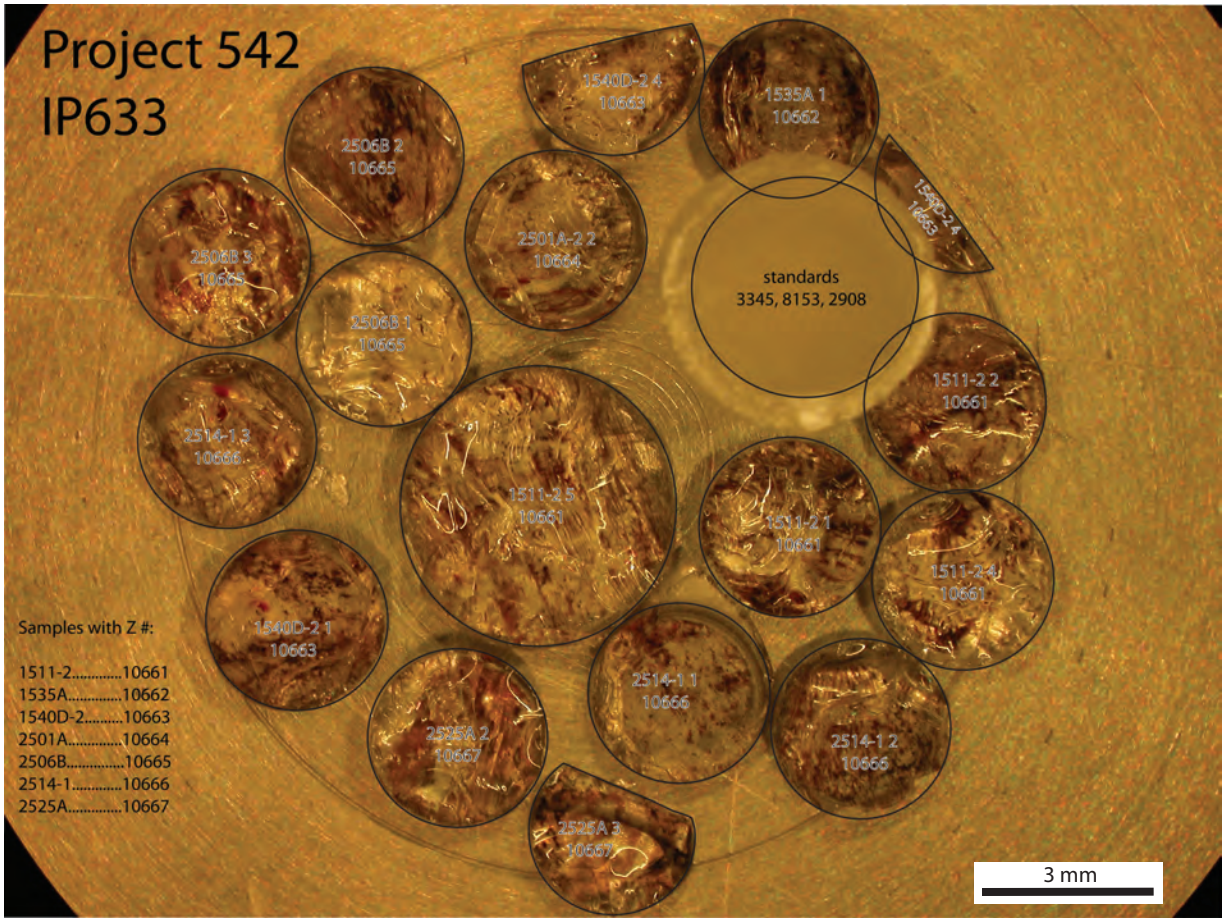


**Appendix E.** Grain mount made for U-Pb SHRIMP geochronological analysis of monazite grains in-situ at the Geological Survey of Canada, Ottawa. Project number 542. A drill press with a 3 or 5 mm diamond drill bit hole saw was used to excise disks of thin section containing selected monazite grains. Each disk contains one or more monazite grains. The mount was imaged with the SEM to locate desired targets.

APPENDIX F

## Mineral abbreviations and ideal chemistries

| Phase | Abbreviation | Ideal formula |
|---|---|---|
| Alkali feldspar (Microcline) | Ksp | $KAlSi_3O_8$ |
| Andalusite/Sillimanite/Kyanite | And, Sil, Ky | $Al_2SiO_5$ |
| Biotite | Bt | $K(Fe,Mg)_3AlSi_3O_{10}(OH)_2$ |
| Chlorite | Chl | $(Fe,Mg)_5Al_2Si_3O_{10}(OH)_8$ |
| Cordierite | Crd | $(Fe,Mg)_2Al_4Si_5O_{18}\cdot 0.5H_2O$ |
| Corundum | Crn | $Al_2O_3$ |
| Garnet | Grt | $(Fe,Mg)_3Al_2Si_3O_{12}$ |
| Granitic melt | L | - |
| Ilmenite | Ilm | $FeTiO_3$ |
| Muscovite | Ms | $KAl_3Si_3O_{10}(OH)_2$ |
| Plagioclase | Plg | $NaAlSi_3O_8$-$CaAl_2Si_2O_8$ |
| Quartz | Qtz | $SiO_2$ |